UNIVERSITY OF CALIFORNIA
RIVERSIDE

Competing Models for the Timing of Cryogenian Glaciation: Evidence From the Kingston Peak Formation, Southeastern California

A Dissertation submitted in partial satisfaction
of the requirements for the degree of

Doctor of Philosophy

In

Geological Sciences

By

David Douglas Mrofka

August 2010

Dissertation Committee:
Dr.Martin J. Kennedy, Chairperson
Dr. Mary M. Droser
Dr.Richard A. Minnich

The Dissertation of David Douglas Mrofka is approved:

_____

_____

_____

Committee Chairperson

ACKNOWLEDGEMENTS

First and foremost, I thank my advisor, Martin J. Kennedy, for his patience, commitment to communicating the importance of scientific thinking, consistent honest criticism and unwavering interest in my many academic endeavors. He never failed to provide me with the funding and analytical facilities needed to better investigate a wide range of geological questions. More importantly, he inspired me to better understand Earth history in general and during the Neoproterozoic specifically. I deeply appreciate his friendship and obvious commitment to my development. I am deeply thankful to Mary L. Droser for her consistent support, encouragement and friendship. I was honored to learn about Australia and the Ediacaran Fauna under her guidance at the beginning of my graduate work. She has been an unwavering supporter and source of practical advice for understanding both "real" and academic life. Very importantly, I owe her a great debt of gratitude for helping me to see the wisdom in making the single best personal decision of my life. I will be buying her venti lattes for many years to come…gladly. Finally, I am thankful to Richard A. Minnich for helping me to understand the relevance of atmospheric science to the study of deep time climate change. I greatly appreciate his willingness to share in the responsibilities of being on my committee and bettering my dissertation. I look forward to many helpful conversations in the future as I continue to better understand climate change science.

My time in this department would be a shadow of what it is without the friendship and camaraderie of the "Noonday Boys." Thanks to Damon DeYoung, Karl Thompson and Thomas Bristow for consistently lightening the load and for their faithful friendship. Special thanks to Thomas for his continued friendship and advice. A special note of thanks to Bill Phelps, whom I

will always think of as a good friend and terrific field mate. Thank you to many other people from UC Riverside that have helped me both in the field and for valuable friendship, including Noriko Noshino, Ganqing Jiang, Keith Morrison, Camille Partin, Erwan LeGuerroue, Kristin Keenan and Aaron Sappenfield.

No Death Valley geology project can miss the valuable scrutiny of Bennie Troxel and Lauren Wright. They provided me with many ideas, field locations and suggestions for what I might be missing. Thanks to Bennie for remembering more than I ever know about the Kingston Peak Formation; thanks to Lauren for encouragement, a place to stay on cold nights and for picking me up in the middle of the night on Highway 127 when I had to walk out of the southern Valjean Hills.

Research was funded by the National Science Foundation (grant EAR 0345207), NASA Exobiology (grant NWG04GjJ42G), a Geological Society of America Student Research Grant, the American Association for Petroleum Geologists Grant-in-Aid program and several quarters of the Department of Earth Sciences Blanchard Fellowship.

Last, I thank the person finally responsible for giving me the strength and desire to see this through, my wife, Ellen Mrofka Fauver. She spent many hours at home and here in the department editing my dissertation and suggesting many helpful alternatives to prolific run-on sentences. Though nearly undone by the wonderful quality of life change I experienced when my life intersected with hers and that of her (our) beautiful boys, I could not have completed this without her. She has been unwavering in her support of my dreams. I hope I can do the same for her.

ABSTRACT

Competing Models for the Timing of Cryogenian Glaciation: Evidence from the Kingston Peak Formation, Southeastern California

by

David Douglas Mrofka

Doctor of Philosophy, Graduate Program in Geological Sciences
University of California, Riverside, August 2010
Dr. Martin J.Kennedy, Chairperson

The Neoproterozoic (~750-635 Ma) Kingston Peak Formation, southeastern California, is a coarse-grained siliciclastic interval, with laterally extensive carbonate marker horizons, deposited in extensional basins between two regionally extensive carbonate intervals.

Thirty sections measured and two geologic maps produced show a wedge-shaped geometry unique to extensional settings and clarify the conformable relationship between the coarse-grained deposits and the overlying Noonday Dolomite. Carbonate intervals were sampled extensively to determine the value of chemostratigraphic correlation in this interval. A newly mapped regional unconformity near the base of the formation serves to separate the overlying tectonic sequence of the Kingston Peak Formation from the underlying deposits related to the platformal Beck Spring Dolomite. A glacigenic influence is inferred based on the presence of striated clasts in one of several basins, facilitating global correlation with similar coarse-grained deposits thought to record the Earth's most severe ice age.

The Kingston Peak Formation provides a rare example of ancient glacial successions in which the relationship between the sedimentary packaging in vertical and lateral dimensions is

apparent in outcrop. This allows the influence on stratigraphic development by the series of tectonic and climate events to be reconstructed without relying on regional or global correlation. These relations show the progressive development of extensional basins from northwest to southeast in the Death Valley region. The exceptional exposure in this region reveals bounding synsedimentary faults allowing tectonic and climate influence on coarse-grained facies to be resolved as well as the lateral persistence and stacking of course grained units. Through-going carbonate marker beds recording regional sea level rise provide timelines allowing the reconstruction and relative timing of climate and rifting events. These relations identify that the Kingston Peak Formation records a complicated regional history in which the record of rifting and climate are intimately related through fault subsidence and the creation of accommodation space.

The availability of accommodation space from tectonism biases the sedimentary record of climate change. Glacial deposits are not necessarily uniquely timed with glacial conditions, but with preservational conditions. This interplay between tectonism and related coarse-grained deposits obscures both the timing and extent of similar coarse-grained deposits related to glaciation.

Table of Contents

LIST OF FIGURES

LIST OF TABLES

CHAPTER 1:

THE NEOPROTEROZOIC EARTH-PROCESS DILEMMA: UNDERSTANDING THE TIMING OF GLOBAL GLACIATION AND THE INFLUENCE OF TECTONISM ON PRESERVATION OF THE CLIMATE RECORD

Extensive debate has centered on the magnitude, frequency and discreteness of Neoproterozoic ice ages because these deposits record perturbations in the Earth system (Allen and Etienne, 2008; Fairchild and Kennedy, 2007; Hoffman and Schrag, 2002) during the critical interval preceding the first appearance of metazoans in the fossil record (Knoll et al., 2006). The climate record, linked through the global carbon cycle to other important biogeochemical cycles such as atmospheric oxygen and oceanic alkalinity, provides important insight into the changes in the planet's biogeochemical systems coinciding with, and perhaps facilitating, the development of complex life (Fairchild and Kennedy, 2007). Aspects of these ice ages may have significant differences from Phanerozoic examples of cold periods (Allen and Etienne, 2008; Evans, 2003), and challenge our understanding of how biogeochemical feedbacks buffer the Earth's potential climate swings, and which of these feedbacks may be a product of life itself (Ridgwell et al., 2003). One of the most basic aspects about this record remains to be resolved, which is the relative timing of glacial deposits preserved in Neoproterozoic basins present across the globe (Fairchild and Kennedy, 2007) and whether these glacial deposits record 1) a prolonged ice age with local glacial evidence a function of paleolatitude (Crowell, 1978; Crowell, 1999), tectonically produced adiabatic cooling (Eyles and Januszczak, 2004; Schermerhorn, 1974, 1975) (ice accumulation due to

elevation gain) or accommodation space, or 2) a generally equable time punctuated by frigid episodes of ice house conditions driven by strong and unbuffered forcing of the climate (Hoffman et al., 1998b; Hoffman and Schrag, 2002).

Late Neoproterozoic successions globally are commonly characterized by intervals containing coarse grained sediments comprised of conglomerate and diamictite (Allen and Etienne, 2008). These sediments are often abruptly overlain by laterally persistent carbonate deposits (Halverson et al., 2005; Hoffman and Schrag, 2002) commonly referred to as cap carbonates because of an abrupt change in lithology to finer grained clastic and chemical sediments (Kennedy, 1996; Roberts, 1976). In most cases, multiple cycles of diamictite and carbonate occur. Diamictite deposits have been variously interpreted, but there is a general consensus of glacial origin or influence on the deposition of these sediments, particularly in cases where other evidence of striated clasts, dropstones, or striated pavements can be demonstrated (Etienne et al., 2007). It is also widely agreed that rift successions are characteristic of these same intervals (Eyles and Januszczak, 2004), and thus must account for some portion of the coarse grained rocks as well as determining the timing of subsidence and accommodation space necessary to capture climate influenced sediment.

Aspects about Neoproterozoic successions suggest fundamental differences to Phanerozoic glacial deposits (Evans, 2003). The global occurrence of discrete intervals of low-latitude glacial facies in most Neoproterozoic basins and abrupt transitions to overlying carbonate platformal deposits taken to indicate warm climates led Harland (1964) to propose that these

deposits shared the common origin of a great global ice age and were largely synchronous. Plate tectonic theory and its obvious implications for the change in latitude of climate paleodeposits combined with sedimentological evidence that all diamictites were not of glacial origin (Crowell, 1957; Dott, 1961) with many examples of a tectonic origin, along with poor time constraints, quelled enthusiasm for interpretation of a single ice age (Crowell, 1977, 1978; Crowell, 1999), raising the specter of similar processes providing similar deposits in diachronous events much as similar debates had occurred in Paleozoic and Cenozoic examples (Eyles et al., 1985). Given the typically poor time resolution for these Precambrian sediments in the absence of higher resolution biostratigraphy, the age constraints on many of these glacial successions can be as great as 100 million years (Etienne et al., 2007). The very real challenge of lithological correlation of sediments that share a similar mechanistic origin has meant that radiometric ages still serve as the only diagnostic test of Harland's (1964) great "InfraCambrian" ice age.

In the past decade, Harland's hypothesis has been reinvigorated by alternative means of correlating these deposits, particularly the use of carbon isotope values in marine carbonate rocks (Halverson et al., 2005; Kaufman et al., 1992; Knoll et al., 1986). Harland's (1964) early low latitude interpretation of glaciers at sea level is now well established with independently confirmed paleomagnetic evidence from glacial-marine sediments at <15° (Evans, 2000; Schmidt et al., 2009; Sohl et al., 1999; Williams, 1996). The extension of ice to the near-equatorial paleolatitudes both identifies the coldest interval in Earth history and implies that glacial deposits resulting from one ice age could have been deposited over much of the planet given appropriately timed accommodation space. Further, the globally similar pattern of conglomeratic sediments overlain by cap carbonates

also argued for a synchronous event, particularly as these carbonate sediments had anomalous carbon isotopic composition and sedimentary structures uncommon elsewhere in the geologic column (Kennedy et al., 1998). In sections where two glacial intervals were each overlain by cap carbonates, the lower cap carbonate was typically black laminated limestone and distinct from the buff colored cap carbonate of the upper interval (Hoffman and Schrag, 2002; Kennedy et al., 1998), a systematic pattern suggesting a global influence. Finally a juxtaposition of cold conditions indicated by glacigenic facies, and platform carbonates suggestive of equable climates implies oscillation between cold and warm periods (Fairchild, 1993) linked through a perturbed global carbon cycle (Kennedy, 1996), rather than gradual changes associated with continental drift from high to low latitudes.

This juxtaposition was most dramatically explained by the Snowball Earth hypothesis of Hoffman et al. (1998). They imagined a climate system dominated by a strong ice albedo feedback, resulting in reduced weathering and buildup of CO_2 in the atmosphere. A critical threshold greenhouse warming from CO_2 resulted in rapid melting and exchange of carbon between the atmosphere and ocean (Hoffman and Schrag, 2002). This exchange of carbon, and enhanced weathering rates in the post-glacial hothouse world, supplied both depleted carbon and alkalinity to the oceans, resulting in the deposition of isotopically depleted carbonate intervals (Higgins and Schrag, 2003) capping coarse-grained deposits.

Alternatively, the alkalinity and depleted carbon necessary for cap carbonate deposition and depleted isotopic values might have been the result of methane clathrate destabilization during

deglaciation (Kennedy et al., 2001). There is support for this idea in both the Cenozoic (Dickens et al., 1995; Nisbet, 1990) and associated with Neoproterozoic cap carbonates (Jiang et al., 2003; Kennedy et al., 2008).

The potential number of these discrete ice ages or "Snowball Earth" events remains controversial with up to four interpreted from correlation of various incomplete records (Kaufman and Knoll, 1995; Kaufman et al., 1997). Most records, however, contain evidence for only two events (Kennedy et al., 1998), an older and younger ice age colloquially referred to as the "Sturtian" (ca. 750 Ma) and the "Marinoan" (ca. 635 Ma) (Halverson et al., 2005).

Identification of global synchronous timing of these events still lies in the correlation of their deposits with the vexing problem that similar looking deposits in most sedimentary systems may have very different ages, and this is apparently the case for Neoproterozoic glacial and cap carbonates as well (Kendall et al., 2006; Kendall et al., 2004). Radiometric ages have proven to be the most reliable means of testing the hypothesis and intensive efforts have been made over the past decade to establish ages within these successions, to interesting effect (Fig. 1.1 and Table 1.1) (Allen and Etienne, 2008; Kendall et al., 2004). While the spread of ages for glacial deposits has increased from 750 Ma to 635 Ma (Allen and Etienne, 2008; Kendall et al., 2006; Kendall et al., 2004), there appears to be convergence on a single termination at 635 Ma confirmed in cap carbonate intervals in Namibia (Condon et al., 2005; Hoffmann et al., 2004a) and south China (Condon et al., 2005; Zhang et al., 2005). These dates suggest termination of the later ice

age ended synchronously with deposition of a global cap carbonate without a subsequent return to glacial conditions, consistent with Harland's (1964) original hypothesis.

Radiometric ages have failed to cluster or constrain distinct grouping of glacial deposits, and are widely scattered through the Cryogenian from different basins (Fig. 1.1 and Table 1.1). In a direct test of the ability to correlate glacial successions based on the properties of the cap carbonates, Kendall et al. (2004) found a 30 million year discrepancy between putatively Sturtian aged cap carbonates in south and central Australia; a correlation previously considered to be robust based on the similar lithological features of the cap carbonates (finely laminated black limestone), carbon isotope patterns of surrounding sediments and geographic proximity (Preiss, 1987). Further, these ages were 70 million years younger than deposits considered Sturtian in age in Namibia (Hoffman et al., 1998a; Hoffmann and Prave, 1996) which were also correlated based on these same criteria (Kaufman et al., 1997). This discrepancy in ages implies that not only do the lithological properties of cap carbonates have little to do with their ages, it is quite possible to have diachronous glacial successions and cap carbonates in adjacent basins. An alternative scenario is that these data support a complex and prolonged (> 100 Ma) Cryogenian ice age, including regional cooling, warming and carbonate deposition, terminated abruptly by cap carbonate deposition at 635 Ma

Neoproterozoic glacigenic rocks within the Kingston Peak Formation (Miller, 1985) of Death Valley California (Fig. 1.2) provide an alternative means of accessing this question of a prolonged ice age versus distinct or discrete ice ages separated by prolonged interglacial

conditions. Continuous exposures revealed in the extensive cliffs of this Tertiary extensional terrain provide a relatively intact view of the physical stratigraphy over >100 km revealing the number and discreteness of glacial intervals and the relation between tectonic and climate influence on coarse-grained facies without depending on correlation. Similar to other successions globally, this succession shows a conglomeratic interval (Fig 1.2) occurring between two regional platformal successions (Miller, 1985). The Kingston Peak Formation has most recently been interpreted to contain the common pattern of two or four discrete glacial intervals overlain by cap carbonate units and is thus commonly viewed as an example of globally correlated Neoproterozoic events (Corsetti and Kaufman, 2003; Prave, 1999). By mapping of key regions and detailed facies analysis of the conglomeratic intervals, data supports the Death Valley succession stratigraphically matching the emerging picture from radiometric ages, indicating complex and long lived diachronous deposition during the Cryogenian and terminating abruptly with the Noonday Dolomite, the Death Valley cap carbonate. This pattern meets Harland's (1964) original interpretation of one profound ice age setting the environmental stage for early animal evolution.

Fig. 1.1. Maximum and minimum age constraints for prominent Neoproterozoic glacial intervals. Faded bars indicate lack of bounding age constraint. Colored green bars indicate radiometric age constraint in interval immediately under or over glacial strata. Blue bars indicate syndepositional age constraint for glacial strata. Bottom bar indicates probable distribution of regional glaciations or glacial-interglacial cycles (modified after Allen and Etienne, 2008)

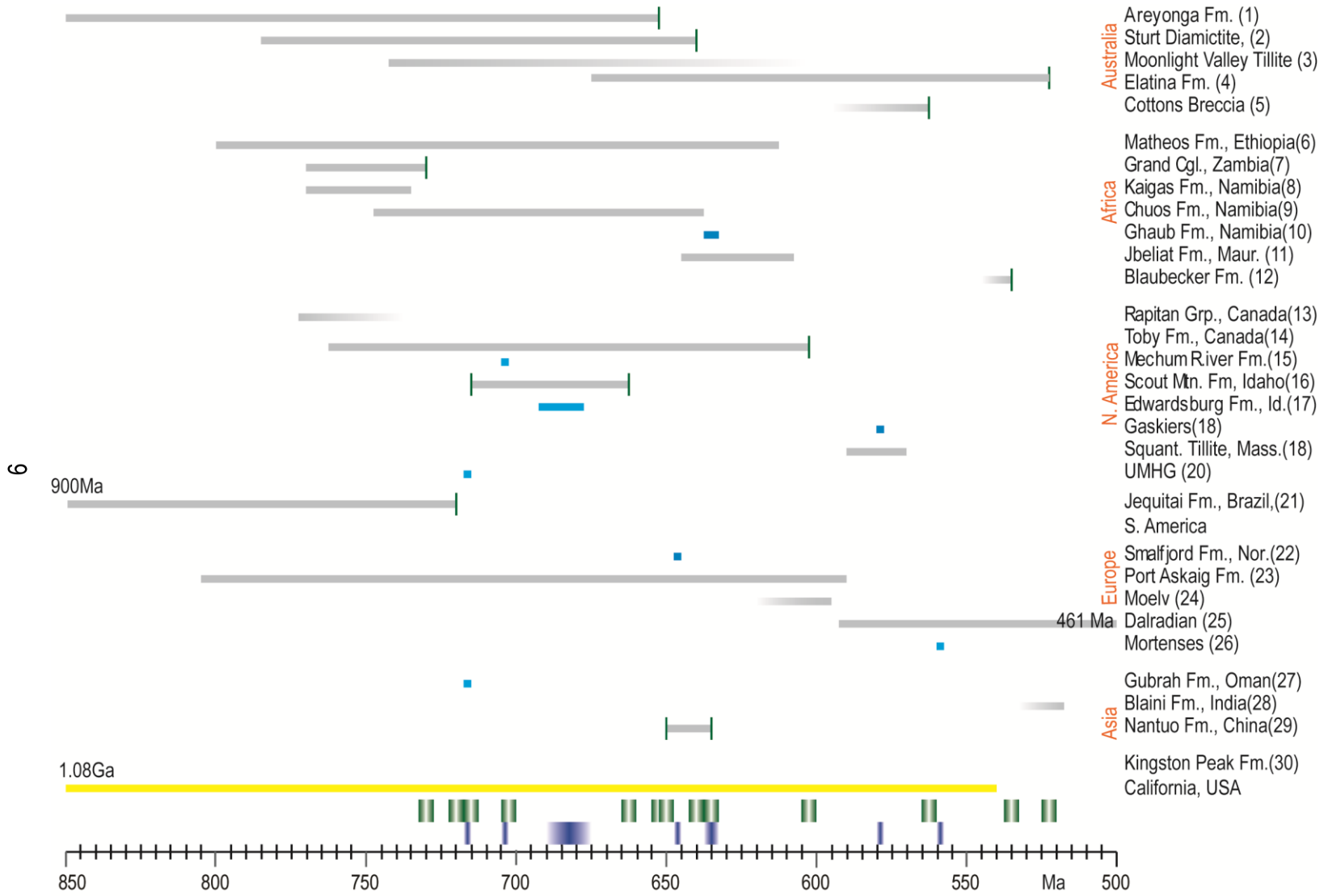
6
900Ma
1.08Ga
461 Ma
Australia
Areyonga Fm. (1)
Sturt Diamictite, (2)
Moonlight Valley Tillite (3)
Elatina Fm. (4)
Cottons Breccia (5)
Africa
Matheos Fm., Ethiopia(6)
Grand Cgl., Zambia(7)
Kaigas Fm., Namibia(8)
Chuos Fm., Namibia(9)
Ghaub Fm., Namibia(10)
Jbeliat Fm., Maur. (11)
Blaubecker Fm. (12)
N. America
Rapitan Grp., Canada(13)
Toby Fm., Canada(14)
Mechum River Fm.(15)
Scout Mtn. Fm, Idaho(16)
Edwardsburg Fm., Id.(17)
Gaskiers(18)
Squant. Tillite, Mass.(18)
UMHG (20)
S. America
Jequitai Fm., Brazil,(21)
Europe
Smalfjord Fm., Nor.(22)
Port Askaig Fm. (23)
Moelv (24)
Dalradian (25)
Mortenses (26)
Asia
Gubrah Fm., Oman(27)
Blaini Fm., India(28)
Nantuo Fm., China(29)
Kingston Peak Fm.(30)
California, USA
850
800
750
700
650
600
550
Ma
500

Table 1.1. Information on age constraints and references for Figure 1.1. Bold numbers indicate a syndepositional age, or blue bar in Figure 1.1. Position indicates a general stratigraphic position relative to the glacigenic interval.

	Fm./Mbr.	Lower Age (Ma)	Position	Upper or syndepo-sitional age (Ma)	Position
1	Areyonga Fm. (Kendall et al., 2006)	897 ± 9	Pre-glacial	657.2 ± 5.4	Immediate post-glacial
2	Sturt Diamictite (Kendall et al., 2006; Walter et al., 2000)	777 ± 7	Pre-glacial	643.0 ± 2.4	Immediate post-glacial
3	Moonlight Valley Tillite (Coats and Preiss, 1980)	672 ± 70	Pre-glacial		
4	Elatina Fm. (Cooper et al., 1992; Walter et al., 2000)	777 ± 7	Pre-glacial	526 ± 4	Post-glacial
5	Cottons Breccia (Calver et al., 2004)			574.7 ± 3	Pre-glacial
6	Matheos Fm. (Beyth et al., 2003)	796		613.4 ± 0.9	Post-glacial
7	Grand Conglomerate (Key et al., 2001)	763 ± 6	Pre-glacial	735 ± 5	Upper glacial contact
8	Kaigas Fm. (Frimmel et al., 2002; Frimmel et al., 1996; Frimmel et al., 2001)	771 ± 6	Pre-glacial	741 ± 6	Post-glacial
9	Chuos Fm. (Hoffmann and Prave, 1996)	758.5 ± 3.5	Pre-glacial	635.5 ± 1.2	Post-glacial
10	Ghaub Fm. (Hoffmann et al., 2004b)			**635.5 ± 1.2**	Within upper glacial correlative
11	Jbeliat Fm. (Attoh et al., 1997; Clauer and Deynoux, 1987)	632 ± 13	Pre-glacial	608 ± 1.2	Post-glacial
12	Blaubecker Fm. (Grotzinger et al., 1995)			545 ± 1	Post-glacial
13	Rapitan Grp. (Ross and Villeneuve, 1997)	755 ± 18	Pre-glacial		
14	Toby Fm. (Kendall et al., 2004)	762-728	Pre-glacial	607.8 ± 4.7	Post-glacial
15	Mechum River Fm. (Bailey and Peters, 1998)			**702-705**	Within glacial

16	Scout Mtn. Mbr. (Fanning and Link, 2004)	709 ± 5	Immediately pre-glacial	667 ± 5	Post-glacial
17	Edwardsburg Fm. (Lund et al., 2003)			**685 ± 7**	Within glacial
18	Gaskiers Fm. (Bowring et al., 2003)			**580**	Within glacial
19	Squantum Tillite (Thompson and Bowring, 2000; Thompson et al., 2000)	587 ± 2	Pre-glacial	570	Post-glacial
20	Upper Mount Harper Group (Macdonald et al., 2010)			**716.47 ± .24**	Within glacial
21	Jequitai Fm.(Babinski and Kaufman, 2003; Babinski et al., 2007)	900	Pre-glacial	740 ± 22	Within cap carbonate
22	Smalfjord Fm. (Gorokhov et al., 2001)			**630**	Within glacial
23	Port Askaig Fm. (Dempster et al., 2002; Halliday et al., 1989)	601 ± 4	Pre-glacial	594 ± 4	Post-glacial
24	Moelv Tillite			612 ± 18	Post-glacial
25	Dalradian Group (Dempster et al., 2002)			590 ± 2	Post-glacial
26	Mortenses Fm. (Gorokhov et al., 2001)			**560**	Within glacial
27	Gubrah Fm.(Allen, 2007; Bowring, 2007; Brasier et al., 2000)			**713.7 ± 0.5**	Within upper glacial
28	Blaini Fm. (Myrow et al., 2003)			525 ± 8	Post-glacial
29	Nantuo Fm. (Condon et al., 2005; Zhang et al., 2008)	654.5 ± 3.8	Immediately pre-glacial	632.5 ± 0.48	Within cap carbonate
30	KPF (Corsetti and Hagadorn, 2000; Heaman and Grotzinger, 1992)	1,008	Pre-glacial	542	Post-glacial

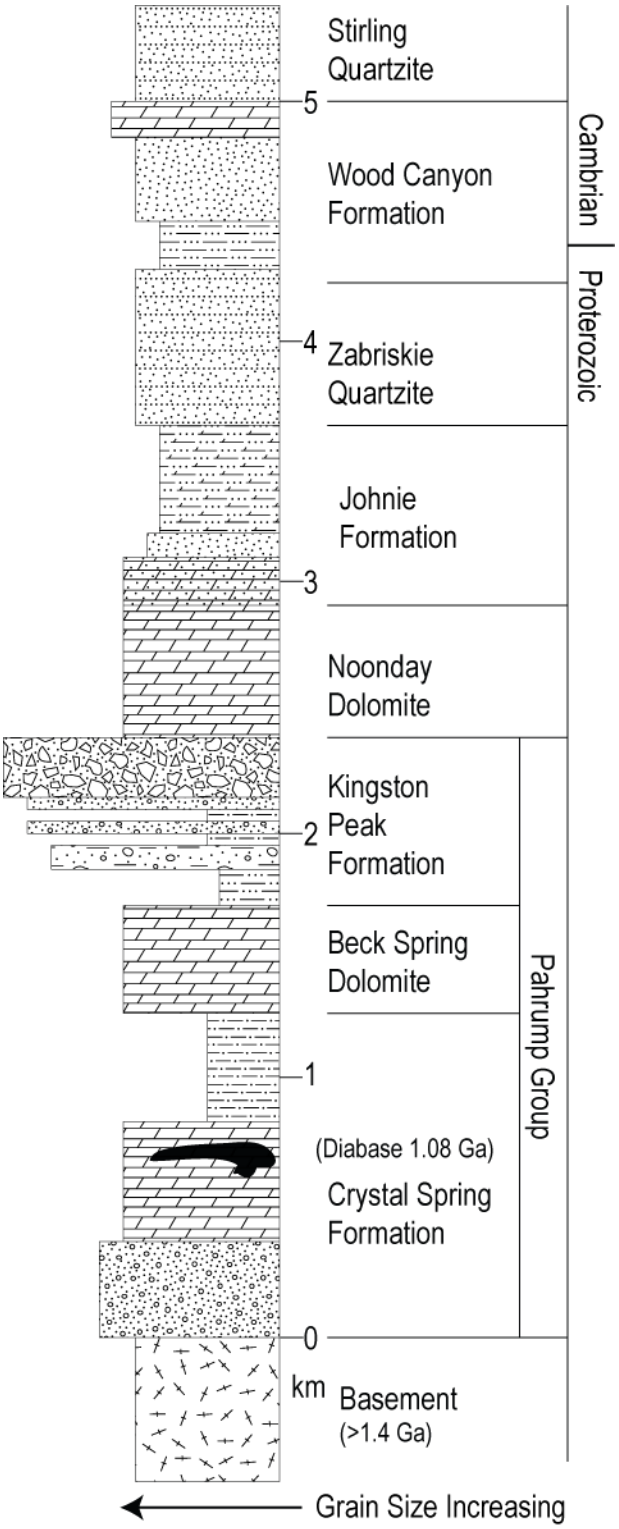

Fig. 1.2. General stratigraphy of the Precambrian strata of the southern Death Valley region (Roberts, 1982). The Kingston Peak Formation, within the Pahrump Group, is bounded by 1.08 Ga diabase in the Crystal Spring Formation (Heaman and Grotzinger, 1992) and by the Cambrian-Precambrian boundary ca. 3 km above (Corsetti and Hagadorn, 2003).

References

Allen, P.A., 2007, The Huqf Supergroup of Oman: Basin development and context for Neoproterozoic glaciation, v. 84, p. 139-185.

Allen, P.A., and Etienne, J.L., 2008, Sedimentary challenge to snowball Earth: Nature Geoscience, v. 1, p. 817-825.

Attoh, K., Dallmeyer, R.D., and Affaton, P., 1997, Chronology of nappe assembly in the Pan-African Dahomeyide Orogen, West Africa; evidence from (super 40) Ar/(super 39) Ar mineral ages: Precambrian Res., v. 82, p. 153–171.

Babinski, M., and Kaufman, A.J., 2003, S. Am. Symp. Isotope Geology 4, Nature Publishing Group, p. 321-323.

Babinski, M., Vieira, L.C., and Trindade, R.I.F., 2007, Direct dating of the Sete Lagoas cap carbonate (Bambui Group, Brazil) and implications for the Neoproterozoic glacial events, v. 19, p. 401-406.

Bailey, C.M., and Peters, S.E., 1998, Glacially influenced sedimentation in the late eoproterozoic MechumRiver Formation, Blue Ridge province, Virginia: Geology, v. 26, p. 623–626.

Beyth, M., Avigad, D., Wetzel, H.-U., Matthews, A., and Berhe, S.M., 2003, Crustal exhumation andindications for Snoball Earth in the East AfricanOrogen: north Ethiopia and east Eritrea: PrecambrianRes., v. 123, p. 187–201.

Bowring, S.A., 2007, Geochronological constraints on the chronostratigraphic framework of the Neoproterozoic Huqf Supergroup, Sultanate of Oman, v. 307, p. 1097-1145.

Bowring, S.A., Myrow, P.M., Landing, E., Ramezani, J., and Grotzinger, J.P., 2003, Geochronological constraints on terminal Neoproterozoic events and the rise of metazoans: Geophysical Research Abstracts, v. 5, p. 13,219.

Brasier, M., McCarron, G., Tucker, R., Leather, J., Allen, P., and Shields, G., 2000, New U-Pb zircon dates for the Neoproterozoic Ghubrah glaciation and for the top of the Huqf Supergroup, Oman: Geology, v. 28, p. 175-178.

Calver, C.R., Black, L.P., Everard, J.L., and Seymour, D.B., 2004, U-Pb zircon age constraints on late Neoproterozoic glaciation in Tasmania: Geology, v. 32, p. 893-896.

Clauer, N., and Deynoux, M., 1987, New information on the probable isotopic age of the late Proterozoic glaciation in West Africa: Precambrian Research, v. 37, p. 89-94.

Coats, R.P., and Preiss, W.V., 1980, Stratigraphic and geochronological reinterpretation of late Proterozoicglaciogenic sequences in the Kimberley region, Western Australia: Precambrian Research, v. 13, p. 181–208.

Condon, D., Zhu, M., Bowring, S., Wang, W., Yang, A., and Jin, Y., 2005, U-Pb Ages from the Neoproterozoic Doushantuo Formation, China: Science, v. 308, p. 95-98.

Cooper, J.A., Jenkins, R.J.F., Compston, W., and Williams, I.S., 1992, Ion-probe zircon dating of a mid-Early Cambrian tuff in South Australia: J. Geol. Soc. London, v. 149, p. 185–192.

Corsetti, F.A., and Hagadorn, J.W., 2000, Precambrian-Cambrian transition: Death Valley, United States: Reply: Geology, v. 28, p. 958-959.

—, 2003, the Precambrian-Cambrian transition in the southern Great Basin, USA: The Sedimentary Record, v. 1.

Corsetti, F.A., and Kaufman, A.J., 2003, Stratigraphic investigations of carbon isotope anomalies and Neoproterozoic ice ages in Death Valley, California: GSA Bulletin, v. 115, p. 916-932.

Crowell, J.C., 1957, Origin of pebbly mudstones: Geological Society of America Bulletin, v. 68, p. 993-1009.

—, 1977, The significance of glaciations in Precambrian correlation, *in* Sidorenko, A.V., ed., Correlation of the Precambrian, Volume 1: Moscow, Izd. Nauka, p. 115-131.

—, 1978, Gondwanan glaciation, cyclothems, continental positioning, and climate change: American Journal of Science, v. 278, p. 1345-1372.

—, 1999, Pre-Mesozoic ice ages; their bearing on understanding the climate system, 106 p.

Dempster, T.J., Rogers, G., Tanner, P.W.G., Bluck, B.J., Muir, R.J., Redwood, S.D., Ireland, T.R., and Paterson, B.A., 2002, Timing of deposition, orogenesis and glaciation within the Dalradian rocks of Scotland: constraints from U–Pb zircon ages: J. Geol. Soc. London, v. 159, p. 83–94.

Dickens, G.R., O'Neil, J.R., Rea, D.K., and Owen, R.M., 1995, Dissociation of oceanic methane hydrate as a cause of the carbon isotope excursion at the end of the Paleocene: Paleoceanography, v. 10, p. 965-971.

Dott, R.H., Jr., 1961, Squantum 'tillite,' Massachusetts; evidence of glaciation or subaqueous mass movements?: Geological Society of America Bulletin, v. 72, p. 1289-1305.

Etienne, J.L., Allen, P.A., Rieu, R., and Le Guerroue, E., 2007, Neoproterozoic glaciated basins; a critical review of the snowball Earth hypothesis by comparison with Phanerozoic glaciations: Special Publication of the International Association of Sedimentologists, v. 39, p. 343-399.

Evans, D.A., 2000, Stratigraphic, geochronological, and paleomagnetic constraints upon the Neoproterozoic climatic paradox: American Journal of Science, v. 300, p. 347-433.

Evans, D.A.D., 2003, A fundamental Precambrian-Phanerozoic shift in earth's glacial style?: Tectonophysics Orogenic Belts, Regional and Global Tectonics: A Memorial Volume to Chris McAulay Powell, v. 375, p. 353-385.

Eyles, C.H., Eyles, N., and Miall, A.D., 1985, Models of glaciomarine sedimentation and their application to the interpretation of ancient glacial sequences: Palaeogeography, Palaeoclimatology, Palaeoecology, v. 51, p. 15-84.

Eyles, N., and Januszczak, N., 2004, 'Zipper-rift': a tectonic model for Neoproterozoic glaciations during the breakup of Rodinia after 750 Ma: Earth-Science Reviews, v. 65, p. 1-73.

Fairchild, I.J., 1993, Balmy shores and icy wastes; the paradox of carbonates associated with glacial deposits in Neoproterozoic times: Sedimentology Review, v. 1, p. 1-16.

Fairchild, I.J., and Kennedy, M.J., 2007, Neoproterozoic glaciation in the Earth system: Journal of the Geological Society of London, v. 164, p. 895-921.

Fanning, C.M., and Link, P.K., 2004, U-Pb SHRIMP ages of Neoproterozoic (Sturtian) glaciogenic Pocatello Formation, southeastern Idaho, v. 32, p. 881-884.

Frimmel, H.E., Foelling, P.G., and Eriksson, P.G., 2002, Neoproterozoic tectonic and climatic evolution recorded in the Gariep Belt, Namibia and South Africa, v. 14, p. 55-67.

Frimmel, H.E., Kloetzli, U.S., and Siegfried, P.R., 1996, New Pb-Pb single zircon age constraints on the timing of Neoproterozoic glaciation and continental break-up in Namibia: Journal of Geology, v. 104, p. 459-469.

Frimmel, H.E., Zartman, R.E., and Spath, A., 2001, Dating Neoproterozoic continental break-up in the Richtersveld Igneous complex, South Africa, v. 109, p. 493-508.

Gorokhov, I.M., Siedlecka, A., Roberts, D., Melnikov, N.N., and Turchenko, T.L., 2001, Rb-Sr dating of diagenetic illite in Neoproterozoic shales, Varanger Peninsula, Northern Norway: Geological Magazine, v. 138, p. 541-562.

Grotzinger, J.P., Bowring, S.A., Saylor, B.Z., and Kaufman, A.J., 1995, Biostratigraphic and geochronologic constraints on early animal evolution: Science, v. 270, p. 598–604.

Halliday, A.N., Graham, C.M., Aftalion, M., and Dymoke, P., 1989, The depositional age of the Dalradian Supergroup: U-Pb and Sm-Nd isotopic studies of the Tayvallich Volcanics, Scotland: J. Geol. Soc. London, v. 146, p. 3–6.

Halverson, G.P., Hoffman, P.F., Schrag, D.P., Maloof, A.C., and Rice, A.H.N., 2005, Toward a Neoproterozoic composite carbon-isotope record: Geological Society of America Bulletin, v. 117, p. 1181-1207.

Harland, B., 1964, Critical evidence for a great infra-Cambrian glaciation: Geologische Rundschau, v. 54, p. 45-61.

Heaman, L.M., and Grotzinger, J.P., 1992, 1.08 Ga diabase sills in the Pahrump Group, California; implications for development of the Cordilleran Miogeocline: Geology (Boulder), v. 20, p. 637-640.

Higgins, J.A., and Schrag, D.P., 2003, Aftermath of a snowball Earth: Geochemistry Geophysics Geosystems, v. 4, p. 431.

Hoffman, P.F., Kaufman, A.J., and Halverson, G.P., 1998a, Comings and goings of global glaciations on a Neoproterozoic tropical platform in Namibia: GSA Today, v. 8, p. 1-9.

Hoffman, P.F., Kaufman, A.J., Halverson, G.P., and Schrag, D.P., 1998b, A Neoproterozoic snowball earth: Science, v. 281, p. 1342-1346.

Hoffman, P.F., and Schrag, D.P., 2002, The snowball earth hypothesis: testing the limits of global change: Terr Nova, v. 14, p. 129-155.

Hoffmann, K.H., Condon, D.J., Bowring, S.A., and Crowley, J.L., 2004a, U-Pb zircon date from the Neoproterozoic Ghaub Formation, Namibia; constraints on Marinoan glaciation: Geology, v. 32, p. 817-820.

Hoffmann, K.-H., Condon, D.J., Bowring, S.A., and Crowley, J.L., 2004b, U-Pb zircon date from the Neoproterozoic Ghaub Formation, Namibia: Constraints on Marinoan glaciation, v. 32, p. 817-820.

Hoffmann, K.H., and Prave, A.R., 1996, A preliminary note on a revised subdivision and regional coorelation of the Otavi Group based on glaciogenic diamictites and associated cap dolostones: Communications of the Geological Survey of Namibia, v. 11, p. 81-86.

Jiang, G., Kennedy, M.J., and Christie-Blick, N., 2003, Stable isotopic evidence for methane seeps in Neoproterozoic postglacial cap carbonates: Nature, v. 426, p. 822-826.

Kaufman, A.J., and Knoll, A.H., 1995, Neoproterozoic Variations in the C-Isotopic Composition of Seawater - Stratigraphic and Biogeochemical Implications: Precambrian Research, v. 73, p. 27-49.

Kaufman, A.J., Knoll, A.H., and Awramik, S.M., 1992, Biostratigraphic and chemostratigraphic correlation of Neoproterozoic sedimentary successions; upper Tindir Group, northwestern Canada, as a test case: Geology, v. 20, p. 181-185.

Kaufman, A.J., Knoll, A.H., and Narbonne, G.M., 1997, Isotopes, ice ages, and terminal Proterozoic earth history: Proceedings of the National Academy of Sciences of the United States of America, v. 94, p. 6600-6605.

Kendall, B., Creaser, R.A., and Selby, D., 2006, Re-Os geochronology of postglacial black shales in Australia: Constraints on the timing of Sturtian glaciation: Geology, v. 34, p. 729-732.

Kendall, B.S., Creaser, R.A., Ross, G.M., and Selby, D., 2004, Constraints on the timing of Marinoan "Snowball Earth" glaciation by 187Re-187Os dating of a Neoproterozoic, post-glacial black shale in Western Canada: Earth and Planetary Science Letters, v. 222, p. 729-740.

Kennedy, M., Mrofka, D., and von der Borch, C., 2008, Snowball Earth termination by destabilization of equatorial permafrost methane clathrate, Nature v. 453, p. 642-645.

Kennedy, M.J., 1996, Stratigraphy, sedimentology, and isotopic geochemistry of Australian Neoproterozoic postglacial cap dolostones; deglaciation, delta (sub 13) C excursions, and carbonate precipitation: Journal of Sedimentary Research, v. 66, p. 1050-1064.

Kennedy, M.J., Christie-Blick, N., and Sohl, L.E., 2001, Are Proterozoic cap carbonates and isotopic excursions a record of gas hydrate destabilization following Earth's coldest intervals?: Geology, v. 29, p. 443-446.

Kennedy, M.J., Runnegar, B., Prave, A.R., Hoffmann, K.H., and Arthur, M.A., 1998, Two or four Neoproterozoic glaciations?: Geology, v. 26, p. 1059-1063.

Key, R.M., Liyungu, A.K., Njamu, F.M., Somwe, V., Banda, J., Mosley, P.N., and Armstrong, R.A., 2001, The western arm of the Lufilian Arc in NW Zambia and its potential for copper mineralization: Journal of African Earth Sciences, v. 33, p. 503-528.

Knoll, A.H., Hayes, J.M., Kaufman, A.J., Swett, K., and Lambert, I.B., 1986, Secular variation in carbon isotope ratios from upper Proterozoic successions of Svalbard and East Greenland: Nature (London), v. 321, p. 832-838.

Knoll, A.H., Walter, M.R., Narbonne, G.M., and Christie-Blick, N., 2006, The Ediacaran Period: a new addition to the geologic time scale: Lethaia, v. 39, p. 13-30.

Lund, K., Aleinikoff, J.N., Evans, K.V., and Fanning, C.M., 2003, SHRIMP U-Pb geochronology of Neoproterozoic Windermere Supergroup, central Idaho: Implications for rifting of western Laurentia and synchroneity of Sturtian glacial deposits: Geological Society of America Bulletin, v. 115, p. 349-372.

Macdonald, F.A., Schmitz, M.D., Crowley, J.L., Roots, C.F., Jones, D.S., Maloof, A.C., Strauss, J.V., Cohen, P.A., Johnston, D.T., and Schrag, D.P., 2010, Calibrating the Cryogenian: Science, v. 327, p. 1241-1243.

Miller, J.M.G., 1985, Glacial and syntectonic sedimentation; the upper Proterozoic Kingston Peak Formation, southern Panamint Range, eastern California: Geological Society of America Bulletin, v. 96, p. 1537-1553.

Myrow, P.M., Hughes, N.C., Paulsen, T.S., Williams, I.S., Parcha, S.K., Thompson, K.R., Bowring, S.A., Peng, S.-C., and Ahluwalia, A.D., 2003, Integrated tectonostratigraphic analysis of the Himalaya and implications for its tectonic reconstruction: Earth Planet. Sci. Lett., v. 212, p. 433–441.

Nisbet, E.G., 1990, The end of the ice age: Canadian Journal of Earth Sciences = Journal Canadien des Sciences de la Terre, v. 27, p. 148-157.

Prave, A.R., 1999, Two diamictites, two cap carbonates, two delta (super 13) C excursions, two rifts; the Neoproterozoic Kingston Peak Formation, Death Valley, California: Geology (Boulder), v. 27, p. 339-342.

Preiss, W.V., 1987, The Adelaide Geosyncline, late Proterozoic stratigraphy, sedimentation, palaeontology, and tectonics: Bulletin - Geological Survey of South Australia, v. 53, p. 438.

Ridgwell, A.J., Kennedy, M.J., and Caldeira, K., 2003, Ocean Science: Carbonate Deposition, Climate Stability, and Neoproterozoic Ice Ages.

Roberts, J.D., 1976, Late Precambrian dolomites, Vendian glaciation, and synchroneity of Vendian glaciations: Journal of Geology, v. 84, p. 47-63.

Roberts, M.T., 1982, Depositional environments and tectonic setting of the Crystal Spring Formation, Death Valley region, California, *in* Cooper, J.D., Troxel, B.W., and Wright, L.A., eds., Geology of selected areas in the San Bernardino Mountains, western Mojave Desert, and southern Great Basin, California: Shohone, CA, United States (USA), Death Valley Publ. Co., p. 143-154.

Ross, G.M., and Villeneuve, M.E., 1997, U–Pb geochronology of stranger stones in eoproterozoic diamictites, Canadian Cordillera: implications forprovenance and ages of deposition, Radiogenic Age andIsotopic Studies, Geol. Surv. Can. Curr. Res., p. 141–155.

Schermerhorn, L.J.G., 1974, Late Precambrian mixtites: Glacial and/or nonglacial?, v. 274, p. 673-24.

—, 1975, Tectonic framework of late Precambrian supposed glacials: Geological Journal, Special Issue, p. 241-274.

Schmidt, P.W., Williams, G.E., and McWilliams, M.O., 2009, Palaeomagnetism and magnetic anisotropy of late Neoproterozoic strata, South Australia: Implications for the palaeolatitude of late Cryogenian glaciation, cap carbonate and the Ediacaran System: Precambrian Research, v. 174, p. 35-52.

Sohl, L.E., Christie-Blick, N., and Kent, D.V., 1999, Paleomagnetic polarity reversals in Marinoan (ca. 600 Ma) glacial deposits of Australia; implications for the duration of low-latitude glaciation in Neoproterozoic time: Geological Society of America Bulletin, v. 111, p. 1120-1139.

Thompson, M.D., and Bowring, S.A., 2000, Age of the Squantum "tillite," Boston Basin, Massachusetts; U-Pb zircon constraints on terminal Neoproterozoic glaciation: American Journal of Science, v. 300, p. 630-655.

Thompson, M.D., Keefe, K.L.D., Martin, M.W., and Bowring, S.A., 2000, Maximum depositional age of the Neoproterozoic Squantum 'Tillite', Boston Basin, Massachusetts; new U-Pb zircon age constraint on Varanger glaciation: Geol. Soc. Am. Abstr. Prog., v. 32, p. 78.

Walter, M.R., Veevers, J.J., Calver, C.R., Gorjan, P., and Hill, A.C., 2000, Dating the 840-544 Ma Neoproterozoic interval by isotopes of strontium, carbon, sulfur in seawater, and some interpretative models: Precambrian Research, v. 100, p. 371-433.

Williams, G.E., 1996, Soft-sediment deformation structures from the Marinoan glacial succession, Adelaide foldbelt; implications for the palaeolatitude of late Neoproterozoic glaciation: Sedimentary Geology, v. 106, p. 165-175.

Zhang, S., Jiang, G., and Han, Y., 2008, The age of the Nantuo Formation and Nantuo glaciation in South China, p. 1-6.

Zhang, S., Jiang, G., Zhang, J., Song, B., Kennedy, M.J., and Christie-Blick, N., 2005, U-Pb sensitive high-resolution ion microprobe ages from the Doushantuo Formation in south China: Constraints on late Neoproterozoic glaciations: Geology, v. 33, p. 473-476.

CHAPTER TWO:

THE KINGSTON PEAK FORMATION OF SOUTHEASTERN CALIFORNIA:

SEDIMENTOLOGY & STRATIGRAPHY FROM ITS TYPE AREA

Chapter Summary

This chapter provides a summary of geologic research for the Kingston Peak Formation (KPF), and places the formation into a context of Neoproterozoic climate and tectonic events. It lays out the rationale for formally naming each of the members of the formation in its type area, describes in detail for the first time the sedimentology and stratigraphic relationships between members and overlying and underlying formations, and discusses the stratigraphic evolution of the KPF deposited in extensional basins. Finally, this chapter discusses the importance of the regional unconformity within the lower KPF and the conformable contact with the overlying Noonday Dolomite. Documenting this conformity resolves the problematic nature of the contact which has been described as "variably conformable and unconformable" and sets the stage for the following chapters, which discuss the value of distinctive carbonate horizons as timelines and the association between local tectonism and the preservation of a climate record.

1. Introduction

The lowermost late Neoproterozoic sedimentary succession in Death Valley is assigned to the Pahrump Group (Fig. 1.2) and is comprised of the mixed siliciclastic-platformal and platformal

successions of the Crystal Spring Formation and the overlying Beck Spring Dolomite, respectively (Hewett, 1940). The Beck Spring Dolomite is overlain by, and locally interbedded with, diamictite, conglomerate and fanglomerate facies of the siliciclastic Kingston Peak Formation (Christie-Blick and Levy, 1989; Miller, 1983) (Fig. 1.2). This interval of coarse-grained deposits is sandwiched in between platform facies of the underlying Beck Spring Dolomite and overlying Noonday Dolomite and was broadly interpreted by Stewart (1972) and Wright *et al.* (1974) to represent the southern Cordilleran transition from Beltian-equivalent deposition to Windermere-age rifting and subsequent passive margin initiation.

Burchfiel (1992) recognized this succession in the Death Valley area as unique because it is one of the few Neoproterozoic successions where the association between rifting and coarse-grained sediments is made clear by the presence of syndepositional normal faults. All three formations are present throughout the Death Valley region. The Beck Spring Dolomite shows a systematic facies change from platformal carbonate in the north to mixed carbonate and siliciclastics in the south; this transition occurs in the Saddle Peak Hills (Fig. 2.1). The Kingston Peak Formation shows much more rapid and locally variable lateral changes in both facies and thickness, from 10 to 3500 meters over distances as short as 8 km. Deposition controlled by tectonism (Miller, 1982) has resulted in these rapid lateral facies changes making lithological correlation of units within the Kingston Peak Formation (Fig. 2.2) problematic and correlation between similar lithologies equivocal. The Kingston Peak Formation is sharply overlain by the Noonday Dolomite (Fig. 1.2) which is a regionally traceable interval, like the Crystal Spring Formation and the Beck Spring Dolomite. Its distinctive carbonate lithology is easily correlated

over its entire outcrop extent (Cloud et al., 1974; Noble, 1934; Williams et al., 1974) and provides a clear correlation that is likely time-significant based on the abrupt change to carbonate lithology and the subsequent difference in the overlying succession to the Kingston Peak Formation (Fig. 2.2a & b).

Much of the interval of coarse-grained sediments comprising the Kingston Peak Formation were first detailed in descriptions of the Panamint Range; Murphy informally named and placed them within the Telescope group (1930; Murphy, 1932) as the Surprise Formation, Sourdough Limestone, Middle Park Formation and Wildrose Formation, from bottom to top respectively. These names have been retained but subsequently assigned to formal member status (Carlisle et al., 1980; Johnson, 1957; Labotka et al., 1980) within Hewett's (1940) Kingston Peak Formation (Fig. 2.2). Noble (1934; Noble, 1941) described the eastern Kingston Peak Formation (Fig. 2.1) and likened it to the "Algonquian" series in the Grand Canyon, suggesting a correlation to Murphy's (1932) Telescope group (later the KPF) in the Panamint Range. Hazzard (1939) interpreted the Kingston Peak Formation to be glacigenic based on the presence of striated clasts in the uppermost Kingston Peak Formation at the Gunsight Mine (Fig. 2.1 #2).

From 1950 to the mid-1980's, relevant research focused on the stratigraphy, sedimentology, paleogeography, and source regions for the different facies of the Kingston Peak Formation (Troxel, 1967, 1982b; Wright, 1952; Wright, 1954; Wright and Troxel, 1966; Wright et al., 1974; Wright et al., 1978; Wright et al., 1984). From the early 1980's onwards, publications primarily addressed the glacial and rift-related features in the eastern and western facies assemblages

Fig. 2.1. The different areas where the Kingston Peak Formation crops out. Western KPF (white), Eastern KPF (light shaded) and Eastern KPF Silurian Hills (formerly "southern facies" of Troxel (1967) (dark shaded). Bold numbers represent measured sections used for this study, whose names and GPS locations are given below:

1=Alexander Hills (35°45'50.02"N, 116° 7'17.58"W), 2=Gunsight Mine (35°50'43.34"N, 116° 7'22.82"W), 3=War Eagle Mine (35°49'10.40"N, 116° 5'25.22"W), 4=Beck Canyon West (35°48'30.65"N, 115°58'26.31"W), 5=Crystal Spring (35°47'53.21"N, 115°57'44.17"W), 6=Silver Rule Mine (35°48'32.94"N, 115°57'23.04"W), 7=Beck Canyon Divide (35°47'48.33"N, 115°55'37.90"W), 8=Horsethief Spring (35°46'28.13"N, 115°53'8.26"W), 9=Kingston North (35°50'16.55"N, 115°51'16.13"W), 10=Jupiter Mine (35°47'17.25"N, 115°50'7.40"W), 11=Snow White Mine (35°46'20.66"N, 115°49'42.85"W), 12=Horsethief Mine (35°41'45.95"N, 115°52'31.30"W), 13=Mesquite North (35°46'2.89"N, 115°45'10.04"W), 14=Mesquite South (35°45'28.93"N, 115°44'42.09"W), 15=Mesquite Small Block (35°44'48.19"N, 115°44'23.71"W), 16=Winters Pass (35°42'29.38"N, 115°41'56.18"W), 17=Southern Valjean Hills (35°40'3.42"N, 116° 7'22.72"W), 18=Sperry Hills (35°42'13.68"N, 116°14'34.72"W), 19=Saddle Peak Hills (35°43'34.55"N, 116°21'44.79"W), 20=Saratoga Hills (35°41'10.90"N, 116°24'43.73"W), 21=Ibex Hills (35°45'32.85"N, 116°26'18.17"W), 22=Eclipse Mine (35°51'57.45"N, 116°21'36.14"W), 23=Virgin Spring Wash south 35°54'51.53"N, 116°38'47.93"W), 24=Virgin Spring Wash north (35°55'2.16"N, 116°38'58.74"W), 25=Silurian Hills, 26=southern Saddle Peak Hills (35°41'43.75"N, 116°20'55.08"W) 35°31'47.42"N, 116° 6'12.55"W), 27=Galena Canyon (36°1'12.06"N, 116°55'30.76"W), 28=Goler Wash (35°51'41.87"N, 117° 8'11.41"W), 29=Wood Canyon (35°56'15.27"N, 117° 7'36.18"W), 30=Sourdough Canyon (36° 8'6.34"N, 117° 5'55.31"W).

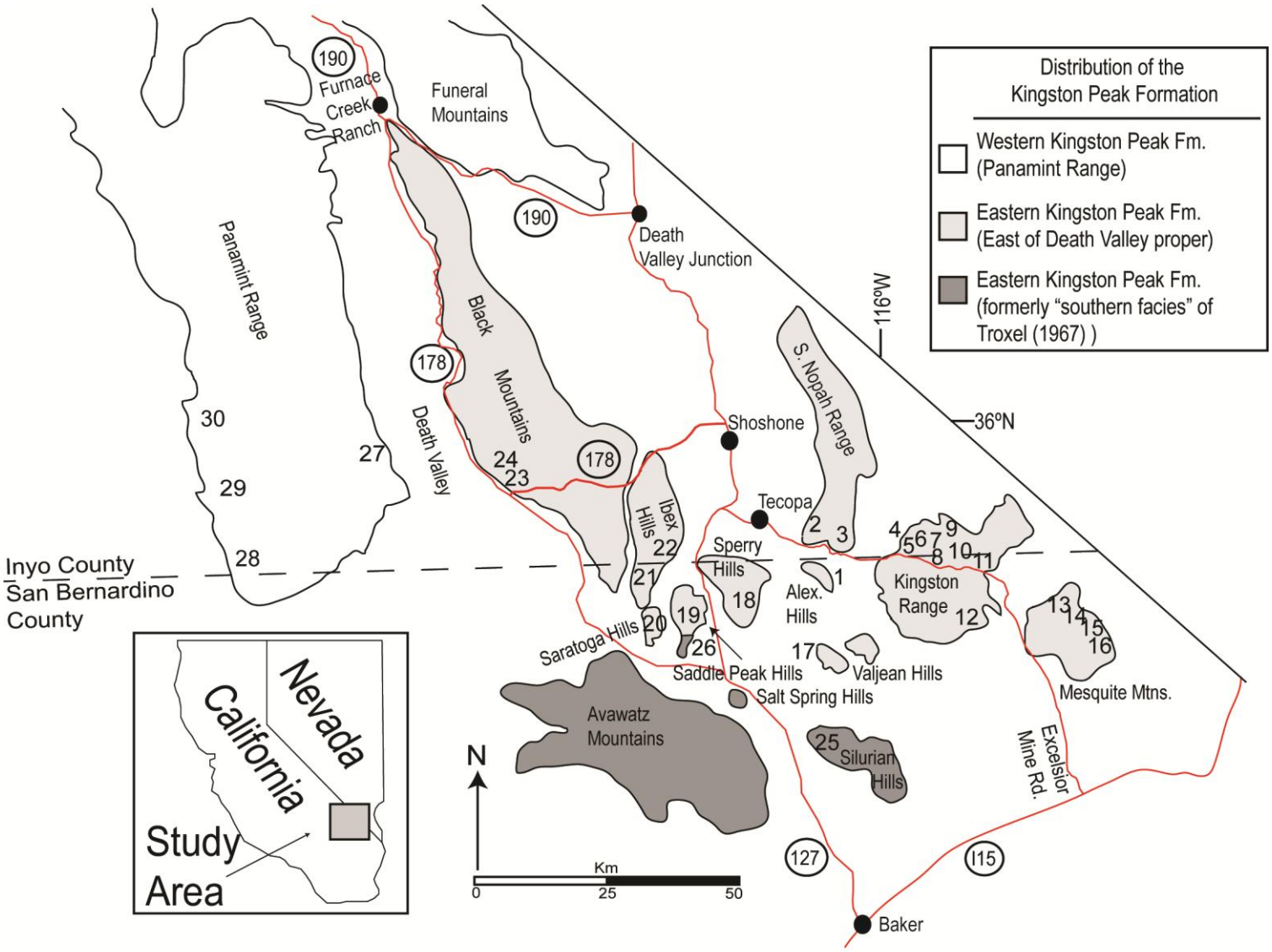
Distribution of the
Kingston Peak Formation
Western Kingston Peak Fm.
(Panamint Range)
Eastern Kingston Peak Fm.
(East of Death Valley proper)
Eastern Kingston Peak Fm.
(formerly "southern facies" of
Troxel (1967))
Furnace
Creek
Ranch
Funeral
Mountains
190
Death
Valley Junction
116°W
36°N
Panamint Range
Black
Mountains
178
Death Valley
S. Nopah Range
Shoshone
Tecopa
Ibex
Hills
Sperry
Hills
Alex.
Hills
Kingston
Range
Saratoga Hills
Saddle Peak Hills
Salt Spring Hills
Valjean Hills
Mesquite Mtns.
Avawatz
Mountains
Silurian
Hills
Excelsior
Mine Rd.
Inyo County
San Bernardino
County
Nevada
California
Study
Area
N
Km
0
25
50
127
I15
Baker

Fig. 2.2. Member division for eastern and western KPF. a) conventional formal names for the western KPF members in the Panamint Range and the informal names given to the different facies in the eastern KPF. Colors indicate correlation of regions based on Prave (1999). b) naming convention used in this work for the eastern KPF. Colors show the correlation suggested in this chapter between different regions.

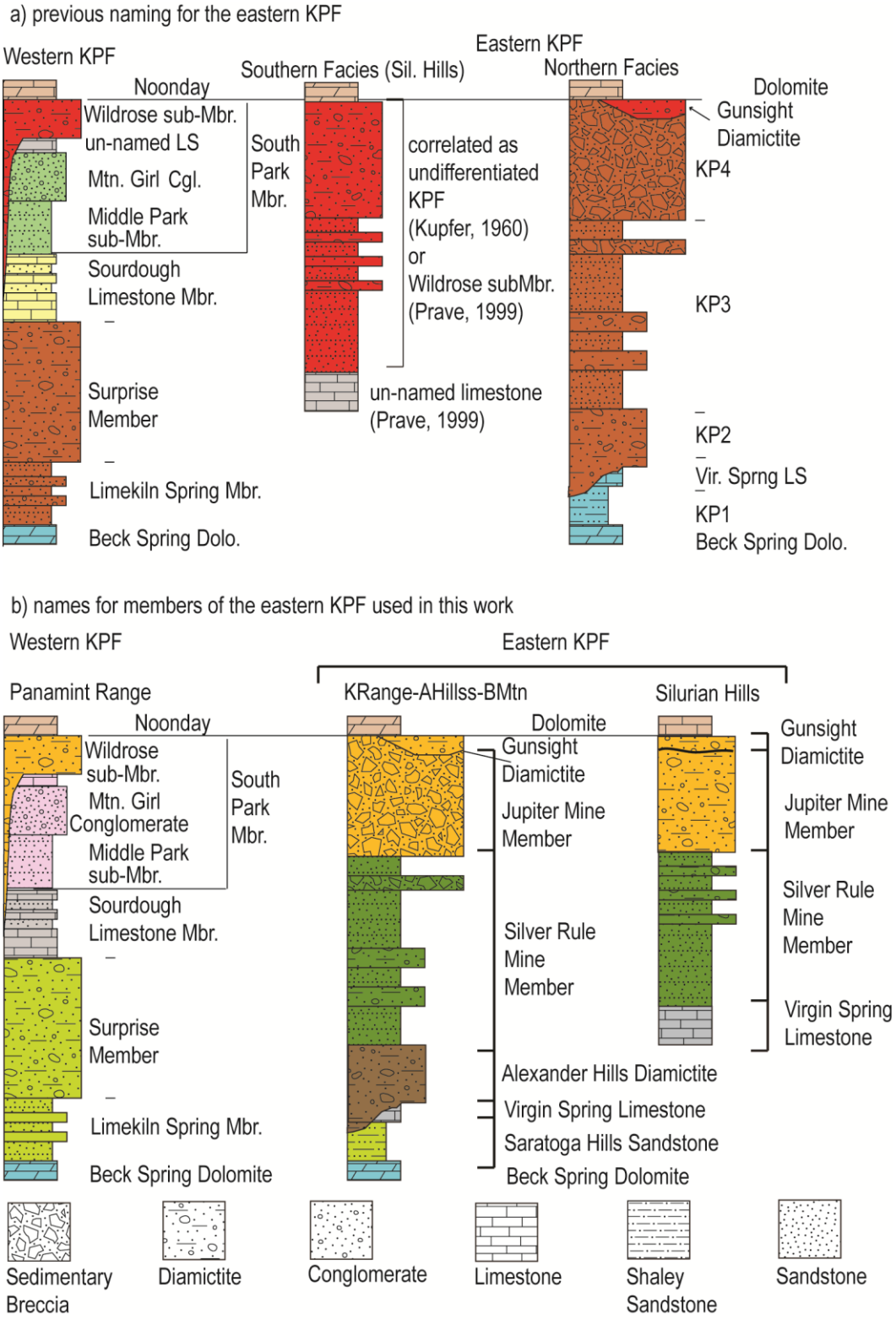
a) previous naming for the eastern KPF
Western KPF
Noonday
Wildrose sub-Mbr.
un-named LS
Mtn. Girl Cgl.
Middle Park sub-Mbr.
Sourdough Limestone Mbr.
Surprise Member
Limekiln Spring Mbr.
Beck Spring Dolo.
South Park Mbr.
Southern Facies (Sil. Hills)
correlated as undifferentiated KPF (Kupfer, 1960) or Wildrose subMbr. (Prave, 1999)
un-named limestone (Prave, 1999)
Eastern KPF
Northern Facies
Dolomite
Gunsight Diamictite
KP4
KP3
KP2
Vir. Sprng LS
KP1
Beck Spring Dolo.
b) names for members of the eastern KPF used in this work
Western KPF
Panamint Range
Noonday
Wildrose sub-Mbr.
Mtn. Girl Conglomerate
Middle Park sub-Mbr.
Sourdough Limestone Mbr.
Surprise Member
Limekiln Spring Mbr.
Beck Spring Dolomite
South Park Mbr.
Eastern KPF
KRange-AHillss-BMtn
Dolomite
Gunsight Diamictite
Jupiter Mine Member
Silver Rule Mine Member
Alexander Hills Diamictite
Virgin Spring Limestone
Saratoga Hills Sandstone
Beck Spring Dolomite
Silurian Hills
Gunsight Diamictite
Jupiter Mine Member
Silver Rule Mine Member
Virgin Spring Limestone
Sedimentary Breccia
Diamictite
Conglomerate
Limestone
Shaley Sandstone
Sandstone

(Christie-Blick and Levy, 1989; Link et al., 1993; Miller, 1982; Miller, 1983; Miller, 1985a; Miller, 1985b, 1987; Miller et al., 1981), providing interpretations for the role of glaciation and rifting in the deposition of the Kingston Peak Formation as well as using the succession to interpret the evolution of the developing passive margin of the western Cordillera (Fedo and Cooper, 2001; Levy and Christie-Blick, 1989, 1991). Most recently, Prave (1999) proposed a chemo- and tectono-stratigraphic correlation for the eastern and western Kingston Peak Formation, suggesting the entire formation fit into a "Snowball Earth" stratigraphic model (Hoffman *et al.* 1998) with a record of two discrete ice ages.

2. Geologic Setting of the Kingston Peak Formation (KPF)

The Kingston Peak Formation (KPF) outcrops in two broad regions: 1) in a number of the ranges east and southeast of Death Valley (eastern KPF of Fig. 2.1) throughout the Panamint Range which borders Death Valley on the west (western KPF of Fig. 2.1) (Miller, 1985b). The eastern KPF, the subject of this study, outcrops throughout a 70x35 km area within a number of ranges of mountains and hills in very well exposed and unmetamorphosed panels displaying the full range of lateral facies and thickness variations and basin-margin relationships. The KPF in this region has been described as having a "northern" and "southern" (dark shaded regions in Fig. 2.1) facies (Troxel, 1967). However, in this work, these facies are correlated with one another and described together as the eastern KPF (Fig. 2.1 & 2.2). Elements of this correlation are discussed throughout the dissertation.

The KPF in the Panamint Range region outcrops in a number of canyons and ridges in a 120 km north-northwest trending belt, mostly along the western limb of a broad anticline defining the axis of the range. This region of the KPF has been the subject of a dissertation and a number of papers (Labotka and Albee, 1977; Miller, 1983; Miller, 1985b; Miller et al., 1981), and formally divided into four members (Fig. 2.2). Panamint Range outcrops have undergone moderate to significant metamorphism (Labotka et al., 1980) with the most southern outcrops undergoing the least alteration.

The eastern KPF crops out extensively in a readily accessible 30 km long belt along the northern and eastern flanks of the Kingston Range (Hewett 1940) and is superbly exposed in a panel extending from the Silver Rule Mine (35°48'17" N 115°56'39" W, #6 in Fig. 2.1) to Beck Canyon Divide (35°48'19" N 115°55'31 W, #7 in Fig. 2.1). The northern Kingston Range is the location of three published KPF type sections (Hewett, 1956) (sections #7, #8 and 3 km south of #8 in Fig. 2.1) and because of a relative lack of metamorphism, laterally persistent outcrops and visibility of rapid lateral facies changes is the best location to examine the eastern KPF. Eastern and western regions of the KPF are dominated by similar coarse-grained siliciclastic rocks, but lithostratigraphic correlation is complicated by lateral facies changes within each region (Miller, 1983), an overall difference in the appearance of specific facies between both regions, and the presence in each assemblage of distinctive carbonate intervals bonded by dissimilar facies.

The abrupt transition between the KPF and the Noonday Dolomite has been interpreted as an angular unconformity (Christie-Blick and Levy, 1989; Wright et al., 1992; Wright et al., 1974)

and as conformable with the underlying glacigenic facies (Prave, 1999). The implication of a significant time break at this contact and the genetic relationship of carbonate capping the KPF are critical for both the correlation of KPF and placing the Death Valley succession in context with other global successions. An unconformity separating glacial and carbonate sediments would exclude the Noonday Dolomite from being a cap carbonate. This contact has been interpreted as an angular unconformity because the Noonday Dolomite in the Alexander Hills seems to cap a tilted surface. A number of studies have suggested this relationship resulted from successive truncation of older units down to the basement succession (Hazzard, 1939; Hewett, 1940; Noble, 1934; Wright et al., 1974). Wright and Troxel (1966) suggested this unconformity is the principal indicator of change from provenance for the Pahrump Group to the beginning of the Cordilleran miogeosyncline. Alternatively, Noble (1941) considered the Stirling Quartzite, some 1000 m higher in the succession, to represent the transition to the miogeosyncline.

Stewart (1970, 1972) considered the Beck Spring Dolomite contact with the KPF to represent the transition from Belt-Purcell to Windermere equivalent deposition (Stewart, 1972); he interpreted the KPF to represent continental separation and include the initial deposits of the Cordilleran Geosyncline. Stewart (1970) considered the KPF-Noonday Dolomite contact to be mostly unconformable, but difficult or impossible to detect in some areas. He recognized that in its southern outcrop area (eastern KPF of Fig. 2.1), the KPF rests on successively older units of the Pahrump Group and basement rock, apparently indicating a significant unconformity, but was uncertain about its “extent.” Because the unconformity was not consistently detectable in all areas in the eastern region and difficult to detect in the Panamint Range, he suggested that it may “die

out" to the south, where all members of the KPF were fully developed. This vexing problem of a regional unconformity between the KPF and the Noonday Dolomite being undetectable in much of the region is a key point of discussion in this chapter.

Miller (1985) also interpreted the contact as both unconformable and conformable (interbedded) in the Panamint Range. Christie-Blick and Levy (1989) interpreted the contact as unconformable and "well established but locally cryptic" and thought this unconformity recorded a transition from rifting to passive margin development. Using a 750-635 Ma age for the Noonday Dolomite (Kennedy et al., 1998a), the transition here is significant because it would predate rifting predicted by thermal subsidence models, for the base of the Cambrian, by 100-200 Ma (Bond et al., 1985).

The contact between the KPF and the Noonday Dolomite was recently reinterpreted by Prave (1999), who placed an unconformity within the uppermost KPF and suggested that a diamictite interval (Gunsight Diamictite; Fig. 2.2) locally fills channels overlying the unconformity and is conformable with the Noonday Dolomite. Thus, he interpreted the Noonday Dolomite as a cap carbonate related in time and process to the end of KPF glaciation consistent genetic models for other Snowball Earth successions. The maximum age for initiation of rifting is 700-800 Ma based on deposits along the Cordillera interpreted to be equivalent to the KPF (Dalrymple and Narbonne, 1996; Ross, 1991; Young, 1995). It is improbable that rifting extended from this maximum age (700-800 Ma) to 590 Ma, the age suggested by thermal subsidence models for the post-rift transition (Bond et al., 1985; Christie-Blick and Levy, 1989; Fedo and Cooper, 2001).

This problem was addressed by Prave (1999), who suggested the Kingston Peak Formation contained evidence of several distinct rift events timed with a Sturtian (~720 Ma) and Marinoan (~635 Ma) glacial interval. This provided consistency with other global successions typified by two glacial and two cap carbonates. It is problematic for continuous rift facies to extend from ~800 Ma (Stewart, 1976) to around 580 Ma as suggested by thermal subsidence modeling and youngest rift-related deposits (Bond et al., 1985). Prave (1999) addressed this problem by suggesting that rifting was not continuous but occurred in two discrete episodes. Further, he went on to suggest that the KPF succession was similar to the characteristic Neoproterozoic stratigraphic succession globally with two discrete glacial-cap carbonates sequences. The stratigraphic and sedimentary evidence for intra-KPF rifting is explored below.

2.1. Proposed Formalization of member names for the eastern KPF

Description of the eastern KPF has been complicated by the informal and non-descriptive naming (Wright, 1954, 1974) of its various members and lack of association with any characteristic type sections. This has also contributed to the difficulty in understanding how correlations might be drawn between the eastern and western KPF regions. These name changes will be suggested in a future publication, and are summarized below and shown in Fig. 2.2b.

Saratoga Hills Sandstone (formerly kp1): The sandstone interval that comprises the base of the KPF is dramatically different from the coarse-grained lithologies of the remaining KPF. Prave (1999) pointed out that the sandstone would be more appropriately considered part of the underlying Beck Spring Dolomite “depositional cycle” and not associated with KPF deposition.

While finer-grained sandstones appear above the overlying diamictite, they are associated both vertically and laterally with debrites and conglomerates. Most importantly, this sandstone is erosionally truncated by a regionally extensive unconformity of unknown duration.

The southern Saratoga Hills is suggested as the type section (35°41'5.66"N 116°24'46.01"W) for this member because: 1) it is very easy to access by well-maintained gravel roads, 2) the overlying limestone unit is well-preserved, 3) the overlying unconformity can be seen truncating both the sandstone and the overlying limestone, 4) all the various fine-grained facies (siltstone, fine- to medium-grained sandstone and carbonate-rich sandstone) are present, and 5) the contacts between the sandstone and the overlying limestone and underlying Beck Spring Dolomite are sharp and easy to walk out.

Virgin Spring Limestone: I am suggesting that the Virgin Spring Limestone, informally named by Tucker (1986), remain so named. Although the limestone is thickest and best preserved in the Ibex Hills, the section is both difficult to access and has a difficult to locate contact with a m-thick section of the Saratoga Hills Sandstone.

In the Virgin Spring Wash, the limestone (35°54'50.68"N 116°38'51.52"W) is 1) well-preserved in several sections, 2) bounded below by an easily accessible contact with a section of the Saratoga Hills Sandstone over 100 m in thickness, 3) bounded above by a characteristic section of the overlying diamictite, 4) preserves m-scale erosional truncation through the limestone and into the underlying Saratoga Hills Sandstone, and 5) clearly exhibits erosional truncation of the

limestone which can be easily described and walked out. At this erosional contact, m-scale blocks of limestone are broken up in the base of the overlying diamictite.

The Saratoga Hills Sandstone and the Virgin Spring Limestone are separated from the overlying coarse-grained deposits of the KPF by a regional unconformity. The sandstone and limestone intervals also indicate very different depositional environments than the overlying KPF and bear a closer genetic relationship to the underlying Beck Spring Dolomite than to the units above. They both should be raised to formation status and assigned as members of the Beck Spring Dolomite.

Silurian Hills Limestone: A dark gray laminated limestone interval in the Silurian Hills shares a number of critical characteristics with the Virgin Spring Limestone (see Chapter 3) and is re-interpreted herein to be equivalent with the Virgin Spring Limestone (Fig. 2.2). Kupfer (1960) interpreted this limestone to be the southern equivalent of the Beck Spring Dolomite based on its position above (200-300 m) talc facies belonging to the Crystal Spring Formation and below coarse-grained debrites and diamictite of the KPF. Prave (1999) interpreted this limestone to be stratigraphically far above the Beck Spring Dolomite and equivalent to a laterally discontinuous limestone interval between the Mountain Girl Conglomerate submember and the Wildrose Diamictite Member in the Panamint Range. This correlation was based on shared positive $\delta^{13}C$ values from three samples from each interval and similar underlying conglomerate intervals.

I consider this limestone in the Silurian Hills to be equivalent to the Virgin Spring Limestone based on one, the very similar facies succession above the limestone in the Silurian

Hills and above Virgin Spring Limestone and, two, the sequence boundary that truncates it throughout the Kingston Range, Alexander Hills and Black Mountains (Fig. 2.3). In the Silurian Hills, the limestone is overlain by a several thousand meter thick section of turbidites interbedded with debrites and coarsens upwards into diamictite and debrite intervals with dam-scale olistoliths of the Crystal Spring Formation. The turbidite interval is overlain by 400-500 m of diamictite and sedimentary breccia, and is capped by a thin limestone interval equivalent to the Noonday Dolomite. The Johnie Oolite (Summa, 1993) is a regional marker bed in the Johnie Formation (Fig. 1.2) and is located ~50 m above the Noonday Dolomite correlative in the Silurian Hills. This stratigraphic section duplicates the stratigraphic relations seen in the same basinal interval (Horsethief Mine, Fig. 2.1) in the Kingston Range.

Alexander Hills Diamictite (formerly kp2): This diamictite is described in detail below, but is preserved regionally in all hanging wall sections and ubiquitously blankets the underlying unconformity. There are a number of well preserved diamictite intervals throughout the Kingston Range and in the southern Black Mountains. The diamictite in the Alexander Hills (35°45'49.12"N 116° 7'7.29"W) is easily accessible from the Alexander Hills Mine (35°45'46.86"N 116° 6'56.27"W) or the Great Western Talc Mine (35°46'42.08"N 116° 7'29.77"W). It is characteristic of many other sections and 1) is easy to access, 2) is associated with well-studied and well-exposed sections of the underlying Crystal Spring and Beck Spring Dolomite Formations, 3) is comprised of the variety of clasts and diamictite matrices that are found in most intervals, 4) contains both clasts of the Virgin Spring Limestone and black calcitic matrix in basal diamictite beds indicating the Virgin Spring Limestone was an important source of material, 5) records a m-scale finer-grained interval

seen in several other sections, and 6) has well-defined and easy to trace contacts with the Saratoga Hills Sandstone and the overlying member.

Silver Rule Mine Member (formerly kp3): The interval above the Alexander Hills Diamictite is coarse-grained overall, but contains many finer-grained beds (sandstone) in its lower half and represents a clear lithological transition from the underlying diamictite. This member is well-preserved throughout the Kingston Range, but is easiest to access from several locations in Beck Canyon. All of the features characteristic of this member are easily observed and well preserved near the Silver Rule Mine (35°48'29.56"N 115°57'39.87"W). The mine is located in drainage in the Noonday Dolomite just west of a fault next to a fault contact between the dolomite and the Beck Spring Dolomite-KPF interval.

The contact (ca. 35°48'33.99"N 115°57'25.47"W) between the Alexander Hills Diamictite and the Silver Rule Mine Member is located east of this fault, above the drainage. This section is comprised of all the features characteristic of this interval, including 1) numerous types of diagnostic sedimentary structures in sandstone intervals, 2) a well-preserved oncolitic marker bed present in many other sections, 3) mega-clast intervals and monomictic sedimentary breccias composed of Beck Spring Dolomite clasts, and 4) clear contacts between the underlying Alexander Hills Diamictite and the overlying sedimentary breccia interval.

This member may be easily viewed and is also very well-preserved near the Crystal Spring Mine and near an un-named mine (35°48'10.51"N 115°55'7.76"W) at the southern end of Beck

Canyon which may be accessed via Mesquite Valley Road at the northern (35°47'42.61"N 115°58'41.57"W) or southern (35°46'29.18"N 115°53'20.65"W) ends of Beck Canyon.

Jupiter Mine Member (formerly kp4): The uppermost interval of the KPF has a gradational contact with the underlying Silver Rule Mine Member (coarsening upwards) and is interbedded with the overlying Noonday Dolomite (see below) but is distinct from both of these bounding units. It is dominated by channelized sedimentary breccias interpreted to be fanglomerate deposits. These deposits are often monomictic and composed of Beck Spring Dolomite clasts.

These fanglomerate intervals are easily accessed throughout the Kingston Range, but near the Jupiter Mine (35°47'28.51"N 115°50'7.76"W) preserve several distinct geologic relationships important for understanding the importance of tectonism in the deposition of the KPF. This section (35°47'13.98"N 115°50'1.11"W) 1) thickens from meters to hundreds of meters over several kilometers (a distinctive wedge-shaped geometry), 2) is floored by a monomictic sedimentary breccia composed of Beck Spring Dolomite clasts, 3) transitions gradationally to mixed-source breccias and 4) abuts the footwall of a synsedimentary normal fault upon which the entire Beck Spring Dolomite and much of the Crystal Spring Formation has been erosionally truncated during KPF deposition. This thickening relationship can be seen clearly in Figure 2.3, which compares the thickness of the KPF atop a footwall section at the Jupiter Mine to the KPF thickness 1.4 km away in the hanging wall. The same relationship can be seen in Figure 4.11 and in Figure 2.4 by comparing sections 1 (Beck Canyon West; section #4 in Fig. 2.1) and 2 (Crystal Spring Mine; section #5 in Fig. 2.1).

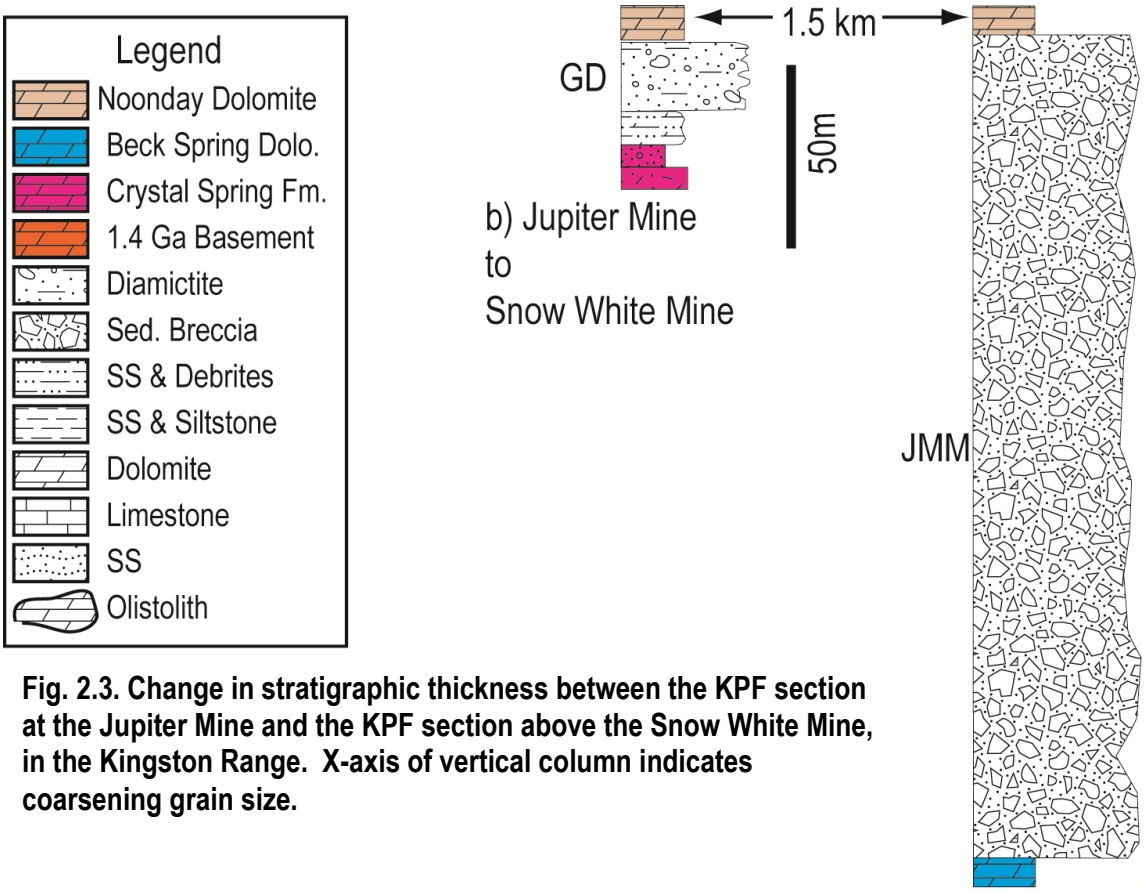

Fig. 2.3. Change in stratigraphic thickness between the KPF section at the Jupiter Mine and the KPF section above the Snow White Mine, in the Kingston Range. X-axis of vertical column indicates coarsening grain size.

Fig. 2.4. Cross-section of Kingston Range sections and the section measured in the Silurian Hills. Inset map shows location of sections. X-axis of measured sections denotes relative changes in grain size. Horizontal scale shown with line between sections 6 & 7.
Section Names (see Fig. 2.1 for location information):
Section 1: Beck Canyon West
Section 2: Crystal Spring
Section 3: Silver Rule Mine
Section 4: Beck Canyon Divide
Section 5: Horsethief Springs
Section 6: Horsethief Mine
Section 7: Silurian Hills

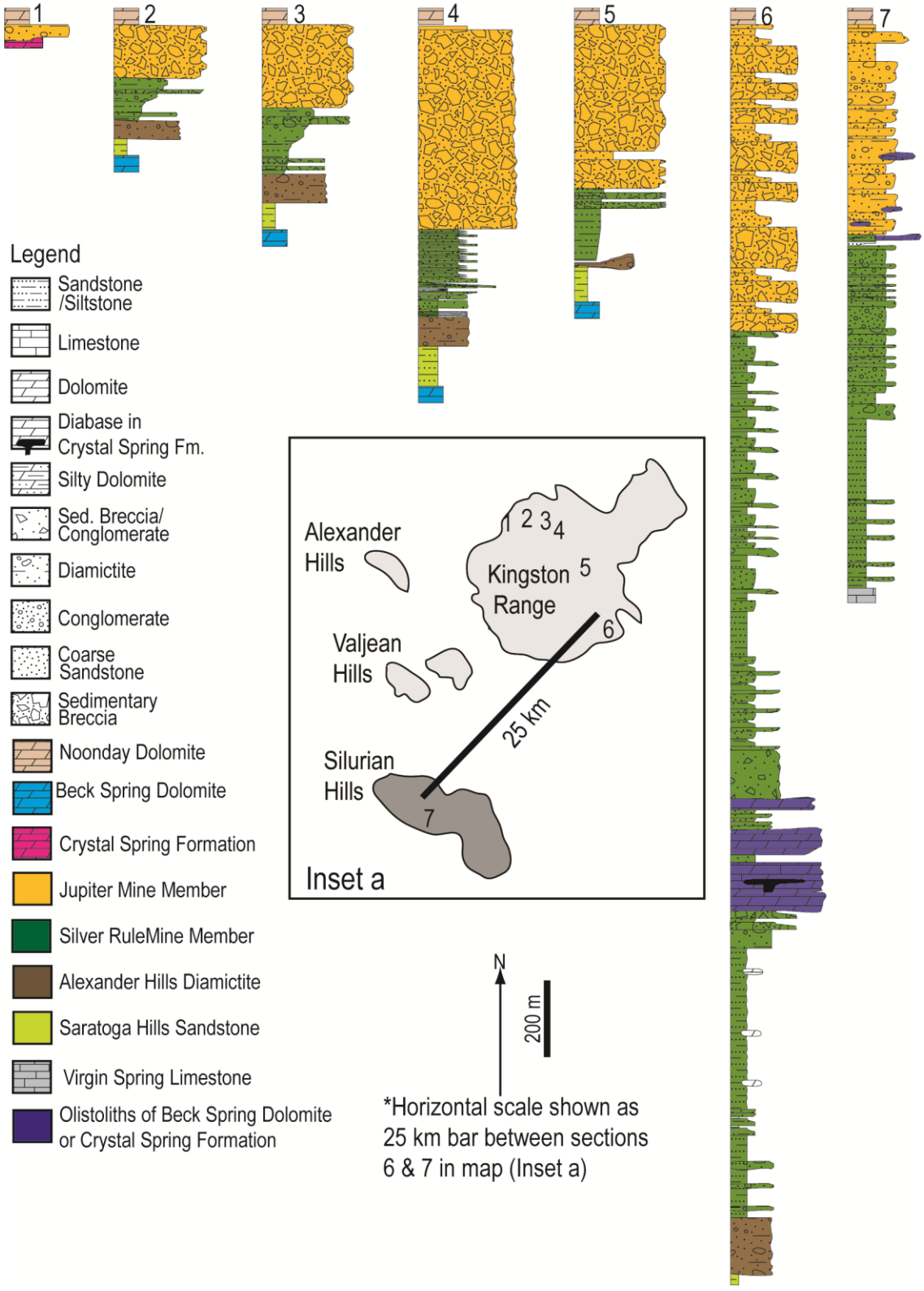
1
2
3
4
5
6
7
Legend
Sandstone /Siltstone
Limestone
Dolomite
Diabase in Crystal Spring Fm.
Silty Dolomite
Sed. Breccia/ Conglomerate
Diamictite
Conglomerate
Coarse Sandstone
Sedimentary Breccia
Noonday Dolomite
Beck Spring Dolomite
Crystal Spring Formation
Jupiter Mine Member
Silver RuleMine Member
Alexander Hills Diamictite
Saratoga Hills Sandstone
Virgin Spring Limestone
Olistoliths of Beck Spring Dolomite or Crystal Spring Formation
Alexander Hills
Kingston Range
Valjean Hills
Silurian Hills
25 km
Inset a
N
200 m
*Horizontal scale shown as 25 km bar between sections 6 & 7 in map (Inset a)

Gunsight Diamictite: The diamictite interval below the Noonday Dolomite at the Gunsight Mine (35°50'35.45"N 116° 7'22.15"W) in the southern Nopah Mountains was informally named the Gunsight member by Troxel (per. comm.. 2002). I am suggesting this interval be referred to as the Gunsight Diamictite. This distinctive interval at the Gunsight Mine 1) contains abundant basement clasts, 2) contains glacially striated and faceted clasts, and 3) overlies the Crystal Spring Formation. In most cases it is preserved in channels atop truncated Pahrump Group rocks but is interbedded with the Jupiter Mine Member.

This diamictite interval is present in all sections between the southeastern Panamint Range and the Kingston Range where the Noonday Dolomite overlies erosionally truncated Pahrump Group lithologies. The diamictite is also present at the Jupiter Mine but contains some lithologies and sedimentary features unique to that section. The interval is present in full sections of the KPF as well (where the Saratoga Hills Sandstone overlies untruncated Beck Spring Dolomite) but does not contain striated clasts and has different clast compositions.

2.2. Structural Framework

The KPF is concentrated in syndepositional extensional basins with accommodation space attributed to rifting along the western margin of North America between 850–600 Ma (Christie-Blick and Levy, 1989; Stewart, 1972). Extension and uplift along normal faults resulted in basins that were filled with sediments derived from successively older stratigraphic levels of the underlying Pahrump Group (Wright *et al.* 1976; Burchfiel *et al.* 1992; Wright *et al*.1992). This process resulted in distinctive patterns of lateral thickness changes associated with synsedimentary normal faulting

(Fig. 2.4); this will be discussed below and in Chapter 3. Evidence for extension includes a preponderance of coarse-grained sediments including km-scale olistoliths (Miller 1985), syndepositional normal faults in the Kingston Range (mapped by the author), the southern Nopah Range (Wright *et al.* 1976, 1978) and the Panamint Range (Prave 1999) and thoeleitic (Hammond, 1983) pillow lavas in the Panamint Range (Miller 1985). Vertical offsets on the faults are > 400 m in the Kingston Range at Jupiter Mine (Fig. 2.1) as demonstrated by removal of the Beck Spring Dolomite on the footwall side of faults ~500 m from extant Beck Spring Dolomite in the hanging wall (Fig. 2.3). Possibly as much as 3 km of uplift may have occurred on these faults (Burchfiel *et al.* 1992).

Sedimentation in the Death Valley region was relatively continuous throughout the Paleozoic (Abolins et al., 2000) but underwent compressional shortening in the Permian (Snow, 1992) and again in the Mesozoic (Levy and Christie-Blick, 1989). Compressional shortening and associated plutonic intrusion was accompanied by metamorphism to the KPF in the Panamint Range (western KPF) that increases south-to-north and east-to-west and reaches upper amphibolites grade (Labotka et al., 1980). Shortening associated metamorphism did not affect the eastern KPF (Fig. 2.1). In the Kingston Range, north–northeastwards tilting strata of the eastern KPF are generally offset along north–south trending normal faults. In the southern Kingston Range, a detachment system in the southern Kingston Range is related to Cenozoic extension of the Basin and Range province (Davis et al., 1993). Levy & Christie-Blick (1989) estimated ca. 150% extension in the Cenozoic following the initial compressive phase in the Mesozoic. Other estimates for Cenozoic extension range from ca. 50–500% with higher estimates recently called

into question by the findings of Renik *et al.* (2008). In the southern Black Mountains, the eastern KPF has undergone significant structural complication due to Cenozoic extension (Miller, 1991; Noble, 1941; Troxel and Wright, 1987).

2.3. Paleolatitude

There is no published paleolatitude data for the KPF, and paleomagnetism test holes in the Silver Rule Mine Member in the Alexander Hills yielded data that showed later remagnetization (Wright 2002, pers. comm.). Evans (2000, page 365) estimated a ca. 9° paleolatitude for the KPF at 723 ±3 Ma based on stratigraphic correlation and continental reconstruction, placing the KPF on a nearly equal line of latitude with the Toby Formation in Western Utah (Christie and Fahrig, 1983; Heaman and Grotzinger, 1992). The 9° paleolatitude is speculative given that the Cryogenian Period glacial deposits range between 750–634 Ma (Condon et al., 2005; Kendall et al., 2006) and there is no absolute age within the KPF (see below).

2.4. Geochronological Constraints

The maximum age of the Pahrump Group and the Kingston Peak Formation is loosely constrained between a sub-Pahrump Group unconformity and the underlying basement intruded by 1.3 Ga granitic dikes (Lanphere et al., 1964). The middle Crystal Spring Formation contains 1.08 Ga diabase dikes (Heaman and Grotzinger, 1992). The Cambrian boundary provides a minimum age, but it is several kilometers up section (Corsetti and Hagadorn, 2000) within the Lower Wood Canyon Formation (Fig. 1.2).

Relative timing constraints include lithologic similarities to other coarse-grained glacigenic successions outcropping along the western margin of North America (Fig. 2.5) as well as unconformities bounding depositional sequences (Christie-Blick and Levy, 1989). Diamictites within the Kingston Peak formation have been correlated with other diamictic intervals in a northward trending line extending into northern British Columbia (Christie-Blick and Levy, 1989; Stewart, 1970, 1972). These glacial successions are interpreted to be timed with the earlier of two rift events that began after 721 Ma (Evenchick et al., 1984) in the northwestern Cordillera, and whose most active phase lasted from 717-685 Ma in the central-western Cordillera (Fanning and Link, 2004). Deposition of broadly similar but non-correlated coarse-grained strata in Idaho is bounded by a lower limit of 717±3 Ma (Fanning & Link 2004, U-Pb Shrimp) and upper limit of 685±7 Ma (Lund et al., 2003). Miller (1985) suggested the KPF was between 1,200 and 700-800 Ma based on: 1) correlation between the Crystal Spring diabase and Apache Group diabase (this was prior to Heaman and Grotzinger (1992) which documented a 1.08 Ga age for the middle Crystal Spring) and 2) correlation of Noonday Dolomite stromatolites with others of Riphean (Sturtian) age. Miller (1985) pointed out that the KPF might be younger than 700 Ma based on regional correlations with other coarse-grained successions (Fig. 2.5). Christie-Blick and Levy (1989) suggested the KPF was Late Proterozoic based on Miller (1985). They also discussed the transition between the middle to earliest Late Neoproterozoic sedimentary rocks of the Cordillera that overly the crystalline basement. They pointed out that it is variably unconformable to conformable and is suggested to be 770-720 Ma in age based on radiometric ages (Armstrong et al., 1982; Devlin et al., 1985; Devlin et al., 1988; Evenchick et al., 1984). If so, the overlying

Noonday Dolomite was deposited more than 100 Ma before the later rifting event occurring between 560-590 Ma (Bond et al., 1985). Christie-Blick & Levy (1989) correlate a sequence boundary in the upper Johnie Formation with one capping the Inkom Formation in Utah that is located ~200 m below intrusive dikes dated at ~580 Ma Kennedy et al. (1998b) interpreted the Noonday Dolomite to be the Marinoan cap carbonate (~635 Ma) based on geochemical trends and unique lithological features shared by other Marinoan cap carbonates.

2.5. Other Characteristics

Corsetti *et al.* (2003) documented complex microfossils preserved in chert and carbonate from the oncolitic dolostone bed within the Silver Rule Mine Member, similar to microfossils identified in chert nodules from the Beck Spring Dolomite (Horodyski and Knauth, 1994; Pierce and Cloud, 1979). These microfossils indicate shallow-water microbial activity, which argues against the frozen global ocean proposed by Hoffman *et al. (*1998).

3. Stratigraphic and Sedimentary Summaries of the Two KPF Outcrop Regions

The KPF crops out in two distinct regions to the east and west of the Death Valley region (Fig. 2.1). East and southeast of the Death Valley region, the KPF crops out in a number of ranges in laterally continuous and unmetamorphosed sections (Fig. 2.1). This coarse-grained siliciclastic eastern KPF was suggested to be divisible into a northern and southern facies but is interpreted in this work as simply the eastern KPF. The reason for the separation was not based on a difference in facies, but of difference in clast composition. Diamictite intervals to the north are dominated by gneissic clasts in the south vs. carbonate clasts in the north (Troxel, 1967). In the southern Saddle

Fig. 2.5. Distribution of coarse-grained deposits of Neoproterozoic age located along the Cordillera. These deposits are commonly interpreted as glacial in origin or as being influenced by glaciations and most recent age constraints shown for 4 intervals (adapted from Link et al., 1993; Etienne et al., 2007 and Miller, 1985)

Peak Hills, diamictite dominated by clasts derived from the Beck Spring Dolomite (characteristic of northern outcrops) is interbedded with diamictite dominated by granitic and gneissic clasts (characteristic of southern outcrops). This relationship can be seen near 35°40'1.78"N 116°21'44.65"W, 35°40'1.09"N 116°21'43.70"W and 35°39'56.41"N 116°21'54.12"W. Northern and southern outcrops are dominated by course-grained lithologies and can be correlated based on the presence of a distinct shared limestone interval (the Virgin Spring Limestone) overlain by very similar facies in each area (Fig. 2.2). Thus, while clasts in coarse-grained intervals may have been sourced from different margins of a shared paleobasin, these outcrops are described herein as simply the eastern KPF. The KPF also crops out in variably metamorphosed intervals throughout the Panamint Range, which borders Death Valley proper to the west (see above, Fig. 2.1) (Miller, 1983). Limited outcrops of highly metamorphosed KPF are also present in the Funeral Mountains, but not easily associated with other KPF sections, other than being coarse-grained and having a similar stratigraphic position.

3.1 KPF east of Death Valley Proper: Black Mountains through Mesquite Mountains

KPF outcrops east of Death Valley proper are the focus of this research and are formally separated here into the Saratoga Hills Sandstone through the Jupiter Mine members (Fig. 2.2) and are described in detail in the proceeding section. These members coarsen upwards from fine-grained laminated sandstone (Saratoga Hills Sandstone), massive diamictite (Alexander Hills Diamictite), mixed diamictite, conglomerates and turbidite deposits (Silver Rule Mine Member), and debris flows, mega-breccias and fanglomerates (Jupiter Mine Member). Locally, erosional

remnants of a thinly laminated black limestone, the Virgin Spring Limestone (Tucker, 1986), caps the Saratoga Hills Sandstone. Regionally, a thin diamictite or conglomerate interval, the Gunsight Diamictite, lies within the uppermost Jupiter Mine Member.

3.2. Compositional and Lithological Similarities within the Silurian Hills and the Southern Salt Spring Mountains

Outcrops of the southernmost eastern KPF (dark gray shading in Fig. 2.1) are limited to a ca. 8 km-wide belt of quartzite, conglomerate, and diamictite that crops out in the southern Saddle Peak Hills, the southern Salt Spring Hills, and the Silurian Hills. These localities contain an assemblage of clasts different from those in the northern sections, most distinctly a dominant component of granite and gneiss (Troxel, 1967). Mesozoic compression and Cenozoic extension, possibly as great as 100-200% (Snow and Wernicke, 2000; Topping, 1993), have made palinspastic reconstruction controversial and call into question the original shape of the basin during KPF time (Christie-Blick and Levy, 1989) and make challenging the bed-by-bed correlation between these southernmost sections and those sections to the north. Nonetheless, there are several specific points of comparison that assist in correlation at a larger scale.

Southern sections are more limited in outcrop than the northern outcrops and best observed in the Silurian Hills (Fig. 2.1) and in the southern Salt Spring Hills. A general correlation between these locations is based on shared presence of coarse siliciclastic sediments (i.e. diamictite, conglomerate and olistoliths lithofacies) and stratigraphic position between the lower Pahrump Group and the overlying Noonday Dolomite in the Silurian Hills or Johnie Formation in

the southern Salt Spring Hills. In the Salt Spring Hills, a thick section of quartzite and pebble conglomerate beds is capped by a unit of diamictite dominated by basement clasts (Fig. 2.6a). The diamictite is lithologically dissimilar from the carbonate-bearing diamictite and conglomerate beds of the more northern outcrops. Troxel (1982a) showed this diamictite to be interbedded with the carbonate-dominated diamictite facies in the Southern Saddle Peak Hills. This interbedding indicates a transition zone between two contributing source areas. This distinctive basement clast-bearing diamictite outcrops at the very southernmost tip of the Saddle Peak Hills and several km to the north is interbedded with Silver Rule Mine Member conglomerate beds containing only Beck Spring Dolomite (35°39'56.41"N, 116°21'54.12"W). This interbedding relationship times deposition of the diamictite facies in the south with the same facies in the Silver Rule Mine Member.

In the Silurian Hills, Kupfer (1960) described a 2 km thick section of coarse siliciclastic deposits above a 40 m-thick dark gray laminated limestone interval (Fig. 2.6c & d). Due to its stratigraphic position below coarse-grained strata similar to the KPF, Kupfer (1960) correlated the limestone to the Beck Spring Dolomite. Alternatively, Prave (1999) correlated the limestone to a discontinuous limestone interval below the Wildrose submember in the Panamint Range (Fig. 2.2) based on $\delta^{13}C$ values and the presence of a quartzite cobble conglomerate below both limestone intervals. This limestone unit overlies a quartz cobble conglomerate, has a karsted upper contact and is lithologically similar to the Virgin Spring Limestone, with the addition of several m-scale sandstone interbeds. The section above the limestone coarsens upwards and contains normally graded sandstone and conglomerate, diamictite and dam-scale megaclasts (Fig. 2.6b). This interval is comprised of >400 m of interbedded turbiditic sandstone beds and graded debrites

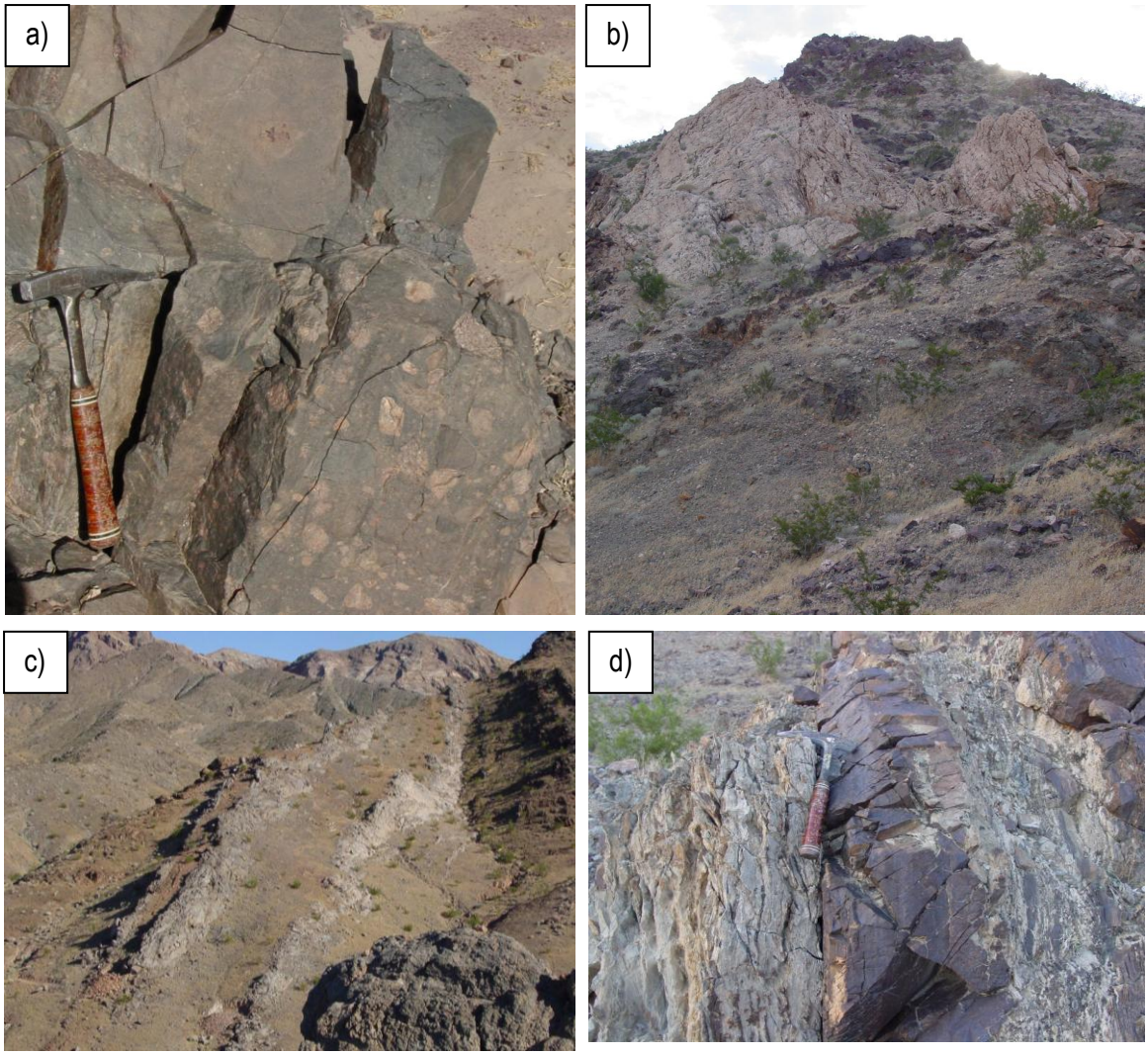

Fig. 2.6. Coarse facies in what was previously referred to as the "southern facies" (Troxel, 1967). a) basement gneiss bearing diamictite in the southern Saddle Peak Hills; b) dam-scale olistolith of Crystal Spring Fm. in upper KPF (Silurian Hills); c) Virgin Spring Limestone equivalent (Silurian Hills); d) interbedded sandstone and limestone of the Virgin Spring Limestone equivalent (Silurian Hills).

overlain by 1000 m of massive diamictite containing dam-scale olistoliths of the Crystal Spring Formation in its base (Fig. 2.6b). This interval of dark laminated limestone overlain by an almost 1500 m sequence of turbidites, debrites and diamictites is very similar to the Virgin Spring Limestone-Jupiter Mine Member interval <10 km to the northwest in the Sperry Hills and <30 km to the northeast in the southern Kingston Range. Capping the KPF in the Silurian Hills is a 5 m interval of sandy buff-colored limestone similar to the Noonday Dolomite in Sperry Wash. Similarities between the northern and southern sections include karsted and laminated limestone facies, sandstone beds, a coarsening-upwards trend above the karsted limestone intervals, and megaclasts.

3.3. KPF in the Western Region (Panamint Mountains)

Correlation between the two regions of Kingston Peak sediments east and west of Death Valley has proven problematic over as little distance as 50 km. Various palinspastic reconstructions call for Cenozoic extension of between 50-500% (see above) between mountain ranges from the Spring Mountains in western Nevada through the Panamint Range. Sediment in the eastern Panamint Range may have been deposited <10 km or less from KPF sections of the eastern region in the southern Black Mountains (Topping, 1993). In both regions, the Kingston Peak Formation has similar lower and upper lithostratigraphy (Fig. 2.2) and is bounded conformably below by the platform carbonate of the Beck Spring Dolomite and bounded above by the distinctive and laterally traceable Noonday Dolomite (Fig. 1.2).

As in the eastern region, siliciclastic sediments are interbedded with the Beck Spring Dolomite (Labotka and Albee, 1977; Labotka et al., 1980); however, these sediments are sandy and conglomeratic (the Limekiln Spring Member; Fig. 2.2), and suggest a marked difference in depositional environment to the siltstone and fine sandstone in the equivalent stratigraphic position in the eastern sections (the Saratoga Hills Sandstone; Fig. 2.2). Clast-supported conglomerates and sandstones give way to laterally continuous massive diamictite (Fig. 2.7a; Surprise Member Fig. 2.2) that is sharply overlain by a regionally persistent, 5-40 m thick, grey, thinly-laminated limestone (Fig. 2.7b-1.7d; Sourdough Limestone; see Fig. 2.2) (Miller, 1983; Miller, 1985b). Where this limestone is preserved near synsedimentary faults (Goler Wash; sec #28 Fig. 2.1), it contains clasts, up to m-scale, of angular sandstone (Fig. 2.7c) and is associated with dam-scale olistoliths in the overlying KPF. The Sourdough Limestone in turn is interbedded with an overlying sandstone unit (Middle Park Member; Fig. 2.2) and conglomerate unit (Fig. 2.7e) (Mountain Girl submember; Fig. 2.2) that is also overlain by a second, thin (~ 12 m), laterally persistent limestone (the "unnamed" limestone; Prave (1999). The uppermost KPF in the Panamint Range is comprised of basement-clast bearing diamictite (Fig. 2.7f) (Wildrose submember; Fig. 2.2 (Miller, 1983; Miller, 1985b)) that caps a syndepositional fault in Goler Wash (Prave, 1999) and overlies an erosional surface that has been documented (Miller, 1983; Prave, 1999) to cut down through lower units to the Surprise Member.

4. Boundary Relations Between the Northern Facies of the KPF in its Type Area and Overlying and Underlying Units

4.1. Underlying Beck Spring Dolomite

The lower and middle formations in the Pahrump Group (Fig. 2.2) record a transition from mixed carbonate–siliciclastic marine and fluvial facies of the Crystal Spring Formation (Roberts, 1974) to the Beck Spring Dolomite, comprised of shallow-water carbonates in the north and mixed carbonate–siliciclastic fluvial–tidal deposits south of the central Saddle Peak Hills (Marian and Osborne, 1992) (Fig. 2.1). In the Kingston Range, Marion & Osborne (1992) divided the Beck Spring Dolomite into: 1) a lower laminated cherty member, 2) a laminated member with angular intraclasts and columnar stromatolites, 3) a relatively thinner oolitic-pisolitic member, and 4) a partially silicified upper member with abundant chert, shale lenses and stromatolites.

4.2. Beck Spring Dolomite-KPF Contact

The contact between the KPF in the Panamint Range and the underlying Beck Spring Dolomite has been described by Miller (1985) as conformable, inter-fingering, and unconformable, depending on the locality. Christie-Blick and Levy (1989) suggested the contact might be regional based on an subtle erosion surface in some localities. Kenny & Knauth (2001) describe karstification of the upper Beck Spring Dolomite in a number of localities. In the Alexander Hills and Saratoga Hills, the Saratoga Hills Sandstone is described as transitional with the top of the Beck Spring Dolomite over 10 m (Wright et al., 1992). This relationship can be seen in the Alexander Hills (35°46’2”N, 116°7’10”W, #1 in Fig. 2.1) and in the southern Black Mountains (35°54’45”N, 116°38’50”W, #23 in Fig. 2.1) where there is a sharp contact between the Beck

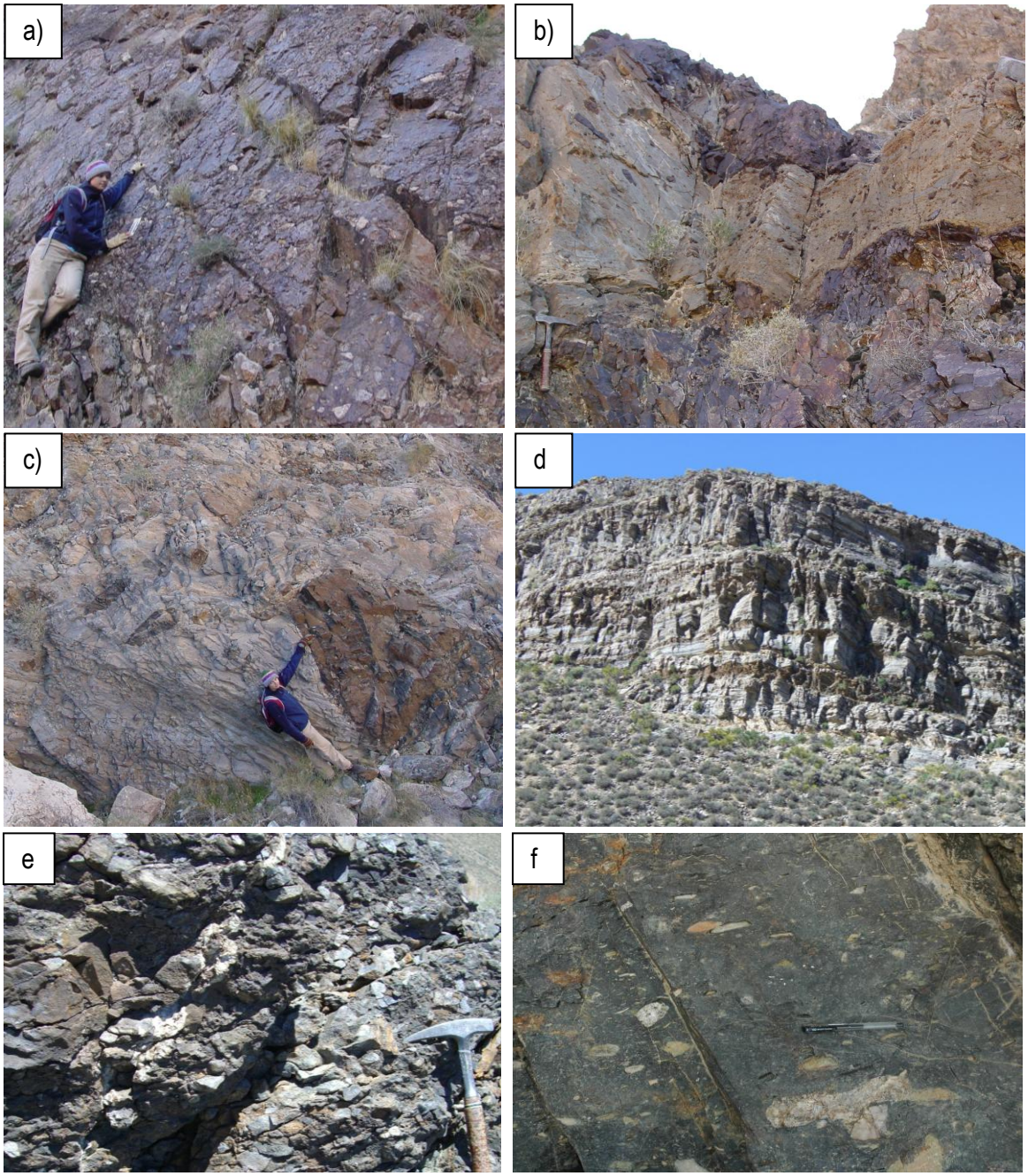

Fig. 2.7. Various members of the western KPF in the Panamint Range; a) Surprise Member diamictite facies (Goler Wash); b) sandstone clast-bearing debris flow of Sourdough Limestone material, Sourdough Limestone Member (Goler Wash; c) m-scale sandstone clast within the Sourdough Limestone Member (Goler Wash); d) bedded Sourdough Limestone Member (Wildrose Canyon); e) Mountain Girl Conglomerate submember (Wildrose Canyon); f) Wildrose Diamictite submember (Goler Wash).

Spring Dolomite and the Saratoga Hills Sandstone, followed by interbedding between cm-scale dolomite and sandstone beds over the next several meters.

4.3. Kingston Peak Formation–Noonday Dolomite Contact

The interpretation for the contact between the eastern KPF and the overlying Noonday Dolomite is contentious and has been reported as regionally unconformable (Noble, 1934; Wright et al., 1978), locally unconformable (Christie-Blick and Levy, 1989) and locally conformable (Miller, 1987). An unconformable relationship has been suggested because the Noonday Dolomite seems to cap tilted strata (Cloud et al., 1974; Wright et al., 1974) between the Alexander Hills and the southern Nopah Range. The Noonday Dolomite also appears to overlay successively older units, ultimately straddling the contact between the Crystal Spring Formation and the basement at the War Eagle Mine. Prave (1999) suggested that the Gunsight Diamictite lies between an unconformity and the Noonday Dolomite, placing an erosional event immediately prior to Gunsight Diamictite deposition. He suggested that the Gunsight Diamictite was conformable with the Noonday Dolomite (Prave, 1999).

Detailed field studies of this contact indicate uninterrupted deposition beginning at the base of the Alexander Hills Diamictite and continuing through the Noonday Dolomite, demonstrated by the following four sedimentary relationships. First, Jupiter Mine Member sedimentary breccia in the Alexander Hills is interbedded (Fig. 2.8) with the basal Noonday Dolomite (35°45’56”N, 116°6’55”W). Second, the base of the Noonday Dolomite commonly contains clasts (Fig. 2.9 a & b) from the Beck Spring Dolomite and Crystal Spring Formation (i.e. 35°45’46”N, 116°6’50”W); this

likely indicates that during incipient Noonday Dolomite deposition, loose clasts from an unlithified Jupiter Mine Member surface were reworked along with carbonate material from the flanks of Noonday Dolomite mounds. Third, in footwall sections, the contact between the Noonday Dolomite and underlying strata is commonly interrupted by a 1–10 m layer of Gunsight Diamictite; this diamictite interval appears conformable with the underlying Jupiter Mine Member in the Alexander Hills. Fourth, in the southern Valjean Hills (35°39'40"N, 116°7'22"W, #17 in Fig. 2.1) and in the Ibex Hills (DeYoung, pers. comm.), Noonday Dolomite clasts are included in diamictite of the Jupiter Mine Member or are in diamictite interbedded with Jupiter Mine Member sedimentary breccia. Alternatively, Corsetti & Kaufman (2005) interpreted Ibex Hills interbedded diamictite to post-date KPF deposition.

4.4. Overlying Noonday Dolomite

The Noonday Dolomite overlying the eastern KPF is divided into a lower cream-colored laminated microbial dolomite member and an upper laminated silty dolomite member (Wright et al., 1978). The cm-scale laminations in the basal several meters of the lower member are parallel and horizontal (Fig. 2.9e). The contact between the upper and lower members outlines synoptic relief of up to 200 m (Williams et al., 1974). Alternatively, Summa (1993) suggested apparent mound topography was due to an intra-formational erosion surface. The lower member contains distinctive vertical tubes (Fig. 2.9c & d) possibly related to vertical transport of fluids (Cloud et al., 1974; Kennedy et al., 2001) or vertical tube-shaped stromatolites (Corsetti and Grotzinger, 2005) and cm-scale pockets of sparry cement) (Cloud et al., 1974; Williams et al., 1974). In the east, the

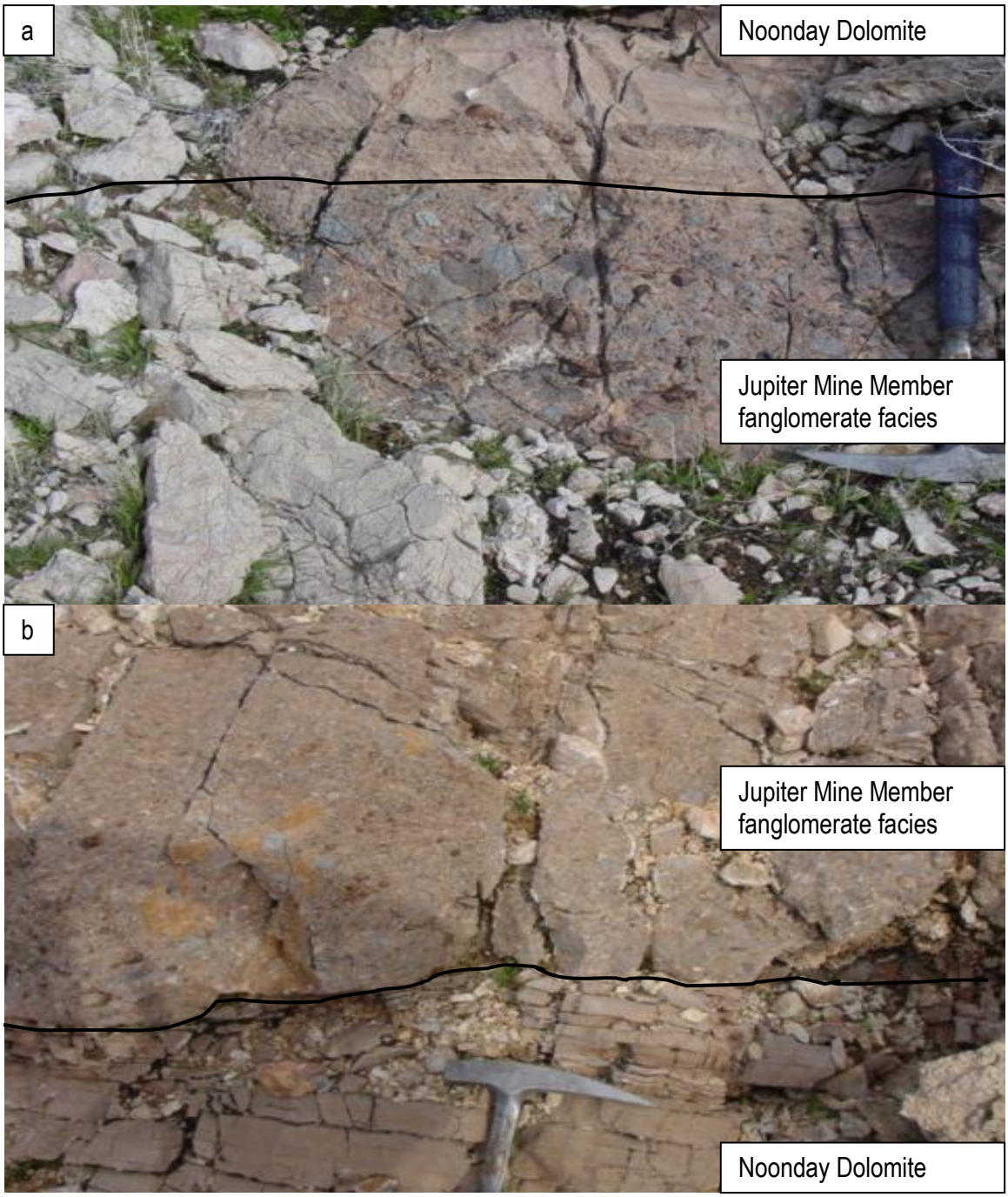

Fig. 2.8. Composite photograph of interbedded Jupiter Mine Member breccia and lower Noonday Dolomite (Alexander Hills). 1 m of cover separates upper and lower photographs. a) gradational contact between sedimentary breccia (dominated by clasts of the Beck Spring Dolomite) of the Jupiter Mine Member and overlying lower Noonday Dolomite ; b) base of the lower Noonday Dolomite capped by basal interbed of the overlying sedimentary breccia

Noonday Dolomite transitions southwards to a siliciclastic-rich facies assemblage (Ibex Formation) (Troxel, 1982a) which includes an arkosic siltstone member, a shaley-limestone member and a quartz-dolomite member (DeYoung, 2005; Williams et al., 1974).

5. Stratigraphy and Sedimentology of the KPF in its Type Area: Kingston Range, Alexander Hills and Southern Black Mountains

The KPF in the southeast Death Valley region (Fig. 2.1) is preserved in a wedge-shaped geometry that thickens away from basin margins (Fig. 2.10; see also 1.3). This geometry owes its origin to syndepositional Precambrian normal faults. Three regions investigated in this study, the Kingston Range, the Alexander Hills and the Southern Black Mountains, all display this wedge-shaped geometry and similar facies and are the basis for the following description of the KPF members. This description includes: 1) the nature of the contact between the Beck Spring Dolomite and the basal KPF, 2) facies and thickness variability at different positions in these wedges (i.e. from the basin margin to the deeper basin positions), 3) lateral facies and thickness variation within individual members, which are critical to understanding the timing of tectonism, and 4) the contact between the KPF and the overlying Noonday Dolomite. As discussed above, this contact – which is important to any geochemical interpretation of the KPF-Noonday Dolomite interval – has been interpreted as an angular unconformity (Christie-Blick and Levy, 1989; Stewart, 1970) but is reinterpreted here as conformable based on evidence of on lap of successive overlying facies toward faulted basin margins.

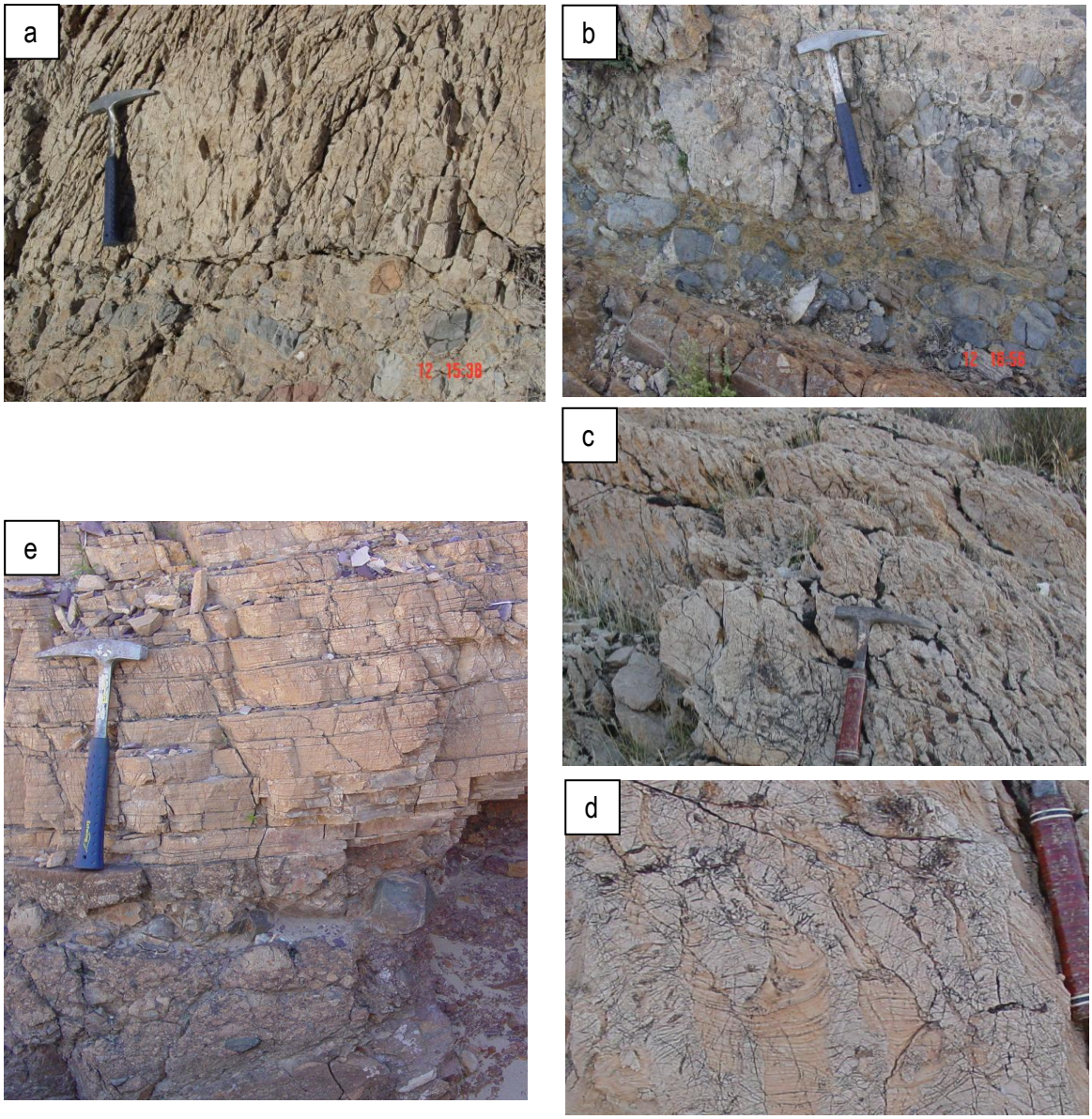

Fig. 2.9. Various features of the Noonday Dolomite; a) near the Snow White Mine the base of the Noonday Dolomite is comprised of a transitional layer composed of a buff-colored dolomite matrix and what must have been loose clasts (primarily Beck Spring Dolomite) of an unlithified Jupiter Mine Member fanglomerate; scattered clasts are found up to several meters within the basal Noonday Dolomite; b) west of the Horsethief Mine section (Fig. 2.1 # 12) there are a number of similar transitional layers comprised of a dolomitic Noonday matrix and primarily Beck Spring Doilomite clasts; c) closely-clustered vertical tubes (Alexander Hills); d) sometimes tubes have much more irregular outlines and are far wider (Alexander Hills); e) lowermost laminated Noonday Dolomite overlying KPF (Ibex Hills).

The best area to observe this wedge-shaped stratigraphy is in a ~20 km long gently curving belt in the northern thru eastern Kingston Range. Fig. 2.10 shows the KPF thickening rapidly to the south through the Kingston Range. The Kingston Range is also the location of the Pahrump Group type sections, in the vicinity of Crystal and Beck Springs (see note on Fig. 2.1) (Hewett, 1940).

5.1. Description of the Saratoga Hills Sandstone

Sedimentary Description: The fine-grained siliciclastic Saratoga Hills Sandstone represents an abrupt change in lithology from stromatolitic, oncolitic and oolitic features of the underlying Beck Spring Dolomite. The Saratoga Hills Sandstone is from 1 to 180 m thick and comprised of 2-5 cm beds of fine quartz-arkosic sandstone and siltstone (Fig. 2.11) which has weathered to green to yellow-green in outcrop. Sandstone beds are characterized by ubiquitous planar mm-scale parallel laminations, but may include rare gentle cross-lamination, massive unlaminated <5 cm thick beds, and beds with gently scoured bases and pock-marked and wavy textures on bedtops resemble microbial mat surfaces (Franks and Stolz, 2009; Noffke et al., 2008). At Crystal Spring, parallel laminated sandstone beds dominate, but are sometimes siltstone, rare sub-dm beds of graded sandstone with coarse sandy bases, or massive siltstones with mud intraclasts. Carbonate

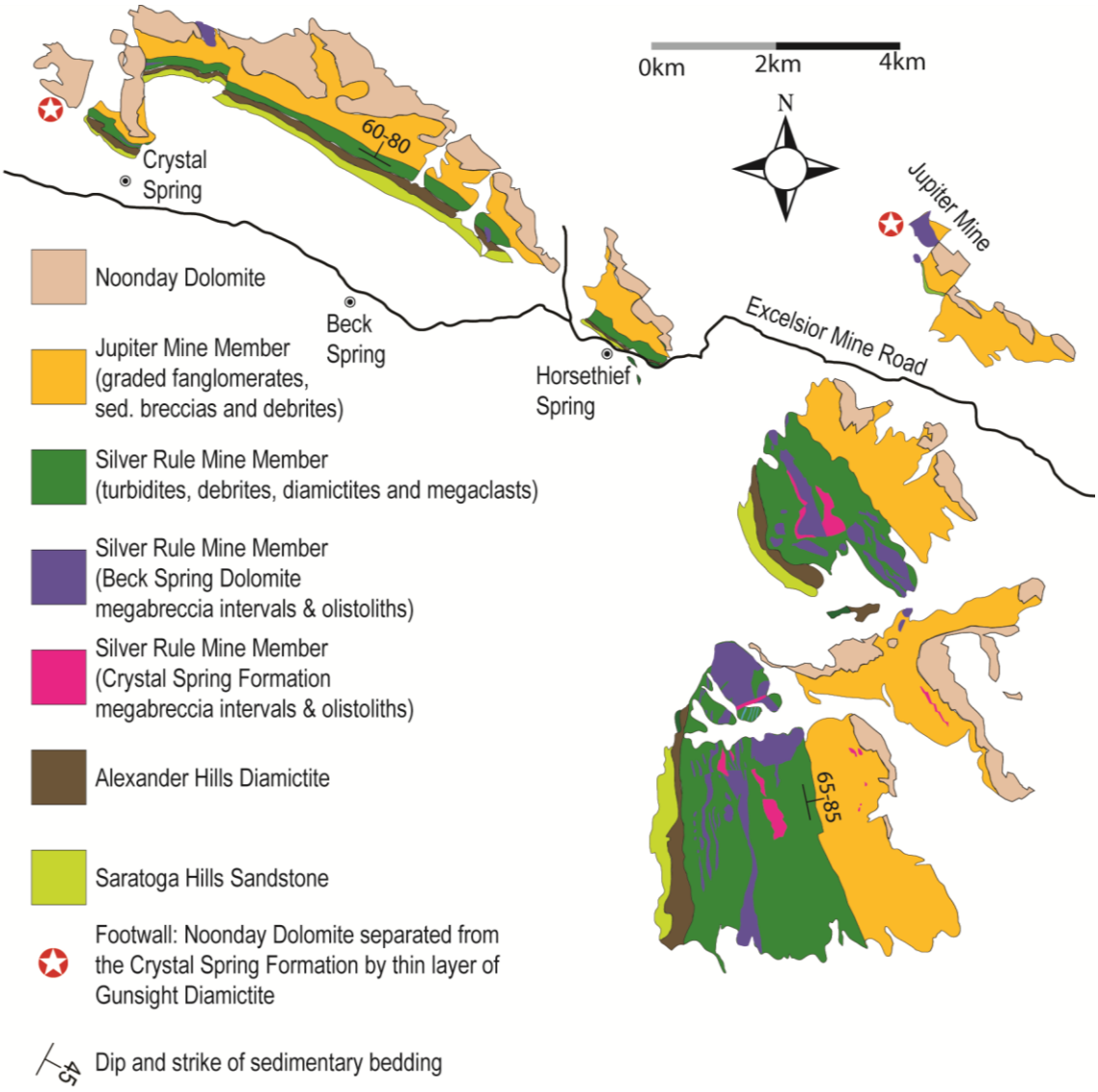

Fig. 2.10. Changing trends in thickness in KPF members throughout Kingston Range (map modified after Calzia et al, 2000).

cemented beds increase upsection toward the Alexander Hills Diamictite contact, and several beds beneath the contact are dolomitic sandstones.

Mineralogy: The sandstones have various grain-to-grain relationships and matrices. Grains are normally angular to sub-angular (Fig. 2.12b & e) but may be sub-rounded (Fig. 2.12a), and more often poorly sorted. Sandstone beds are divided between being grain supported (Fig. 2.12b & e) and matrix supported (Fig. 2.12a & f). Matrix material is normally composed of quartz silt and clay, but can also be carbonate or carbonate-rich (Fig. 2.12f) at the base of the member near the gradational contact with the Beck Spring Dolomite and also at the top of the member. Lithic grains (Fig. 2.12d) are also common in many beds.

Sedimentary Contacts: The contact between the Saratoga Hills Sandstone and the underlying Beck Spring Dolomite is interbedded. In the Virgin Spring Wash, Alexander Hills, and Beck Canyon, 5-10 m thick intervals of laminated dolomitic sandstone appear throughout the upper 50-70 m of the microbially laminated Beck Spring Dolomite. In the Alexander Hills, basal Saratoga Hills Sandstone siltstone and sandstone beds are interbedded with upwards thinning microbially laminated dolomite beds across a ~40 m transitional interval. These dolomite beds have enriched $\delta^{13}C$ and $\delta^{18}O$ values (see Table 2.2) similar to the underlying Beck Spring Dolomite in the Alexander Hills and not as characteristic of carbonates above the Saratoga Hills Sandstone or of the overlying Noonday Dolomite. There is no evidence of erosional truncation between the Saratoga Hills Sandstone and the Beck Spring Dolomite and 10-15 m siliciclastic-carbonate cycles suggest a prolonged transition from the carbonate system of the Beck Spring Dolomite to the

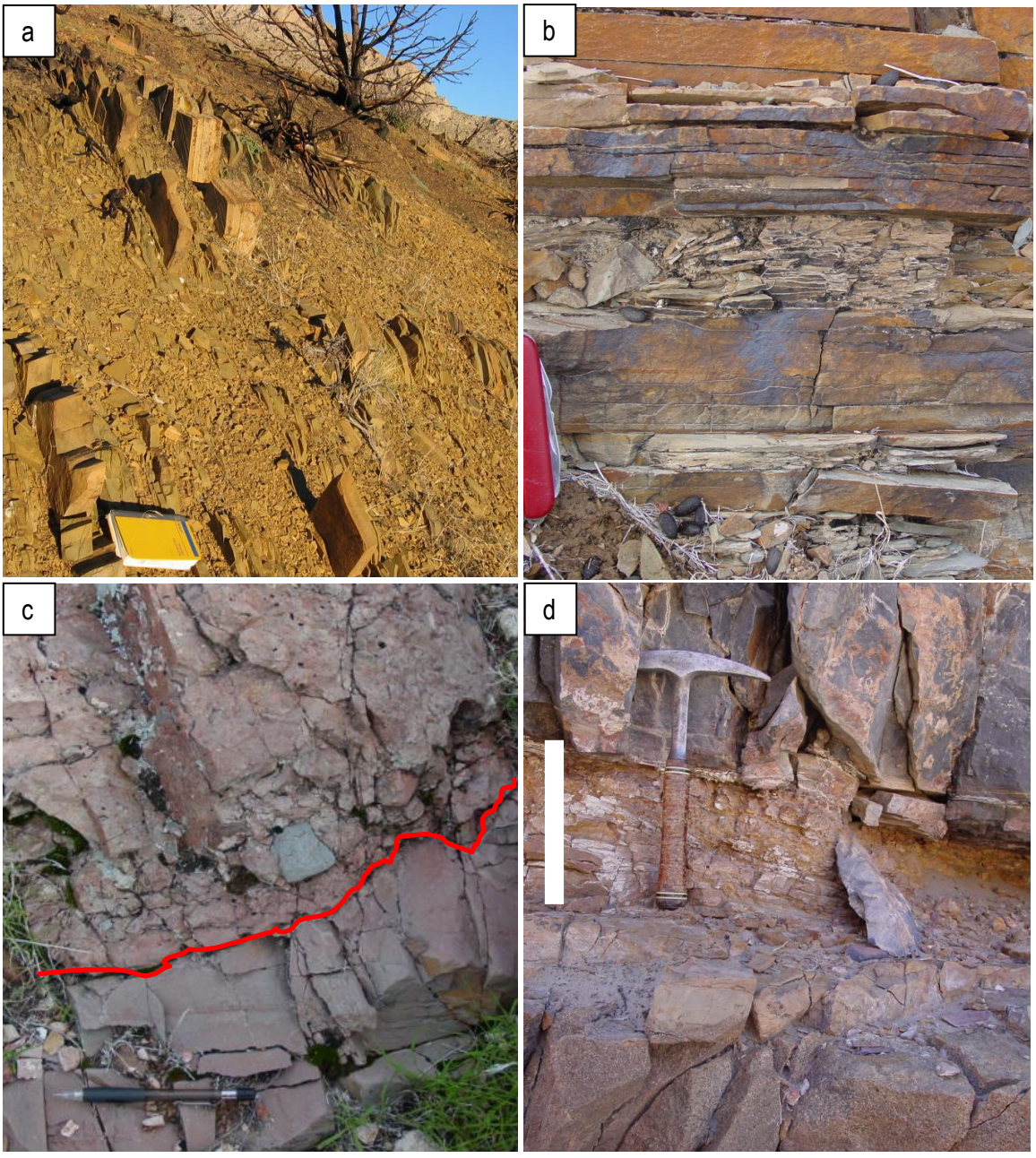

Fig. 2.11. Typical facies and important features of the Saratoga Hills Sandstone; a) cm-scale interbedded sandstone and siltstone (Beck Canyon Divide); b) bedded sandstone and siltstone (Crystal Spring); c) irregular erosional contact (red line) between the Saratoga Hills Sandstone and the overlying Alexander Hills Diamictite (Alexander Hills); d) contact between thin (<1 m) Saratoga Hills Sandstone section(total thickness shown with white bar) and overlying Virgin Spring Limestone in the Ibex Hills.

siliciclastic lower KPF and shutdown of the carbonate factory. Basinwards in the Saratoga Hills and Saddle Peak Hills, this member contains a higher proportion of siltstone and shale.

The top of the Saratoga Hills Sandstone has been erosionally truncated in all sections. In the southern Black Mountains, near Virgin Spring Wash, 30 m of Saratoga Hills Sandstone has been truncated over a distance of ~100 m. In the Alexander Hills and Beck Canyon sections, erosional truncation is sharp, irregular and m-scale (Fig. 2.11c). The black laminated limestone overlying the Saratoga Hills Sandstone is rarely preserved due to this truncation; in one of two locations where the contact is preserved (Virgin Spring Wash), it is sharp and the underlying Saratoga Hills Sandstone is 105 m thick.

Variability: The Saratoga Hills Sandstone varies between >180 m and <1 m in thickness within the sections measured. In the Ibex Hills (Fig. 2.1) there is a <1 m thick section of Saratoga Hills Sandstone (Fig. 2.11d) comprised of thinly interbedded siltstone, laminated fine sandstone and very coarse well-rounded sandstone. The uncharacteristic thinness may be explained by the position of the Ibex section relative to the basin, as this is also a location where the Noonday Dolomite platformal to basinal facies transition has been documented (DeYoung, 2005; Troxel, 1982a). The Saratoga Hills Sandstone does not appear to systematically vary in thickness away from the basin margin. At the western end of the Kingston Range near Crystal Spring, the entire KPF is limited to a section limited to ~20 m of diamictite unconformably overlying the Crystal Spring Formation. The basin margin, possibly defined by a syndepositional Precambrian normal fault, lies between that contact and the section measured near Crystal Spring (Fig. 2.1). Where all four KPF

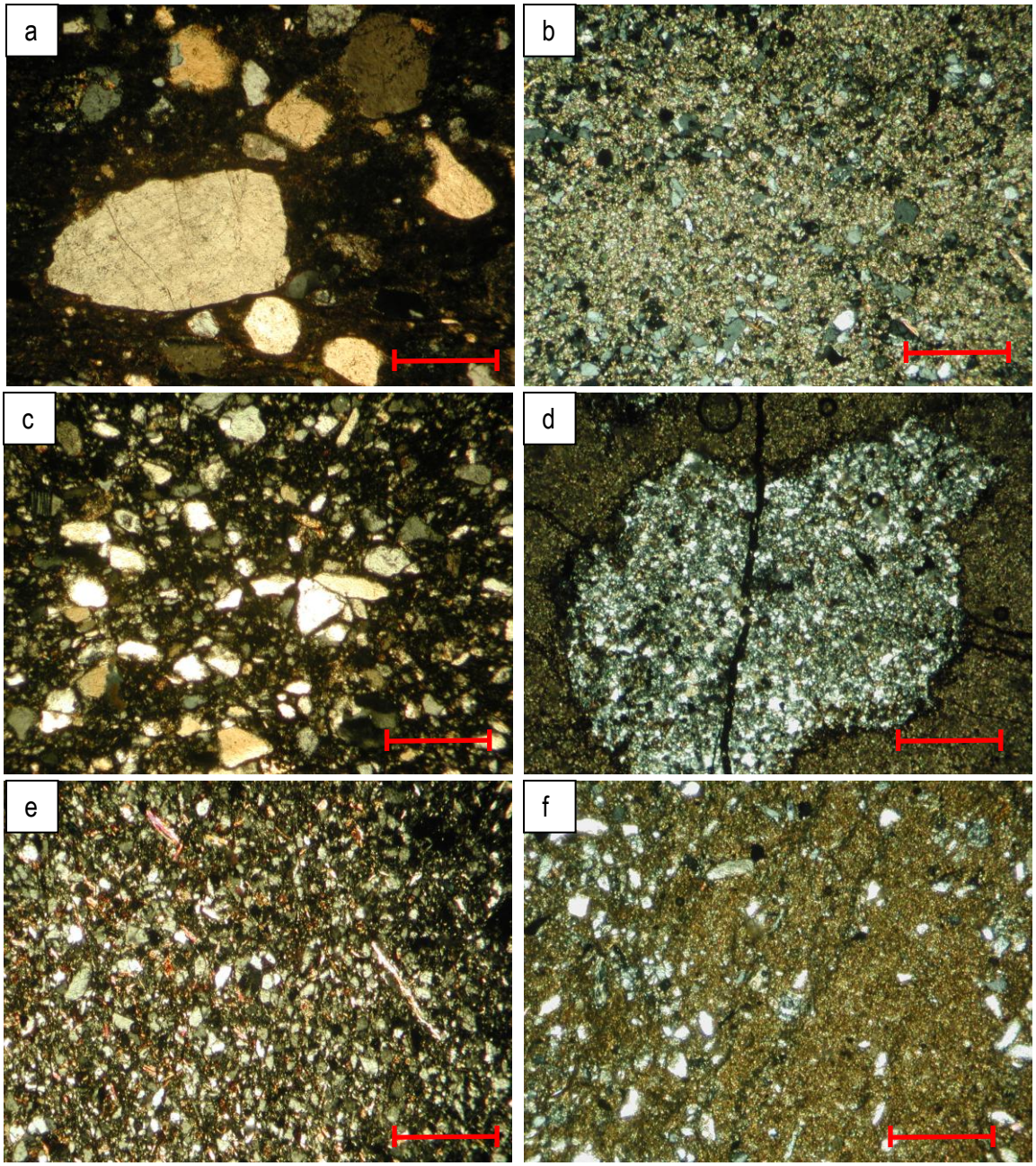

Fig. 2.12. Mineralogy of the Saratoga Hills Sandstone. Scale bar = 0.5 mm. Sample locations are indicated in Appendix A.

a. 011306-2
b. 121706-12
c. 121706-6
d. 013105-3
e. 013105-1
f. 013105-1

members are present, the Saratoga Hills Sandstone conformably overlies Beck Spring Dolomite. The Saratoga Hills Sandstone is present eastwards throughout the remainder of the Beck Canyon (Crystal Spring-to-Horsethief Spring, Fig. 2.1), and thickens systematically from 43 m at Crystal Spring to 158 m at Horsethief Spring, some 8 km away. In the Alexander Hills, the Saratoga Hills Sandstone is 181 m thick <1 km from the basin margin contact, where 40-60 m of diamictite unconformably overlies Beck Spring Dolomite and is sharply overlain by the Noonday Dolomite. Because of the erosional truncation of the upper Saratoga Hills Sandstone, it is not possible to estimate the pre-erosional thickness of these sections.

5.2. Description of the Virgin Spring Limestone

Sedimentary Description: A distinctive unit (3-17 m thick) of parallel laminated black limestone overlies the Saratoga Hills Sandstone in the Saratoga Hills, the Ibex Hills and Virgin Spring Wash. Beds are between 2-15 cm thick and typically comprised of sub-mm scale laminations (Fig. 2.13a). Sedimentary structures are generally limited to parallel lamination, but include rare massive 2-5 cm thick beds, folded beds and tight overturned folds generally 5-10 cm in height. These overturned folds are probably a result of mass movement downslope (Tucker, 1986); their axes are often oriented in the same direction and may be steeply overturned. There is no evidence of other laminated microbial fabric. In thin section both ooids and non-laminated peloids are abundant. In the Ibex Hills, some m-scale intraclastic beds are comprised of limestone mud flakes and angular chips and interbedded with laminated facies. Cm-scale sandstone beds with sharp bases appear throughout each section (Fig. 2.13b).

Mineralogy & Geochemistry: Thin sections studied (n=23) reveal the Virgin Spring Limestone is composed entirely of calcite with no evidence of dolomite. Tucker (1986) interpreted the mineralogy to have been originally aragonitic based on high Sr content (avg. 1770 ppm) and very low Mg content (avg. 0.26 %). A negative correlation between Sr and Fe + Mn provides evidence that Sr was not added during diagenesis. Isotopic data for all three sections of the Virgin Spring Limestone is summarized in Table 2.1. For the Virgin Spring Wash and Ibex Hills sections $\delta^{13}C$ values average +2.0‰ PDB (n=7) (Tucker, 1986) and +2.5‰ PDB (n=16) respectively, while the mean of $\delta^{18}O$ values is -15.8‰ PDB and -13.3‰ PDB respectively. In the Saratoga Hills, where karst features penetrate more deeply into the limestone (Fig. 2.13c), the mean of $\delta^{13}C$ and $\delta^{18}O$ values (n=13) are +0.5‰ PDB and -16.0‰ PDB respectively and there is a systematic 2.0‰ increase in $\delta^{13}C$ upsection. There is no co-variation between $\delta^{13}C$ and $\delta^{18}O$ in any of the three sections.

Sedimentary Contacts: The Virgin Spring Limestone sharply overlies the Saratoga Hills Sandstone across a depositional contact at the Ibex Hills and Virgin Spring Wash. In the Saratoga Hills, laterally extensive (several hundred meters) limestone beds overlie the Saratoga Hills Sandstone but the contact is faulted. The top surface of the Virgin Spring Limestone is karsted and erosionally truncated; sandstone fills grikes that penetrate 30-50 cm down into the limestone in the Saratoga Hills and cross-sections of 20-30 cm diameter oval cavities several meters below the top of the limestone in the Ibex Hills are similarly filled with sandstone (Fig. 2.13c). In the southern Saratoga Hills, the Virgin Spring Limestone is gradually beveled out to the south as it is erosionally truncated. This erosional surface penetrates down on into the Saratoga Hills Sandstone and

		$\delta^{18}O$				$\delta^{13}C$			
	n=	Avg	Std Dev	Min	Max	Avg	Std Dev	Min	Max
VSL-s	71	-14.3	3.1	-24.3	-7.3	2.4	2.0	-4.4	6.7
VSL-n	74	-13.3	4.0	-23.3	-1.2	1.6	-1.2	1.1	3.4
SDL	158	-14.5	1.7	-17.8	-6.3	-2.0	1.7	-7.2	4.8

Table 2.1. Isotope statistics for samples run in this study for main carbonate intervals of interest in the eastern and western KPF (VSL-s = Silurian Hills; VSL-n = Saratoga Hills, Ibex Hills & Virgin Spring Wash; SDL = Sourdough Limestone); see Table 3.2 as well.

defines the regional Saratoga Hills Sandstone-Alexander Hills Diamictite unconformity, as described above.

Variability: Because of erosional truncation, it is impossible to estimate the original stratigraphic thickness of the Virgin Spring Limestone. The Virgin Spring Limestone is the thickest (17 m) in the Ibex Hills (Fig. 2.13d) but is still karsted, indicating some erosional thinning may not be ruled out. The limestone in the Ibex Hills is underlain by the Beck Spring Dolomite and because of their similar colors, may be easily confused with the dolomite. The following four sedimentary and geochemical relationships distinguish the Virgin Spring Limestone from the Beck Spring Dolomite in the Ibex Hills. One, the underlying dolomite contains large ooids and stromatolitic features, often chertified, characteristic of the Beck Spring Dolomite; the overlying limestone is laminated. Two, the underlying dolomite has very diagnostic enriched $\delta^{18}O$ values (see Table 2.2) while the overlying limestone has very depleted $\delta^{18}O$ values characteristic of the Virgin Spring Limestone (see Table 2.2), beginning immediately above the fault contact. Three, in a wash at the west end of the faulted contact, a small section of the Saratoga Hills Sandstone is preserved. It is <1 m thick but contains a very characteristic coarse-grained sandstone also found at the top of the Saratoga Hills Sandstone in the Saratoga Hills. Four, the overlying basal Alexander Hills Diamictite is almost entirely comprised of a black calcitic matrix, identical to many other basal Alexander Hills Diamictite sections.

In the Saratoga Hills, the 3 m thick limestone member lies the farthest of any section from a basin margin, and yet has been thinned by erosion. The limestone is 7-8 m thick in the southern

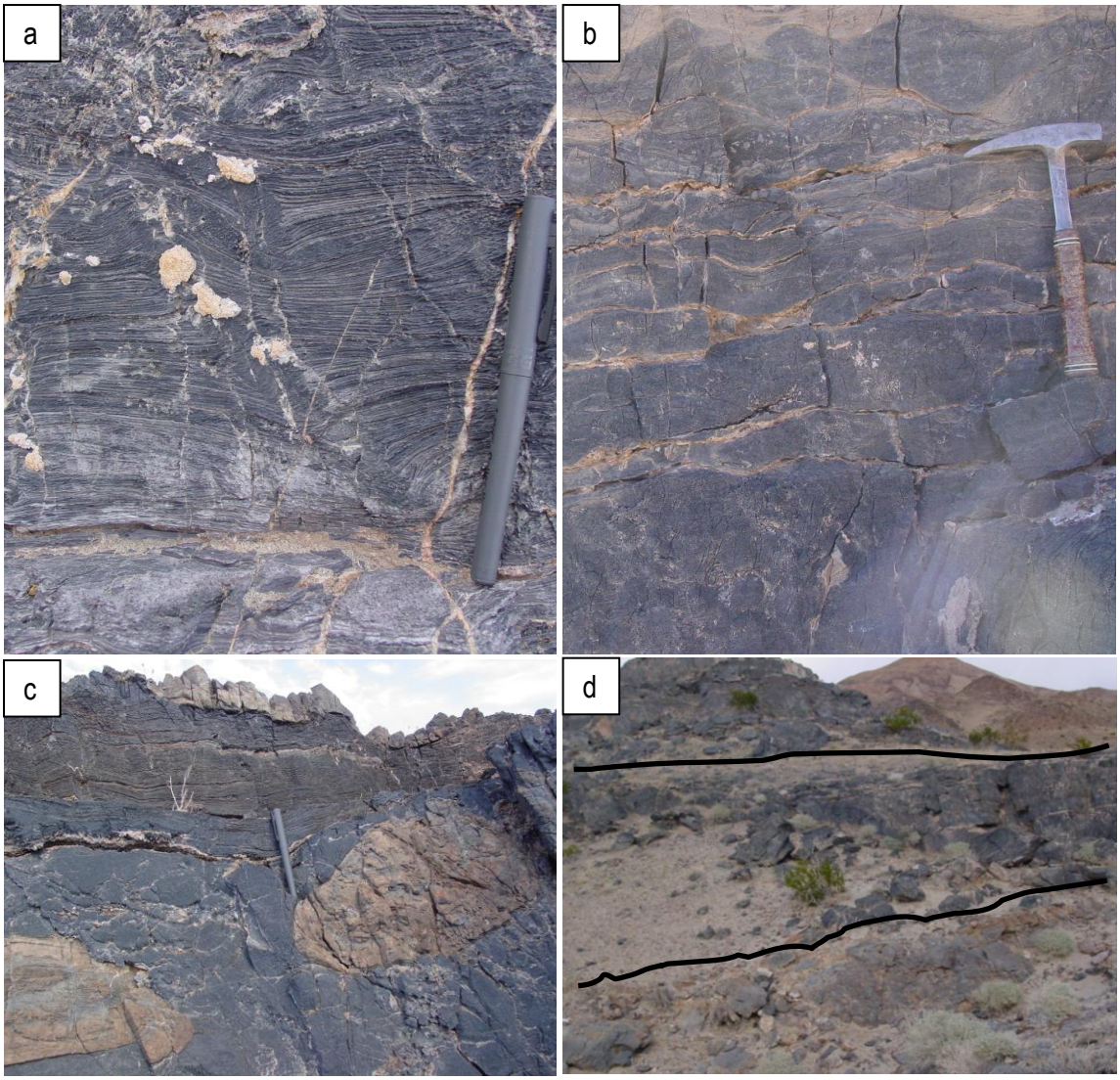

Fig. 2.13. Various features of the Virgin Spring Limestone; a) arcuate planar laminations (Ibex Hills); b) wavy laminations in interbedded limestone and sandstones layers with wavy upper surface (top picture) from down-slope movement (Ibex Hills); c)sandstone fills karst features within the upper Virgin Spring Limestone (Ibex Hills); d) thickest Virgin Spring Limestone section at Ibex Hills sandwiched in between overlying Alexander Hills Diamictite (above upper black line) and underlying Beck Spring Dolomite (below lower black line).

Black Mountains at Virgin Spring Wash, within 1 km of a transition to the basin rim where discontinuous lenses of diamictite are sandwiched between Beck Spring Dolomite and the Noonday Dolomite. The Virgin Spring Wash section is also the location of 30 m of erosional truncation into the Saratoga Hills Sandstone (see above). Where the Saratoga Hills Sandstone is thinnest (75 m), dam-scale blocks of Virgin Spring Limestone lie in close contact to the Saratoga Hills Sandstone, but are underlain by a thin layer of diamictite belonging to the overlying Alexander Hills Diamictite. This marks the edge of the Virgin Spring Limestone as it failed, collapsed and was included into the overlying Alexander Hills Diamictite. In the Ibex Hills, the limestone is 17 m thick (Fig. 2.13d) but thins laterally over a distance of several hundred meters to several meters in thickness. The upper limestone here has numerous beds of limestone intraclast flake breccias interbedded with the laminated facies and may be thicker due to deposition in a submarine channel, or other seafloor topography. The Virgin Spring Limestone likely was laterally extensive and covered most, if not all, of the Saratoga Hills Sandstone, based on its incorporation as clasts into the overlying Alexander Hills Diamictite in most sections.

Diamictite of the overlying Alexander Hills Diamictite commonly includes Virgin Spring Limestone clasts in almost all sections. Sometimes diamictite interbedded up to 100 m into the Silver Rule Mine Member (throughout Beck Canyon) contain clasts of the Virgin Spring Limestone, indicating that either platforms of limestone were exposed and being eroded into Silver Rule Mine Member deposit, or that Alexander Hills Diamictite was sometimes reworked.

5.3. Description of the Alexander Hills Diamictite

Sedimentary Description: The Alexander Hills Diamictite is dominated by a single facies of massive cobble-to-boulder diamictite (Fig. 2.14a), averages ~100 m in thickness, contains lesser intervals of laminated and cross-laminated siltstones, is regionally persistent, fills erosional topography, contains a conspicuous proportion of clasts from the underlying Virgin Spring limestone (Fig. 2.14b) and comprises the first coarse-grained deposit of the Kingston Peak Formation. Striated and faceted clasts are scattered but present in some sections, suggesting a glacial influence.

The massive diamictite facies of the Alexander Hills Diamictite commonly provides few clues as to depositional processes because of a heavy weathering rind that obscures sedimentary bedding and the rarity of associated more diagnostic facies. Where fresh surfaces are exposed, the massive diamictite facies is comprised of m-scale composite bedding defined by variation in clast and matrix size (Fig. 2.14c & d). In some locations, and particularly near the middle of the massive diamictite, laminated silt and fine sandstone intervals suggest the nature of background sedimentation. In the Saratoga Hills, silt and fine sandstone laminated sediments are cross cut by channelized diamictite beds indicating reworking. These fine grained sediments show herringbone cross stratification and well developed tidal bundles indicative of deposition under tidal influence (Fig. 2.15). Near Crystal Spring, Alexander Hills Diamictite like massive diamictite facies are also interbedded with subaqueous debris flows of the Silver Rule Mine Member that have sharp bases, graded intervals and laminated fine grained tops that have not been reworked by wave or storm

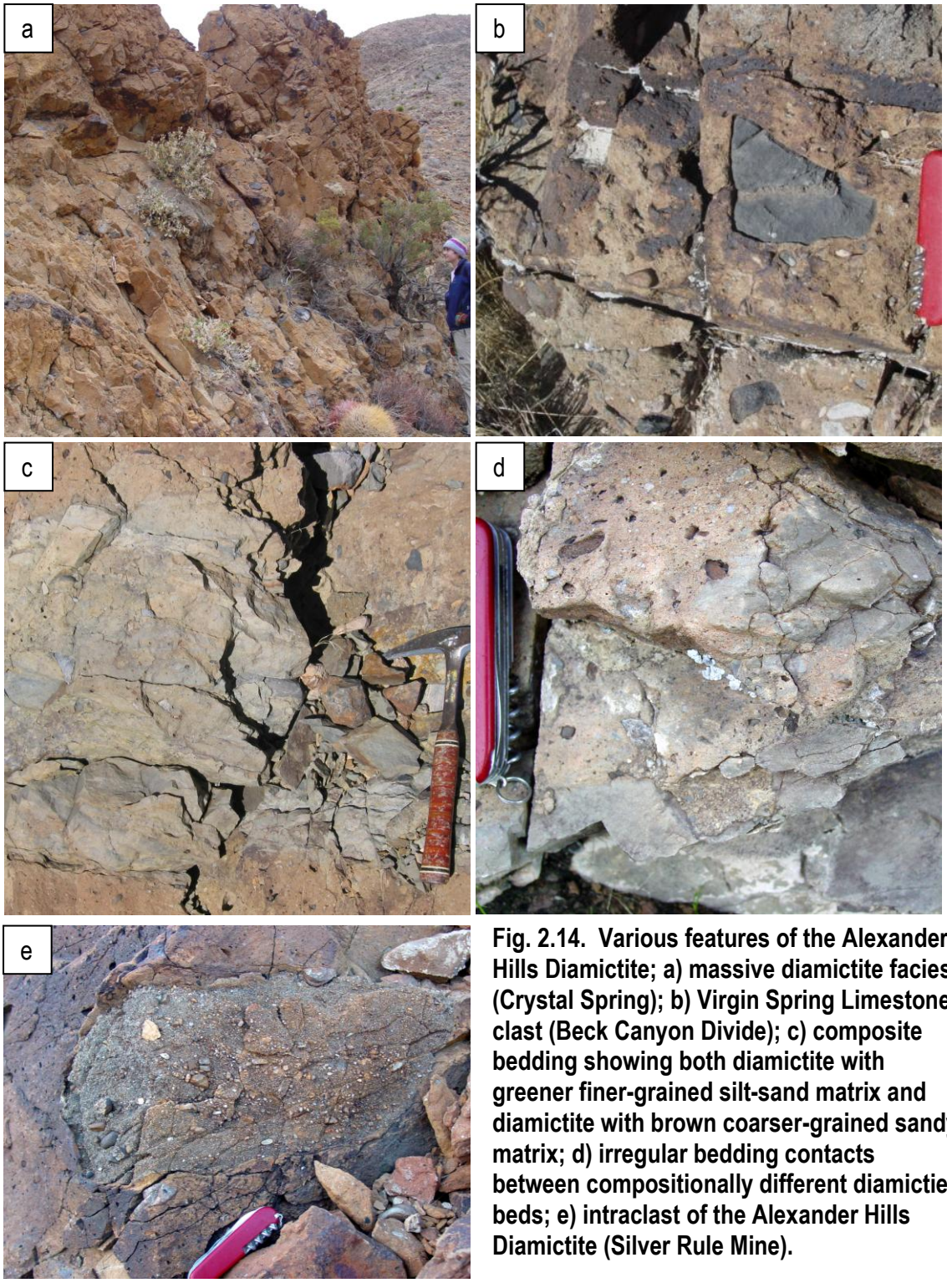

Fig. 2.14. Various features of the Alexander Hills Diamictite; a) massive diamictite facies (Crystal Spring); b) Virgin Spring Limestone clast (Beck Canyon Divide); c) composite bedding showing both diamictite with greener finer-grained silt-sand matrix and diamictite with brown coarser-grained sandy matrix; d) irregular bedding contacts between compositionally different diamictie beds; e) intraclast of the Alexander Hills Diamictite (Silver Rule Mine).

energy. The massive diamictite facies of Alexander Hills Diamictite thus occur in tidal associated settings, likely in shallow water as well as deeper water settings.

Clast composition in the massive diamictite facies of Alexander Hills Diamictite is dominated by local lithologies and includes: 1) sub-angular blue-gray oolitic and cherty dolostone from the underlying Beck Spring Dolomite, 2) rounded vein quartz and quartzite, 3) sub-angular green siltstone and black limestone from the immediately underlying Saratoga Hills Sandstone-Virgin Spring Limestone, 4) sub-angular tan microbially laminated dolostone of the Crystal Spring Formation, and 5) sub-rounded basement gneiss and granite. Intraclasts of what appear to have been unlithified Alexander Hills Diamictite material also occur, indicating some internal reworking (Fig. 2.14e). The Virgin Spring Limestone clasts are distinguished from other carbonate units by parallel laminations, ooids, black color, more positive $\delta^{13}C$ and more depleted $\delta^{18}O$ and a calcitic mineralogy and are readily recognizable in the basal sections of the Alexander Hills Diamictite. The majority of clasts is cobble-sized, but range from pebble-sized to the occasional m-scale boulder. Larger clasts are typically quartzite, from the Beck Spring Dolomite or the Crystal Spring Formation. Striations and facets are present on scattered clasts of chert, fine-grained quartzite or siltstone in most sections, though comprise only a small proportion of clasts and are difficult to locate.

Diamictite within the Alexander Hills Diamictite varies from bed to bed as well as regionally by clast composition and matrix. Where the massive diamictite facies occurs at the base of the Alexander Hills Diamictite, it contains a black calcitic bimodal matrix composed of silt-sized detrital

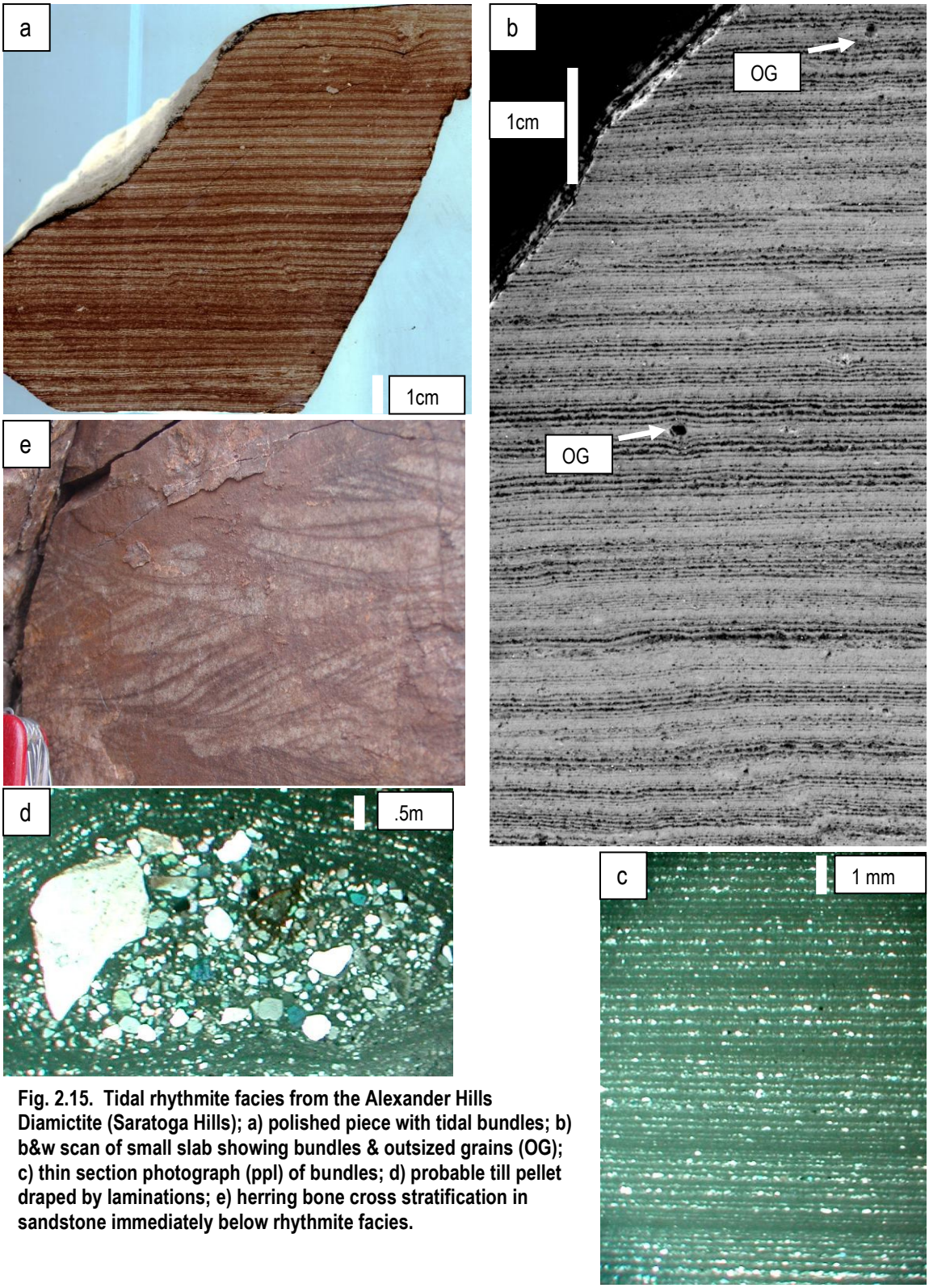

Fig. 2.15. Tidal rhythmite facies from the Alexander Hills Diamictite (Saratoga Hills); a) polished piece with tidal bundles; b) b&w scan of small slab showing bundles & outsized grains (OG); c) thin section photograph (ppl) of bundles; d) probable till pellet draped by laminations; e) herring bone cross stratification in sandstone immediately below rhythmite facies.

calcite grains and coarse to sub-rounded quartz sand associated with a high percentage of Virgin Spring Limestone clasts indicating local derivation with only minor transport. Other diamictite matrices are roughly grouped into two categories that are interbedded: 1) light brown and composed of quartz silt and coarse quartz sand or 2) green and composed of fine quartz sand along with some medium- to coarse-grained quartz sand and chlorite (Fig. 2.14c). Absent fresh surfaces, chipping away weathering rinds through most sections reveals diamictite with composite bedding of alternating types of matrix and clasts.

Finer-grained intervals appear in at least three Alexander Hills Diamictite sections. In the Saratoga Hills, an ~20 m thick fining-upwards interval of interbedded coarse sandstone with herring-bone cross-bedding (Fig. 2.15e), pebble conglomerate, graded beds with wavy cross-lamination, reactivation surfaces, pebble-conglomerate bases and sandy tops, diamictite beds with erosional bases and very fine-grained green planar laminated sandstones. This green planar laminated sandstone is comprised of bundles of light-dark laminae couplets (Fig. 2.15a-c).

Bundles average 7-10 couplets each and individual couplets contain a light colored fine quartz sand laminae, often 1-2 grains in thickness, capped by a dark-colored silt and clay laminae; the upper third to quarter of each bundle is composed of the same silt and clay forming the upper laminae in each couplet and possible till pellets are found within bundles (Fig. 2.15d). Laterally and vertically this interval is cut out by a continuous succession of stacked channelized beds within the massive diamictite facies. The geometry of this window of fine grained sediments suggests deposition as background sediment truncated by an active area of subaqueous diamicton debris

flows. In the southern Saddle Peak Hills, a 10 m thick interval of interbedded sandstone and siltstone also appears within the middle of the Alexander Hills Diamictite. In the lower third of the Alexander Hills Diamictite section in the Alexander Hills, a 4-5 m thick interval of cross-stratified and channelized pebble-conglomerate indicates deposition by traction currents and is separated by a several meter thick bed of diamictite from a 10 cm thick bed of laminated siltstone.

Mineralogy: Thin sections studied (n=40) reveal diamictite bi-modal smaller component grains are sub-rounded to very-angular and poorly sorted (Fig. 2.16). Grains are dominantly quartz, but feldspar (Fig. 2.16b) and lithic grains (Fig. 2.16f) are also present. Matrix material is either composed of very fine quartz sand (Fig. 2.16a), greenish-yellow clay (Fig. 2.16c) or carbonate (Fig. 2.16d). Towards the base, the diamictite contains a higher percentage of Virgin Spring Limestone clasts and the diamictite matrix is more typically dark black to the eye, carbonate-rich (Fig. 2.16d) and often contains spherules from the Virgin Spring Limestone.

Sedimentary Contacts: The Alexander Hills Diamictite overlies erosionally truncated Saratoga Hills Sandstone and siltstone (Fig. 2.11c) in all localities. The typical amount of erosional relief is between 10 and 30 cm over lateral distances of several meters, although up to 30 m of erosional relief occurs at Virgin Spring Wash. In some localities, such as the Coral Section, the Alexander Hills Diamictite fills vertical walled erosional cuts indicating the Saratoga Hills Sandstone was lithified prior to Alexander Hills Diamictite deposition. At Virgin Spring Wash, Ibex Hills and the Saratoga Hills, Alexander Hills Diamictite overlies laminated black limestone. The Alexander Hills Diamictite rests on Beck Spring Dolomite in the central Alexander Hills (Fig. 1.2) where it can be

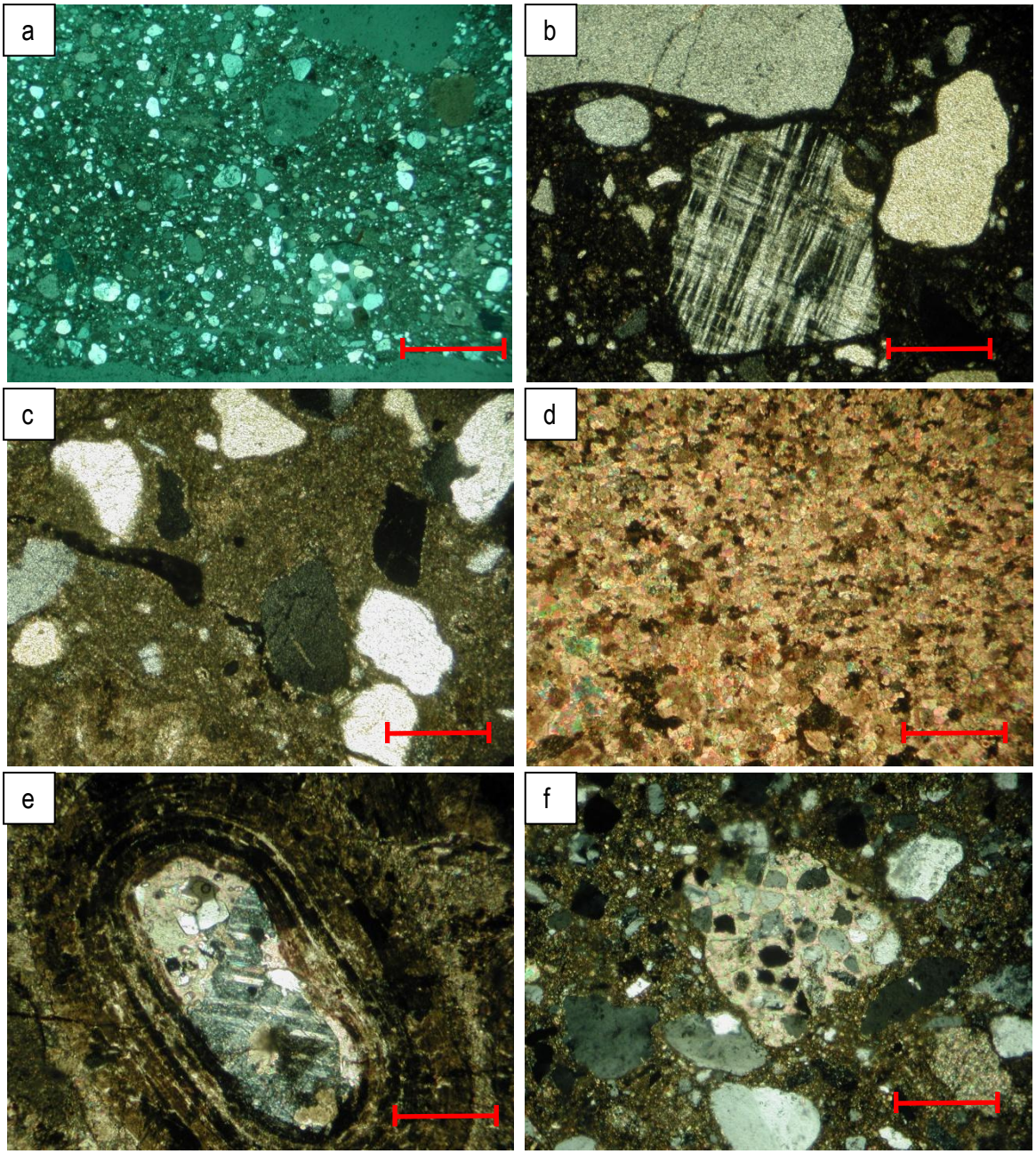

Fig. 2.16. Thin section micrographs of the Alexander Hills Diamictite. Scale bar = 0.5 mm. Sample locations are indicated in Appendix A.

a. 110605-6
b. 120305-4
c. 031906-3
d. 032505-2
e. 030505-3
f. 121706-2

traced continuously resting on progressively older horizons from the south to north. The contact with the lower Silver Rule Mine Member is abrupt. The massive diamictite facies characteristic of Alexander Hills Diamictite is interbedded with Silver Rule Mine Member up to 30 m above the transition.

Variability: Like the Saratoga Hills Sandstone, thickness variation in the Alexander Hills Diamictite does not appear to be dependent on the position of the section relative to the basin margin. Thickness varies from 5 to >200 m over <10 km within the Kingston Range. From the west end of Beck Canyon to the Horsethief Springs, the diamictite thickens and thins between 5 and 80 m. In the Horsethief Mine section (Fig. 2.1 and Fig. 2.4 #6), the thickest section measured, the diamictite varies laterally between 50 and >200 m over a distance of several km. Clast composition in the Kingston Range Alexander Hills Diamictite sections are dominated by more angular carbonate clasts while those to the southwest, Saratoga Hills, Saddle Peak Hills and the Ibex Hills, contain a significantly higher proportion of well-rounded quartz.

5.4. Description of the Silver Rule Mine Member

Sedimentary Description: The Silver Rule Mine Member initiates a prominent coarsening-upwards trend in the upper KPF. It is >2 km thick, dominated by event beds and gradationally coarsens upwards from shallow marine laminated siltstones and graded debrites into megabreccias and km-scale olistoliths of underlying platformal carbonates. It terminates with >1000 m of terrestrial fanglomerates and talus paleoslope deposits (Fig. 2.4 #6). The interval is wedge-shaped in outcrop pattern across the two mapped regions as well as through the entire Kingston Range (Fig.

2.10), thickens laterally away from paleo-fault scarps from 100 to 3000 m over 8 km and represents an abrupt transition from glacial to tectonic control on sedimentation and consequent preservation of the underlying glacigenic deposits. Though the interval is dominated by coarse tectonic deposits, diamictite with striated clasts in the lower 100 m and at its upper contact with the Noonday Dolomite preserves a periodic climate signal.

The Silver Rule Mine Member is 110 to 2300 m thick (Fig. 2.4 & Plates 2 & 3) and can be roughly divided into a lower relatively finer grained shallow marine facies succession (Fig. 2.17) and an upper coarsening-upward succession of interbedded sandstone and siltstone, debrite, diamictite, megabreccia and km-scale olistoliths (Fig. 2.18). In the Kingston Range-Alexander Hills area, the lower and upper facies of the member are separated from each other by a gradational transition from bedded sandstones and siltstones of the lower facies to debrite and mega-breccia deposits in the upper facies. The lower facies sharply overlies the Alexander Hills Diamictite with no evidence of truncation or topographic relief in the underlying diamictite and marks an abrupt change from coarse-grained Alexander Hills diamictite to 5-15 cm beds of finely laminated green to lavender quartz siltstone and sandstone. Interbedded with the siltstone and sandstone beds and often filling shallow channels are similar-sized beds of graded debris flows and diamictite. Many of the sandstone and siltstone beds contain outsized clasts, but in most cases these beds are vaguely graded with coarse-sand or pebble bases and laterally (along bed) sediments coarsen over meters into debrites; outsized clasts have not been observed completely isolated within continuous beds of laminated fine-grained sediments. Depending on the section measured, 2 to 5 beds of diamictite, lithologically similar to the Alexander Hills Diamictite, occur within the first 30-50

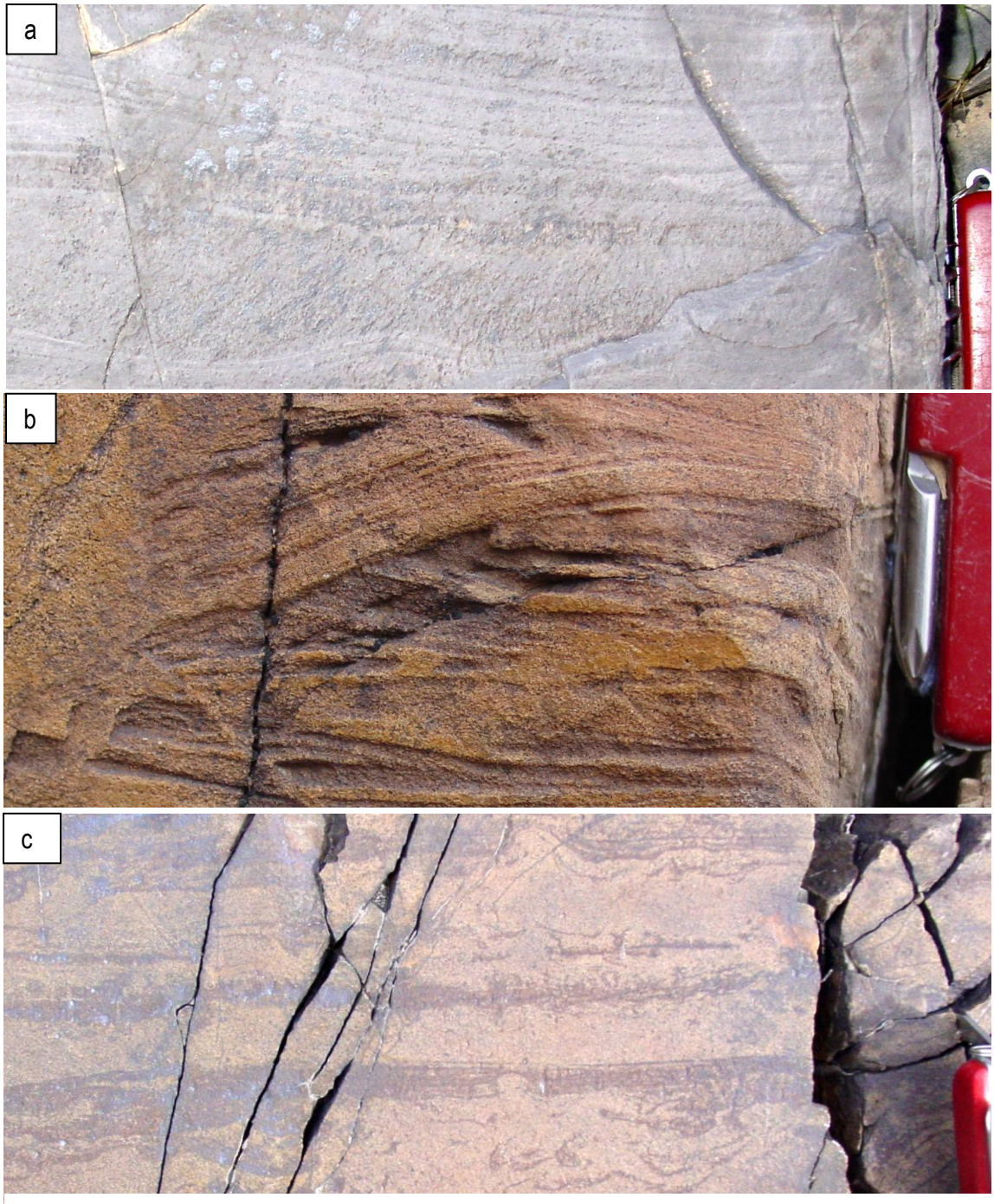

Fig. 2.17. Various sedimentary structures in the finer-grained Silver Rule Mine Member intervals; a) alternating massive sandstone infilling wavy and parallel laminated sandstone with ripples (Horsethief Mine); b) cross-laminations and ripples (Crystal Spring); c) massive sandstone with caps of parallel laminated fine-grained sandstone; sandstone has ripples, dewatering and injection of massive sandstone into overlying laminations (Beck Canyon Divide).

m of the lower Silver Rule Mine Member. These m-scale diamictite intervals contain the same mixture of clasts as the Alexander Hills Diamictite, including clasts of the Virgin Spring Limestone. Fine-grained facies are typically planar laminated but may also display soft-sediment deformation, cross-lamination, convolute and diffuse bedding contacts and tee-pee folds (Fig. 2.17a-c).

The transition to the upper coarse-grained facies of the Silver Rule Mine Member in the Kingston Range occurs above a 2-3 m thick dolostone marker bed and is characterized by the appearance of boulder- to m-scale outsized clasts within conglomerates and debris flows both below and above the dolostone bed. The dolostone bed is comprised of oncolitic, microbially laminated and intraclastic facies as well as microfossil-bearing chert (Corsetti et al., 2003), is discontinuous between sections and often has karstic features on its upper surface. The upper part of the member is comprised of interbedded diamictites, conglomerates, sandstone and megabreccia. In deeper sections sandstones are within turbididte intervals (Fig. 2.18a). Diamictites in the upper Silver Rule Mine Member have erosional bases, a quartz sand matrix with angular clasts of Beck Spring dolomite and rounded quartzite; they do not contain striated clasts or material from the Virgin Spring Limestone (Fig. 2.18b & c). Conglomerates are both normally- and reverse-graded, sometimes have erosional lower contacts, and fill 20-40 m wide shallow (<1 m) channels and are interbedded with massive or thickly (~1 cm) laminated quartz sandstone beds. Conglomerates are composed of clasts of angular to sub-angular Beck Spring Dolomite and rounded quartzite (Fig. 2.18d) in a coarse quartz sand matrix. Another characteristic facies in the upper Silver Rule Mine Member are 10-30 m thick wedge-shaped layers of sedimentary breccia

Fig. 2.18. Characteristic intervals within the upper Silver Rule Mine Member; a) turbidites interbedded with debrite and sedimentary breccia (Horsethief Mine); b) contact between massive sandstone, sedimentary breccia and diamictite facies (Crystal Spring); c) contact between siltstone and normally graded conglomerate facies (Alexander Hills); d) quartz cobble diamictite (Beck Spring Divide).

derived from the Beck Spring Dolomite and that fill steep and narrow (i.e. 20 m wide x 10-20 m deep) channels and cut out underlying units.

The Beck Spring Dolomite is the primary source of clasts in the coarse-grained facies of the Silver Rule Mine Member. However, sandstone and carbonate clasts from the Crystal Spring Formation as well as m-scale rounded granite boulders from the underlying basement are not uncommon. Scattered rounded to sub-angular cobbles and small boulders begin to appear in the lower Silver Rule Mine Member below the dolostone oncolitic marker bed and increase in size upward to several meters in diameter within the Beck Canyon sections and in the Alexander Hills. These large clasts are scattered throughout less coarse facies, but are spatially associated with debrites. South of Beck Canyon along the eastern flank of the Kingston Range, the Silver Rule Mine Member hosts km-scale olistoliths (Wise et al., 1999; Wright et al., 1974) and megabreccia comprised of m-scale to dam-scale blocks of Beck Spring dolomite. In some cases, the upper Crystal Spring Formation remains attached to the base of Beck Spring Dolomite olistoliths (Calzia et al., 2000) and one 1.4 km long olistolith derived from the Crystal Spring Formation was large enough to mine for associated talc deposits. Olistoliths of the Crystal Spring Formation appear stratigraphically above Beck Spring Dolomite olistoliths in reverse of their stratigraphic order.

West of the Kingston Range, the Silver Rule Mine Member becomes less varied and consists of a continuous succession of interbedded turbidites, graded debrites, diamictites and occasional sandstone beds. In the Sperry Hills, Saddle Peak Hills, Saratoga Hills and Ibex Hills, the Silver Rule Mine Member is less variable and largely comprised of 5-50 cm graded beds with

pebbly conglomeratic bases and coarse sandy tops interbedded with comparatively thicker diamictite beds filling shallow channels and massive sandstones. The majority of clast material is derived from the Beck Spring Dolomite, but includes a larger percentage of rounded quartz cobbles in these western sections than in the Kingston Range and Alexander Hills.

Mineralogy: Thin sections studied (n=52) reveal sandstone beds and matrix of diamictite and debrite beds are both compositionally and physically immature (Fig. 2.19). Quartz grains are poorly sorted overall and sub-rounded to very angular (Fig. 2.19a-c). Some beds are cemented with calcite (Fig. 2.19d) and others contain grains of carbonate (Fig. 2.19f). Diamictite beds in the upper Silver Rule Mine Member are similar to the diamictite in the underlying member and contain clasts of the Virgin Spring Limestone, including the characteristic spherules (Fig. 2.19e).

Sedimentary Contacts: While the lower contact with the Alexander Hills Diamictite is sharp without evidence of erosion, the upper contact with the Jupiter Mine Member is gradational and marked by disappearance of siltstone and sandstone interbeds and is characterized by the presence of graded breccias comprised primarily of Beck Spring dolomite or, in basinal sections, an increasing abundance of sedimentary breccias and conglomerates. In some basinal sections, like the Saddle Peak Hills, this transition is more difficult to define and based on a subtler increase of graded debris flows and conglomerates and a marked decrease in siltstone facies.

Variability: The Silver Rule Mine Member records the greatest amount of lateral variability of any of the four members. In the Kingston Range, its thickness changes over a distance of 8 km from 110 m at the Crystal Spring Mine to >2300 m at the Horsethief Mine (Fig. 2.4, Plate 2 and Plate 3),

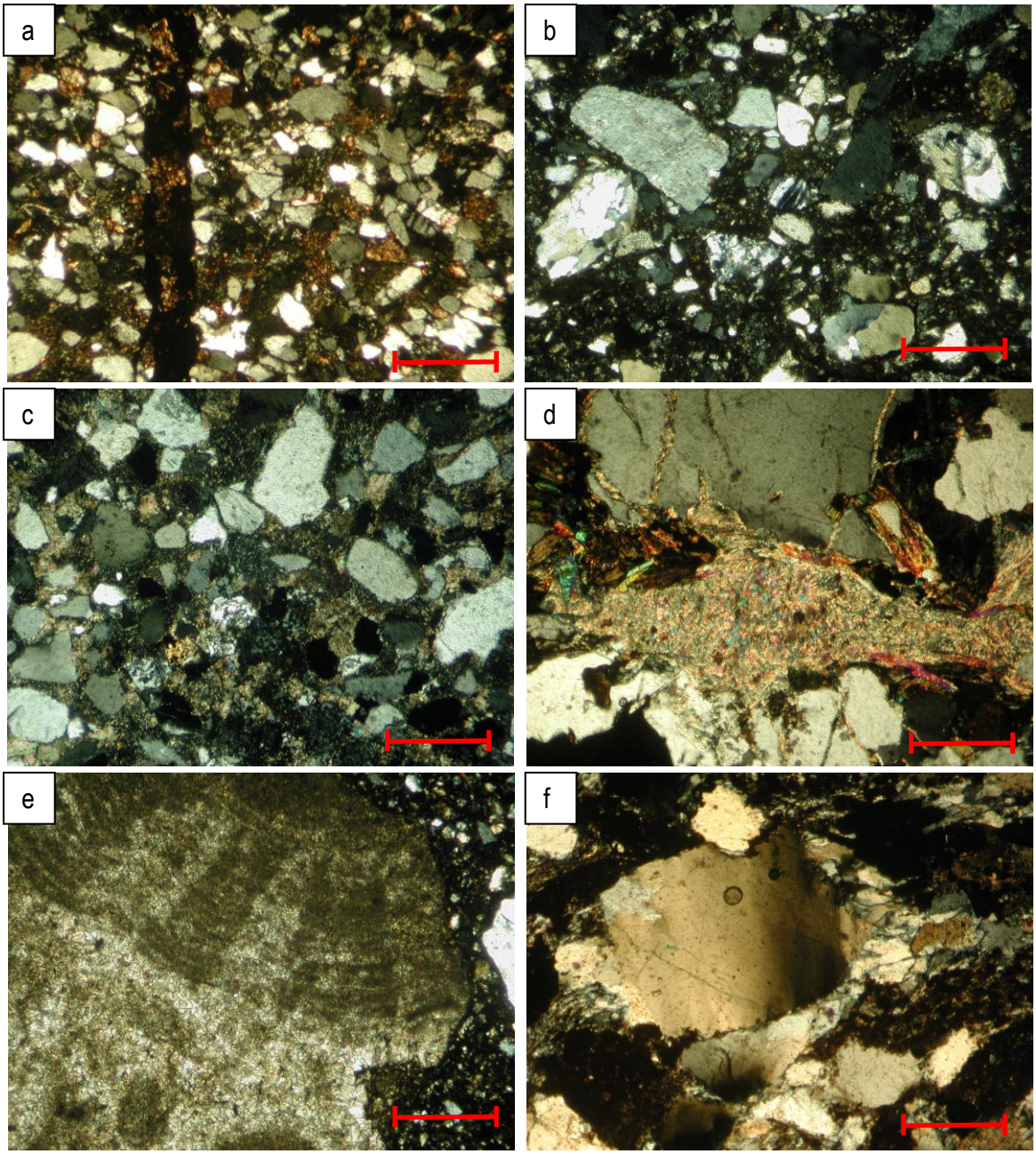

Fig. 2.19. Thin section micrographs of the Silver Rule Mine Member. Scale bar = 0.5 mm. Sample locations are indicated in Appendix A.

a. 0111705-20
b. 011705-14
c. 011705-21
d. 021405-2
e. 112005-14-16
f. 032105-4

where it comprises the bulk of the thickest KPF deposits (2300 of 3200 m; see Fig. 2.4 #6). The entire member records a vertical and lateral transition to coarser facies. Between the Sperry Hills and the Saddle Peak Hills, upper coarse-grained facies are limited to debrites with <m-scale outsized clasts while Beck Canyon margin slope sections include dam-scale mega-breccias filling channels and m-scale clasts. Ultimately, km-scale blocks of underlying platform carbonate were shed into the Silver Rule Mine Member in the southern Kingston Range in the deepest part of the clastic wedge (Fig. 2.10).

5.5. Jupiter Mine Member: Sedimentary Breccia and Conglomerate Facies

Sedimentary Description: The Jupiter Mine Member in the Kingston Range and in the Alexander Hills is comprised of massive ungraded sedimentary breccias and graded beds of breccia and conglomerate (Fig. 2.20). Graded beds are typically composed of angular carbonate and sub-rounded quartzite (Fig. 2.20a) with sandy tops. Carbonate clasts are dominantly Beck Spring Dolomite, which are the only lithology comprising many debrites (Fig. 2.20b & c) and graded beds (Fig. 2.20b). Other beds are composed of coarse sandstone, sometimes graded with pebble bases. Contacts between beds are planar to gently inclined, defining shallow dam-scale channels filled with breccia. Monomictic ungraded intervals often fill more steeply inclined channels. Graded sedimentary breccias beds are identical to fanglomerate beds forming in the region today (Fig. 2.20d). Mega-breccia beds may have m-scale clasts, but very few outsized clasts (i.e. m-scale clasts associated with graded beds of dm-scale clasts). Near the Snow White Mine in the Kingston

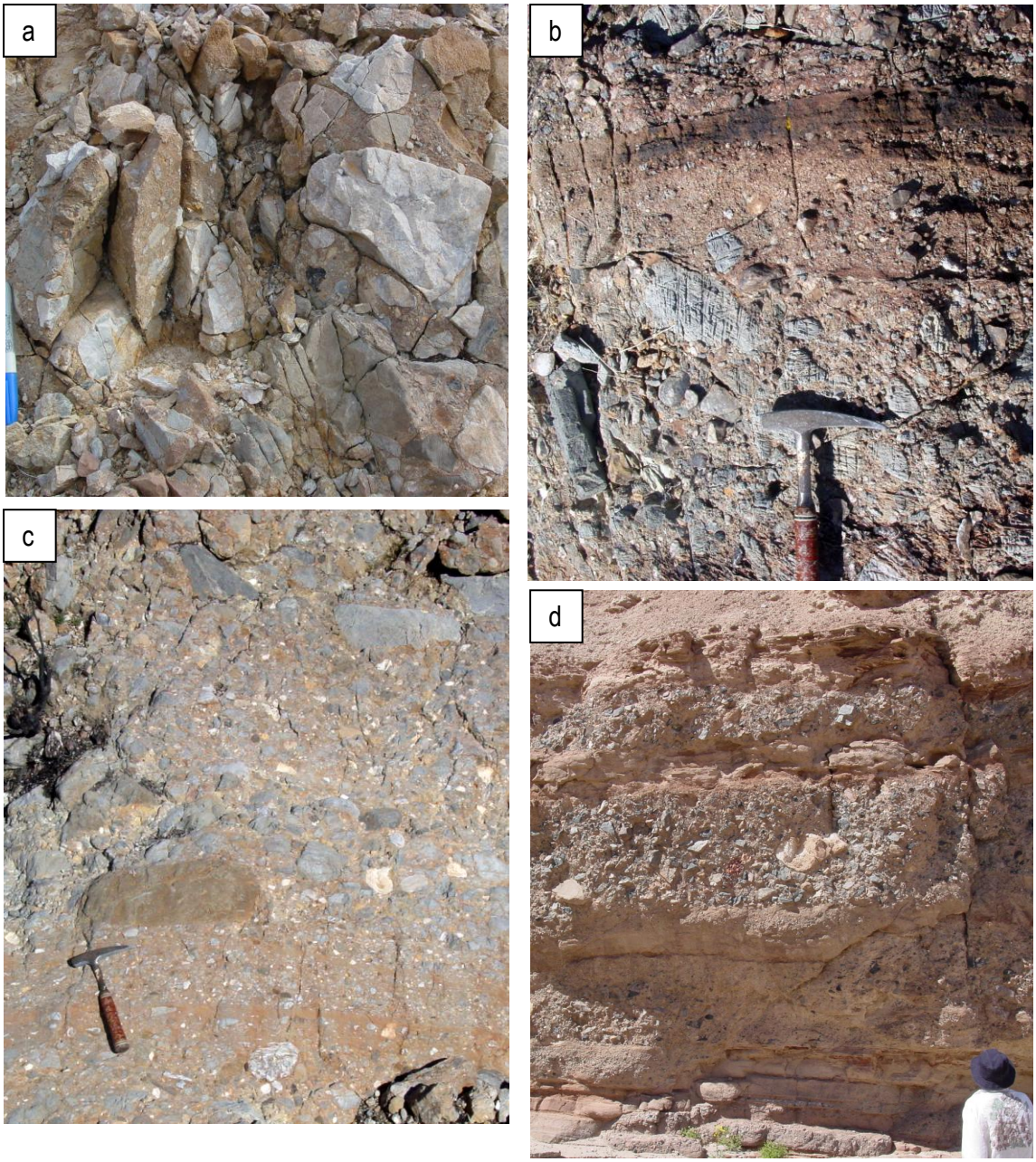

Fig. 2.20. Coarse-grained facies of the Jupiter Mine Member; a) angular quartz cobbles in diamictite--6" pen for scale (Snow White Mine); b) graded fanglomerate with coarse-grained sandy cap (Beck Canyon Divide); c) Beck Spring clast dominated fanglomerate (Snow White Mine); d) modern analog to Jupiter Mine Member-modern fan deposits (CC Canyon).

Range, 50-100 m thick monomictic breccias of Beck Spring dolomite define the basal Jupiter Mine Member wedging in between the upper Crystal Spring Formation and the overlying Noonday Dolomite. This monomictic Beck Spring Dolomite breccia is overlain by a wedge of polymictic graded breccia and conglomerate beds that thickens southwestwards and northwestwards into the full Jupiter Mine Member.

Mineralogy: Thin sections studied (n=23) reveal matrix material of debrites and sedimentary breccias if compositionally and physically immature, as with the rest of the formation (Fig. 2.21a-c). Some beds retain carbonate-rich matrices (Fig. 2.21a). Grains are usually more rounded than in the underlying Silver Rule Mine Member but very poorly sorted. Lithic grains (Fig. 2.21c) are common.

Sedimentary Contacts: The contact with the underlying Silver Rule Mine Member is gradational and defined by the disappearance of siltstone and finer-sandstone facies, disappearance of sedimentary structures indicating rapid deposition and a further coarsening in grain size. The Silver Rule Mine Member-Jupiter Mine Member sequence thus represents the primary coarsening upwards interval in the Kingston Peak Formation. The contact with the overlying Noonday Dolomite is often faulted where sections of now inclined Noonday Dolomite have slipped down slopes of the underlying KPF. The contact normally has undergone alteration from fluid movement along the fault contacts. Where the sedimentary contact is preserved it is normally sharp, recording a rapid change in depositional setting and resumption of the carbonate factory. This contact has been interpreted as an angular unconformity (Wright et al., 1974) in the past, but is

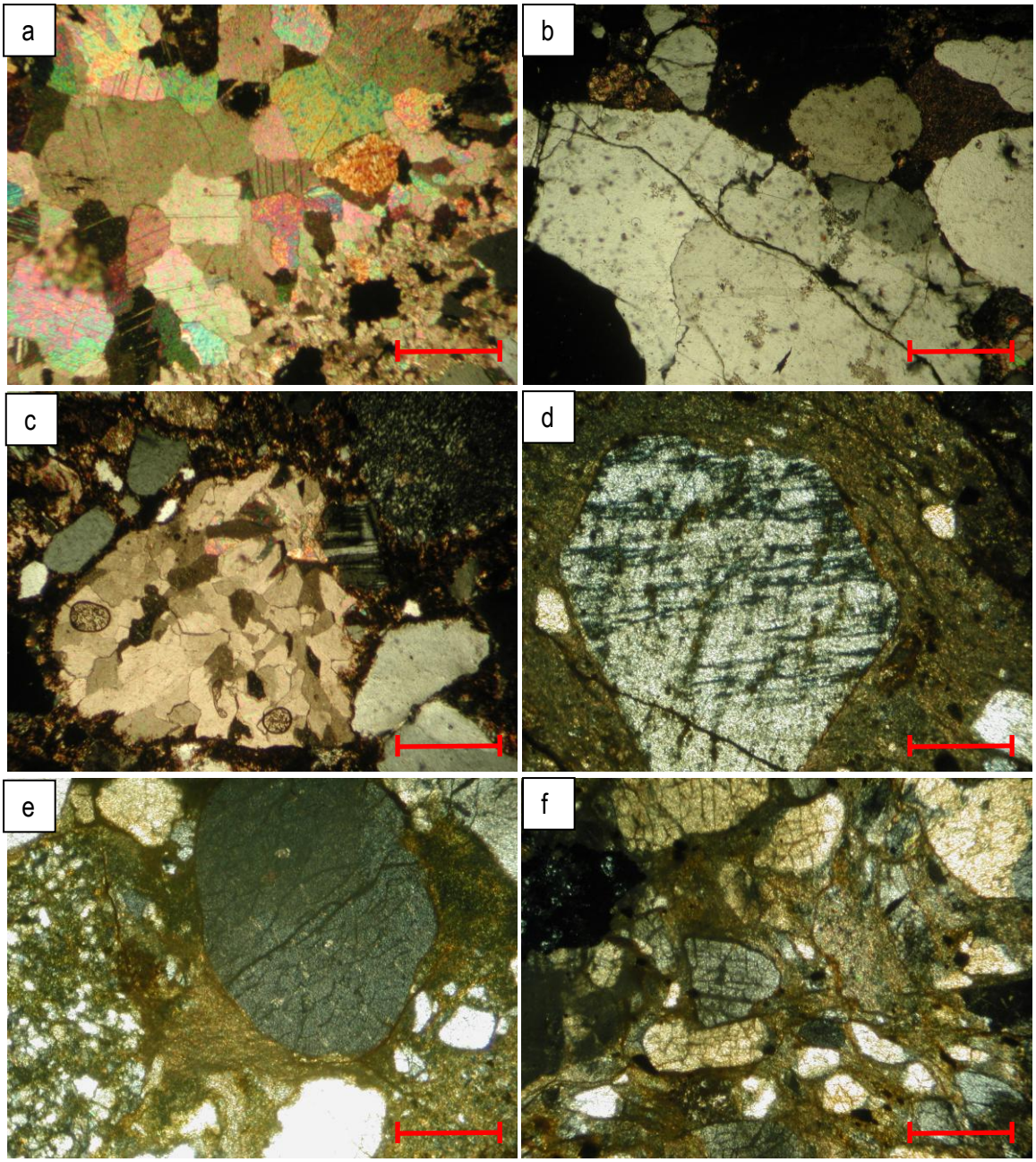

Fig. 2.21. Thin section micrographs of the Jupiter Mine Member. Scale bar = 0.5 mm. Sample locations are indicated in Appendix A.

a. 032105-2
b. 022705-3
c. 011705-5
d. DS 65
e. 013106-5
f. 020106-8

here reinterpreted as conformable based on the observations summarized above (also section 4.3, Fig. 2.8 & 2.9) and described in more detail below.

In the Alexander Hills, the uppermost Alexander Hills Diamictite is interbedded with the lowermost Noonday Dolomite. Several thin (20-50 cm) beds of sedimentary breccia dominated by clasts of Beck Spring dolomite are interbedded several meters above the initial contact between the Noonday Dolomite identifying contemporaneous deposition. The clasts in the basal Noonday Dolomite are not comprised of Noonday dolomite intraclasts, but of the same distinct suite of lithologies making up the underlying Alexander Hills Diamictite. They are also not derived from a reworking of lithified Alexander Hills Diamictite surface but appear to represent a mixture of the two ongoing depositional processes.

In the Alexander Hills and throughout the Kingston Range, it is common to see clasts up to 50 cm in size, but normally <10 cm, floating in the base of the Noonday Dolomite. Clasts are not comprised of broken pieces of the multi-lithologic Alexander Hills Diamictite breccia below but are individual clasts of angular carbonate or sub-rounded quartzite floating in the dolomitic matrix of the basal Noonday Dolomite in what appears to be mass flows shed from the flanks of growing Noonday Dolomite mounds and mixed with clasts of the unlithified and loose Alexander Hills Diamictite.

The above relationship is similar to that seen in the Ibex Hills where dm-scale blocks of the Noonday Dolomite occur in debris flows of the Alexander Hills Diamictite that were unlithified at the time of slope failure (DeYoung, 2005; Troxel, 1982a; Wright et al., 1974). Four, in the southern

Valjean Hills, a distinct diamictite with buff-colored carbonate clasts is interbedded with Alexander Hills Diamictite diamictite rich in Beck Spring Dolomite clasts. Approximately ½ mile away, these buff-colored carbonate clasts appear stratigraphically above debris flows laden with Noonday Dolomite material.

Variability: In the Kingston Range, the Jupiter Mine Member thickens from 140 to 900 m over 8 km between Crystal Spring, at the basin margin, and Horsethief Mine in the basin center. In the Alexander Hills, where the Alexander Hills Diamictite-Jupiter Mine Member interval wedges in between the Noonday Dolomite and the underlying Saratoga Hills Sandstone erosional truncation, the Jupiter Mine Member-Noonday Dolomite contact is faulted and consequentially some of the Jupiter Mine Member breccia may have been thinned here by faulting, but geologic mapping (Plates 1 & 4) and contact relations show a systematic thickening and onlapping of the Jupiter Mine Member away from the basin margin (Fig. 2.10, Fig. 4.9 & Plates 2 & 3). In the Kingston Range, the proportion of sandy turbidites in the Jupiter Mine Member increases basinwards; this relationship is most apparent in the Horsethief Mine section (Fig. 4.17). West of the Kingston Range in the Sperry/Saddle Peak/Saratoga/Ibex Hills sections, there are fewer differences between the Silver Rule Mine Member and Jupiter Mine Member, which are both largely comprised of interbedded sandy turbidites, diamictites and graded conglomerate/breccia beds.

5.6. Gunsight Diamictite

Sedimentary Description: At the Jupiter Mine, a thin (2-30 m) interval of striated clast-bearing diamictite is sandwiched between beveled Crystal Spring Formation and the Noonday Dolomite

(Fig. 2.22a & b). This member was informally named the "Gunsight Diamictite" (Troxel, per comm. 2002.) after the diamictite underlying the Noonday Dolomite at the Gunsight Mine where striated and faceted clasts were first documented in the KPF by Hazzard (1939). Excellent exposures of this striated clast-bearing diamictite can be seen along the entire margin of the basin, especially the west end of Beck Canyon, the War Eagle Mine in the southern Nopah Mountains and throughout the eastern Kingston Range and in the Mesquite Mountains, many kilometers from the presumed basin margin. The matrix of the diamictite varies from coarse sand to silty, the clast composition is dominated by quartzite (Fig. 2.23), basement clasts, and chert instead of carbonate and diamictite outcrops typically weather to a dark black to purple.

Mineralogy: Examination of thin sections (n=21) show the smaller grain component of diamictite is composed of sub-rounded to sub-angular grains, grains are very poorly sorted but compositionally and physically more mature than underlying diamictite intervals (Fig. 22d-f). Matrices observed are typically some combination of clay and silt; no carbonate matrix was observed.

Sedimentary Contacts: The lower and upper contacts with the diamictite are sharp and abrupt. At Jupiter Ridge the Gunsight Diamictite overlies a brecciated erosional contact in the upper Crystal Spring Formation. In the eastern Kingston Range and in the Mesquite Mountains a thin (1-10 m) layer of diamictite overlies basement, has been heavily altered, and is in turn sharply overlain by the Noonday Dolomite. No interbedding has been observed between the Gunsight Diamictite and the Noonday Dolomite, as with the Jupiter Mine Member and the Noonday Dolomite.

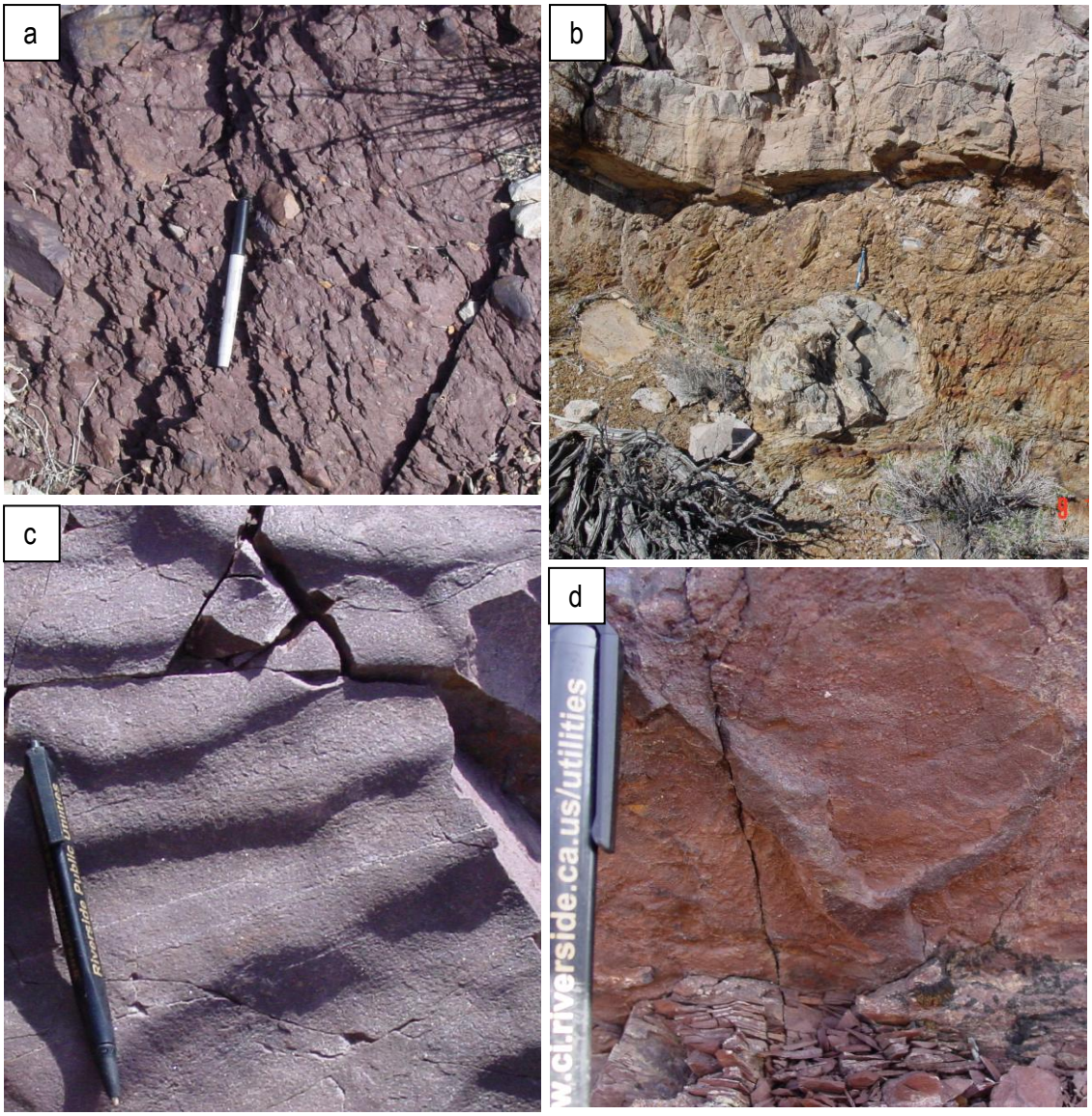

Fig. 2.22. Various facies within the Gunsight Diamictite; a) striated clast bearing diamictite (Jupiter Mine); b) 8" rounded quartz cobble clast in diamictite beneath sharp contact with Noonday Dolomite (Jupiter Mine); c) ripple casts on the soles of sandstone beds from rare finer-grained facies (Jupiter Mine); d) cast of mud cracks from sandstone (Jupiter Mine).

Variability: The Gunsight Diamictite varies between 1 and ~60 m in thickness. Near the basin margin it is typically 1-10 m thick and ubiquitously massive and unbedded. Basinwards, several meters of a quartzite-bearing diamictite is often sandwiched between the Noonday Dolomite and the Jupiter Mine Member; this can appear as one or more distinct beds of massive diamictite with clast compositions distinctly different than the underlying Jupiter Mine Member carbonate dominated breccias. The clast composition of the Gunsight Diamictite varies by section. A more complex section of the Gunsight Diamictite is located at Jupiter Ridge where facies include interbedded quartzite filling m-scale channels, cm-scale bedded siltstone with ripples and mudcracks and diamictite with striated clasts (Fig. 2.22c & d). In the sections west of the Alexander Hills-Kingston Range, there is no obvious distinctly different diamictite interval between the Jupiter Mine Member and the Noonday Dolomite. However, in the southern Black Mountains near the Jubilee Mine, several meters of diamictite fills small channels in discontinuous lenses between the Beck Spring Dolomite and the Noonday Dolomite. This diamictite thickens southward over several km to ~20 m at Virgin Spring Wash between the Alexander Hills Diamictite and the basin facies of the Noonday Dolomite. The Gunsight Diamictite is also present between the Crystal Spring Formation and the Noonday Dolomite at the Eclipse Mine in Ibex Hills. Thirty km northwest in the Panamint Range, a similar several meter interval of diamictite rests between the Noonday Dolomite and the Crystal Spring Formation in Galena Canyon.

5.7. Clast Composition of coarse-grained members

Table 2.2 shows the compilation of clast counts from coarse-grained units (diamictite and fanglomerate) in the Kingston Peak Formation. Clasts that stand out both visually and statistically are both those of the Virgin Spring Limestone and the Beck Spring Dolomite. The base of many Alexander Hills Diamictite sections is dominated by clasts of the Virgin Spring Limestone. Coarse-grained intervals in the Jupiter Mine Member are dominated by clasts of the Beck Spring Dolomite. Trends in clast composition support a progressive unroofing sequence. These trends are discussed in detail in Chapter Three.

	Alexander Hills Diamictite: clast composition basal sections	Alexander Hills Diamictite: clast composition middle sections	Alexander Hills Diamictite: clast composition upper sections	Alexander Hills Diamictite: clast composition all complete sections	Silver Rule Mine Member: diamictite facies	Jupiter Mine Member: fanglomerate facies	Gunsight Diamictite
Quartzite	13%	61%	45%	27%	20%	19%	13%
Basement (igneous)	3%	13%	10%	9%	11%	0%	0%
Basement (metamorphic)	2%	0%	0%	1%	0%	0%	24%
Crystal Spring Formation (carbonate)	0%	9%	1%	4%	7%	10%	47%
Crystal Spring Formation (sandstone)	0%	4%	0%	1%	0%	3%	0%
Crystal Spring Formation Diabase	0%	0%	0%	2%	0%	0%	0%
Beck Spring Dolomite	4%	0%	0%	2%	26%	65%	0%
Saratoga Hills Sandstone	1%	6%	30%	9%	11%	3%	16%
Saratoga Hills Sandstone (coarse facies)	3%	0%	4%	5%	1%	0%	0%
Virgin Spring Limestone	73%	6%	11%	38%	24%	0%	0%

Table 2.2: Clast compositions of different Kingston Peak Formation members, by percentage.

6. Discussion

The Saratoga Hills Sandstone parallel-laminated sandstone was interpreted by Tucker (1986) as having been deposited on a marine shelf by storm currents and the overlying laminated Virgin Spring limestone as a deeper water carbonate environment with periodic input of sand and

Fig. 2.23. Intrusion and injection of Jupiter Mine Member sedimentary breccia, dominated by Beck Spring Dolomite clasts, into compositionally varying Gunsight Diamictite (Horsethief Mine).

ooids by storms. The unconformity that truncates the Virgin Spring limestone might be a result of either sea level fall from glaciation or tilting of hanging wall blocks during normal faulting. Erosional truncation in hanging wall sections indicates that while clasts from the underlying Pahrump Group in the Alexander Hills Diamictite provide a clear signal for initiation of tectonism, initial exposure and erosion across the region may have been the result of ice growth and sea level change prior to local tectonism, as indicated by the presence of striated clasts. Another alternative is that the Saratoga Hills Sandstone and the Virgin Spring Limestone are lacustrine, deposited in rift lakes; this possibility is discussed in more detail in Chapter 2.

The Alexander Hills Diamictite was likely deposited in a glacio-marine setting. It either underwent gradual downslope reworking (Boulton and Deynoux, 1981) on the same broad shallow shelf on which the Saratoga Hills Sandstone and Virgin Spring limestone were deposited, or was subject to retransport down oversteepened debris aprons. There is no evidence of laminations within the diamictite facies hosting outsized clasts expected from rainout of ice rafted debris. Convolute bedding contacts between diamictite event beds indicate rapid deposition. The presence of tidalites indicates deposition in a marine setting by Alexander Hills Diamictite time.

The Silver Rule Mine Member records the greatest lateral thickness changes of all the KPF members and represents the most active phase of tectonism in the KPF, perhaps equivalent to a rift climax (Prosser et al., 1993). The relatively finer-grained deposits at the base of the member and associated olistoliths likely represent the climax stage of rifting in a sediment-balanced or sediment-overfilled rift basin. At this stage rift related subsidence is much greater than sediment

supply (Ravnas and Steel, 1998) coarser-grained deposits are relegated to settings near fault scarps. Diamictite intervals within the Silver Rule Mine Member with striated clast are interbedded with coarse-grained deposits interpreted to be a result of gravity driven debris flows down a rapidly tectonically steepening margin. The Horsethief Mine section (Fig. 2.4 #6) represents the deepest part of the basin preserved in the Kingston Range. The Silver Rule Mine Member there is comprised of a coarsening upwards sequence of interbedded coarse sandy turbidite intervals, coarse sand and pebble conglomerate and diamictite dominated with clasts of the Beck Spring Dolomite. Overall the deposits are finer-grained and than in Beck Canyon and the presence of dam-scale channels filled with coarse sandstone beds with low-angle cross-bedding indicates sedimentation was the result of reworking of more proximal deposits and delivery in both channels and s turbidity flows.

The Jupiter Mine Member is dominated by largely monomictic channelized sedimentary breccia deposits that likely represent terrestrial fanglomerate facies (Hewett, 1956). Lateral inter-fingering relations evident in the Kingston Range between graded sedimentary breccias beds, channels, and coarse sandstone beds suggests initial reworking of more proximal Jupiter Mine Member sediments with eventual infilling of the basin with distal fanglomerate facies as the availability of accommodation space slowed and was great outplaced by tectonically derived sediments.

The Gunsight Diamictite represents the initial transgressive deposit resulting from deglacial sea level rise and flooding of Jupiter Mine Member terrestrial deposits. Striated clasts may indicate

a final pulse of glaciation or simply a change in sediment supply from local fault scarps and reworking of glacigenic sediments. The abrupt and conformable transition to the overlying and regionally continuous platformal Noonday Dolomite and thickness of its microbial mounds (>200 m) suggest rapid flooding led to the condensed Gunsight Diamictite interval being covered by high stand deposits of the prograding Noonday Dolomite. Sea level rise may also be related, in part, to sediment loading. Regional cessation of tectonism cut off any source of siliciclastic sediments, facilitating construction of the Noonday Dolomite platform.

Tectonic and glacial deposits of the eastern KPF are bounded by the Beck Spring Dolomite and Noonday Dolomite carbonate platforms, overlie a regional unconformity, and record an abrupt change to siliciclastic sedimentation resulting from tectonic uplift. The wedge-shaped packaging of the KPF strata next to tilted and erosionally truncated segments of the underlying Pahrump Group and basement conforms to rotation of the hanging wall and footwall sections in extensional systems (Faerseth et al., 1997; Jackson et al., 2005; Jackson and White, 1989). Coarse-grained facies are primarily the product of local tectonic activity as indicated by: 1) syndepositional normal faults and erosional beveling of footwall blocks, 2) a systematic and consistent pattern of coarsening upwards from sand and angular cobble debrites to sedimentary breccia and km-scale olistoliths, 3) a transition from marine debris-flow facies to terrestrial fanglomerates and 4) a systematic pattern of unroofing of the underlying Pahrump group as seen in the sequence of dominant clasts. The occurrence of striated clasts in the Alexander Hills Diamictite and Silver Rule Mine Members indicates a glacigenic influence that is sporadic and limited to specific stratigraphic intervals.

The wedge-shaped geometry of the KPF (Fig. 2.10) is discussed in more detail in Chapter 4 and is characteristic of extensional terranes. Together with the presence of the regional unconformity, the problem of how the KPF-Noonday Dolomite contact can be interpreted as both conformable and unconformable can be resolved. The unconformity is present beneath the Noonday Dolomite in footwall sections and absent in hanging wall sections because it is an erosion surface generated by uplift, likely along rift flanks.

7. Conclusion

The Kingston Peak Formation in the Death Valley region is one of the few areas in the southern Cordillera where the association between extension and resulting Neoproterozoic sedimentation is clear (Burchfiel et al., 1992). This allows three competing hypotheses for the origin of Neoproterozoic glacial deposits to be tested. One, glacial sediments record a globally synchronous climate event (Snowball Earth) or two, glacial sediments record regional glaciation attributed to tectonism and terminated with the cessation of extension (i.e. zipper-rift model of Eyles & Januszczak (2004). Three, glacial sediments comprise an incomplete record of either regional glaciation or a long-term (50–100 Ma) Cryogenian glacial era (Allen and Etienne, 2008) with sedimentary evidence of glaciation only preserved during periods of tectonism and generation of accommodation space. In hypothesis two and three, the preservation of glacigenic sediments is linked with regional tectonism and therefore results in a diachronous record of glaciation.

Each of the three hypotheses makes specific predictions for the sedimentary record. In the first case, if the transgressive deposits of the Noonday Dolomite are related to global

deglaciation and not cessation of extension, syndepositional faulting should continue through the Noonday Dolomite. In the second case, carbonate deposition is related to transgression during thermal subsidence when tectonism ends; rising sea-level confines glacial evidence up-dip or may be entirely lacking because of slowdown in adiabatic cooling provided by uplift. In the last case, evidence for normal faulting should end underneath or at the base of the Noonday Dolomite; extension and uplift would provide accommodation space in shallow marine to terrestrial environments that rapidly preserve glacial sediments and provide a record of glaciation and climate change whose continuity and completeness is controlled by local tectonism. Glacial conditions may not be uniquely timed with glacial deposits, but rather glacial conditions were sampled by depositional conditions that allowed for these deposits to be preserved.

The intimate association between localized tectonically created uplift, accommodation space, and conglomeratic facies brings into question the suggestion that KPF strata record a regional component of synchronous glacial sedimentation associated with a global Neoproterozoic ice ages (Corsetti and Kaufman, 2003; Prave, 1999). The lack of geochronological data makes any global correlation problematic. Evidence in the Kingston Peak Formation provides more support for hypotheses two and three, supporting diachronous glacial deposition and cap carbonate deposition. These data support the argument that the Kingston Peak Formation, along with an increasing number of other Neoproterozoic deposits worldwide (Allen and Etienne, 2008), record part of a continual and diachronous climate record spanning the Cryogenian Period.

References

Abolins, M., Oskin, R., Prave, T., Summa, C., and Corsetti, F.A., 2000, Neoproterozoic glacial record in the Death Valley region, California and Nevada: GSA Field Guide, v. 2, p. 319-335.

Allen, P.A., and Etienne, J.L., 2008, Sedimentary challenge to snowball Earth: Nature Geoscience, v. 1, p. 817-825.

Armstrong, R.L., Eisbacher, G.H., and Evans, P.D., 1982, Age and stratigraphic-tectonic significance of Proterozoic diabase sheets, Mackenzie Mountains, northwestern Canada: Canadian Journal of Earth Sciences = Journal Canadien des Sciences de la Terre, v. 19, p. 316-323.

Bond, G.C., Christie-Blick, N.H., Kominz, M.A., and Devlin, W.J., 1985, An Early Cambrian rift to post-rift transition in the Cordillera of western North America: Nature, v. 315, p. 742-746.

Boulton, G.S., and Deynoux, M., 1981, Sedimentation in glacial environments and the identification of tills and tillites in ancient sedimentary sequences: Precambrian Research, v. 15, p. 397-422.

Burchfiel, B.C., Cowan, D.S., and Davis, G.A., 1992, Tectonic overview of the Cordilleran Orogen in the Western United States, *in* Burchfiel, B.C., Lipman, P.W., and Zoback, M.L., eds., The Cordilleran Orogen; conterminous U.S.: United States (USA), Geol. Soc. Am.

Calzia, J.P., Troxel, B.W., Wright, L.A., Burchfiel, B.C., Davis, G.A., and McMackin, M.R., 2000, Geologic map of the Kingston Range, southern Death Valley, California, Open-File Report - U. S. Geological Survey, p. 2 sheets.

Carlisle, D., Kettler, R.M., and Swanson, S.C., 1980, Geological study of uranium potential of the Kingston Peak Formation, Death Valley region, California, Open File Report, U.S. Department of Energy.

Christie, K.W., and Fahrig, W.F., 1983, Paleomagnetism of the Borden dykes of Baffin Island and its bearing on the Grenville Loop: Canadian Journal of Earth Sciences = Revue Canadienne des Sciences de la Terre, v. 20, p. 275-289.

Christie-Blick, N., and Levy, M., 1989, Stratigraphic and tectonic framework of upper Proterozoic and Cambrian rocks in the Western United States, *in* Christie-Blick, N., Levy, M., Mount, J.F., Signor, P.W., and Link, P.K., eds., ???: 28th International Geological Congress field trip guide series 7-21: Washington D.C., American Geophysical Union, p. 7-21.

Cloud, P., Wright, L.A., Williams, E.G., Diehl, P.E., and Walter, M.R., 1974, Giant Stromatolites and Associated Vertical Tubes from the Upper Proterozoic Noonday Dolomite, Death Valley Region, Eastern California: Geological Society of America Bulletin, v. 85, p. 1869-1882.

Condon, D., Zhu, M., Bowring, S., Wang, W., Yang, A., and Jin, Y., 2005, U-Pb Ages from the Neoproterozoic Doushantuo Formation, China: Science, v. 308, p. 95-98.

Corsetti, F.A., Awramik, S.M., and Pierce, D., 2003, A complex microbiota from snowball Earth times: Microfossils from the Neoproterozoic Kingston Peak Formation, Death Valley, USA: Proceedings of the National Academy of Sciences of the United States of America, v. 100, p. 4399-4404.

Corsetti, F.A., and Grotzinger, J.P., 2005, Origin and Significance of Tube Structures in Neoproterozoic Post-glacial Cap Carbonates: Example from Noonday Dolomite, Death Valley, United States: Palaios, v. 20, p. 348-362.

Corsetti, F.A., and Hagadorn, J.W., 2000, Precambrian-Cambrian transition: Death Valley, United States: Geology, v. 28, p. 299-302.

Corsetti, F.A., and Kaufman, A.J., 2003, Stratigraphic investigations of carbon isotope anomalies and Neoproterozoic ice ages in Death Valley, California: GSA Bulletin, v. 115, p. 916-932.

—, 2005, The relationship between the Neoproterozoic Noonday Dolomite and the Ibex Formation: New observations and their bearing on 'snowball Earth': Earth-Science Reviews, v. 73, p. 63-78.

Dalrymple, R.W., and Narbonne, G.M., 1996, Continental slope sedimentation in the Sheepbed Formation (Neoproterozoic, Windermere Supergroup), Mackenzie Mountains, N.W.T: Canadian Journal of Earth Sciences = Revue Canadienne des Sciences de la Terre, v. 33, p. 848-862.

Davis, G.A., Fowler, T.K., Bishop, K.M., Brudos, T.C., Friedmann, S.J., Burbank, D.W., Parke, M.A., and Burchfiel, B.C., 1993, Pluton pinning of an active Miocene detachment fault system, eastern Mojave Desert, California: Geology, v. 21, p. 627-630.

Devlin, W.J., Bond, G.C., and Brueckner, H.K., 1985, An assessment of the age and tectonic setting of volcanics near the base of the Windermere Supergroup in northeastern Washington; implications for latest Proterozoic-earliest Cambrian continental separation: Canadian Journal of Earth Sciences = Journal Canadien des Sciences de la Terre, v. 22, p. 829-837.

Devlin, W.J., Brueckner, H.K., and Bond, G.C., 1988, New isotopic data and a preliminary age for volcanics near the base of the Windermere Supergroup, northeastern Washington, U.S.A: Canadian Journal of Earth Sciences = Journal Canadien des Sciences de la Terre, v. 25, p. 1906-1911.

DeYoung, D.P., 2005, The Neoproterozoic Ibex Formation, eastern California: Stratigraphic and Sedimentological Constraints on Ice Age and Carbonate Precipitation Events of Southern Death Valley [MSc thesis]: Riverside, University of California, Riverside.

Evenchick, C.A., Parrish, R.R., and Gabrielse, H., 1984, Precambrian gneiss and late Proterozoic sedimentation in north-central British Columbia: Geology, v. 12, p. 233-237.

Faerseth, R.B., Knudsen, B.E., Liljedahl, T., Midboe, P.S., and Soderstrom, B., 1997, Oblique rifting and sequential faulting in the Jurassic development of the northern North Sea: Journal of Structural Geology, v. 19, p. 1285-1302.

Fanning, C.M., and Link, P.K., 2004, U-Pb SHRIMP ages of Neoproterozoic (Sturtian) glaciogenic Pocatello Formation, southeastern Idaho: Geology, v. 32, p. 881-884.

Fedo, C.M., and Cooper, J.D., 2001, Sedimentology and sequence stratigraphy of Neoproterozoic and Cambrian units across a craton-margin hinge zone, southeastern California, and implications for the early evolution of the Cordilleran margin: Sedimentary Geology, v. 141, p. 501-522.

Franks, J., and Stolz, J.F., 2009, Flat-laminated microbial mat communities: Earth-Science Reviews, v. 96, p. 163-172.

Hammond, J.G., 1983, Late Precambrian diabase intrusions in the southern Death Valley region, California: Their petrology, geochemistry, and tectonic significance [PhD thesis], University of Southern California.

Hazzard, J.C., 1939, Possibility of pre-Cambric glaciation in southeastern California: Pan-American Geologist, v. 71, p. 47-48.

Heaman, L.M., and Grotzinger, J.P., 1992, 1.08 Ga diabase sills in the Pahrump Group, California; implications for development of the Cordilleran Miogeocline: Geology (Boulder), v. 20, p. 637-640.

Hewett, D.F., 1940, New formation names to be used in the Kingston Range, Ivanpah Quadrangle, California: Journal of the Washington Academy of Sciences, v. 30, p. 239-240.

—, 1956, Geology and mineral resources of the Ivanpah Quadrangle, California and Nevada, p. 23-99.

Horodyski, R.J., and Knauth, L.P., 1994, Life on land in the Precambrian: Science, v. 263, p. 494-498.

Jackson, C.A.L., Gawthorpe, R.L., Carr, I.D., and Sharp, I.R., 2005, Normal faulting as a control on the stratigraphic development of shallow marine syn-rift sequences; the Nukhul and Lower Rudeis Formations, Hammam Faraun fault block, Suez Rift, Egypt: Sedimentology, v. 52, p. 313-338.

Jackson, J.A., and White, N.J., 1989, Normal faulting in the upper continental crust; observations from regions of active extension: Journal of Structural Geology, v. 11, p. 15-36.

Johnson, B.K., 1957, Geology of a part of the Manly Peak Quadrangle, southern Panamint Range, California: University of California Publications in Geological Sciences, v. 30, p. 353-423.

Kendall, B., Creaser, R.A., and Selby, D., 2006, Re-Os geochronology of postglacial black shales in Australia: Constrains on the timing of [ldquo]Sturtian[rdquo] glaciation, v. 34, p. 729-732.

Kennedy, M.J., Christie-Blick, N., and Sohl, L.E., 2001, Are Proterozoic cap carbonates and isotopic excursions a record of gas hydrate destabilization following Earth's coldest intervals?: Geology, v. 29, p. 443-446.

Kennedy, M.J., Runnegar, B., Prave, A.R., Hoffman, K.-H., and Arthur, M.A., 1998a, Two or four Neoproterozoic glaciations?, v. 26, p. 1059-1063.

Kennedy, M.J., Runnegar, B., Prave, A.R., Hoffmann, K.H., and Arthur, M.A., 1998b, Two or four Neoproterozoic glaciations?: Geology, v. 26, p. 1059-1063.

Kenny, R., and Knauth, L.P., 2001, Stable isotope variations in the Neoproterozoic Beck Spring Dolomite and Mesoproterozoic Mescal Limestone paleokarst; implications for life on land in the Precambrian: Geological Society of America Bulletin, v. 113, p. 650-658.

Kupfer, D.H., 1960, Thrust faulting and chaos structure, Silurian Hills, San Bernardino County, California: Geological Society of America Bulletin, v. 71, p. 181-214.

Labotka, T.C., and Albee, A.L., 1977, Late Precambrian depositional environment of the Pahrump Group, Panamint Mountains, California.: California Division of Mines and Geology-Special Papers, v. 129, p. 93-100.

Labotka, T.C., Albee, A.L., Lanphere, M.A., and McDowell, S.D., 1980, Stratigraphy, structure, and metamorphism in the central Panamint Mountains (Telescope Peak Quadrangle), Death Valley area, California: Geological Society of America Bulletin, v. 91 Part II, p. 843-933.

Lanphere, M.A., Wasserburg, G.J.F., Albee, A.L., and Tilton, G.R., 1964, Redistribution of strontium and rubidium isotopes during metamorphism, World Beater Complex, Panamint Range, California, Chapter 20.

Levy, M., and Christie-Blick, N., 1989, Pre-Mesozoic palinspastic reconstruction of the eastern Great Basin (Western United States): Science, v. 245, p. 1454-1462.

—, 1991, Tectonic subsidence of the early Paleozoic passive continental margin in eastern California and southern Nevada: Geological Society of America Bulletin, v. 103, p. 1590-1606.

Link, P.K., Christie-Blick, N., Devlin, W.J., Elston, D.P., Horodyski, R.J., Levy, M., Miller, J.M.G., Pearson, R.C., Prave, A., Stewart, J.H., Winston, D., Wright, L.A., and Wrucke, C.T., 1993, Middle and late Proterozoic stratified rocks of the western U.S. Cordillera, Colorado Plateau, and Basin and Range Province, *in* Reed, J.C.J., Bickford, M.E., Houston, R.S., Link, P.K., Rankin, D.W., Sims, P.K., and Van Schmus, W.R., eds., Precambrian-conterminous U.S.: The geology of North America: Denver, CO, United States Geological Survay, p. 463-595.

Lund, K., Aleinikoff, J.N., Evans, K.V., and Fanning, C.M., 2003, SHRIMP U-Pb geochronology of Neoproterozoic Windermere Supergroup, central Idaho: Implications for rifting of western Laurentia and synchroneity of Sturtian glacial deposits: Geological Society of America Bulletin, v. 115, p. 349-372.

Marian, M.L., and Osborne, R.H., 1992, Petrology, petrochemistry, and stromatolites of the middle to late Proterozoic Beck Spring Dolomite, eastern Mojave Desert, California: Canadian Journal of Earth Sciences = Journal Canadien des Sciences de la Terre, v. 29, p. 2595-2609.

Miller, J.M.G., 1982, Kingston Peak Formation in the southern Panamint Range; a glacial interpretation, *in* Cooper, J.D., Troxel, B.W., and Wright, L.A., eds., Geology of selected areas in the San Bernardino Mountains, western Mojave Desert, and southern Great Basin, California: Geological Society of America Cordilleran Section Field Trip Guidebook and Volume: Shohone, California, Death Valley Publ. Co., p. 155-164.

—, 1983, Stratigraphy and sedimentolgy of the upper Proterozoic Kingston Peak Formation, southern Panamint Range, eastern California [Doctoral thesis]: Santa Barbara, University of California.

—, 1985a, Glacial and syntectonic sedimentation: The upper Proterozoic Kingston Peak Formation, southern Panamint Range, eastern California, v. 96, p. 1537-1553.

—, 1985b, Glacial and syntectonic sedimentation; the upper Proterozoic Kingston Peak Formation, southern Panamint Range, eastern California: Geological Society of America Bulletin, v. 96, p. 1537-1553.

—, 1987, Paleotectonic and stratigraphic implications of the Kingston Peak-Noonday contact in the Panamint Range, eastern California: Journal of Geology, v. 95, p. 75-85.

Miller, J.M.G., Wright, L.A., and Troxel, B.W., 1981, The late Precambrian Kingston Peak Formation, Death Valley region, California, *in* Hambrey, M.J., and Harland, W.B., eds.: Cambridge, Cambridge Univ. Press.

Miller, M.G., 1991, High-angle origin of the currently low-angle Badwater turtleback fault, Death Valley, California: Geology, v. 19, p. 372-375.

Murphy, F.M., 1930, Geology of the Panamint silver district, California: Economic Geology and the Bulletin of the Society of Economic Geologists, v. 25, p. 305-325.

—, 1932, Geology of a part of the Panamint Range, report 27 of the state mineralogist: California Journal of Mines and Geology, v. 28, p. 329-356.

Noble, L.F., 1934, Rock formations of Death Valley, California; science, n. s., vol. 80, no. 2069.

—, 1941, Structural features of the Virgin Spring area, Death Valley, California: Geological Society of America Bulletin, v. 52, p. 941-999.

Noffke, N., Beukes, N., Bower, D., Hazen, R.M., and Swift, D.J.P., 2008, An actualistic perspective into Archean worlds; (cyano-)bacterially induced sedimentary structures in the siliciclastic Nhazatse section, 2.9 Ga Pongola Supergroup, South Africa: Geobiology, v. 6, p. 5-20.

Pierce, D., and Cloud, P., 1979, New microbial fossils from approximately 1.3 billion-year-old rocks of eastern California: Geomicrobiology Journal, v. 1, p. 295-309.

Prave, A.R., 1999, Two diamictites, two cap carbonates, two delta (super 13) C excursions, two rifts; the Neoproterozoic Kingston Peak Formation, Death Valley, California: Geology (Boulder), v. 27, p. 339-342.

Prosser, S., Williams, G.D., and Dobb, A., 1993, Rift-related linked depositional systems and their seismic expression: Geological Society Special Publications, v. 71, p. 35-66.

Ravnas, R., and Steel, R.J., 1998, Architecture of marine rift-basin successions: AAPG Bulletin, v. 82, p. 110-146.

Renik, B., Christie-Blick, N., Troxel, B., Wright, L., and Niemi, N., 2008, Re-evaluation of the middle Miocene Eagle Mountain Formation and its significance as a piercing point for the interpretation of extreme extension across the Death Valley Region, California, U.S.A.: Journal of Sedimentary Research, v. 78, p. 199-219.

Roberts, M.T., 1974, Stratigraphy and Depositional Environments of the Crystal Spring Formation, Southern Death Valley Region, California, Guidebook; Death Valley Region, California and Nevada (see Geological Society of America): Shoshone, California, Death Valley Publ. Co., p. 49-57.

Ross, G.M., 1991, Tectonic setting of the Windermere Supergroup revisited: Geology, v. 19, p. 1125-1128.

Snow, J.K., 1992, Large-magnitude Permian shortening and continental-margin tectonics in the southern Cordillera: Geological Society of America Bulletin, v. 104, p. 80-105.

Snow, J.K., and Wernicke, B.P., 2000, Cenozoic tectonism in the central Basin and Range: magnitude, rate, and distribution of upper crustal strain: American Journal of Science, v. 300, p. 659-719.

Stewart, J.H., 1970, Upper Precambrian and Lower Cambrian strata in the southern Great Basin, California and Nevada, U. S. Geological Survey Professional Paper, p. 206.

—, 1972, Initial deposits in the Cordilleran geosyncline: Evidence of a late Precambrian (<850 m.y.) continental separation: Geological Society of America Bulletin, v. 83, p. 1345-1360.

—, 1976, Late Precambrian evolution of North America: Plate tectonics implication: Geology, v. 4, p. 11-15.

Summa, C.L., 1993, Sedimentologic, stratigraphic, and tectonic controls of a mixed carbonate-siliciclastic succession; Neoproterozoic Johnnie Formation, Southeast California [Doctoral thesis], Massachusetts Institute of Technology, Cambridge, MA, United States (USA).

Topping, D.J., 1993, Paleogeographic reconstruction of the Death Valley extended region: Evidence from Miocene large rock-avalanche deposits in the Amargosa Chaos Basin, California: Geological Society of America Bulletin, v. 105, p. 1190-1213.

Troxel, B.W., 1967, Sedimentary rocks of late Precambrian and Cambrian age in the southern Salt Spring Hills, southeastern Death Valley, California: Special Report - California Division of Mines and Geology, p. 33-41.

—, 1982a, Basin facies (Ibex Formation) of the Noonday Dolomite, southern Saddle Peak Hills, southern Death Valley, California, *in* Cooper, J.D., Troxel, B.W., and Wright, L.A., eds., Geology of selected areas in the San Bernardino Mountains, western Mojave Desert, and southern Great Basin, California: Geological Society of America Cordilleran Section Field Trip Guidebook and Volume: Shohone, Death Valley Publ. Co., p. 43-48.

—, 1982b, Description of the uppermost part of the Kingston Peak Formation, Amargosa Rim Canyon, Death Valley region, California, *in* Cooper, J.D., Troxel, B.W., and Wright, L.A., eds., Geology of selected areas in the San Bernardino Mountains, western Mojave Desert, and southern Great Basin, California: Geological Society of America Cordilleran Section Field Trip Guidebook and Volume: Shohone, Death Valley Publ. Co., p. 61-70.

Troxel, B.W., and Wright, L.A., 1987, Tertiary extensional features, Death Valley region, eastern California: Geological Society of America Centennial Field Guide-Cordilleran Section, p. 121-132.

Tucker, M.E., 1986, Formerly aragonitic limestones associated with tillites in the Late Proterozoic of Death Valley, California: Journal of Sedimentary Petrology, v. 56/6, p. 818-830, 14 Figs., 3 Tabs.

Williams, E.G., Wright, L.A., and Troxel, B.W., 1974, The noonday dolomite and equivalent stratigraphic units, southern Death Valley region, California, Guidebook; Death Valley region, California and Nevada: Shoshone, Death Valley Publ. Co., p. 73-77.

Wise, K.P., Austin, S.A., and Anonymous, 1999, Gigantic megaclasts within the Kingston Peak Formation (Upper Precambrian, Pahrump Group), southeastern California; evidence for basin margin collapse: Abstracts with Programs - Geological Society of America, v. 31, p. 455-456.

Wright, L.A., 1952, Geology of the Superior talc area, Death Valley, California: Special Report - California Division of Mines and Geology, v. 20, p. 1-22.

—, 1954, Geology of the Alexander Hills area, Inyo and San Bernardino counties, *in* Jahns, R.H., ed., Geology of southern California, Calif. Dept. Nat. Res., Div. Mines Bull. 170, p. Map Sheet 17.

—, 1974, Geology of the S.E. 1/4 Tecopa 15-minute quadrangle, San Bernardino and Inyo Counties: San Fransisco, California, Division of Mines and Geology.

Wright, L.A., and Troxel, B.W., 1966, Strata of late Precambrian-Cambrian age, Death Valley region, California-Nevada: Bulletin of the American Association of Petroleum Geologists, v. 50, p. 846-857.

Wright, L.A., Troxel, B.W., and Prave, A.R., 1992, Field traverse of Proterozoic rock units, Alexander Hills and southern Nopah Range, Death Valley region, CA, Late Phanerozoic Penrose Conference, Geological Society of America, p. 1-11.

Wright, L.A., Troxel, B.W., Williams, E.G., Roberts, M.T., and Diehl, P.E., 1974, Precambrian sedimentary environments of the Death Valley region, eastern California: Shoshone, Death Valley Publ. Co.

Wright, L.A., Williams, E.G., and Cloud, P., 1978, Algal and cryptalgal structures and platform environments of the lat pre-Phanerozoic Noonday Dolomite, eastern California: Geological Society of America Bulletin, v. 89, p. 321-333.

Wright, L.A., Williams, E.G., and Troxel, B.W., 1984, Type section of the newly-named Proterozoic Ibex Formation, the basinal equivalent of the Noonday Dolomite (Appendix II). Geology of The northern half of the Confidence Hills 15-minute Quadrangle, Death Valley region, eastern California, v. Map Sheet 34, p. 25-31.

Young, G.M., 1995, Are Neoproterozoic glacial deposits preserved on the margins of Laurentia related to the fragmentation of two supercontinents?: Geology, v. 23, p. 153-156.

CHAPTER THREE:

KINGSTON PEAK FORMATION CARBONATE INTERVALS: GEOCHEMISTRY AND ASSOCIATED TIMELINES, AND THEIR BEARING ON REGIONAL & GLOBAL CORRELATION AND TIMING OF TECTONISM AND GLACIATIONS

Chapter Summary

This chapter provides a detailed description of the sedimentology, stratigraphic relationships and isotopic geochemistry for a distinctive organic-rich, dark, laminated limestone horizon within the KPF. One similar carbonate horizon appears or was at one time present in all areas where the KPF crops out. Also discussed are discontinuous carbonate intervals in the upper KPF, their geochemistry and how they have been used to suggest correlations between the two main regions in which the KPF crops out. The value of these carbonate intervals as timelines and their bounding relationships with variable facies in different outcrop regions is that they establish a diachronous record of progressive rifting between the Panamint Range in the west to the Kingston Range to the west. This provides valuable context for the final chapter, which discusses the importance of the duration of glacigenic conditions vs. the timing of available accommodation space.

1. Introduction

In this chapter I test the hypothesis that carbonate intervals in the eastern and western Kingston Peak Formation (KPF) regions (Fig. 2.1) may serve as timelines between the two regions. The isotopic values of carbonates have been used as a means of correlation in the Neoproterozoic

globally (Halverson et al., 2005) and locally in Death Valley (Corsetti and Kaufman, 2003). The isotope values of KPF carbonate intervals are used to correlate several intervals with enriched values inter-basinally and to correlate an interval with depleted values globally (Prave, 1999). A broader range of samples helps identify the value of chemostratigraphic correlation in understanding the timing of tectonism, glaciation and carbonate deposition in the KPF. Further, understanding the timing of carbonate deposition, glacial deposition and tectonism may provide evidence for or against the possibility of globally synchronous glaciations during the Neoproterozoic.

The coarse-grained KPF lies at the southern extent of a series of similar coarse-grained Neoproterozoic deposits along the Cordillera (Stewart, 1972) and has been interpreted as a product of both tectonism and glaciation (Marian, 1979; Miller, 1985; Wright et al., 1974). Prave (1999) proposed a chemo- and tectono-stratigraphic correlation for the eastern and western succession of the KPF, suggesting the entire formation fit into a "Snowball Earth" stratigraphic model (Hoffman et al., 1998) with a record of two discrete ice ages separated by an interglacial interval.

Correlation of the Kingston Peak Formation to other Neoproterozoic sections is confounded by the lack of radiometric constraints. A number of criteria may be useful in correlating sections regionally and globally, including glacial intervals, sequence boundaries, regionally extensive carbonate intervals (i.e. transgressive or highstand systems tracts), or secular isotopic trends. The KPF is clearly bounded above (the Noonday Dolomite) and below (the Beck Spring Dolomite) by regionally extensive carbonate intervals. In order to confirm independent correlation

of glacial strata in the Kingston Peak Formation with other Neoproterozoic glacial strata, through-going surfaces (sequence boundaries) or carbonate horizons must be identified. Prave (1999) and Corsetti and Kaufman (2003) used both lithostratigraphic and chemostratigraphic correlation within the Kingston Peak Formation to propose a global correlation scheme for glacial and tectonic events. A broader data set from a more comprehensive set of sample locations than other studies (Corsetti and Kaufman, 2003; Prave, 1999) reveals an overlap in values that do not support unique chemostratigraphic correlations.

Internal carbonate intervals in both the eastern and western KPF have the potential to be correlated mineralogically, isotopically and sequence stratigraphically. They have undergone extensive alteration including up to amphibolites-grade metamorphic temperatures and shared an original aragonitic mineralogy (Tucker, 1986). Distinctive laminated and originally organic-rich carbonate intervals in the Panamint Range (the Sourdough Limestone) and in the Black Mountains (the Virgin Spring Limestone) have the potential for chemostratigraphic correlation. They represent condensation events (Tucker, 1986), are comprised of detrital grains, and are both overlain by sequence boundaries. Here I investigate their lithological, chemical, mineralogical, isotopic and stratigraphic architecture to see if they provide useable points of correlation that can be used to test the timing of fault movement and glacial facies deposition.

Characteristics shared by the limestone intervals provide a possible means of inter-regional correlation and are discussed below. This comparison also addresses some broader questions relevant to Neoproterozoic geology: One, can carbonate intervals serve as timelines that will help clarify correlation issues and timing of tectonism? Two, do carbonate timelines

support a model of two discrete glacial intervals separated by an interglacial interval? Three, do isotopic trends support using these carbonate intervals as chemostratigraphic timelines?

2. Methods

Isotopic data for over 1000 samples (appendix) was collected primarily on a VG Prism II where precision was better than 0.1‰ for $\delta^{13}C$ and better than 0.2 ‰ for $\delta^{18}O$. Standards used in runs were internal standards calibrated against NBS-19. High resolution sampling of smaller sample sizes and checks for reproducibility were carried out on a Thermo Delta V connected to a gas bench where precision was better than 0.1‰ for $\delta^{13}C$ and better than 0.2 ‰ for $\delta^{18}O$. All isotopic data is reported relative to the VPDB scale. Standards used in runs were both NBS-19 and internal standards calibrated using NBS-19, LSVEC and NBS-18. Mineralogy and petrography were accomplished by standard microscopy, cathode ray luminescence microscopy and SEM. Qualitative mineralogy was also determined on some samples by XRD using a Shimadzu XRD-6000.

3. Data

3.1. Sedimentology of Carbonate Intervals

An interval of dark, relatively organic-rich, parallel laminated limestone is present in the Panamint Range (Sourdough Limestone), the Black Mountains (Virgin Spring Limestone) and in the Silurian Hills. Each interval is bounded by coarse-grained facies, but regional differences in the lithologies of these facies confounds lithostratigraphic correlation. The Sourdough Limestone is present throughout almost the entire western KPF in the Panamint Range. The Silurian Hills

limestone is a continuous marker bed throughout the KPF section in the Silurian Hills. The Virgin Spring Limestone in the Black Mountains is limited to three outcrop areas, but clasts of it in the overlying diamictite indicate a regional extent prior to erosion.

Virgin Spring Limestone (Black Mountains & Saratoga Hills): A distinctive unit (3-17 m thick) of parallel laminated black limestone overlies the Saratoga Hills Sandstone in three locations: the Saratoga Hills, the Ibex Hills and Virgin Spring Wash. Beds are 2-15 cm thick and comprised of sub-mm scale laminations (Fig. 3.1a, 3.2a & 3.2c). Sedimentary structures are generally limited to parallel lamination, but include rare massive 2-5 cm thick beds, folded beds, tight overturned folds generally 5-10 cm in height and cm-scale sandstone layers (Fig. 3.1b). These overturned folds are a result mass movement downslope (Tucker, 1986). There is no evidence of any other laminated microbial fabric. In thin section both ooids and peloids are abundant. Tucker (1986) interpreted this interval to have been subject to retransport of grains during subaqueous grain flows. Sharp lower sedimentary contacts are only preserved in two sections, Ibex Hills and Virgin Spring Wash. The top surface of the Virgin Spring Limestone is karsted and erosionally truncated; sandstone fills grikes that penetrate 30-50 cm down into the limestone in the Saratoga Hills and cross-sections of 20-30 cm diameter oval cavities several meters below the top of the limestone in the Ibex Hills are similarly filled with sandstone (Fig. 3.1c). In the southern Saratoga Hills, the Virgin Spring Limestone is gradually beveled out to the south as it is erosionally truncated, defining the regional Saratoga Hills Sandstone-Alexander Hills Diamictite unconformity described above.

In the Ibex Hills, the Virgin Spring Limestone is 17 m thick (Fig. 3.1d), but thins laterally over a distance of several hundred meters to several meters in thickness, probably due to

truncation by the fault between it and the underlying Beck Spring Dolomite. The upper limestone here is comprised of interbedded limestone and intraclast flake breccias interbedded with the laminated facies. Prior to erosional truncation, the Virgin Spring Limestone likely covered most, if not all, of the Saratoga Hills Sandstone, based on its consistent incorporation as clasts and matrix into the overlying Alexander Hills Diamictite in most sections.

Petrographic analysis shows that the limestone is composed of recrystallized ooids and peloids of uncertain origin. Both spherical grains are recrystallized but remnant concentric laminae are still visible. Ooids are usually precipitated around a grain of quartz. Tucker (1986) interpreted the dark color to be a product of disseminated organic matter.

Silver Rule Mine Member oncolitic marker bed: Near the middle of the Silver Rule Mine Member, an oncolitic marker horizon of dolomite roughly delineates the relatively finer-grained lower member from the rapidly coarsening upwards upper part of the member. This marker bed is present in most sections, but discontinuous. It is 2-4 m thick and often has well-defined oncoids that appear to be no longer rooted to a substrate, but have been broken and transported. Where the oncoids are clear, they appear in beds with ooids that are sometimes graded. This bed looks very similar to the exceptional exposure of oncolitic dolostone capping the top of the Beck Spring Dolomite at Crystal Spring. The bed appears unbrecciated and intact near the Beck Canyon Divide locality (Fig. 2.1 #7), but in most other sections may be entirely brecciated or have a brecciated lower and upper surface. This horizon was also used to identify microfossils in chert and establish the existence of an active biota during this interval {Corsetti, 2003 #805}.

Sourdough Limestone Member: western KPF (Panamint Range): The Sourdough Limestone may be as little as several meters thick in the southern Panamint Range and thickens northward to over 30 m in Wildrose Canyon (Fig. 3.2). In the Central Panamint Range it is truncated by an erosion surface overlain by the Wildrose Diamictite Member (Fig. 3.1c). It is characterized by (Miller, 1983; Tucker, 1986): 1) tight asymmetric dam-scale compressional folds (Fig. 3.1b & 3.2b), 2) boudinization of sandstone beds into lenses (Fig. 3.1e & f), 3) sucrosic recrystallization with light-dark lamina couplets preserved (Fig. 3.2d), 4) sandstone interbeds, and 5) sharp lower contacts and gradational upper contacts. Towards the southern tip of the Panamint Range, the Sourdough Limestone is comprised of debris flows of carbonate grains with up to m-scale sandstone clasts (Fig. 3.1d). In Wildrose Canyon it is not completely limestone, but includes interbedded dolostone beds with sharp bedding boundaries and dolomitized zones with irregular diffuse boundaries. Any original primary fabric has been obliterated by recrystallization.

Limestone in the Silurian Hills: This heavily recrystallized and sucrosic limestone unit in the Silurian Hills (Fig. 3.2e) was measured in two localities ~2 km apart. Both sections are ca. 40 m thick, contain abundant veins of spar, boudinization, tight asymmetric folds, color changes with sharp and diffuse boundaries, and have karsted upper contacts. Like the Sourdough Limestone, it is interbedded with several sandstone horizons and, due to recrystallization, has lost any primary fabric.

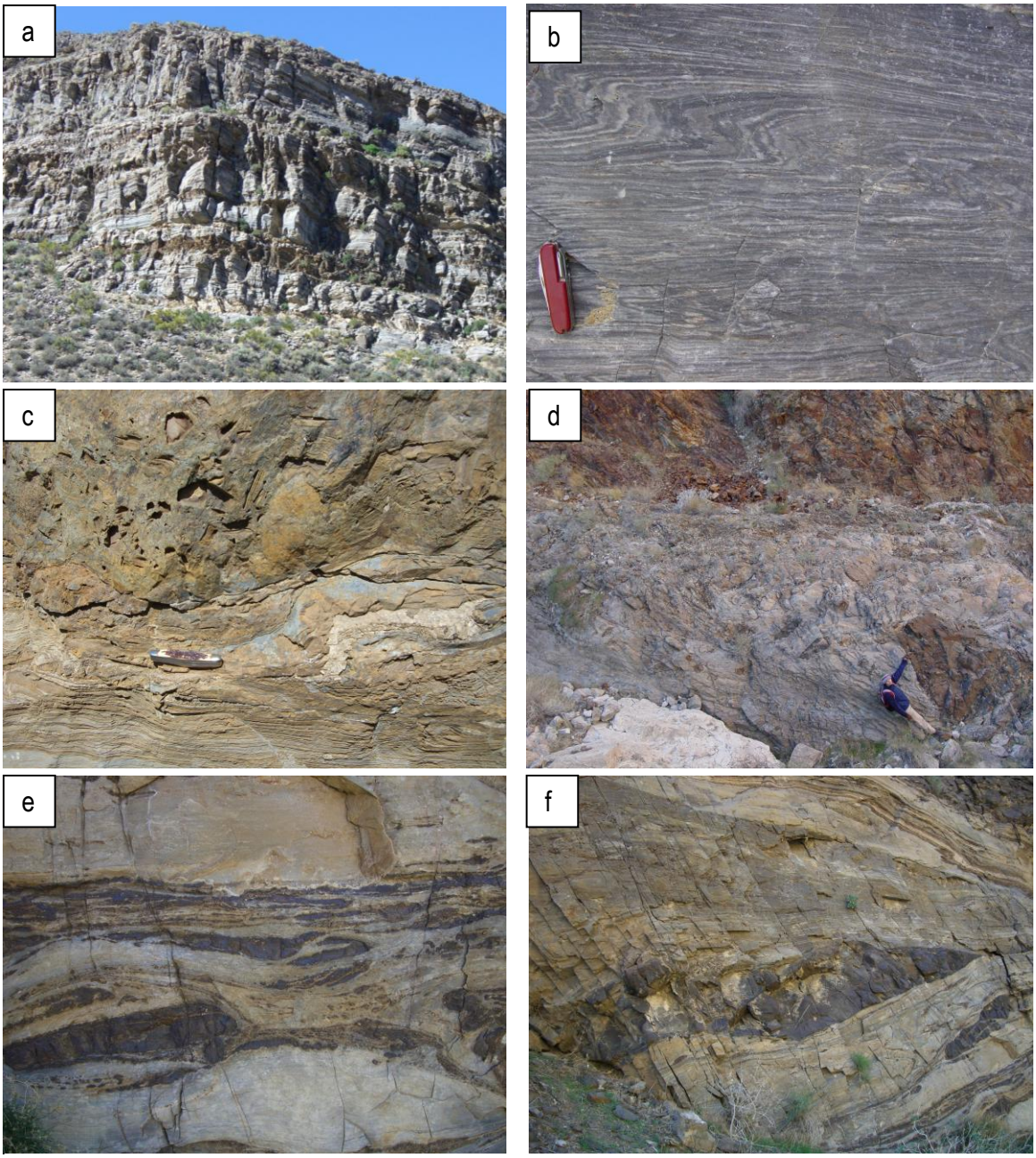

Fig. 3.1. Various features of the Sourdough Limestone; a) 30m section interbedded with sandstone (Wildrose Canyon); b) post-depositional folding (Wood Canyon); c) erosion surface between limestone and overlying Wildrose Diamictite (Cooper Mine); d) m-scale sandstone clast in Sourdough Limestone (Goler Wash); e) boudins interbedded sandstone (Pleasant Canyon); f) sandstone boudin and folding (Pleasant Canyon).

Fig. 3.2. Various polished slabs of KPF limestones show fabric and textures. a) Virgin Spring Limestone, Saratoga Hills; b) Sourdough Limestone, Goler Wash; c) Virgin Spring Limestone Virgin Spring Wash; d) Sourdough Limestone, Sourdough Canyon; e) Silurian Hills limestone; f) un-named limestone, Wildrose Canyon; g) un-named limestone; Sourdough Canyon.

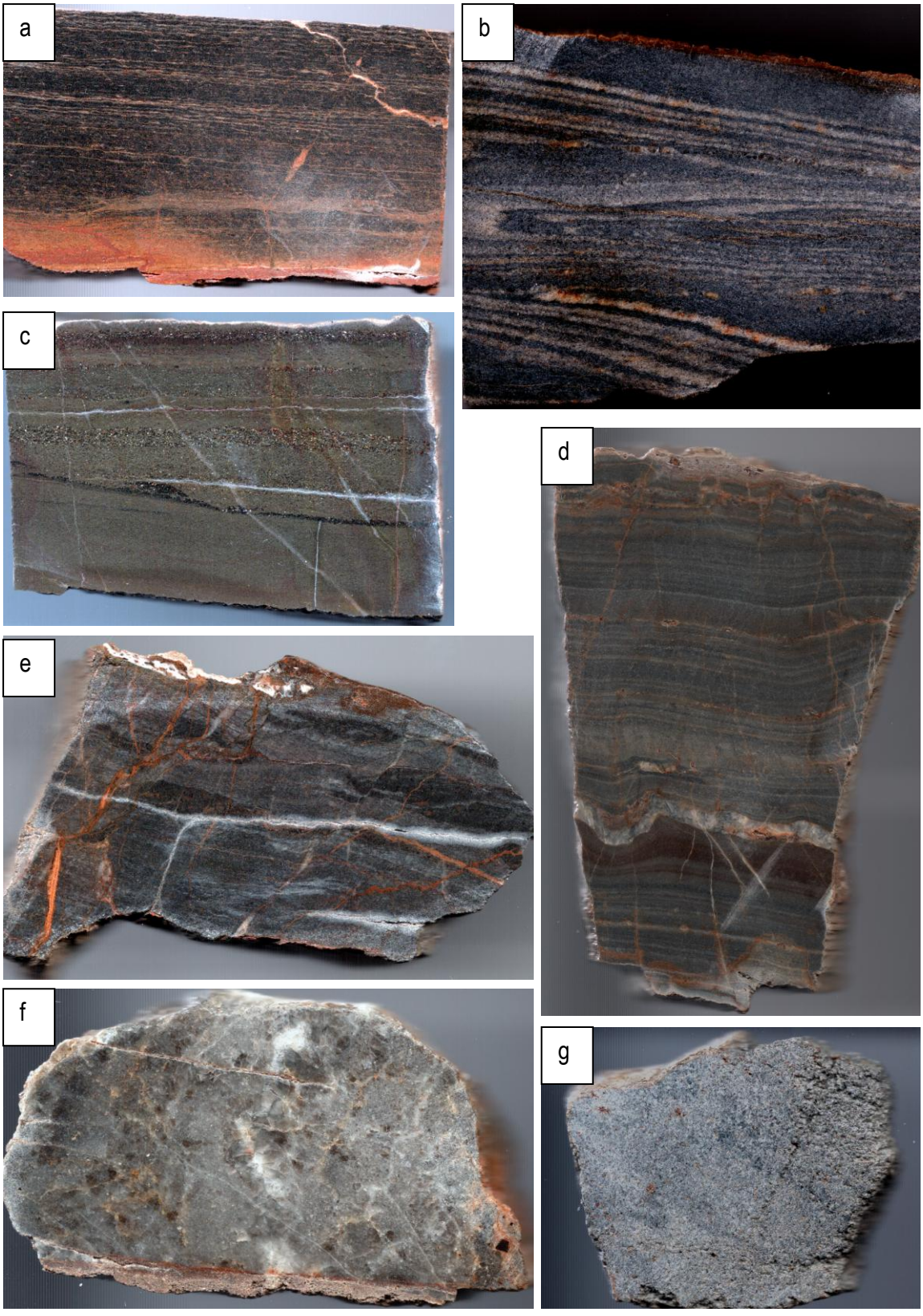
a
b
c
d
e
f
g

Un-named limestone (Panamint Range): A discontinuous carbonate interval occurs beneath the Wildrose Diamictite throughout the Panamint Range. It is thinly bedded (2-5 cm), fine-grained with vague laminations to coarsely recrystallized (Fig. 3.2e & f), light-colored and 3-20 m thick. Like the Sourdough Limestone, recrystallization has obscured any primary fabric. Fresh surfaces are light in color and do not contain the dark color banding evident within the Virgin Spring or Sourdough Limestones. In Sourdough Canyon, the un-named limestone is alabaster white, recrystallized and similar in appearance to three overlying carbonate intervals occurring between the Wildrose Diamictite and the Noonday Dolomite. In Wildrose Canyon the un-named limestone is comprised of interbeddded dolostone and limestone.

3.3 Mineralogy of Carbonate Intervals

Thin sections show that the Virgin Spring Limestone is composed of coarse brown calcite crystals. This recrystallization has not obscured the original fabric of the limestone and ooids and spherules with concentric banding are visible. The Sourdough Limestone has been heavily recrystallized and only coarse calcite crystals and abundant spar veins are visible. The Virgin Spring Limestone and the Sourdough Limestone have high levels of Strontium, up to 3,650 ppm and 3,100 ppm, respectively (Tucker, 1986). These levels, along with the radial structure of peloids and neomorphic texture of ooids in the Virgin Spring Limestone,, were the basis of Tucker's (1986) interpretation for an originally aragonitic mineralogy. The concentration of Strontium in the un-named limestone has not been determined.

**Table 3.1: Isotope statistics for all samples analyzed by the
and included in this study.**

		$\delta^{18}O$			$\delta^{13}C$		
Section	**n=**	**Avg.**	**Min.**	**Max.**	**Avg.**	**Min.**	**Max.**
Beck Spring Dolomite-Saratoga Hills Sandstone transitional beds (Alex. Hills)	7	-5.1	-6.8	-2.4	0.9	-0.7	2.3
Beck Spring Dolomite-immediately below Virgin Spring Limestone (Ibex Hills)	7	-5.0	-10.5	-1.2	2.5	1.8	3.5
Saratoga Hills Sandstone-basal carbonate cemented (Alex. Hills)	5	-4.9	-10.0	-2.5	-0.4	-2.9	0.9
Saratoga Hills Sandstone-upper carbonate cemented beds (various locations)	3	-17.6	-23.8	-13.9	-2.3	-5.4	2.1
Virgin Spring Limestone-laminated facies (Ibex Hills)	16	-13.4	-18.7	-9.4	2.5	1.2	3.4
Virgin Spring Limestone-brecciated facies (Ibex Hills)	29	-13.4	-18.9	-8.8	2.0	0.3	3.4
Virgin Spring Limestone (Saratoga Hills)	13	-16.0	-19.9	-13.4	0.5	-1.2	2.5
Virgin Spring Limestone (Virgin Spring Wash (Tucker, 1986))	7	-15.8	-16.5	-15.2	2.0	1.0	4.3
Virgin Spring Limestone 1 (Silurian Hills)	29	-13.9	-18.2	-8.5	2.6	-0.5	5.5
Virgin Spring Limestone 2 (Silurian Hills)	26	-13.6	-20.1	-7.3	2.9	-1.2	6.7
Silver Rule Mine Member: oncolitic marker bed	13	-6.1	-11.2	-2.1	-1.6	-4.0	1.1
Alexander Hills Diamictite-basal tabular clasts (various locations)	4	-15.1	-15.5	-14.6	-6.2	-7.4	-3.9
Alexander Hills Diamictite-black laminated limestone clasts (various locations)	9	-12.4	-16.7	-2.1	2.4	-1.1	4.9
Alexander Hills Diamictite-black matrix (various locations)	5	-12.4	-13.10	-10.0	0.6	0.2	1.0
Alexander Hills Diamictite-green matrix (Saratoga Hills)	1	-14.7			-8.8		
Silver Rule Mine Member-debrite matrix (Beck Divide)	8	-9.2	-12.2	-3.7	1.3	-1.1	2.9
Silver Rule Mine Member-green matrix interbedded diamictite (Beck Divide)	3	-10.4	-11.2	-9.5	-3.3	-4.2	-1.8
Silver Rule Mine Member-brown matrix interbedded diamictite (Beck Divide)	3	-11.7	-12.6	-11.1	-0.3	-0.9	0.2
Silver Rule Mine Member-oncolite marker bed (Horsethief Springs)	4	-6.2	-9.7	-2.5	-0.6	-1.7	0.4
Silver Rule Mine Member-oncolite marker bed (Beck Divide)	2	-7.4	-11.6	-3.3	-1.0	-2.8	0.9
Silver Rule Mine Member-oncolite marker bed, Corsetti Locality 1 (Corsetti, 2003)	9	-6.1	-11.2	-2.1	-2.0	-4.0	1.1
Silver Rule Mine Member-oncolite marker bed, Corsetti Locality 2 (Corsetti, 2003)	4	-6.2	-8.3	-3.9	-0.7	-1.9	1.0
Silver Rule Mine Member-BSD clasts from diamictite (Alexander Hills)	4	-0.3	-1.2	0.0	3.4	1.8	4.0
Jupiter Mine Member-BSD clasts from fanglomerate (various locations)	4	-3.3	-8.6	-0.1	1.8	-2.6	5.3

Jupiter Mine Member-cements fringing clasts (Alex. Hills)	6	-5.4	-5.8	-5.0	-3.5	-4.0	-2.8
Jupiter Mine Member-BSD clasts in interbedded Jupiter Mine Member (Alexander Hills)	3	-0.1	-1.5	1.3	3.4	1.2	4.7
Noonday Dolomite-matrix around clasts in basal Noonday Dolomite (Alex. Hills)	1	-6.0			-1.8		
Noonday Dolomite-below interbedded Jupiter Mine Member (Alex. Hills)	13	-5.7	-6.1	-5.2	-3.0	-3.8	-2.7
Noonday Dolomite-above interbedded Jupiter Mine Member (Alex. Hills)	2	-6.2	-6.3	-6.1	-3.1	-3.3	-3.0
Noonday Dolomite Equivalent Silurian Hills	10	-13.4	-17.6	-9.3	-4.2	-4.6	-3.6
Panamint Range							
Sourdough Limestone: Cooper Mine	8	-13.8	-15.2	-12.3	-3.5	-4.1	-2.8
Sourdough Limestone: Goler Wash	15	-15.4	-16.8	-10.8	-2.0	-3.5	-0.9
Sourdough Limestone: Sourdough Canyon	36	-12.9	-16.3	-11.0	-2.7	-3.9	-1.5
Sourdough Limestone: Wildrose Canyon (thick section)	16	-13.0	-14.3	-7.2	2.3	-4.6	4.8
Sourdough Limestone: Wildrose Canyon (cycles)	8	-14.2	-17.3	-10.8	-2.1	-6.3	2.5
Sourdough Limestone: Wood Canyon	58	-15.7	-20.2	-11.9	-2.8	-5.8	-1.8
Un-named Limestone: Cooper Mine	5	-14.8	-15.8	-13.4	-3.8	-4.3	-3.4
Un-named Limestone: Wildrose Canyon	11	-12.7	-14.2	-11.4	0.5	-2.5	4.7
Un-named Limestone: Sourdough Canyon	15	-13.8	-15.3	-11.3	3.0	0.5	5.6
First Carbonate Cycle above Un-named Limestone	5	-9.5	-10.3	-8.8	-2.4	-2.9	-2.0
Second Carbonate Cycle above Un-named Limestone	1	-14.3			-5.0		

3.4. Isotopic Data

Stable carbon isotopic data (Tables 2.1 & 3.1) have been used in this study to test for any shared isotopic characteristics of the three prominent Limestone Members in the KPF: 1) the Virgin Spring Limestone in northern sections of the eastern KPF, 2) the Virgin Springs Limestone in the Silurian Hills, and 3) the Sourdough Limestone in the Panamint Range.

Virgin Spring Limestone in the Black Mountains and the Saratoga Hills: Data for the Virgin Spring Limestone is presented in Tables 3.1 and in Fig. 3.3 for two sections measured in this study, Saratoga Hills and the Ibex Hills, as well as the Virgin Spring Wash from Tucker (1986). $\delta^{13}C$ values (n=74) for all three sections average 1.7‰ (min.= -1.2‰ & max.= 3.5‰). There is no obvious isotopic trend in any of the sections. In the Ibex Hills variability of >2‰ is seen in samples between angular mm-scale allochems and surrounding matrix or laminae and in some samples across sharp color change boundaries. $\delta^{18}O$ values average -13.4‰ (min.= -23.4 & max.= -1.2).

Polished slabs (Fig. 3.4) show a variety of textures, including laminations, flake breccias, mottled features and diagentic zoning in the samples from Ibex Hills (see Appendix B for sample descriptions). These pieces reveal abundant fracturing and veins which can provide pathways for diagenetic fluids. Isotopic values vary by up to 3‰ and 6‰ at cm-scales for $\delta^{13}C$ and $\delta^{18}O$ respectively. In the Ibex Hills the Beck Spring Dolomite is separated from the Virgin Spring Limestone by only a meter of sand- and siltstone. Several samples of the dolomite taken near the contact with the Virgin Spring Limestone are included in Fig. 3.4 to show the large difference in $\delta^{18}O$ values (up to 18‰).

Fig. 3.3. Isotopic profiles for the Virgin Spring Limestone (Ibex Hills; 35°45'18.00"N 116°26'12.00"W) and the Silurian Hills limestone interval (35°32'7.44"N 116° 5'59.42"W).

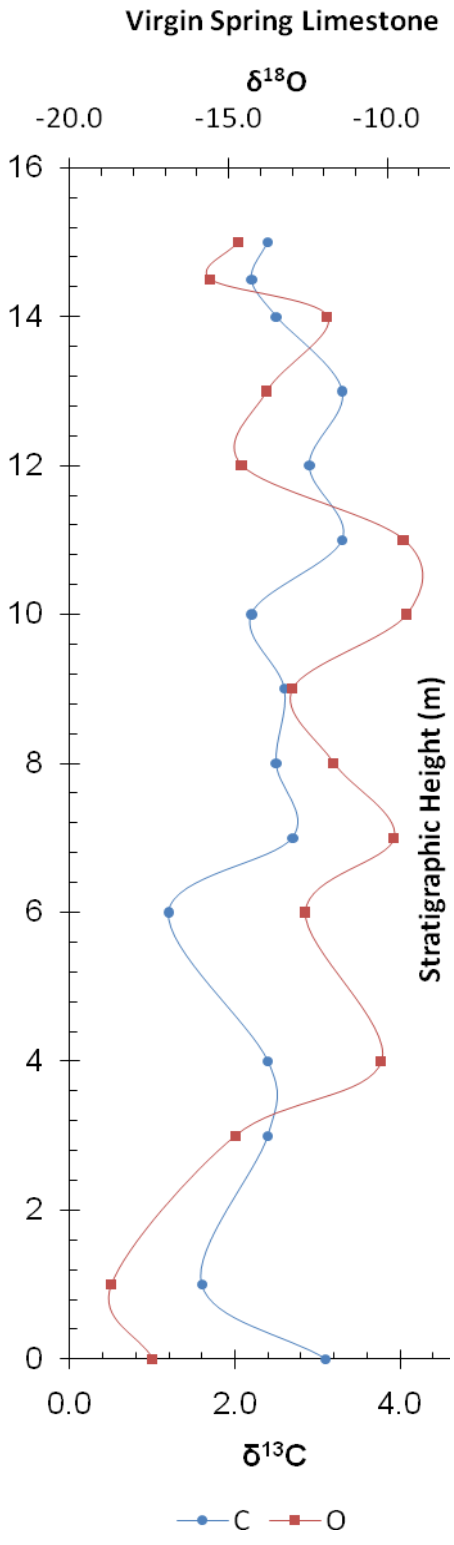
Virgin Spring Limestone
δ18O
-20.0
-15.0
-10.0
16
14
12
10
8
6
4
2
0
Stratigraphic Height (m)
0.0
2.0
4.0
δ13C
C
O

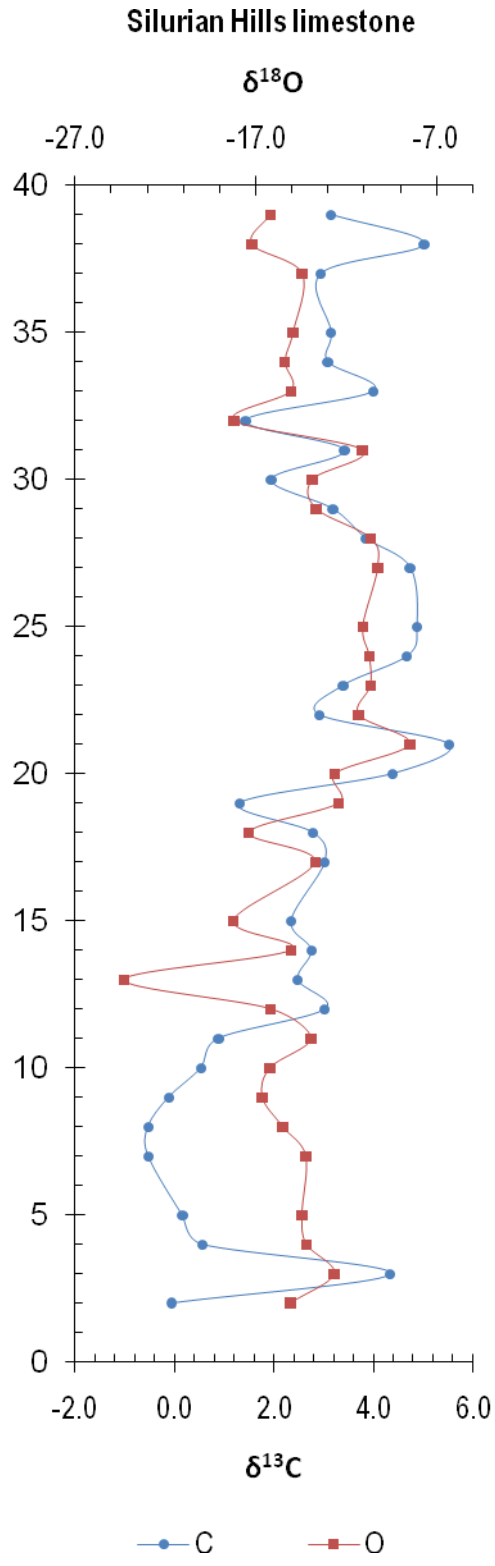
Silurian Hills limestone
δ18O
-27.0
-17.0
-7.0
40
35
30
25
20
15
10
5
0
-2.0
0.0
2.0
4.0
6.0
δ13C
C
O

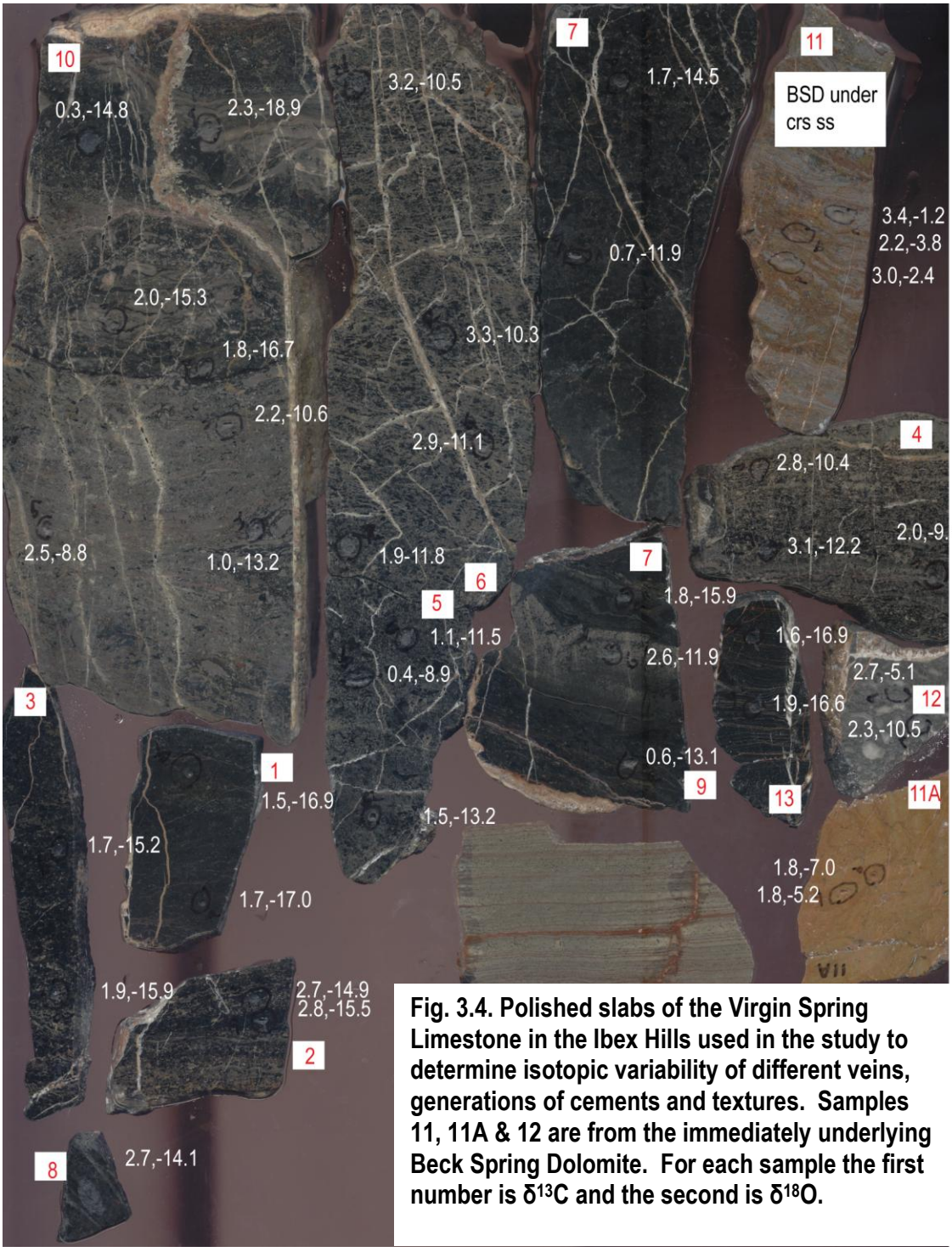

Fig. 3.4. Polished slabs of the Virgin Spring Limestone in the Ibex Hills used in the study to determine isotopic variability of different veins, generations of cements and textures. Samples 11, 11A & 12 are from the immediately underlying Beck Spring Dolomite. For each sample the first number is $\delta^{13}C$ and the second is $\delta^{18}O$.

Virgin Spring Limestone in the Silurian Hills: $\delta^{13}C$ values (n=71) for combined data set (Table 2.1) average 2.4‰ (min.= -4.4‰ & max.= 6.7‰). There is an overall positive trend upwards (Fig. 3.3) and a resulting shift in values from ~ 1‰ to ~ 6‰ in each section (second section not shown). There is <cm-scale isotopic variability of 1-2‰ both across color change boundaries and between different spots in isotopic variability of 1-2‰ both across color change boundaries and between different spots in hand samples that were taken from grike contacts. $\delta^{18}O$ values average -14.3‰ (min.= -24.3 & max.= -7.3).

Oncolitic Marker Bed, Silver Rule Mine Member: This marker bed was sampled north of Horsethief Mine (35°45'10.75"N 115°51'25.61"W) and within the Horsethief Spring section (Fig. 2.1 #8; 35°46'28.08"N 115°53'0.39"W). $\delta^{13}C$ and $\delta^{18}O$ values average -1.6‰ (min.= --4.0‰ & max.= 1.1‰) and -6.4‰ (min.= -11.2‰ & max.= -2.1‰) respectively (Table 3.1).

Sourdough Limestone Member and "un-named" limestone (Panamint Range): Data from the Sourdough Limestone in the Panamint Range is presented from five different localities: Wildrose Canyon, Sourdough Canyon, Wood Canyon, Pleasant Canyon and Goler Wash. $\delta^{13}C$ values (n=158) for combined data set (Table 2.1) average -2.8‰ (min.= -7.2‰ & max.= 4.8‰). While $\delta^{13}C$ values for the Sourdough Limestone are generally reported as depleted, or <0‰, the sections in Wildrose Canyon provide more enriched values (Fig. 3.5 & 3.6), that overlap values for the Silurian Hills and Virgin Spring Limestones (Table 3.1, Fig. 3.3 and Fig. 3.12).

The stratigraphic position of the Sourdough Limestone is clear. Both the south (Fig. 3.5) and north (Fig. 3.6) sections overlie Surprise Member diamictite. The northern section is overlain in normal stratigraphic order (Fig. 1.2) by the Middle Park Quartzite, the Mountain Girl

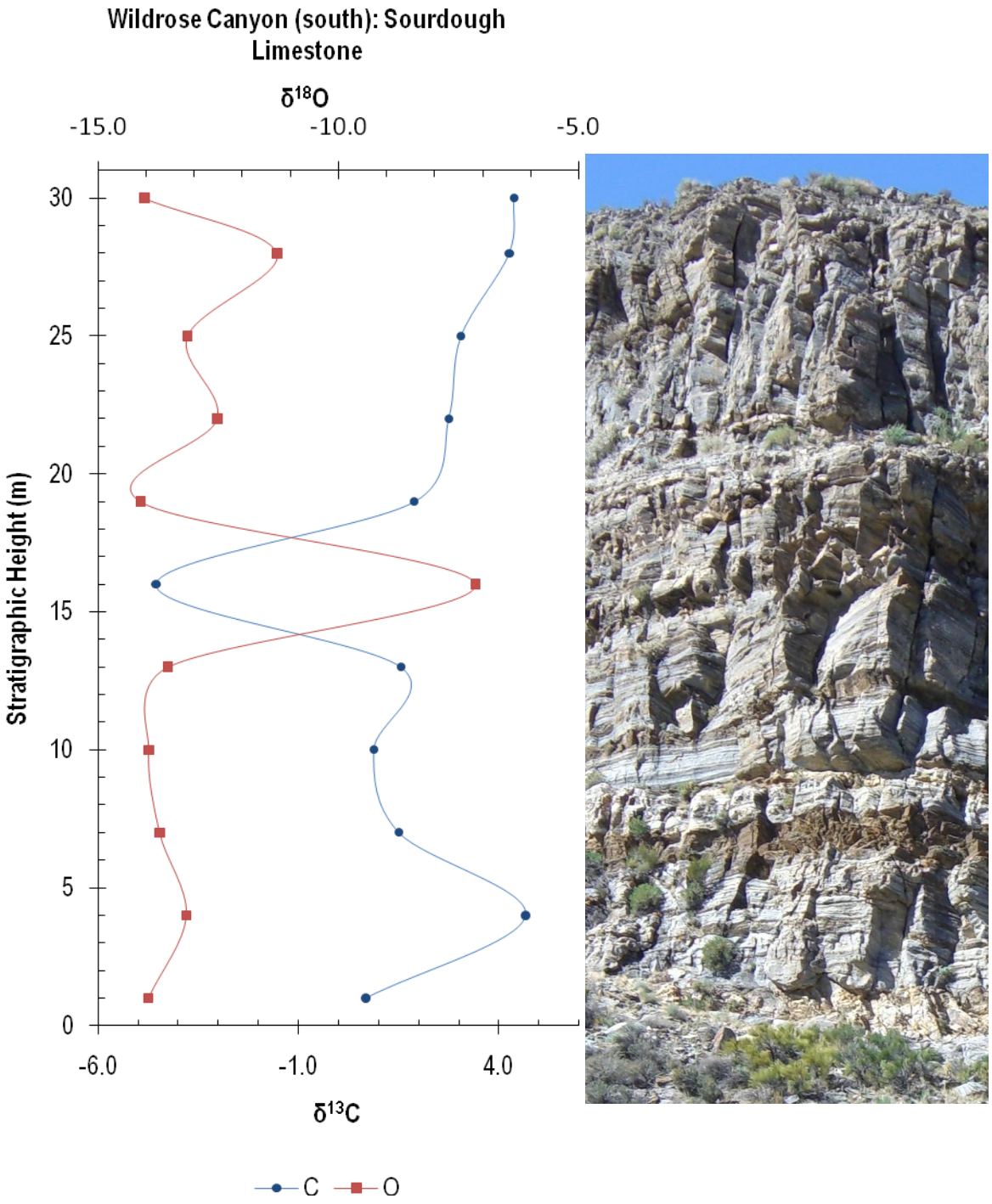

Fig. 3.5. Isotopic profile for the Sourdough Limestone in Wildrose Canyon (south; 36°14'47.82"N 117° 8'20.79"W). Photograph shows the section measured in the study.

Conglomerate and finally the un-named limestone capped by the Wildrose Member.

The un-named limestone also shares a positive-to-negative spectrum of $\delta^{13}C$ values in the sections measured (Figs. 3.6, 3.7 & 3.8). In both Wildrose Canyon (Fig. 3.6) and at the Cooper Mine in Pleasant Canyon (Fig. 3.7), $\delta^{13}C$ values are negative. The Sourdough Canyon (Fig. 3.8) and Wood Canyon (Fig. 3.9) sections both show a pattern of $\delta^{13}C$ isotopic depletion corresponding to sandstone intervals. In Wood Canyon $\delta^{13}C$ values remain steadily close to -2‰ except in proximity to sandstone intervals where they generally decrease to ~ -4‰. There is negligible isotopic variability in hand samples and an extensive set (n=37) of light-dark couplets analyzed showed no systematic differences (Fig. 3.10). $\delta^{18}O$ values average -14.5‰ (min.= -17.8 & max.= -6.3). Wood Canyon $\delta^{18}O$ values show a similar pattern to $\delta^{13}C$ with the most depleted values corresponding to sandstone intervals.

Three carbonate intervals appear between the Wildrose Diamictite and the Noonday Dolomite in Sourdough Canyon (Fig. 3.8). They are coarse-grained due to recrystallization and thinly bedded (3-5 cm). These intervals have positive $\delta^{13}C$ values and, like the un-named limestone in this section, are light-colored and marbleized. These light-colored carbonate intervals further complicate correlation of the underlying un-named limestone (actually limestone and dolostone) in the upper KPF with dark organic-rich limestone intervals in the base of the KPF. $\delta^{18}O$ values average -14.5‰ (min.= -17.8 & max.= -6.3). Wood Canyon $\delta^{18}O$ values show a similar pattern to $\delta^{13}C$ with the most depleted values corresponding to sandstone intervals.

Fig. 3.6. Paired isotopic profile and measured section for the Sourdough Limestone in Wildrose Canyon (north side road; 36°15'13.56"N 117° 5'34.48"W). Isotopic values for the un-named limestone are shown at the top of the section within inset with different vertical scale. Vertical scale is in meters and x-axis of measured section shows sediment coarsening trend.

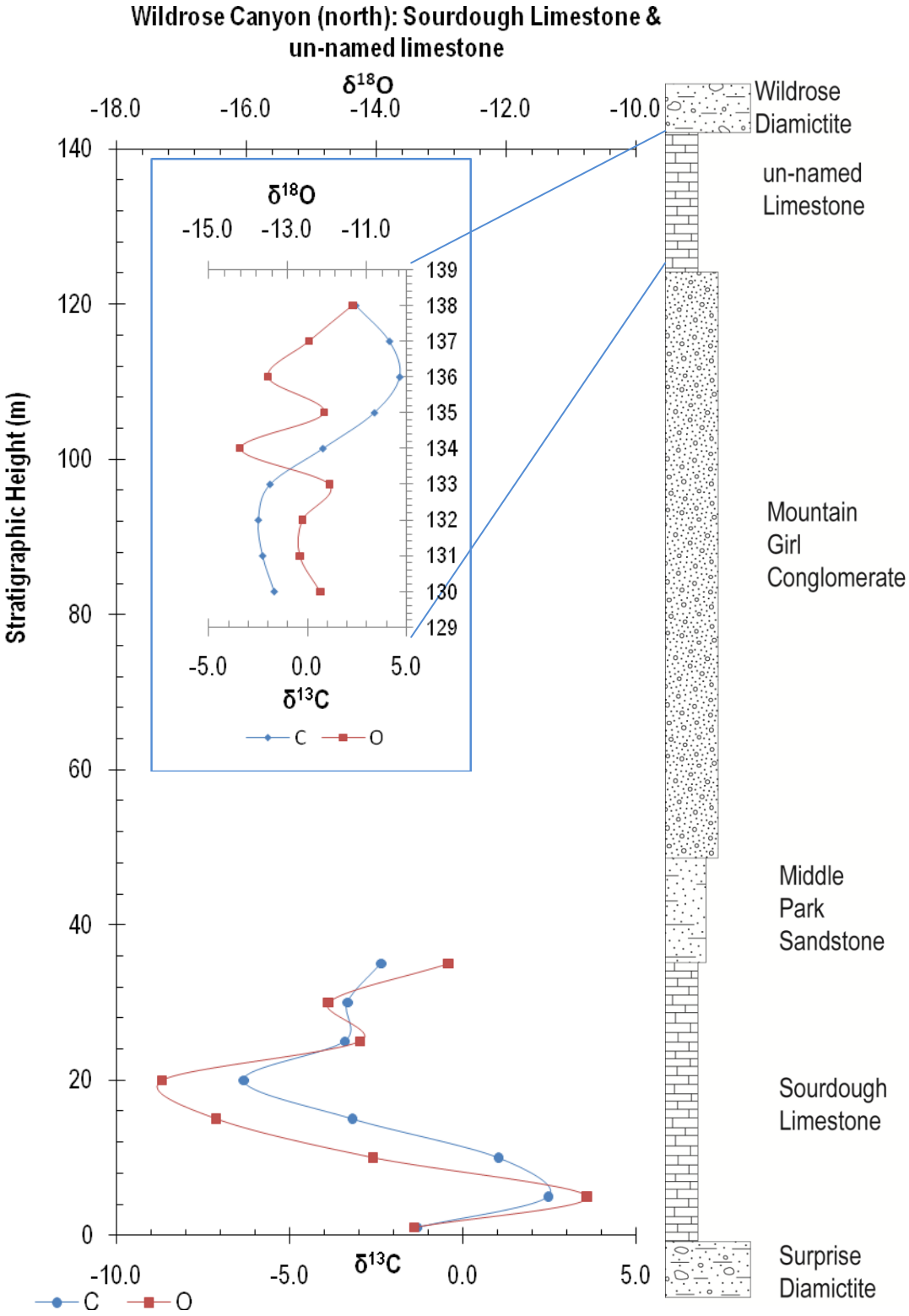
Wildrose Canyon (north): Sourdough Limestone & un-named limestone
δ18O
-18.0
-16.0
-14.0
-12.0
-10.0
Stratigraphic Height (m)
140
120
100
80
60
40
20
0
δ13C
-10.0
-5.0
0.0
5.0
C
O
δ18O
-15.0
-13.0
-11.0
139
138
137
136
135
134
133
132
131
130
129
-5.0
0.0
5.0
δ13C
C
O
Wildrose Diamictite
un-named Limestone
Mountain Girl Conglomerate
Middle Park Sandstone
Sourdough Limestone
Surprise Diamictite

Fig. 3.7. Paired isotopic profiles and measured section for the Sourdough Limestone in Pleasant Canyon (Cooper Mine; 36° 2'35.63"N 117° 4'33.95"W). Top of the profile includes the un-named limestone. Vertical scale in meters and grain size indicated by x-axis of measured section.

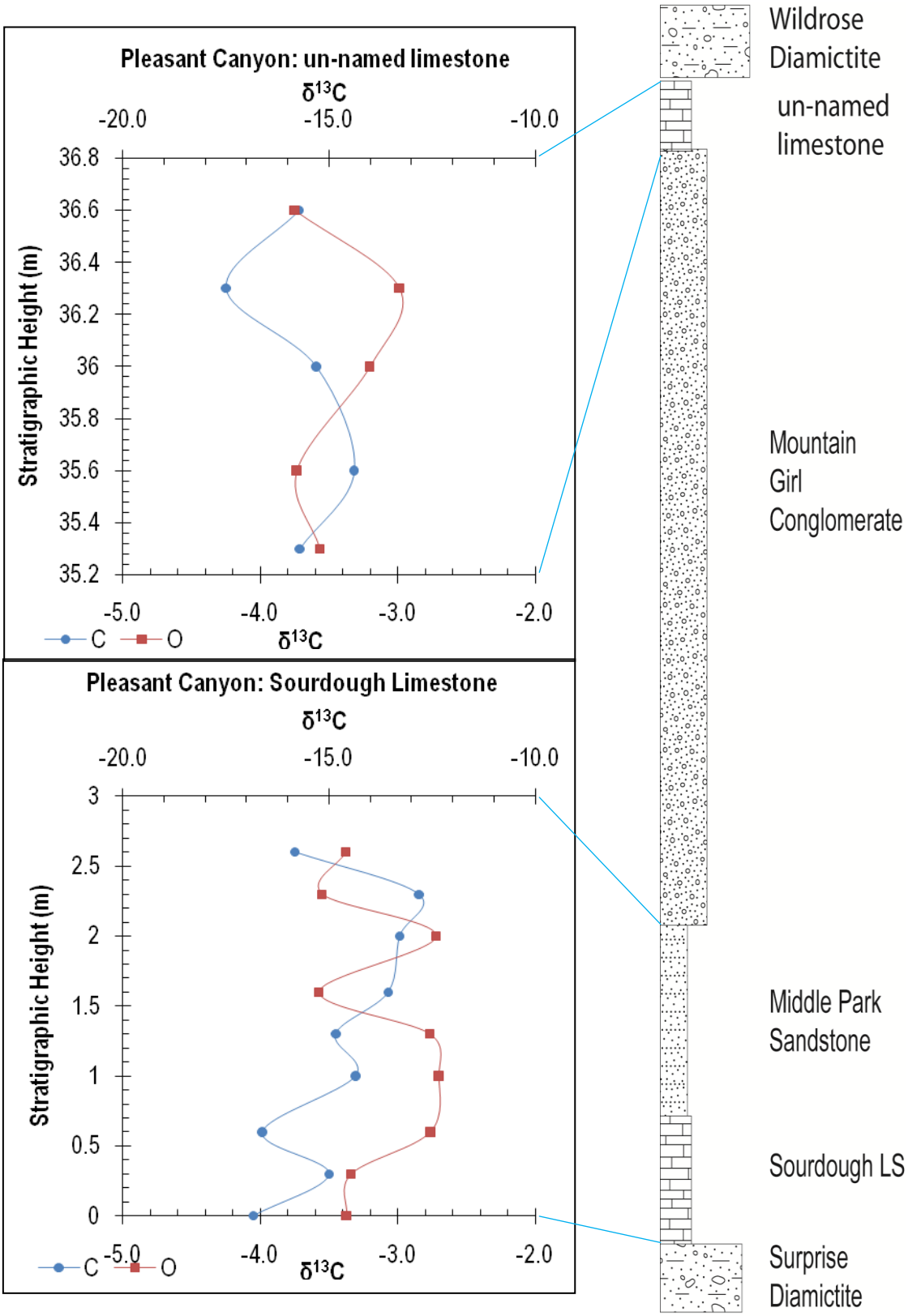
Pleasant Canyon: un-named limestone
δ13C
-20.0
-15.0
-10.0
36.8
36.6
36.4
36.2
36
35.8
35.6
35.4
35.2
Stratigraphic Height (m)
-5.0
-4.0
-3.0
-2.0
C
O
δ13C
Pleasant Canyon: Sourdough Limestone
δ13C
-20.0
-15.0
-10.0
3
2.5
2
1.5
1
0.5
0
Stratigraphic Height (m)
-5.0
-4.0
-3.0
-2.0
C
O
δ13C
Wildrose Diamictite
un-named limestone
Mountain Girl Conglomerate
Middle Park Sandstone
Sourdough LS
Surprise Diamictite

Fig. 3.8. Paired isotopic profile and measured section for the Sourdough Limestone in Sourdough Canyon (36° 7'56.78"N 117° 5'57.67"W). Both the section and profile show the more complicated carbonate stratigraphy sandwiched between the Wildrose Diamictite and the lowermost Noonday Dolomite (the Sentinel Peak Member). The photograph shows three separate carbonate intervals (height at base of photograph and two buff-colored cycles below the alabaster-white Sentinal Peak Member of the Noonday Dolomite) between the Wildrose Diamictite and the lowermost Noonday Dolomite. Vertical scale in meters and x-axis of measured section denotes changing grain size.

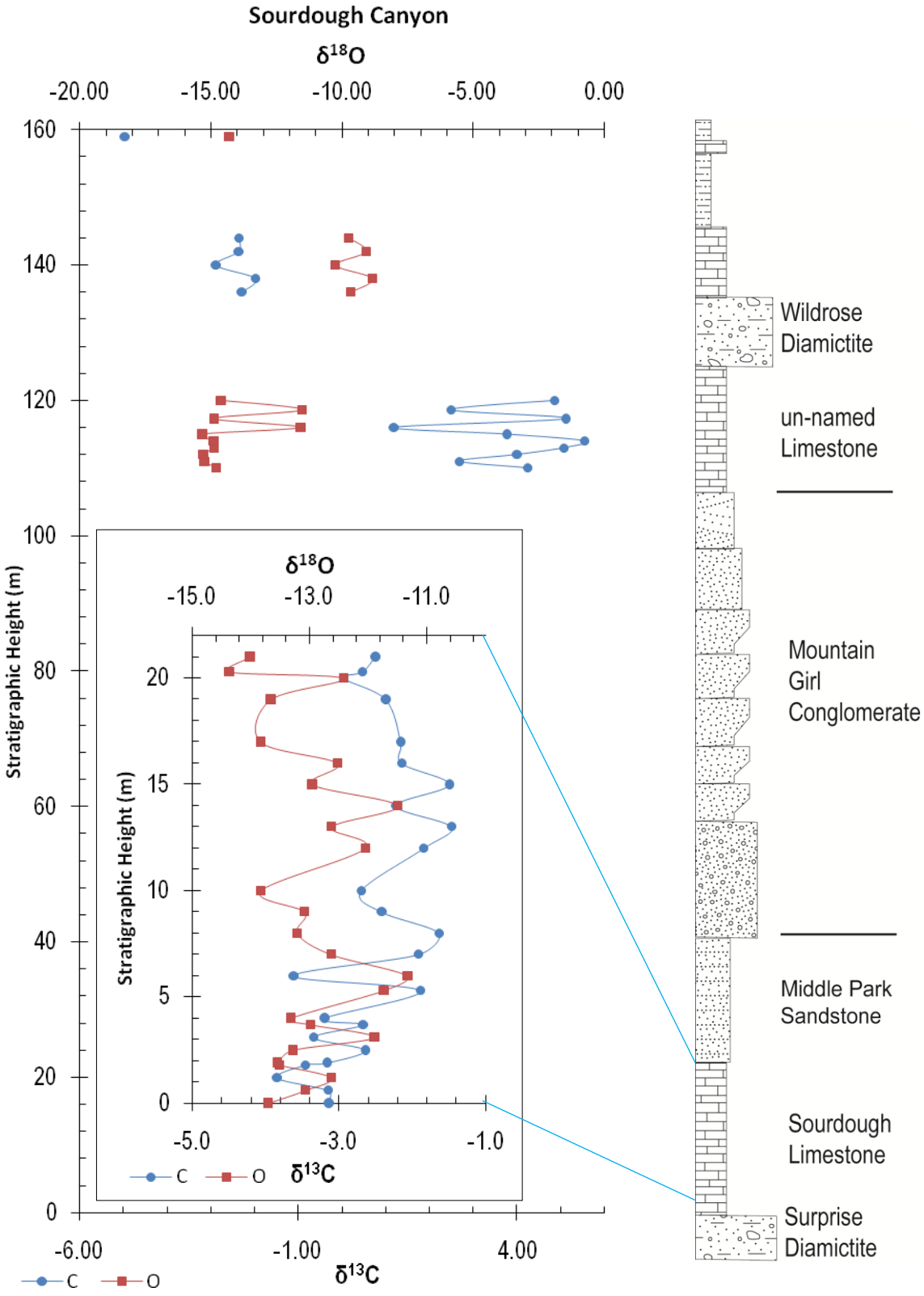
Sourdough Canyon
δ18O
-20.00
-15.00
-10.00
-5.00
0.00
160
140
120
100
80
60
40
20
0
Stratigraphic Height (m)
-6.00
-1.00
4.00
δ13C
C
O
δ18O
-15.0
-13.0
-11.0
20
15
10
5
0
Stratigraphic Height (m)
-5.0
-3.0
-1.0
δ13C
C
O
Wildrose Diamictite
un-named Limestone
Mountain Girl Conglomerate
Middle Park Sandstone
Sourdough Limestone
Surprise Diamictite

Fig. 3.9. Paired isotopic profile and measured section for Wood Canyon (35°56'12.97"N 117° 7'33.85"W) showing both the Sourdough Limestone and all three members of the Noonday Dolomite (right) and isotopic profile for bottom 30 km of the Sourdough Limestone (right) underlain by photograph of the section sampled. The Sourdough Limestone here is ca. 40 m thick and composed of three cycles separated by sandstone beds. The profile on the right shows distinct dips in isotopic values adjacent to sandstone intervals (the bottom sand interval is not visible). On the left, the upper two members of the Noonday Dolomite show a mineralogical change from the Sentinal Peak Member to limestone. Vertical scale in meters and x-axis of measured section reflects coarsening grain size.

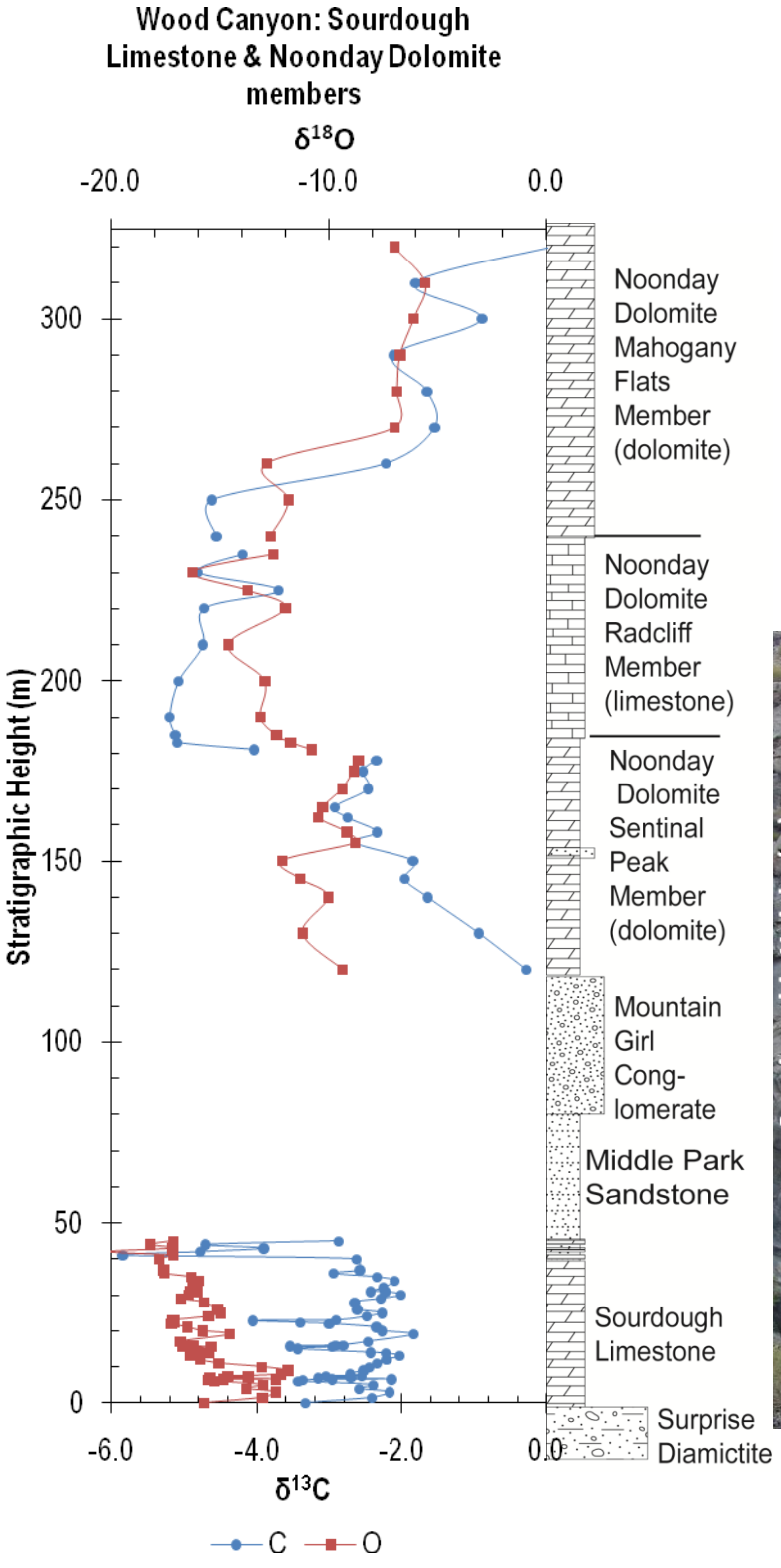
Wood Canyon: Sourdough Limestone & Noonday Dolomite members
δ18O
-20.0
-10.0
0.0
300
250
200
150
100
50
0
Stratigraphic Height (m)
Noonday Dolomite Mahogany Flats Member (dolomite)
Noonday Dolomite Radcliff Member (limestone)
Noonday Dolomite Sentinal Peak Member (dolomite)
Mountain Girl Cong-lomerate
Middle Park Sandstone
Sourdough Limestone
Surprise Diamictite
-6.0
-4.0
-2.0
0.0
δ13C
C
O

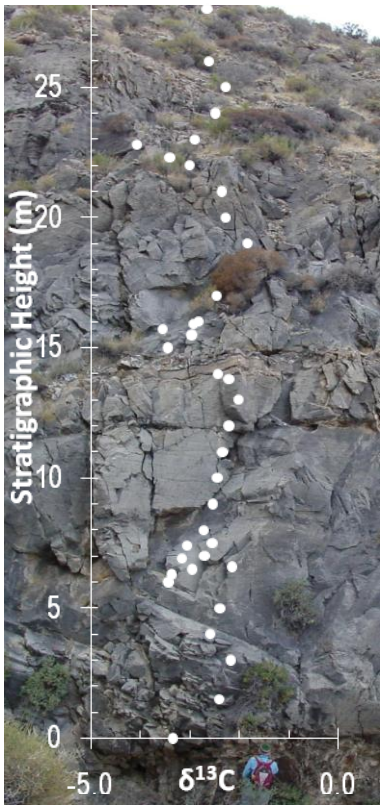
Wood Canyon: Sourdough Limestone
25
20
15
10
5
0
Stratigraphic Height (m)
-5.0
δ13C
0.0

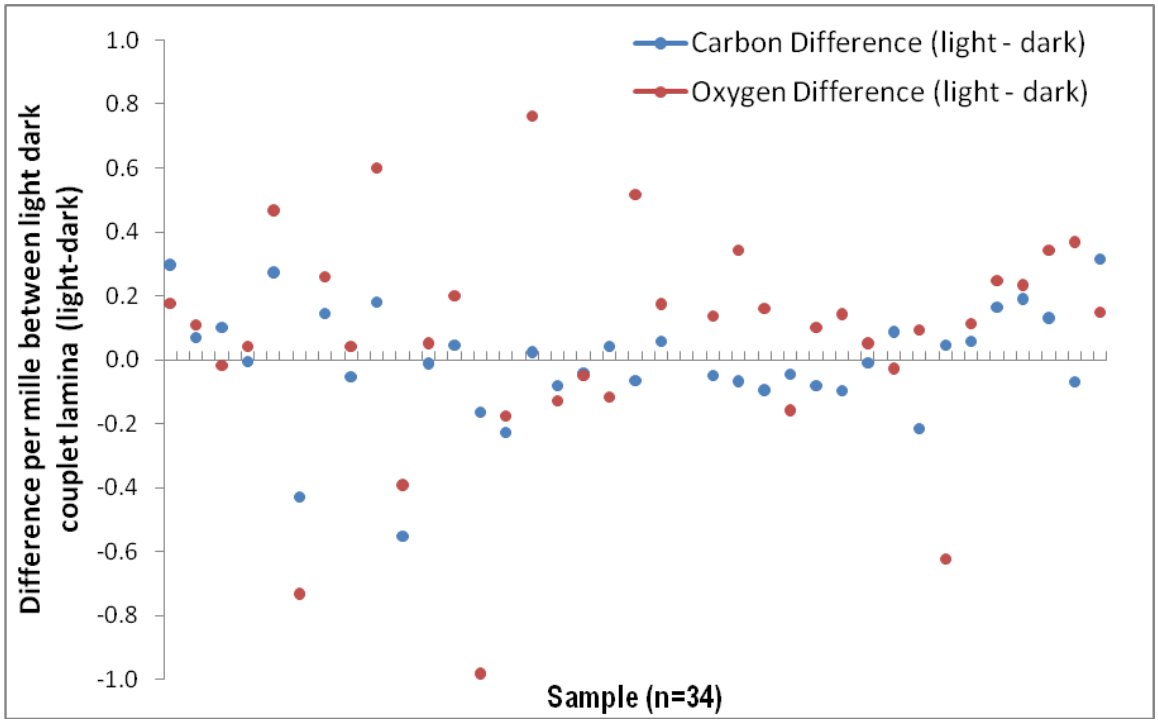

Fig. 3.10. The Sourdough Limestone is characterized by light-dark coupled laminations. This Figure shows the difference in isotopic values for both carbon and oxygen between light-dark couplets. Positive values indicate light lamination is heavier than its corresponding dark lamination (n=34).

4. Discussion

A variety of processes have been shown to influence both the $\delta^{13}C$ and $\delta^{18}O$ values of carbonate minerals, ranging from synsedimentary processes like biological fractionation during mineral precipitation (Andres et al., 2006; Sumner, 2001), facies control due to a marine isotopic gradient (Giddings and Wallace, 2009; Hotinski et al., 2004; Shen et al., 2005) to post-depositional processes like diagenetic alteration during and after lithification and burial (Banner and Hanson, 1990).

Two questions need to addressed to determine the usefulness of limestone intervals as timelines. One, do isotopic values represent primary values from carbonate grains precipitated during deposition making them a reasonable basis for correlation? Two, based on characteristics other than isotopic values can the carbonate intervals and overlying sequence boundaries serve as timelines and assist in correlation between the eastern and western KPF successions?

4.1. Diagenesis

During lithification, the mineralogy of carbonates is usually "set" under the influence of either vadose or phreatic waters of meteoric origin (Hudson, 1975; Irwin et al., 1977; Knauth and Kennedy, 2009; Land, 1970; Pingitore, 1976). During recrystallization during progressive burial, isotopic values often come into carbon and oxygen isotopic equilibrium with available pore water containing a variable fraction of meteoric, deep basinal fluids and marine values from dissolved phases. Meteoric and deep basinal fluids contain both oxygen from water and carbon from carbon dioxide that are more depleted than primary marine values. These modifications to fluids result in

alteration of primary mineralogy and precipitation of secondary cements that have more depleted $\delta^{13}C$ and $\delta^{18}O$ values (Hudson, 1975; Land, 1986). Alteration by meteoric water may impose a systematic covariation between $\delta^{13}C$ and $\delta^{18}O$ recording mixing contributions of different fluids (Gross and Tracey, 1966). Mineralogy may play an important role in determining the timing of isotopic equilibration, with early dolomitization stabilizing the isotopic value of carbonate minerals during subsequent burial.

Both the Sourdough Limestone in the Panamint Range and the limestone in the Silurian Hills are recrystallized, have lost most of the finer-scale details, and have abundant spar veins, boudinized sandstone layers, and high-angle post-burial compressional folds. The Virgin Spring Limestone in the Black Mountains retains more fine-scale features but has abundant spar veins, and, along with the limestone in the Silurian Hills, has well-developed karst features. All $\delta^{18}O$ values cluster around -14‰. These values suggest remineralization in the presence of highly depleted high temperature burial fluids.

Knauth and Kennedy (2009) describe several diagenetic processes to which all carbonates are subject during stabilization and lithification. These processes create distinctive trends when $\delta^{13}C$ and $\delta^{18}O$ values are plotted against one another. Cross-plots of $\delta^{13}C$ and $\delta^{18}O$ for KPF limestone samples (Fig. 3.11) show such trends and suggest values for $\delta^{13}C$ have become depleted after precipitation and burial. The purple block arrow in Figure 3.11 separates the "forbidden zone" (Knauth and Kennedy, 2009) on the right from the "lithification domain" on the left. While primary isotopic values for oxygen and carbon might have been closer to modern values for marine waters (blue oval, Fig. 3.11), over time both isotopes trend toward more depleted values

under the influence of meteoric waters ($\delta^{13}C$ and $\delta^{18}O$ become more depleted). During later diagenesis, carbonates undergo further alteration in the presence of highly depleted burial fluids ($\delta^{18}O$ values becomes more depleted); this is shown by the red arrows. Derry (2010) modeled burial diagenetic environments that produce covariation and depletion of both $\delta^{13}C$ and $\delta^{18}O$ under the influence of high pCO_2 fluids.

Isotopic values for the Beck Spring Dolomite and the Noonday Dolomite, the two platformal carbonates that bound the KPF, are also plotted in Figure 3.11. As a group they show a strong positive co-variation (R^2=0.7). Limestone values cross-plot differently. The difference in diagenetic trends between dolomite and limestone groups suggests several different alteration pathways are shown in Figure 3.11. The Virgin Spring and Silurian Hill limestone intervals are largely positive and the Sourdough Limestone is largely negative, but they occupy a region of shared values (Fig. 3.12). The position of the limestone values on the cross-plot and occasional co-variation suggests depletion of isotopic values by burial fluids was more important than isotopic change imposed by meteoric fluids.

4.2. Chemostratigraphic Correlation of Limestone Intervals

Regional comparison of isotopic values is meaningless without considering the full range of values present. Recrystallization and $\delta^{18}O$ depletion suggest that these carbonate horizons have undergone locally controlled alteration. Few depositional processes result in enrichment of ^{13}C, while all common diagenetic processes result in depletion. All three limestone intervals (Sourdough, Virgin Spring and Silurian Hills) share highly enriched values (Fig. 3.12) and these values make the most reasonable basis for isotopic comparison.

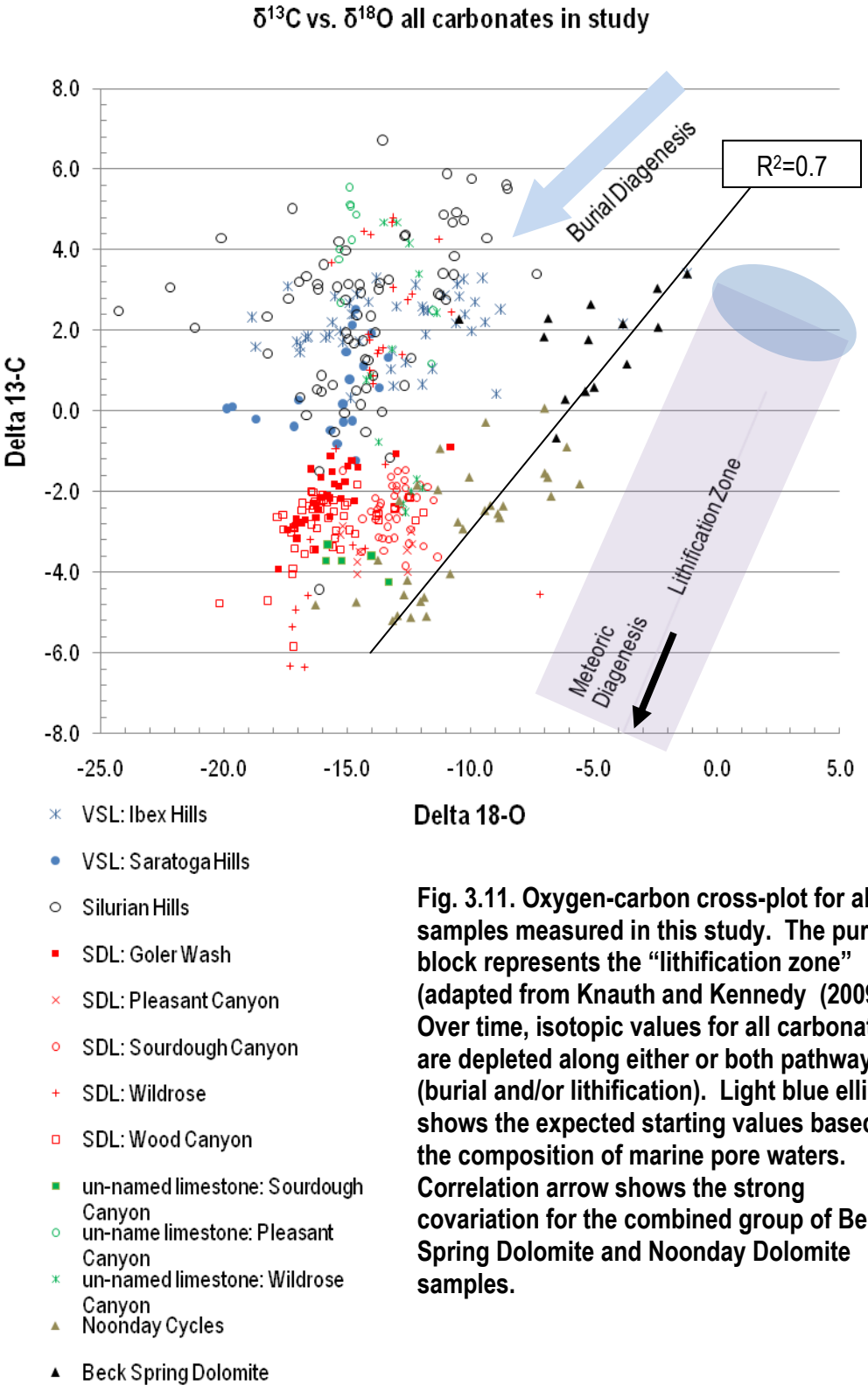

Fig. 3.11. Oxygen-carbon cross-plot for all samples measured in this study. The purple block represents the "lithification zone" (adapted from Knauth and Kennedy (2009)). Over time, isotopic values for all carbonates are depleted along either or both pathways (burial and/or lithification). Light blue ellipse shows the expected starting values based on the composition of marine pore waters. Correlation arrow shows the strong covariation for the combined group of Beck Spring Dolomite and Noonday Dolomite samples.

Figure 3.12 shows the range of $\delta^{13}C$ values for all of the carbonate samples measured. The large overlap in values suggests either alteration of primary values in most of the carbonate intervals or some heterogeneous mixing of detrital components with different isotopic values. Data from Prave (1999) is plotted on Figure 3.12 as open red circles and, given the limited number of samples, the enriched values in the un-named limestone and Silurian Hills limestone made a reasonable correlation. However, the positive vales identified in the Sourdough from Wildrose Canyon (Fig. 3.5 & 3.6) indicate that all carbonate units can be equally correlated on the basis of Prave's same criteria: positive carbon isotopic values. The anomalous negative values of some Sourdough sections he used to separate this unit in time are more likely to be an artifact of local post-depositional alteration as suggested by Bergfeld (1996) (Fig. 3.12 and Table 2.1) and do not record secular variation.

4.3 Lithostratigraphic Correlation of Limestone Intervals

In the east, the Virgin Spring Limestone and the Silurian Hills limestone are 20 km apart but share similar stratigraphic positions at the base of coarsening-upwards turbidite-diamictite-breccia successions. The Virgin Spring Limestone is karstic or truncated by a regional unconformity and the Silurian Hills limestone's upper surface is a karst surface. Both limestones have enriched δ13Cvalues.

Between the western and eastern regions, Tucker (1986) documented a number of similarities between the Sourdough and Virgin Spring Limestones including similar facies and depositional environment and a probable original aragonitic mineralogy; he suggested they might be related (Tucker, 1986).

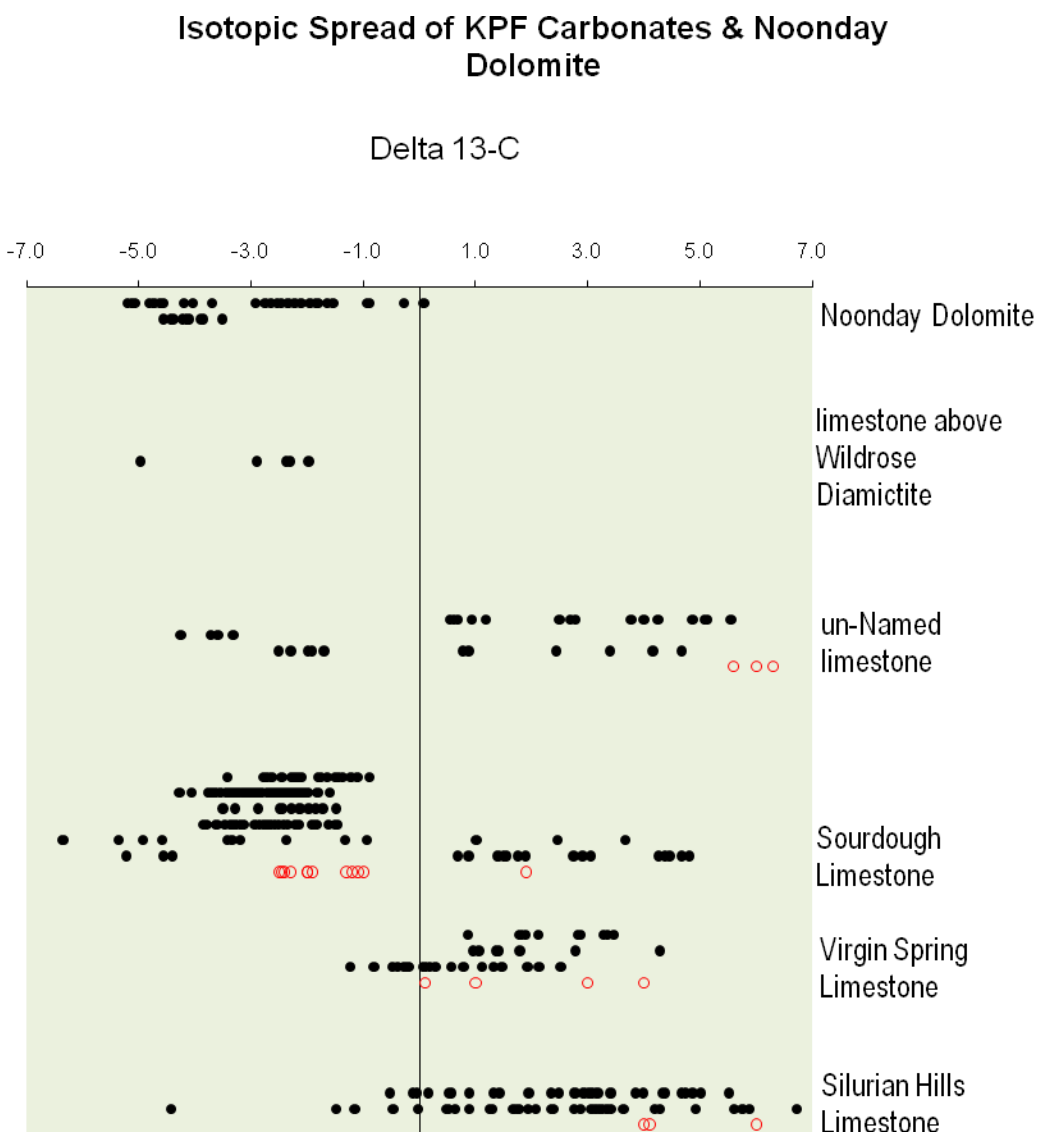

Fig. 3.12. Distribution in isotopic values for the carbonate intervals in the Kingston Peak Formation, along with the Noonday Dolomite; separate lines within each group represent different sections measured. These values are derived from table 2; multiple sample spots on each hand sample are not included. Open red circles represent isotopic values from Prave (1999).

The Virgin Spring Limestone in the Black Mountains, in the Saratoga Hills, and in the Silurian Hills, share lithological similarity, regional continuity, and distinctive and singular appearance within each section (Tucker, 1986) with the Sourdough Limestone. The Sourdough and Virgin Spring Limestones are now 30 km apart; however, prior to Cenozoic extension, the closest currently exposed sections of the Sourdough Limestone and Virgin Spring Limestone (Warmsprings Canyon and Virgin Springs Wash respectively) were likely <10 km apart (Topping, 1993).

4.4. Sequence Stratigraphic Correlation of Eastern and Western KPF Successions

In this sedimentary environment dominated by tectonism and given to lateral facies changes, potentially through-going carbonate horizons linked regionally as a product of relative sea level rise provide the best correlative surfaces between the southeastern KPF with that in the Panamint Range. Along with the Noonday Dolomite and the Beck Spring Dolomite, limestone intervals may provide important timelines that can be used to separate local tectonism from regional glacial signals in similar coarse grained sediments.

Sea Level Rise, Carbonate Highstand Deposits and Tectonism in the Panamint Range: The Virgin Spring, Sourdough and Silurian Hills Limestone intervals likely represent condensed intervals deposited in a deep water setting. The Virgin Spring Limestone is composed of detrital grains (ooids and spherules) transported into deeper waters, along with sand, by periodic storm currents. These grains are not visible in the heavily recrystallized Sourdough and Virgin Spring Limestones, but they also received periodic sands, likely from storm currents, and show the same sedimentary structures as the better preserved Virgin Spring Limestone. These deposits would have been

transported into deeper waters by storms during a sea level high stand. This depositional model is common: sea level rises, the basin is starved of siliciclastic input and carbonates and other chemical precipitates are deposited {Kennedy, 1996 #615}.

This common horizon helps to time the initiation of tectonism in the KPF. In the Panamint Range, the Surprise Member is comprised largely of diamictite facies, has rift-related basaltic pillow lava, is devoid of glacial evidence and underlies the Sourdough Limestone (Fig. 1.2). This horizon also argues for pulsed and progressive extension across the region. In the east, the Saratoga Hills Sandstone conformably underlies the Virgin Spring Limestone and is also conformable with the underlying Beck Spring Dolomite. The sand was likely deposited by storm currents in a part of the basin, or connected basin, not impacted by the incipient tectonism in the Panamint Range.

Sea Level Fall, Erosional Truncation and Tectonism in the East: A prominent erosional surface is identified in the KPF in the southeast. This surface cuts down through the Virgin Spring Limestone as well as up to 30 m of the underlying Saratoga Hills Sandstone Member and is overlain by Alexander Hills Diamictite. In the Panamint Range a similar surface cuts down through much of the KPF and into the Crystal Spring Formation (Miller, 1983) and is overlain by the Wildrose submember diamictite. In the southern Panamint Range, the uppermost KPF, the Wildrose submember can be seen resting on all of the underlying units of the KPF, except the Limekiln Springs (Miller, 1985), signaling a change in base level of hundreds of meters.

There are two possible interpretations for the cause of this erosional truncation: 1) it represents a eustatic change, or 2) lowering of local base level due to tectonism. In the first instance, assuming the Saratoga Hills Sandstone and the Limekiln Springs Members can be

correlated on the basis of their interbedding with the Beck Spring Dolomite, such a high-magnitude sea level change seems unlikely given the lack of a correlative event of similar magnitude in the eastern KPF. The sequence boundary below the Alexander Hills Diamictite does not appear to cut out more than 30 m of section. In Goler Wash, the Wildrose submember rests on a beveled surface cutting across the KPF, a Precambrian normal fault, and the basement. The Sourdough Limestone here was deposited as debris flows of retransported limestone mixed with lithified sandstone clasts shed from a tectonic high, timing tectonism in the western KPF with deposition of the Sourdough Limestone. A similar transition ~25 km to the east exists in Galena Canyon where a thin diamictite interval lies between the Crystal Spring Formation and the Noonday Dolomite. Less than 4 km to the south, near Warm Springs Canyon, a number of KPF members are present (Johnson, 1957; Wrucke et al., 1995).

These thin diamictite intervals have been preserved on top of uplifted horsts that were stripped of underlying Pahrump Group rocks during uplift and deposition of the KPF. These abrupt syndepositional fault transitions are identical to footwall-hanging wall transitions seen in the southeast and discussed in the following chapter. Given these stratigraphic relationships, proximity to similar faulted basins in the southeast and abundant evidence for local tectonism the sub-Wildrose truncation is interpreted to be a product of syndepositional tectonism. As in the southeast, the KPF in the Panamint Range thickens and undergoes facies changes away from these faulted margins (to the north). The same tectonic processes driving deposition of coarse-grained sediments in the Kingston Range also were responsible for coarse-grained sediments in the Panamint Range. This explains the absence of glacigenic sediments (i.e. striated clasts) in any members of the western KPF.

A remaining question is how the sequence boundary below the Alexander Hills Diamictite in the southeast is expressed in the Panamint Range. There is no apparent correlative sequence boundary immediately overlying the Sourdough Limestone. If the Sourdough Limestone and the Virgin Spring Limestone are correlative, the surface between the deeper water Sourdough Limestone and the interbedded shallower water Middle Park Member sandstones could represent a correlative conformity to the unconformity overlying the Virgin Spring Limestone. In the eastern KPF, there is not a similar correlative conformity to the sequence boundary to the later -Wildrose submember.

Two separate erosional events in the Panamint Range are suggested by 1) the transition from the Middle Park Sandstone to the fluvial deposits of the Mountain Girl Conglomerate and 2) the truncation of KPF members beneath the Wildrose Diamictite. The lower event may likely correlate with the sequence boundary in the eastern KPF, while the upper event, beneath the Wildrose submember, would be a product of tectonism, perhaps closely timed with syntectonism in the eastern KPF. These erosional surfaces, coarse-grained deposits and their timing relative to the through going carbonate horizons identify a pattern of progressive extension and diachronous creation of accommodation space between basins.

Sea Level Rise, Cessation of Tectonism and Deposition of High Stand Deposits: Deposition of coarse-grained, tectonic facies in both the Panamint Range and southeastern ranges ended abruptly with deposition of the Noonday Dolomite, although local interbedding at the base is common including some synsedimentary slides (DeYoung, 2005). The base of the Noonday Dolomite is continuous across the entire Death Valley region, recording a scale of process that

exceeded the more localized fault bound basins typical of the preceding Kingston Peak units. This shift in depositional style may indicate the cessation of rifting (Christie-Blick and Levy, 1989) and/or transgression, possibly caused by deglaciation. The geochemical and lithological affinities of the Noonday Dolomite are consistent with Marinoan cap-like carbonates in other basins globally, and the intimate relation with glacigenic diamictite, evidence for transgression and eustasy exceeding 200 m, regional deposition, and an abrupt shift to non-glacial sediment is characteristic of abrupt termination of the Marinoan ice age and the onset of the Ediacaran Period.

5. Conclusion

The dark, laminated, and lithologically distinctive thin, limestone units present regionally may provide an important time line across the different tectonic regions of Death Valley. This is based on the following observations described in this chapter. One, the Sourdough, Virgin Spring and Silurian Hills Limestones have positive carbon isotope end member values. Two, all three limestone horizons share a number of sedimentary characteristics. Three, all three horizons indicate a regional, or inter-basinal, sea level rise. Four, the Virgin Spring Limestone is eroded beneath the unconformity at the base of Alexander Hills Diamictite and in the Panamint Range 60 km to the west, the Sourdough Limestone is overlain by a possible correlative conformity.

The Virgin Spring Limestone, in the Black Mountains and in the Silurian Hills, and Sourdough Limestone make a plausible correlation, and one that would provide an important time line between these regions. While the basal Kingston Peak succession shows conformable interbedding of Beck Spring platformal carbonates with siliciclastics in both the Panamint Range (Labotka et al., 1980) and the eastern region, the cobble conglomerate and diamictite of the

Limekiln Spring and Surprise Members in the Panamint Range are fundamentally different than the fine siliciclastics of the Saratoga Hills Sandstone in the southeastern outcrops, and indicate that faulting began earlier in the northwest. This is supported by rift-related volcanics below this limestone datum in the west (Miller, 1983) and the abundant tectonic deposits above the limestone datum (the Silver Rule Mine Member) in the east.

Correlation of these carbonate horizons establishes the relative timing of different tectonic events. Fault-derived conglomerate postdating the Beck Spring Dolomite platformal deposits but underlying this horizon in the west identify well developed fault basins likely correlating with fine-grained facies underlying the Virgin Spring Limestone in the east. This suggests a step-wise progression from the northwest of localized fault basins (Eyles and Januszczak, 2004) filled by material derived from the underlying Beck Spring platform. The tectonic progression from north to south, accommodation space timing, and abrupt termination of coarse clastic deposits coinciding with regional flooding and transgression recorded by the Noonday dolomite suggest that tectonic control dominated the timing and sediment properties of the Kingston Peak formation with lesser modification by a climate influence. This record contrasts with the prevailing paradigm of two or more discrete global ice ages separated by tens of millions of years that are interpreted for many Neoproterozoic basins globally and suggests an alternative scenario of tectonically controlled creation of accommodation space against the background of a single prolonged Cryogenian ice age.

Termination of glacial influence beneath the Noonday Dolomite, the continuity of this signal across the region beyond the influence of local rift basins, and sea-level extent necessary for

deposition of >200 m stromatolitic Noonday Dolomite mounds argues for an external forcing of the stratigraphy by a abrupt end to the Marinoan glaciation. This supports the correlation of the Noonday Dolomite with other Marinoan Cap carbonates (Kennedy et al., 1998) and growing evidence of a synchronous end to the Marinoan ice age (Condon et al., 2005; Hoffmann et al., 2004). The timing of diamictite deposits with initiation of rifting further complicates a glacial interpretation by implying that the Sturtian global climate event was either fortuitously tied to the initial rift created accommodation space or somehow causally linked. Comparison between the KPF in the Panamint Range and the southeast across the Beck Spring Dolomite to Virgin Spring Limestone interval, however, indicates rifting was likely diachronous across the Death Valley region, making the coincidence of timing of rift basins and global ice ages even less likely.

The association of rift-related basin formation and glacial deposits is not unique to Death Valley but has been discussed extensively in numerous places (Eyles, 1993; Ross et al., 1995; Young et al., 1976). This stratigraphic finding is consistent with increasing geochronological evidence showing a spread of dates for "Sturtian aged" (or older) glacial deposits (Fig. 1.1) exemplified by recent Re-Os dates of the Sturtian type interval in south Australia, which showed diachronous ages for the lower interval even into central Australia- a previously confident correlation with relatively similar lithologic successions and cap carbonates (Kendall et al., 2006; Kendall et al., 2004). In southern Namibia, the depositional age of the earliest "Sturtian" glacial has been constrained to be ca. 754 Ma (Hoffmann *et al*., 2006) representing a 14 Ma extension to the age of the oldest Sturtian aged deposits. Kendall *et al*. (2004) demonstrate a 30 million year time difference between Sturtian-age deposits in south and central Australia. This latter result is important because these deposits epitomize the lithologic and chemostratigraphic correlation

forming the basis of Harland's original "global event" concept and reinforce the growing scatter in radiometric ages (Allen and Etienne, 2008; Fanning and Link, 2004; Halverson et al., 2005) suggesting protracted or diachronous diamictite deposition. This scatter, sometimes ascribed to be a result of dubious radiometric data or regional glaciation (Halverson et al., 2005), suggests controls on glacial deposition relied not on an earlier and later discrete global climate "event" but instead on protracted glaciation and the timing of basin formation.

The possibility that the Sourdough Limestone is a Sturtian cap carbonate (Prave, 1999) because it directly overlies the Surprise diamictite and maintains similar lithological features of some cap carbonates needs to be balanced against: 1) the current lack of independent evidence for glacial origin of diamictite within the Surprise or Limekiln Members (i.e. striations, facets or dropstones), 2) the evident tectonic influence on the succession that could account for diamictite lithologies by gravity flow, 3) the absence of glacial influence 50 km away in potentially correlative strata of the Saratoga Hills Sandstone (dropstones), or 4) the presence of a post Virgin Spring interglacial record in any of the basin transects in the eastern area.

The sedimentary succession in the eastern KPF area provides an alternative to the paradigm of two or more discrete and global Neoproterozoic ice ages. It is more suggestive of a second order glacial modification of a dominant tectonic control with timing determined by fault-controlled creation of accommodation space. This record is also consistent with an association between alpine glaciation and tectonic uplift during rifting, such as the glacial record associated with 4-5 km Cenozoic uplift of escarpments in the West Antarctic rift system (Behrendt and Cooper,

1991). Glacial conditions may have been more easily initiated with subtle changes in uplift since Kingston Peak deposition coincided with the ambient cold climate conditions of the Cryogenian.

References

Allen, P.A., and Etienne, J.L., 2008, Sedimentary challenge to snowball Earth: Nature Geoscience, v. 1, p. 817-825.

Andres, M.S., Sumner, D.Y., Reid, R.P., and Swart, P.K., 2006, Isotopic fingerprints of microbial respiration in aragonite from Bahamian stromatolites: Geology, v. 34, p. 973-976.

Banner, J.L., and Hanson, G.N., 1990, Calculation of simultaneous isotopic and trace element variations during water-rock interaction with applications to carbonate diagenesis: Geochimica et Cosmochimica Acta, v. 54, p. 3123-3137.

Behrendt, J.C., and Cooper, A.K., 1991, Evidence of rapid Cenozoic uplift of the shoulder escarpment of the West Antarctic rift system and a speculation on possible climate forcing: Geology, v. 19, p. 315-319.

Bergfeld, D., Nabelek, P.I., and Labotka, T.C., 1996, Carbon isotope exchange during polymetamorphism in the Panamint Mountains, California, USA: Journal of Metamorphic Geology, v. 14, p. 199-212.

Christie-Blick, N., and Levy, M., 1989, Stratigraphic and tectonic framework of upper Proterozoic and Cambrian rocks in the Western United States, *in* Christie-Blick, N., Levy, M., Mount, J.F., Signor, P.W., and Link, P.K., eds., ???: 28th International Geological Congress field trip guide series 7-21: Washington D.C., American Geophysical Union, p. 7-21.

Condon, D., Zhu, M., Bowring, S., Wang, W., Yang, A., and Jin, Y., 2005, U-Pb Ages from the Neoproterozoic Doushantuo Formation, China: Science, v. 308, p. 95-98.

Corsetti, F.A., and Kaufman, A.J., 2003, Stratigraphic investigations of carbon isotope anomalies and Neoproterozoic ice ages in Death Valley, California: GSA Bulletin, v. 115, p. 916-932.

DeYoung, D.P., 2005, The Neoproterozoic Ibex Formation, eastern California: Stratigraphic and Sedimentological Constraints on Ice Age and Carbonate Precipitation Events of Southern Death Valley [MSc thesis]: Riverside, University of California, Riverside.

Eyles, N., 1993, Earth's glacial record and its tectonic setting: Earth-Science Reviews, v. 35, p. 1-248.

Eyles, N., and Januszczak, N., 2004, 'Zipper-rift': a tectonic model for Neoproterozoic glaciations during the breakup of Rodinia after 750 Ma: Earth-Science Reviews, v. 65, p. 1-73.

Fanning, C.M., and Link, P.K., 2004, U-Pb SHRIMP ages of Neoproterozoic (Sturtian) glaciogenic Pocatello Formation, southeastern Idaho, v. 32, p. 881-884.

Giddings, J.A., and Wallace, M.W., 2009, Facies-dependent [delta]13C variation from a Cryogenian platform margin, South Australia: Evidence for stratified Neoproterozoic oceans?: Palaeogeography, Palaeoclimatology, Palaeoecology, v. 271, p. 196-214.

Gross, M.G., and Tracey, J.I., Jr., 1966, Oxygen and carbon isotopic composition of limestones and dolomites, bikini and eniwetok atolls: Science, v. 151, p. 1082-1084.

Halverson, G.P., Hoffman, P.F., Schrag, D.P., Maloof, A.C., and Rice, A.H.N., 2005, Towards a Neoproterozoic composite carbon isotopic record, v. 117, p. 1181-1207.

Hoffman, P.F., Kaufman, A.J., Halverson, G.P., and Schrag, D.P., 1998, A Neoproterozoic snowball earth: Science, v. 281, p. 1342-1346.

Hoffmann, K.H., Condon, D.J., Bowring, S.A., and Crowley, J.L., 2004, U-Pb zircon date from the Neoproterozoic Ghaub Formation, Namibia; constraints on Marinoan glaciation: Geology, v. 32, p. 817-820.

Hotinski, R.M., Kump, L.R., and Arthur, M.A., 2004, The effectiveness of the Paleoproterozoic biological pump; a delta (super 13) C gradient from platform carbonates of the Pethei Group (Great Slave Lake Supergroup, NWT): Geological Society of America Bulletin, v. 116, p. 539-554.

Hudson, J.D., 1975, Carbon Isotopes and Limestone Cement: Geology (Boulder), v. 3, p. 19-22.

Irwin, H., Curtis, C., and Coleman, M., 1977, Isotopic evidence for source of diagenetic carbonates formed during burial of organic-rich sediments: Nature, v. 269, p. 209-213.

Johnson, B.K., 1957, Geology of a part of the Manly Peak Quadrangle, southern Panamint Range, California: University of California Publications in Geological Sciences, v. 30, p. 353-423.

Kendall, B., Creaser, R.A., and Selby, D., 2006, Re-Os geochronology of postglacial black shales in Australia: Constrains on the timing of [ldquo]Sturtian[rdquo] glaciation, v. 34, p. 729-732.

Kendall, B.S., Creaser, R.A., Ross, G.M., and Selby, D., 2004, Constraints on the timing of Marinoan "Snowball Earth" glaciation by 187Re-187Os dating of a Neoproterozoic, post-glacial black shale in Western Canada: Earth and Planetary Science Letters, v. 222, p. 729-740.

Kennedy, M.J., Runnegar, B., Prave, A.R., Hoffman, K.-H., and Arthur, M.A., 1998, Two or four Neoproterozoic glaciations?, v. 26, p. 1059-1063.

Knauth, L.P., and Kennedy, M.J., 2009, The late Precambrian greening of the Earth, v. 460, p. 728-732.

Labotka, T.C., Albee, A.L., Lanphere, M.A., and McDowell, S.D., 1980, Stratigraphy, structure, and metamorphism in the central Panamint Mountains (Telescope Peak Quadrangle), Death Valley area, California: Geological Society of America Bulletin, v. 91 Part II, p. 843-933.

Land, L.S., 1970, Phreatic versus vadose meteoric diagenesis of limestones: evidence from a fossil water table: Sedimentology, v. 14, p. 175-185, 6 Figs.

—, 1986, Limestone diagenesis - some geochemical considerations, *in* Mumpton, F.A., ed., Studies in diagenesis: U.S. Geological Survey Bulletin 1578, Volume 1578, p. 129-137.

Marian, M.L., 1979, Sedimentology of the Beck Spring Dolomite, eastern Mojave Desert, California [Master's thesis]: Los Angeles, University of Southern California.

Miller, J.M.G., 1983, Stratigraphy and sedimentolgy of the upper Proterozoic Kingston Peak Formation, southern Panamint Range, eastern California [Doctoral thesis]: Santa Barbara, University of California.

—, 1985, Glacial and syntectonic sedimentation: The upper Proterozoic Kingston Peak Formation, southern Panamint Range, eastern California, v. 96, p. 1537-1553.

Pingitore, N.E., 1976, Vadose and phreatic diagenesis, process, products and their recognition in corals, v. 46, p. 985-1006, 10 Tabs.

Prave, A.R., 1999, Two diamictites, two cap carbonates, two delta (super 13) C excursions, two rifts; the Neoproterozoic Kingston Peak Formation, Death Valley, California: Geology (Boulder), v. 27, p. 339-342.

Ross, G.M., Bloch, J.D., and Krouse, H.R., 1995, Neoproterozoic strata of the southern Canadian Cordillera and the isotopic evolution of seawater sulfate: Precambrian Research, v. 73, p. 71-99.

Shen, Y., Zhang, T., and Chu, X., 2005, C-isotopic stratification in a Neoproterozoic postglacial ocean: Precambrian Research

Stable Isotopes, Life and Early Earth History, v. 137, p. 243-251.

Stewart, J.H., 1972, Initial deposits in the Cordilleran geosyncline: Evidence of a late Precambrian (<850 m.y.) continental separation: Geological Society of America Bulletin, v. 83, p. 1345-1360.

Sumner, D.Y., 2001, Microbial influences on local carbon isotopic ratios and their preservation in carbonate: Astrobiology, v. 1, p. 57-70.

Topping, D.J., 1993, Paleogeographic reconstruction of the Death Valley extended region: Evidence from Miocene large rock-avalanche deposits in the Amargosa Chaos Basin, California: Geological Society of America Bulletin, v. 105, p. 1190-1213.

Tucker, M.E., 1986, Formerly aragonitic limestones associated with tillites in the Late Proterozoic of Death Valley, California: Journal of Sedimentary Petrology, v. 56/6, p. 818-830, 14 Figs., 3 Tabs.

Wright, L.A., Troxel, B.W., Williams, E.G., Roberts, M.T., and Diehl, P.E., 1974, Precambrian sedimentary environments of the Death Valley region, eastern California: Shoshone, Death Valley Publ. Co.

Wrucke, C.T., Stevens, C.H., and Wooden, J.L., 1995, The Butte Valley and Layton Well thrusts of eastern California; distribution and regional significance: Tectonics, v. 14, p. 1165-1171.

Young, G.M., Williams, G.E., and Schermerhorn, L.J.G., 1976, Late Precambrian mixtites; glacial and/or nonglacial?: American Journal of Science, v. 276, p. 366-384.

CHAPTER FOUR:

THE INFLUENCE OF TECTONISM ON PRESERVATION OF THE CRYOGENIAN CLIMATE RECORD:

KINGSTON PEAK FORMATION, SOUTHEASTERN DEATH VALLEY REGION

Chapter Summary

This final chapter discusses the range of sedimentary and stratigraphic evidence for the role of glacial and tectonic processes in the KPF and places it into context with the global record of climate change during the Neoproterozoic. Specifically, observations made in the KPF contribute to resolving the timing of Neoproterozoic climate change. Does the relationship between tectonism and preservation of glacigenic sediments support the snowball Earth model of discrete and globally synchronous climate events, or a model of a long-lived Cryogenian glacial ice age with regional cycles of ice growth and retreat? Stratigraphic packaging of the KPF in extensional basins into distinct wedge-shaped geometries, a regional unconformity identifying initiation of tectonism, through-going carbonate intervals that serve as timelines for progressive tectonism, and the conformable relationship with the overlying Noonday Dolomite demonstrate a record of a long-lived Cryogenian ice age and the important role that tectonism, and accompanying accommodation space, has in biasing the record of climate change.

1. Introduction

The stratigraphic record of Late Neoproterozoic glacial intervals provides insight into how the Earth's ancient climate transitioned between hothouse and icehouse conditions and how this interval differed from the better understood Phanerozoic mode of climate transition. This interval also resides at the critical transition between a biosphere populated solely by unicellular life and the advent of metazoans. Direct evidence of glaciation is the clearest proxy for ancient climate change and can assist in understanding the drivers, rates of change, magnitude, and duration of ice ages. Comparison to Phanerozoic ice ages helps identify changes in the behavior of the planet's climate system through time and identifies changes in the biosphere that coincide with important evolutionary events and permanent Earth system changes.

Central to interpretation of the climate record using glacial intervals are two concerns: one, is there reliable direct evidence for glaciation in preserved sediments and, two, is there a complete record of shifting climate conditions (warm-cold-warm) in the stratigraphic record? One reason for the absence of sedimentary evidence for glaciation during an ice age is erosional truncation. However, sedimentary evidence might also be absent due to a hiatus in preservation due to the lack of available accommodation space (i.e. an available basin in which to preserve deposits).

In the Cenozoic, various proxies for climate change are preserved in the deep ocean. Deep ocean sedimentary records are absent in ancient sections and glacial deposits rely on tectonically driven accommodation space in continental and near shore environments for preservation. Accommodation space is necessary for preservation of a complete record of climate

conditions and transitions. However, tectonism and accommodation space creation (i.e., rift-related extension) happen independent of climate change and so there is little reason to expect tectonism to coincidentally begin and end before and after climate shifts, thus the full complexity of change is not recorded. .

This chapter addresses these concerns by asking two important questions. One, does a detailed examination of the sedimentological features of one key stratigraphic interval interpreted to be glacial provide enough positive criteria (i.e. striated clasts, striated pavements, dropstones) or equivocal but supporting criteria (i.e. rapid changes in facies and diamictic intervals) to support a glacial interpretation? Two, does the stratigraphic record bounding glacial intervals provide evidence for controls on deposition and timing of accommodation space? This last question is fundamental to understanding ancient climate change as it addresses the assumption of the completeness of a geological record that is confounded by the association of accommodation space with tectonic events, which also provides many of the same sedimentological criteria used to interpret glaciation.

This study of the KPF: 1) examines the criteria for glaciation within the Neoproterozoic interval in Death Valley, 2) records the interplay between two important depositional processes (i.e. tectonism and glaciation) and 3) interprets Late Neoproterozoic basin evolution.

1.1. Earth's Glacial History

Earth's climate record is punctuated with at least five ice ages that resulted in sedimentary evidence of glaciation (Fig. 4.1). The earliest evidence for the action of ice in the sedimentary

record occurs from 2.7-2.3 Ga, known as the "Huronian," and appears in outcrops primarily in North America and in Southern Africa (Crowell, 1999). Because of the age of these deposits, it is unclear if there was any Cenozoic-style episodicity and if icy conditions were global in extent (Deynoux et al., 1994; Eyles, 2008).

The next ice age, and possibly the most severe and extensive (Deynoux et al., 1994; Hoffman and Schrag, 2002), occurred during the Cryogenian Period between ~750-635 Ma, includes evidence for ice at tropical latitudes (Schmidt et al., 2009; Sohl et al., 1999), and may have involved several globally synchronous glacial events (Hoffman et al., 1998; Hoffman and Schrag, 2002; Kennedy et al., 1998) or a number of diachronous glacial advances (Allen and Etienne, 2008; Kendall et al., 2006; Kendall et al., 2004). This glacial epoch terminated relatively suddenly at 635 Ma (Condon et al., 2005; Zhang et al., 2008; Zhang et al., 2005).

Two briefer and less understood ice ages occurred around 580 Ma (Gaskiers) and from 460-430 Ma (the Andean-Saharan). This latter ice age occurred during the late Ordovician to early Silurian and outcrops are limited to South America and Northern Africa (Crowell, 1999; Deynoux et al., 1994).

The most extensively studied ancient ice age, the Karoo (Crowell, 1978; Crowell and Frakes, 1970; Deynoux et al., 1994), occurred from the middle Carboniferous through the early Permian (350-260 Ma), left extensive deposits in many continents, and appears to have been largely driven by continental drift over the Earth's south pole (Crowell, 1978). During the Cenozoic Era, the planet has been subject to a climate regime where some permanent ice has been present

Fig. 4.1 Timing of Earth's Ice Ages

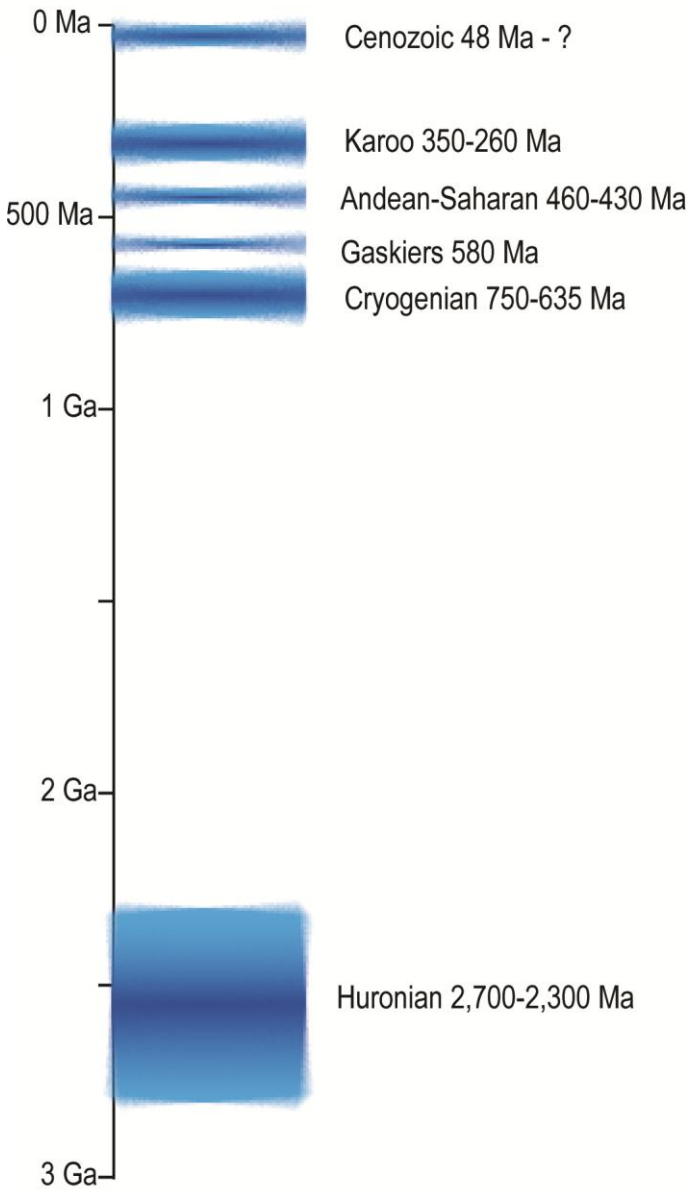

somewhere on the globe for at least the last 34 Ma (Kent et al., 2006; Lear et al., 2008) and possibly as early as 42 Ma, based on the presence of ice-rafted debris (IRD) in sediment cores from the North Atlantic (Tripati et al., 2008). This change to ice age conditions occurred at about 34 Ma after the Eocene-Oligocene climate transition away from Cenozoic greenhouse conditions (Lear et al., 2008). This modern ice age was likely controlled by either greenhouse gas accumulation, orbital forcing, or tectonism and resultant weathering, or a combination of these drivers. Geochemical proxies and ice-growth models indicate that while there may have been some ice present in the Northern Hemisphere, the majority of ice growth was likely limited to Antarctica (Liu et al., 2009) until the beginning of the Pleistocene Epoch. Continental ice was present at mid-latitudes in the Northern Hemisphere by 2.58 Ma, the beginning of the Pleistocene Epoch.

The intricate record of Cenozoic climate change is easier to resolve and glacial-interglacial cyclicity is more apparent than in the older ice ages. This resolution depends on both ice core records and unlithified marine and terrestrial sediments. The resolvability of the climate record becomes more detailed beginning 700 ka when the continental ice records can be examined. An extensive sedimentary and geochemical record indicates a climate system with a series of glacial-interglacial cycles, sudden transitions to warmer conditions after gradual buildup of ice, and complicated pattern of see-saw and synchronous conditions at the poles (Barker et al., 2009; Barker and Knorr, 2007). Given the resolution and preservation of the Cenozoic record, this pattern of diachronous climate conditions and systematic cyclicity is the best starting point from which to understand more ancient climate conditions.

1.2. Cryogenian Glaciation

Interpretation of Cryogenian glaciation commonly represents a significant departure from the model for causes and timing of icehouse conditions during the remainder of Earth history. The Cryogenian Period is characterized by numerous sections of coarse-grained strata that have been assigned a glacial interpretation. These coarse-grained strata occur in many global localities, often occurring as an older (ca. 720 Ma) and younger (ca. 640 Ma) interval separated by an interglacial interval, and may be capped by isotopically distinct carbonate intervals (Hoffman and Schrag, 2002).

However, coarse-grained intervals are associated with a wide range of depositional ages, from about 760 through 635 Ma Without available radiometric ages and any biostratigraphic age constraints, Harland (1964) suggested distinct coarse-grained intervals were synchronous and represented a means of global correlation of Earth's most significant climate event. The implication of this hypothesis is that icehouse conditions during the Cryogenian were global, extending upwards from near-equatorial latitudes, occurred relatively abruptly, and represented global-scale "climate catastrophes" (Harland, 1964). This is a departure from our understanding of later Phanerozoic icehouse conditions which likely depended on a combination of forcing agents, most importantly continental position and tectonic-scale transfer of carbon from the exosphere into the lithosphere (Crowell, 1978), and where ice extent continuously waxed and waned over a much longer 50-100 Ma interval. This departure from Phanerozoic models of icehouse climates has been popularized by the Snowball Earth hypothesis (Hoffman et al., 1998), which posits that there were four discrete global-scale icehouses during the period from 750 through 635 Ma

Alternatively, as with later ice ages, these coarse-grained stratigraphic horizons represent many diachronous intervals of deposition spread out over a 120 million year interval. This model would be similar in extent and timing of regional preservation to the record of coarse-grained glacial deposits representing both the Permo-Carboniferous and present Cenozoic ice ages. This model of Cryogenian glaciation is supported by a growing body of radiometric age constraints from both coarse-grained intervals and from overlying carbonates. In Figure 1.1, prominent coarse-grained strata are recorded as having been deposited across a range of ages from 754 Ma to 640 Ma Snowball Earth proponents would argue that Cryogenian glaciation is unlike Permo-Carboniferous glaciation (Hoffman and Schrag, 2002) based on the presence of carbonate intervals directly above glacial sediments, the depleted carbon isotopic signatures of those carbonates and near-equatorial paleolatitude of at least one glacial interval (Sohl et al., 1999).

One possibility is that intervals of coarse-grained strata are related to tectonism associated with the breakup of Rodinia during the Neoproterozoic. This rifting of Rodinia led to extension of the crust and accommodation space in which to preserve sediments. Because tectonic processes result in many of the same coarse-grained sedimentary characteristics as the action of glacial ice, assigning a glacial status to strata based solely on the presence of coarse-grained sediment, lithostratigraphic correlation is problematic. Such an association between rift-related processes and many stratigraphic intervals interpreted to be Cryogenian glacial deposits has been documented by Eyles & Januszczak (2004).

This relationship between tectonism and preservation of glacial deposits presents an important and obvious complication to understanding the record of ancient climate change in its

entirety and is the central theme of the chapter. Without a deep-marine record, ancient glacial sediments are preserved in the accommodation space provided by tectonic activity and associated subsidence. The preservation of a global climate signal should depend upon the supply of accommodation space, a regional process. This dependence is important, because an incomplete or abbreviated record of climate change remains without continual tectonism coincident with each ancient climate change event.

2. Testing the Timing of Neoproterozoic Climate Change and possibility of Accommodation Space Bias

The Snowball Earth hypothesis (Hoffman et al., 1998; Kirschvink, 1992) seeks to explain the global presence of late Neoproterozoic diamictite intervals. It predicts that a runaway ice-albedo feedback is capable of driving the entire planet into a state of global ice cover, and has done so at least once during the latest Neoproterozoic era (Cryogenian Period) and can only be overcome by external forcing from volcanic CO_2 input. If true, the planet's climate can be driven inescapably and uni-directionally toward a frozen end-member and an unassociated external mechanism (volcanic outgassing in the case of the Snowball Earth hypothesis) is required to drive climate in the opposite direction. The hypothesis is based on several sedimentary and geochemical observations (Allen and Etienne, 2008; Fairchild and Kennedy, 2007) and follows from a hypothesis by Kirschvink (1992) predicting a possible mechanism for the existence of widespread glacial deposits of late Cryogenian age, some apparently deposited at low latitudes.

A clear understanding of the global timing, or synchroneity vs. diachroneity, of Cryogenian glacial intervals, is critical to understanding how to characterize the Cryogenian ice age. Was it a long-lived (i.e. 50-100 Ma) period of regional ice growth and decay, perhaps linked in part to continental position as with later ice ages? Alternatively, was it "non-uniformitarian" in nature and significant because there were one or two globally synchronous climate "events" with ice advancing globally to near the equator and requiring extreme feedback systems to reverse icehouse conditions? Importantly, are we confounded in a proper understanding of ancient climate change because of the possibility that the timing of regional or local tectonism acts like an "on-off" switch on the preservation of glacial sediments?

This chapter tests the hypothesis that syndepositional tectonism played the primary role in controlling the distribution and the timing of glacigenic deposits. Coarse-grained lithologies can be used as evidence for the timing of tectonism and relation to deposition of glacigenic sediments. Tectonism timed with glaciation would bias the climate record by controlling availability of accommodation space in which a sedimentary record of glaciation might be preserved. This can be tested by identifying the stratigraphic relationship between tectonic and glacigenic sediments and determining whether glacigenic sediments are constrained within the period of tectonism. Further, this chapter considers coarse-grained deposits as a function of local tectonism rather than the typical emphasis on the climate origin of these same deposits. This distinction places the emphasis on local and not global climate events. .

The potential for local or regional tectonism to bias the climate record, and confound global correlation of coarse-grained intervals, is shown as a hypothetical model in Figure 4.2. A long-

lasting ice age may entail a complex interval of extensive ice and nearly ice-free conditions, perhaps with brief intervals where no permanent ice exists; this was the case during the Permo-Carboniferous ice age (Crowell, 1999). This interval of climate cycling is shown as a trend between extensive ice and nearly ice-free states in Figure 4.2a. However, tectonically provided accommodation space cannot be expected to be synchronous between different regions of the globe. If, in one region, glacial deposits are preserved due to extension and available accommodation space, they will not be preserved in the second region, as shown in Figure 4.2b. When accommodation space is available in the second region, a similar interval of coarse-grained facies will be preserved. If these separate and diachronous intervals occur within a distinctly different facies association, like a marine carbonate platform, they may give the appearance of being synchronous. While this is a hypothetical model, there is a growing body of radiometric dates supporting the diachroneity of Cryogenian glacial deposits (Fig. 1.1) (Allen and Etienne, 2008). Alternatively, uplift of topography in rift zones may lead to mountain glaciers and deposits of glacigenic sediments in an associated rift basin (see the red line in Fig. 4.2a) (Eyles and Januszczak, 2004).

2.1. The Test Interval: the Kingston Peak Formation

The Kingston Peak Formation (KPF) provides evidence for the important role that tectonism has on the completeness of the stratigraphic record. It is detailed enough in cliff exposures to physically trace the relation between measured sections and determine if there are time breaks between numerous diamictic intervals or if there are really several distinct glacial intervals as

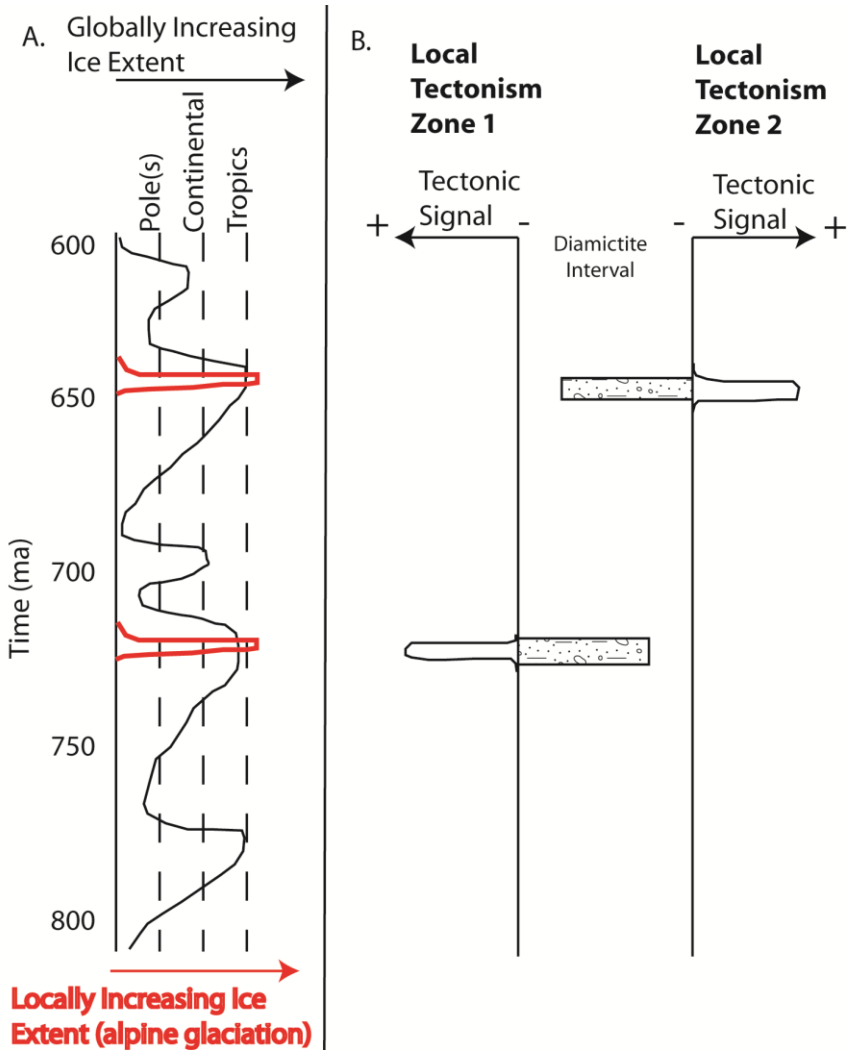

Fig. 4.2. Tectonism climate bias model. Shows a hypothetical situation where climate conditions change over the entire globe while sedimentary evidence is preserved diachronously in two geographically separate regions.

A. Ice volume waxes and wanes between the poles and the equator over the entire planet (global conditions) during a roughly 200 Ma ice age. Alternatively, the red line represents local ice growth in one zone related to adiabatic glacial advance; this might be the case along tectonically uplifted zones where elevation change was sufficient to preserve winter precipitation and build mountain glaciers.

B. In two hypothetical and separate areas a period of local tectonism occurs that provides accommodation space to preserve glacial sediments in that region.

predicted by the model of globally synchronous climate events. In the KPF, syndepositional tectonism was coincident with glaciation, preferentially preserving coarse-grained glacial deposits along with tectonic deposits. This coincidental timing raises doubts about interpreting other Cryogenian intervals as recording several global climate events, especially in light of the close association between many of these intervals and tectonism (Eyles and Januszczak, 2004). Multiple glacial intervals and cap carbonates in the same section may be the result of renewed tectonism and a period of adiabatic (alpine) ice growth or flooding during a relatively warmer or interglacial period.

3. Methods Used

Sedimentary and stratigraphic data was collected by: 1) a detailed examination of sedimentary features, 2) high-resolution (1:6000) geologic mapping across possible paleo footwall-to-hanging wall transitions, and 3) measurement of a variety of stratigraphic sections. Features in interbedded fine-grained and coarse-grained siliciclastic intervals should provide evidence of glacial influence during deposition. Mapping rapidly thickening siliciclastic intervals across syndepositional normal faults clarifies the timing of glacial and tectonic processes and the effect of tectonism on the glacial record. Finally, a number of measured sections across over 100 km of exposed and laterally continuous outcrops allow fault timing and lateral relation to be related to local tectonic and regionally more pervasive glacigenic facies.

4. Data

Data included in this section includes sedimentary evidence for tectonism and glaciation, stratigraphic evidence for timing of tectonism and its role on stratigraphic geometry, and description of contacts with the underlying and overlying formations.

4.1 Stratigraphic and sedimentary evidence for glaciation and tectonism

Saratoga Hills Sandstone: The Saratoga Hills Sandstone is 1 to 180 m thick, comprised of cm-scale beds of parallel laminated sandstone and siltstone and underlies a regional erosional unconformity (Fig. 2.11c). Sedimentary structures are dominated by planar parallel cross-lamination, but include low-angle cross-lamination, beds with scoured bases, rare massive sandstone beds with mudstone chips, and a general coarsening and increase in carbonate cement upsection. In the southern Black Mountain (35°54'45"N, 116°38'50"W, #23 & 24 in Fig. 2.1), the Saratoga Hills Sandstone varies in thickness by ca. 30 m over a lateral distance of 100 m due to erosional truncation.

Virgin Spring Limestone: The Virgin Spring Limestone (Tucker, 1986) is erosionally truncated and karsted (Fig. 2.13c), dark and parallel-laminated, sharply overlies the Saratoga Hills Sandstone, and is preserved in only three localities. The Limestone is 17 m thick and best exposed in the Ibex Hills (35°45'18"N, 116°26'12"W, #21 in Fig. 2.1), but also crops out at Virgin Spring Wash and in the Saratoga Hills where it is <4 m thick and gradually truncated to the south. Tucker (1986) described the Virgin Spring Limestone as comprised of cm- to dm-scale beds of parallel laminated limestone interbedded with <1 mm thick sandstone laminae with scoured bases and occasional

normal grading. Petrographic and sedimentary features include ooids and convoluted or overturned beds attributed to mass sediment movement down the palaeoslope (Tucker, 1986).

Alexander Hills Diamictite: The Alexander Hills Diamictite comprises a regionally extensive blanket of massive- to diffusely-bedded cobble-boulder diamictite that varies from 10 to 250 m in thickness, sharply overlies regionally extensive unconformity defining the top of the underlying Saratoga Hills Sandstone or Virgin Spring Limestone and contains striated and faceted clasts (Fig. 4.3). Diamictite clasts are derived from the underlying Pahrump Group or basement, the matrix is composed of coarse angular quartz sand and illite (mica) or chlorite, and basal diamictite commonly contains black limestone clasts and a carbonate-rich matrix likely derived from the underlying Virgin Spring Limestone. In the Saratoga Hills, southern Saddle Peak Hills, and Alexander Hills, the diamictite facies is interrupted by a 5–20 m interval of finer-grained facies, variably including siltstone and sandstone with parallel laminations, trough cross-bedding, steep bi-modal cross-lamination and normally graded pebble conglomerates with sandy tops.

In the Saratoga Hills, a fine-grained interval in the middle of the Alexander Hills Diamictite was investigated by M.J. Kennedy and found to contain fine-grained sandstone with varved laminations (Fig. 2.15). These varves appear immediately above a coarse-grained sandstone interval containing herring-bone cross lamination (Fig. 2.15e). I investigated the varves and found them to be divided into mm-scale bundles of between 10-14 dark-light coupled laminations (Fig. 2.15b). Light laminations within couplets are composed of one to two layers of sub-rounded to sub-angular coarse sand (Fig. 2.15c). Dark laminations within couplets are composed of silt and

Fig. 4.3 Striated clasts collected from the Alexander Hills Diamictite; a) Alexander Hills Diamictite (Alexander Hills; Fig. 2.1 #1). b) reverse side of Alexander Hills Diamictite in a c) Alexander Hills Diamictite (Horsethief Springs; Fig. 2.1 #8). d) Alexander Hills Diamictite– clast in matrix. Arrow indicates direction of striations (Saratoga Hills; Fig. 2.1 #20). e) Alexander Hills Diamictite (Beck Canyon West; Fig. 2.1 #4)

clay. Outsized grains, much larger than the grain size of sand in the laminations, appear within some bundles (Fig. 2.15b).

Silver Rule Mine Member: The Silver Rule Mine Member is 15 to 2000 m thick, consists of interbedded siltstone and sandstone, diamictite with striated clasts, normally graded conglomerate beds, km-scale olistoliths, and channel-filling sedimentary breccia. The lower Silver Rule Mine Member is comprised primarily of siltstone and sandstone interbedded with minor diamictite and conglomerate. Pebble- to cobble-sized outsized clasts commonly float in sandstone beds that grade laterally to conglomerate or diamictite. Sedimentary structures include normally graded beds, convolute laminations and siltstone with intraclasts and flame structures. A 2–3 m thick oncolitic dolostone in the Kingston Range (35°46'27"N, 115°52'59"W) is found at the top of the finer-grained lower Silver Rule Mine Member and marks a coarsening-upwards transition to interbedded sandstone, normally graded conglomerate and diamictite. As with the Alexander Hills Diamictite, diamictite intervals often have contain black limestone clasts in a black calcitic matrix. The middle to upper Silver Rule Mine Member is characterized by m- to km-scale mega-clasts and olistoliths of the underlying Pahrump Group that form prominent ridges in the Kingston Range around 35°44'43"N, 115°51'5"W and 35°44'35"N, 115°50'22"W (Wright *et al.* 1976).

Cobble to boulder outsize clasts are common in both massive and laminated siltstone and sandstone facies comprising sediment gravity density flows within the Silver Rule Mine Member. At Sperry Wash (35°42'13.76"N 116°14'34.47"W) a 170 m thick section of the Silver Rule Mine Member is excellently exposed, consisting of interbedded graded and massive debrites, diamictites and turbidites, deposited by various sediment gravity flows. Beck Spring Dolomite clasts within

turbidite beds are thicker than the beds containing them and, rarely, appear to form piercement structures at their basal contacts. These clasts have been interpreted as ice-rafted debris (Abolins et al., 2000; Corsetti and Kaufman, 2003) and thus may have important genetic implications for the Silver Rule Mine Member. Conversely, they have been interpreted as outsized clasts on the distal edges of debris flows or as lone clasts rolling down tectonically produced slopes (Troxel, 1982b).

A vertical transect with outsize clasts interpreted as dropstones was measured to understand the relationship between sediment gravity flows and outsized clasts. Clasts in 295 beds in a 2 m wide by 56 m high transect were measured to determine long-axis orientation and proximity to other outsize clasts within the same bed. Of the 33 outsize clasts observed over the 297 beds, 91% had been deposited with their long axes parallel to bedding. Within an along-bed distance of 1 m on each side of every clast, outsize clasts were either associated along bedding to a sandstone-to-debrite transition or with an average of eight additional outsized clasts.

Jupiter Mine Member: The Jupiter Mine Member gradationally overlies the Silver Rule Mine Member and is comprised of 200 to 1300 m of conglomerate, sedimentary breccia and monomictic mega-breccia (Fig.2.20 & 4.4a & b). Conglomerate and breccia beds are commonly normally graded and fill channels 1–2 m deep and 10–50 m wide. Mega-breccia is massive, dominated by up to m-scale angular blocks of Beck Spring Dolomite filling steeper narrower channels than graded beds. In the Kingston Range, sedimentary breccia composed entirely of Beck Spring Dolomite was deposited adjacent to a syndepositional fault (35°47'22"N, 115°50'1"W, #10 in Fig. 2.1). Laterally, sedimentary breccia and conglomerate is interbedded with normally graded to massive sandstone beds with sharp planar lower bed contacts.

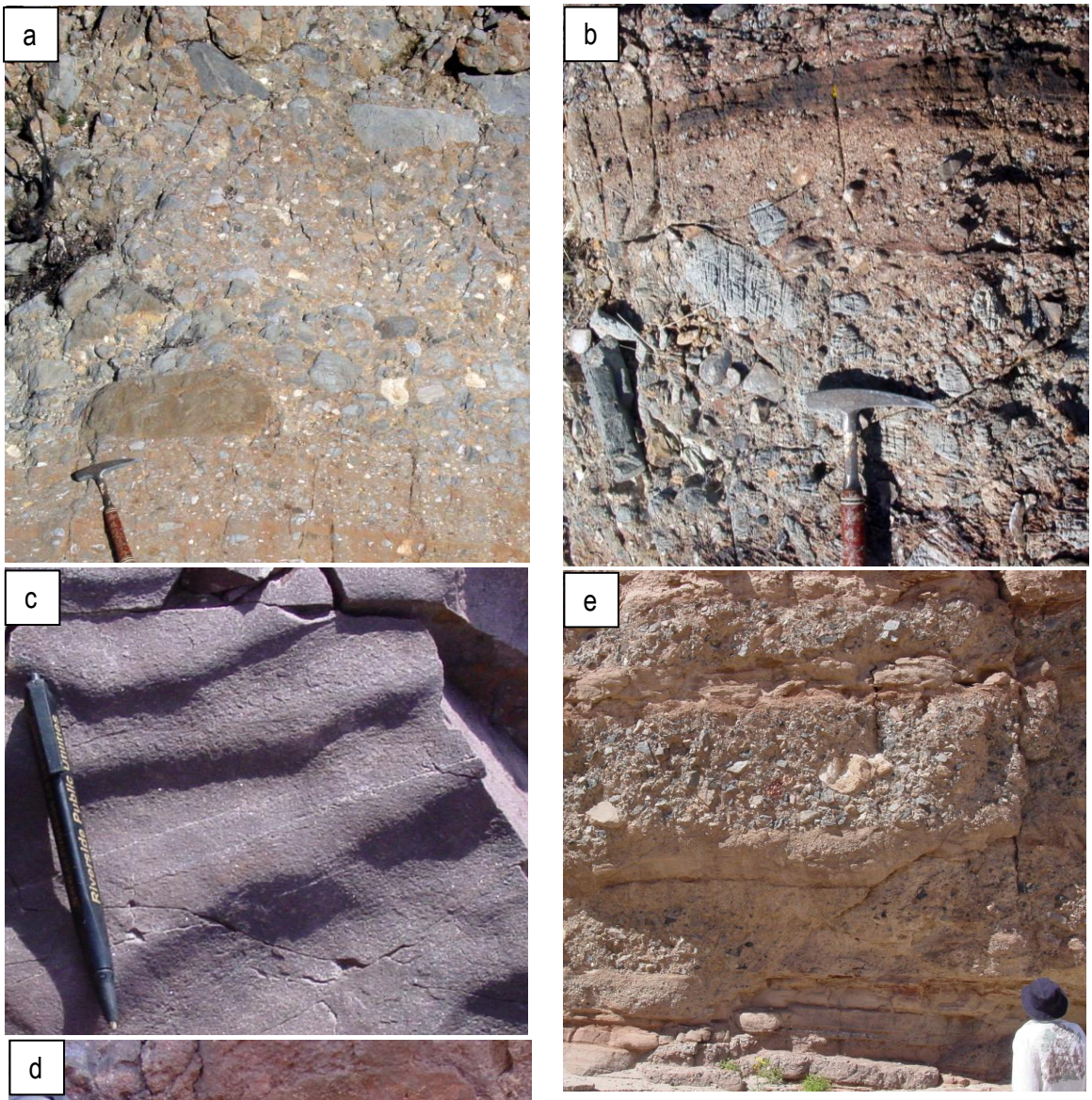

Fig. 4.4. Coarse-grained facies of the Jupiter Mine Member; a) Beck Spring clast dominated fanglomerate (Snow White Mine); b) graded fanglomerate with coarse-grained sandy cap (Beck Canyon Divide); c) ripples on sole surface of Gunsight Diamictite sandstone bed (Jupiter Mine); d) mudcrack on sole surface of Gunsight Diamictite sandstone bed (Jupiter Mine); e) modern analog to Jupiter Mine Member-modern fan deposits (CC Canyon).

Gunsight Diamictite: In footwall sections, the KPF is comprised entirely of a diamictite interval informally named the Gunsight member (Troxel, pers. comm.) and more formally referred to herein as the Gunsight Diamictite. Near the Jupiter Mine (35°47'28"N, 115°50'1"W, #10 in Fig. 2.1), the Gunsight Diamictite includes channelized sandstone with mudcracks and ripples overlain by diamictite with striated clasts (Fig. 4.4 c-d).

4.2. Boundary relations with overlying and underlying non-glacial units

Beck Spring Dolomite–KPF Contact: The contact between the eastern KPF and the underlying Beck Spring Dolomite has been described as conformable, inter-fingering or unconformable (Christie-Blick and Levy, 1989), and shows no evidence of erosional truncation, although Kenny and Knauth (Kenny and Knauth, 2001) describe karstification of the upper Beck Spring Dolomite in a number of localities. In the Alexander Hills and Saratoga Hills, the Saratoga Hills Sandstone is described as transitional with the top of the Beck Spring Dolomite over 10 m (Wright et al., 1992). This relationship can be seen in the Alexander Hills (35°46'2"N, 116°7'10"W, #1 in Fig. 2.1) and in the southern Black Mountains (35°54'45"N, 116°38'50"W, #23 in Fig. 2.1) where there is a sharp contact between the Beck Spring Dolomite and the Saratoga Hills Sandstone, followed by interbedding between cm-scale dolomite and sandstone beds over the next several meters.

KPF–Noonday Dolomite Contact: The contact between the eastern KPF and the overlying Noonday Dolomite is contentious and has been reported as regionally unconformable (Noble, 1934; Wright et al., 1978), locally unconformable (Levy and Christie-Blick, 1989), and locally conformable (Miller, 1987). An unconformable relationship has been suggested because the

Noonday Dolomite seems to cap successively older, seemingly tilted, strata (Cloud et al., 1974; Wright et al., 1976) between the Alexander Hills and the southern Nopah Range, ultimately straddling the contact between the Crystal Spring Formation and the basement at the War Eagle Mine. Alternatively, Prave (1999) suggested the Gunsight Diamictite infills erosional topography and is conformable with the overlying Noonday Dolomite.

Field studies provide evidence for uninterrupted deposition beginning at the base of the Alexander Hills Diamictite and continuing through the Noonday Dolomite, as demonstrated by the following four sedimentary relationships. First, Jupiter Mine Member sedimentary breccias in the Alexander Hills are interbedded with the basal Noonday Dolomite (35°45'56"N, 116°6'55"W) (Fig. 2.8). Second, the base of the Noonday Dolomite commonly contains clasts from the Beck Spring Dolomite and Crystal Spring Formation (i.e. 35°45'46"N, 116°6'50"W) (Fig. 2.9a & b), which likely indicates that during incipient Noonday Dolomite deposition, loose clasts from an unlithified Jupiter Mine Member surface were reworked along with carbonate material from the flanks of transgressing Noonday Dolomite mounds. Third, in footwall sections the contact between the Noonday Dolomite and underlying strata is commonly interrupted by a 1–10 m layer of Gunsight Diamictite; a similar diamictite interval appears conformable with the underlying Jupiter Mine Member. Fourth, in the southern Valjean Hills (35°39'40"N, 116°7'22"W, #17 in Fig. 2.1) and in the Ibex Hills (DeYoung, 2005), Noonday Dolomite clasts are included in diamictite of the Jupiter Mine Member or are in diamictite interbedded with Jupiter Mine Member sedimentary breccia. Alternatively, Corsetti & Kaufman (2005) interpreted Ibex Hills interbedded diamictite to post-date KPF deposition.

4.3. Laminated Debrites with Outsized Clasts

Ice-rafted debris (IRD) is often associated with striated clast bearing till in glacio-marine environments (Harland, 1964) and has been suggested to characterize late Neoproterozoic glacial successions (Condon et al., 2002). Cobble to boulder outsize clasts are common in both massive and laminated siltstone and sandstone facies comprising sediment gravity density flows within the Alexander Hills Diamictite Member. These deposits have been interpreted as either IRD (Condon et al., 2002; Corsetti and Kaufman, 2003) or as outsized clasts on the distal edges of debris flows or lone clasts rolling down tectonically produced slopes (Troxel, 1982b) .

Sperry Wash (35°42'13.68"N 116°14'34.72"W) is often visited as a classic location for looking at clasts that are interpreted as IRD in the Kingston Peak Formation (Abolins et al., 2000; Corsetti and Kaufman, 2003). Outsized clasts in laminated sandstones at Sperry Wash are not striated, do not occur randomly within laminated mudstone, nor show piercement of laminae as should occur for dropstones. They are grouped along common bedding planes and laterally associated along beds with debrites. In other sections this same laminated sandstone and debrite interval hosts dam- scale megaclasts and km-scale olistoliths. Though clasts are outsized compared to the sand-sized grains of the matrix component of coarse-grained deposits, they also appear to be disproportionately larger than thickness of beds. However, this important relationship is greatly exaggerated by the up to 50% post burial compaction in these sandy turbidites and gravity deposits. .

These deposits likely represent the distal edges of debris flows or loose clasts that tumbled down clast-laden slopes because of their association to tectonically emplaced mega-clasts in other sections, clast long axis orientation, and close association of outsize clasts to debrites. Lateral association with faults in the Kingston Range, local derivation, and absence of transport or mechanical grinding indicates this facies is of a tectonic origin with no evidence of glaciation.

4.4. Clast distribution of diamictite

Clast composition within coarse-grained units (diamictite and fanglomerate) show distinct and systematic trends both vertically and laterally. Figures 4.5, 4.6, & 4.7 and Table 4.1 are compiled from 37 clast counts from all the Kingston Peak Formation members with coarse-grained facies, but emphasize trends within the Alexander Hills Diamictite. Clast composition for all sections of the Alexander Hills Diamictite is dominated by the rounded quartzite cobbles and clasts of the Virgin Spring Limestone (Fig. 4.5a).

An important vertical trend within the Alexander Hills Diamictite is shown in Figure 4.5c-d. Clast counts along the basal contact with the underlying Saratoga Hills Sandstone show the dominant component to be Virgin Spring Limestone clasts (Fig. 4.5b). Within middle portions of sections, quartzite is the dominant lithology, basement clasts and Crystal Spring Formation clasts are proportionately increasing and the Virgin Spring Limestone becomes a minor component (Fig. 4.5c). Within upper portions of the Alexander Hills Diamictite measured section quartzite clasts remain the dominant lithology but clasts of both basement and the underlying Saratoga Hills Sandstone increase (Fig. 4.5d). This trend is indicative of systematic unroofing of lithologies

below the unconformity separating the Alexander Hills Diamictite from the Virgin Spring Limestone or Saratoga Hills Sandstone.

A second important lateral trend in clast composition within the Alexander Hills Diamictite is shown in Figure 4.6a-c. Counts have been grouped by their position relative to paleo fault scarps. Proximal or adjacent to these hanging wall-footwall transitions quartzite and Virgin Spring Limestone clasts dominate but basement and Saratoga Hills Sandstone clasts are also important components (Fig. 4.6a). More distal sections are dominated by the Virgin Spring Limestone (Fig. 4.6b). Within the most distal sections, or those thought to represent the deepest or most distal reaches of the basin, clasts of the Virgin Spring Limestone have nearly disappeared, quartzite remains an important component and clasts of the basement and the Saratoga Hills Sandstone increase. This lateral trend within the Alexander Hills Diamictite may indicate: 1) the absence of the Virgin Spring Limestone in more distal sections from lack of deposition, 2) that it was not incised by the sub-Alexander Hills Diamictite erosional event and thus remains preserved but buried in some distal sections, or 3) distal sections have additional sources of clasts, diluting the Virgin Spring Limestone component.

Interestingly, one of the most "distal" sections, located in the Ibex Hills (Fig. 2.1 #21), is completely dominated by quartzite clasts in the upper section (Fig. 4.6d) but nearly completely dominated by clasts of Virgin Spring Limestone in the base of the section (Fig. 4.6e). This is also the location of the thickest *in situ* Virgin Spring Limestone section. This trend seems to indicate that the Virgin Spring Limestone was an important but transient source of material for deposits

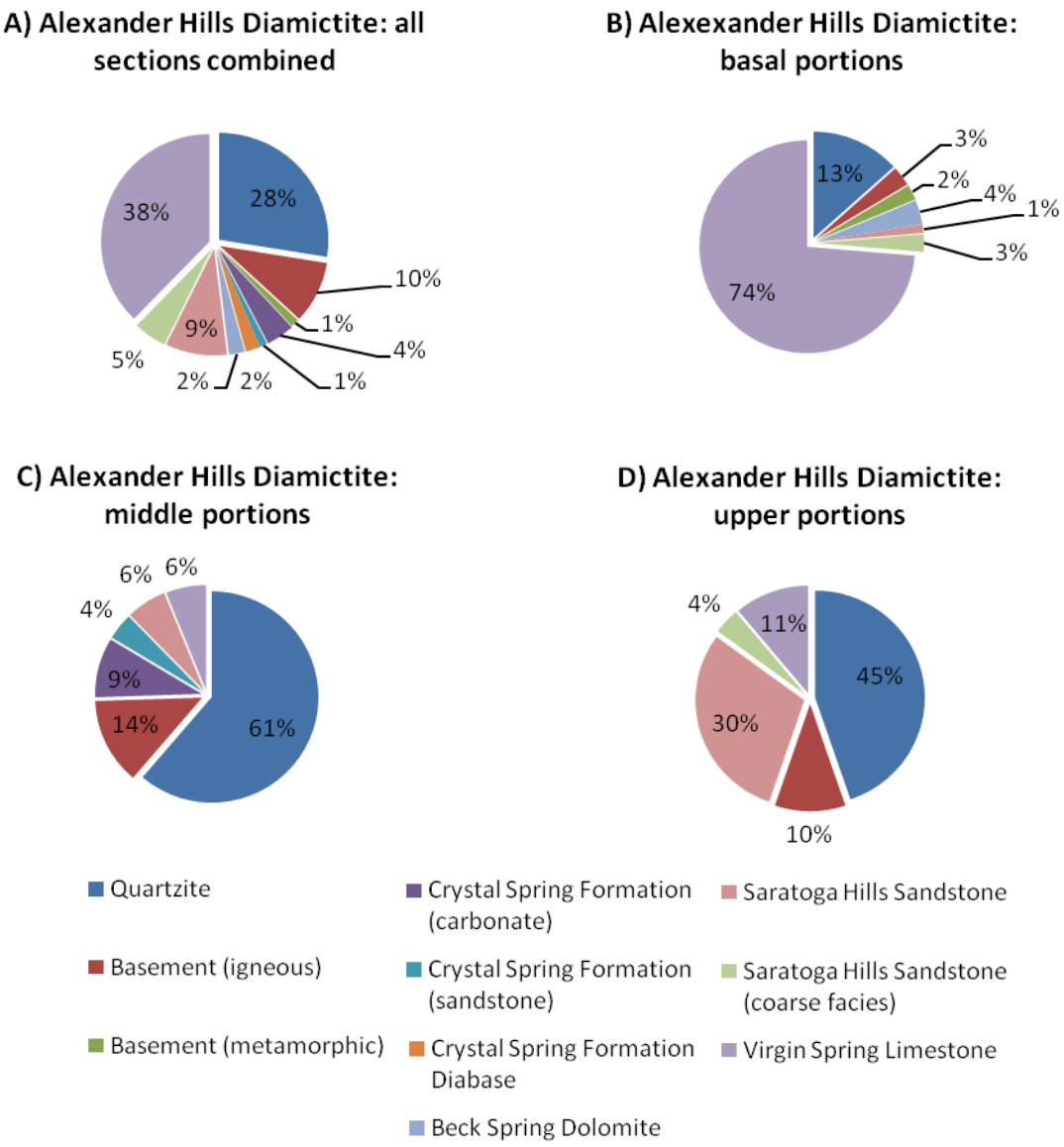

Fig. 4.5. Clast composition of Alexander Hills Diamictite; a) total clast compositions from twenty four clast counts, b) composition of seven basal counts, c) composition of mid-sections and d) composition of four upper clast counts near contact with Silver Rule Mine Member.

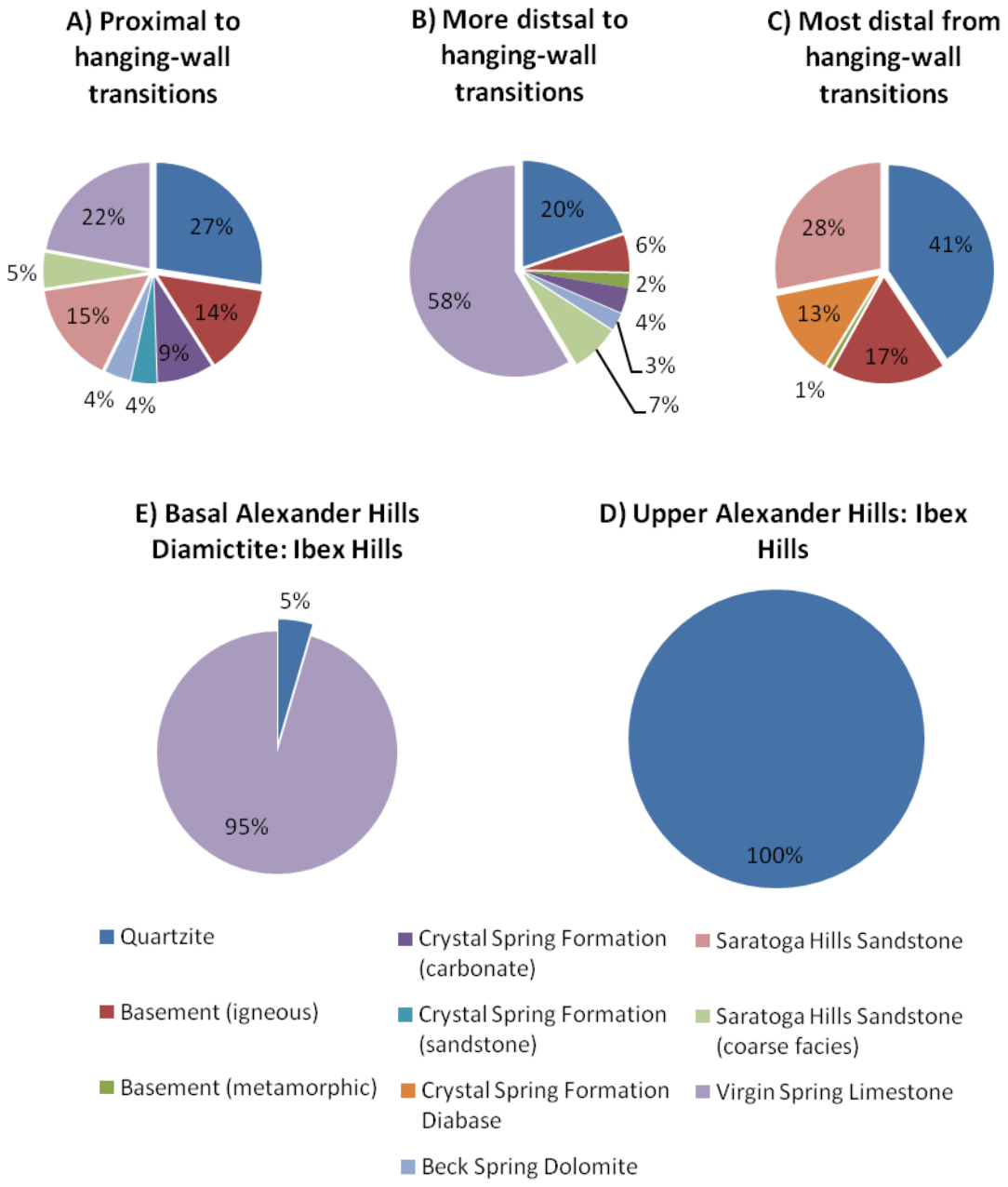

Fig. 4.6. Change in clast composition of Alexander Hills Diamictite between sections proximal to normal faults (a), those more distal (b) and most distal (c). Also shown is the change in clast composition between the upper (d) and basal (e) portions of the Alexander Hills Diamictite in the Ibex Hills, a more distal section.

overlying the sub-Alexander Hills Diamictite unconformity; the limestone was probably rapidly buried and isolated as a source of material.

Vertical trends within the remaining Kingston Peak Formation also indicate successive unroofing of the underlying lithologies. Most sections of the Silver Rule Mine Member contains a number of m-scale diamictite intervals that are lithologically indistinguishable from the underlying Alexander Hills Diamictite, in both clast and matrix composition, except for one important difference. While they contain abundant clasts of the Virgin Spring Limestone, they also contain abundant clasts of the Beck Spring Dolomite as well as basement (Fig. 4.7a). These intervals may have been deposited by the same process responsible for the underlying diamictite interval or represent remobilization of unstable Alexander Hills Diamictite, but the addition of Beck Spring Dolomite clasts indicates additional exposure of the Beck Spring Dolomite in uplifted source areas. Likewise, the fanglomerate facies (Fig. 4.7b) and debris flow facies (Fig. 4.7c) of the Jupiter Mine Member are both dominated by the Beck Spring Dolomite, and in the fanglomerate, there are a significant number of clasts of the Crystal Spring Formation, also indicating successive unroofing. The Jupiter Mine Member in the Silurian Hills is dominated by basement (gneiss) clasts (Fig. 4.7d), which may indicate the influence of tectonic unroofing, but could also represent a contribution from a different source region. The Gunsight Diamictite comprises the uppermost Kingston Peak Formation and is dominated by basement and Crystal Spring Formation clasts. This represents the apex of erosion just prior to sea level rise and deposition of the Noonday Dolomite (Fig. 4.7e).

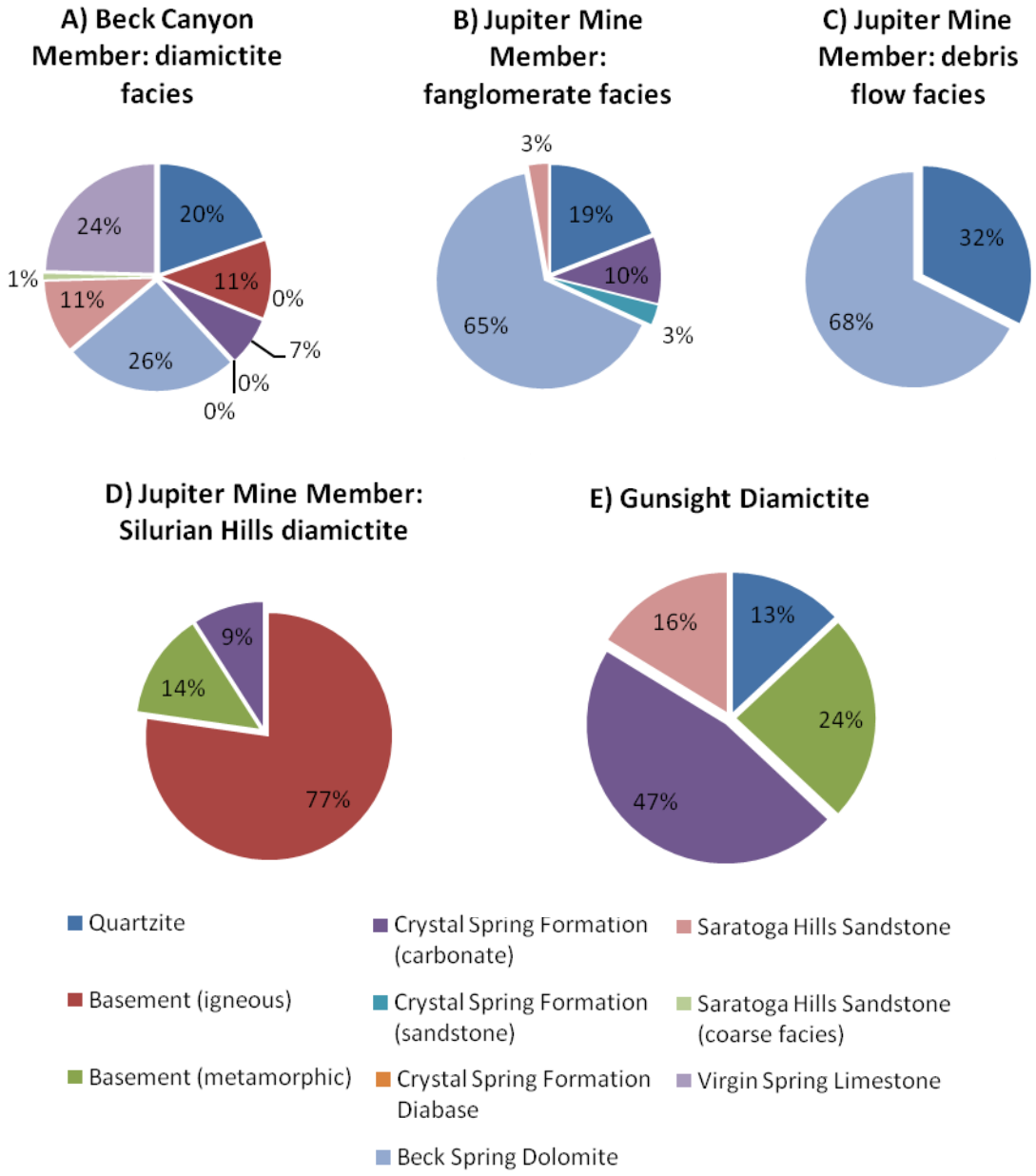

Fig. 4.7. Clast compositions for the diamictite facies within the Silver Rule Mine Member (a), the fanglomerate facies (b) and debris flow facies (c) of the Jupiter Mine Member, the composition of what is interpreted to be the Jupiter Mine Member in the Silurian Hills (d) and the Gunsight Diamictite (e).

Clast Type	AHD basal	AHD middle	AHD upper	AHD ttl	SRM	JMM	GD
Quartzite	13%	61%	45%	27%	20%	19%	13%
Basement (igneous)	3%	13%	10%	9%	11%	0%	0%
Basement (metamorphic)	2%	0%	0%	1%	0%	0%	24%
Crystal Spring Formation (carbonate)	0%	9%	1%	4%	7%	10%	47%
Crystal Spring Formation (sandstone)	0%	4%	0%	1%	0%	3%	0%
Crystal Spring Formation Diabase	0%	0%	0%	2%	0%	0%	0%
Beck Spring Dolomite	4%	0%	0%	2%	26%	65%	0%
Saratoga Hills Sandstone	1%	6%	30%	9%	11%	3%	16%
Saratoga Hills Sandstone (coarse facies)	3%	0%	4%	5%	1%	0%	0%
Virgin Spring Limestone	73%	6%	11%	38%	24%	0%	0%

Table 4.1. Compositions of different Kingston Peak Formation members. AHD=Alexander Hills Diamictite. SRM=Silver Rule Mine Member, JMM=Jupiter Mine Member, GD=Gunsight Diamictite

Regional Variability of Clast composition: Southern outcrops of the eastern KPF (dark gray shading in Fig. 2.1) are limited to an ca. 8 km-wide belt of coarse-grained sediments cropping out in the southern Saddle Peak Hills, the southern Salt Spring Hills, and the Silurian Hills. Unlike coarse-grained deposits in the KPF in the Kingston Range, southern outcrops include a dominant component of granite and gneiss (Troxel, 1967).

4.5. Wedge-shaped Geometry of fault thickened sections

The KPF thickens with the transition from footwall sections to hanging wall sections. This relationship is demonstrated in Figure 4.8, which compares the stratigraphic thickness of the KPF atop four footwall sections to the thickness of the most proximal hanging wall section. The same relationship is demonstrated in Figure 4.9, which shows the extent of thickening, due to extensional faulting, from the northern Kingston Range through the Silurian Hills. In several cases this transition can be traced across syndepositional normal faults. This wedge-shaped geometry is characteristic of extensional tectonism in siliciclastic depositional environments, especially with coarse-grained deposits (Faerseth et al., 1997; Jackson et al., 2005; Jackson and White, 1989). Coarse-grained deposits in the eastern KPF owe their thickness and preservation to the coincidental timing of extensional tectonism. This same relationship has been documented in the western KPF by (Miller, 1983).

4.6. Wedge-shaped thickening in the Alexander Hills

In the Alexander Hills area, the KPF displays a wedge-shaped geometry characteristic of thickening resulting from stripping of sediments from an uplifted region (horst) into available

Fig. 4.8. Footwall-to-Hanging Wall Transitions from four different locations.

a) Alexander Hills Mine, Alexander Hills; b) Jupiter Mine, Kingston Range; c) Beck Canyon, Kingston Range; d) Goler Wash, Panamint Range (adapted from Prave, 1999).

Stratigraphic Units:

Eastern Region: GD=Gunsight Diamictite, JMM=Jupiter Mine Member, SRMM=Silver Rule Mine Member, AHD=Alexander Hills Diamictite, SHS=Saratoga Hills Sandstone.

Western Region (Panamint Range): WD=Wildrose Diamictite, O=Olistolith, M&S=Middle Park and Sourdough Limestone Members, SM=Surprise Member

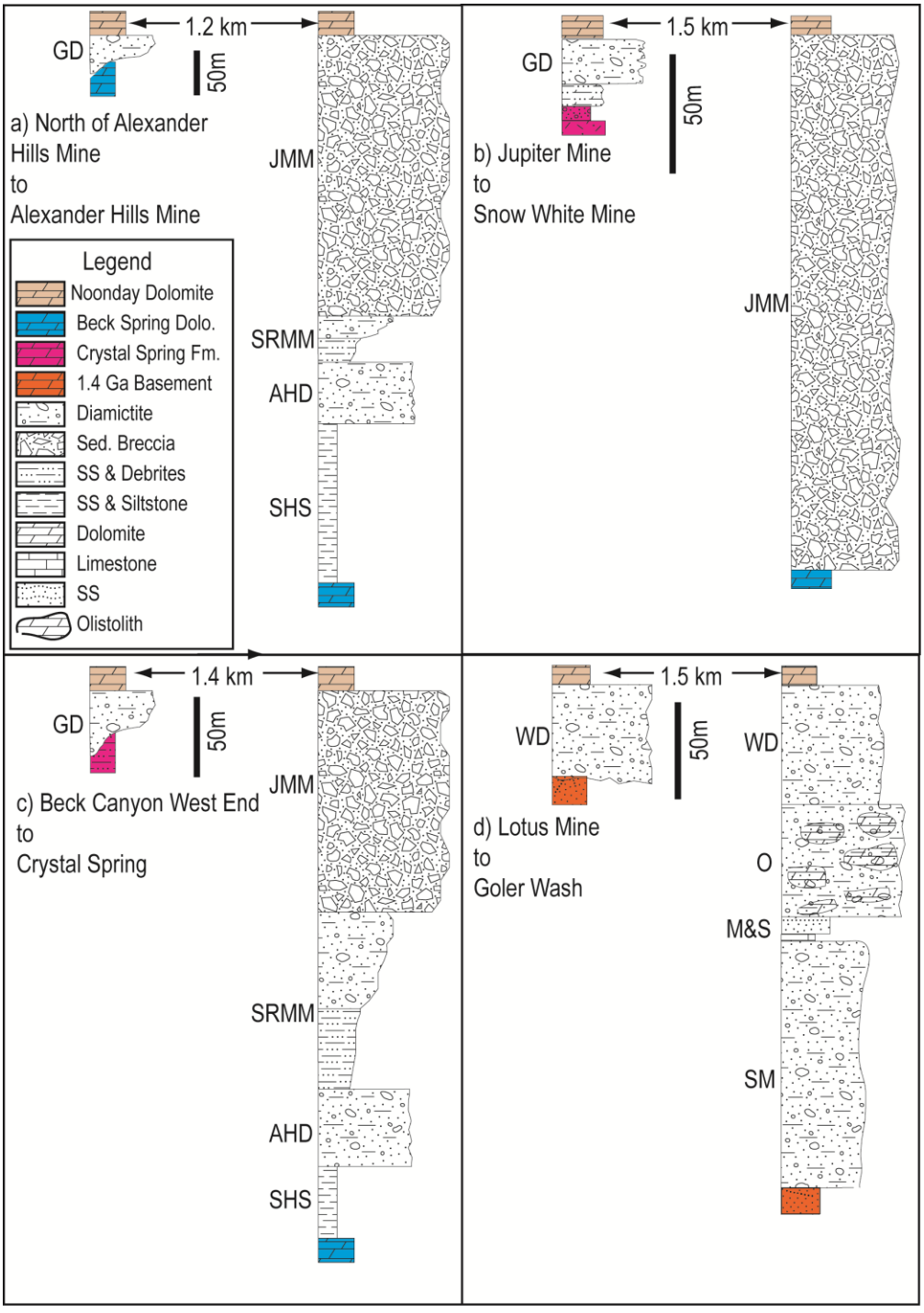
1.2 km
GD
50m
a) North of Alexander Hills Mine to Alexander Hills Mine
JMM
SRMM
AHD
SHS
Legend
Noonday Dolomite
Beck Spring Dolo.
Crystal Spring Fm.
1.4 Ga Basement
Diamictite
Sed. Breccia
SS & Debrites
SS & Siltstone
Dolomite
Limestone
SS
Olistolith
1.5 km
GD
50m
b) Jupiter Mine to Snow White Mine
JMM
1.4 km
GD
50m
c) Beck Canyon West End to Crystal Spring
JMM
SRMM
AHD
SHS
1.5 km
WD
50m
d) Lotus Mine to Goler Wash
WD
O
M&S
SM

Fig. 4.9. Cross-section of four measured sections showing the change in thickness and facies from north to south and across the transition between a footwall section (Beck Canyon West) and sections deposited atop the hanging wall. The transition is labeled in red. Inset a shows the approximate location of the four measured sections. Inset b shows a cartoon model of wedge-shaped geometry of sediments deposited during syndepositional normal faulting.

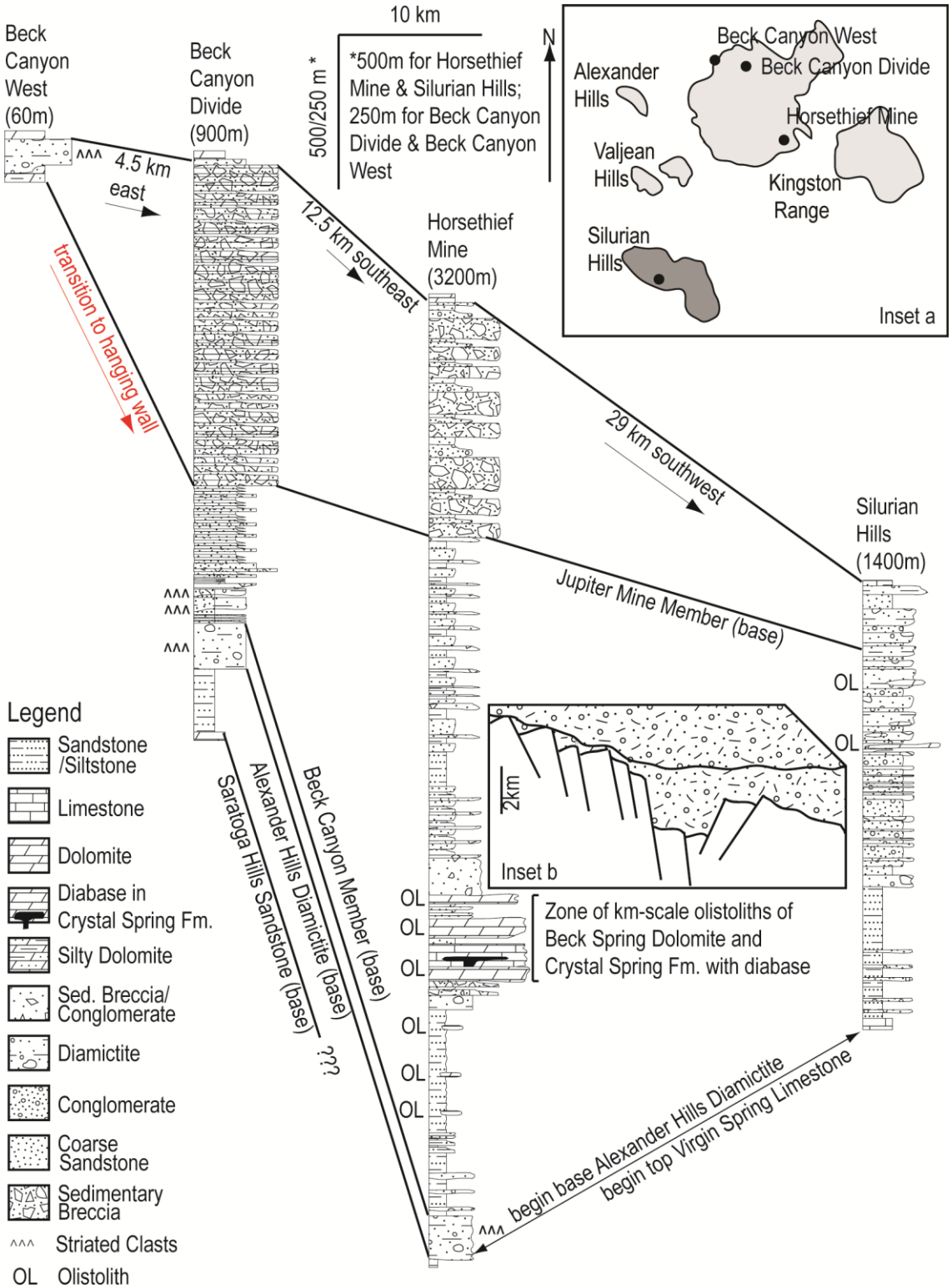
Beck Canyon West (60m)
Beck Canyon Divide (900m)
Horsethief Mine (3200m)
Silurian Hills (1400m)
10 km
500/250 m *
*500m for Horsethief Mine & Silurian Hills; 250m for Beck Canyon Divide & Beck Canyon West
N
Beck Canyon West
Beck Canyon Divide
Alexander Hills
Horsethief Mine
Valjean Hills
Kingston Range
Silurian Hills
Inset a
4.5 km east
12.5 km southeast
29 km southwest
transition to hanging wall
Jupiter Mine Member (base)
Beck Canyon Member (base)
Alexander Hills Diamictite (base)
Saratoga Hills Sandstone (base) ???
2km
Inset b
Zone of km-scale olistoliths of Beck Spring Dolomite and Crystal Spring Fm. with diabase
OL
begin base Alexander Hills Diamictite
begin top Virgin Spring Limestone
Legend
Sandstone /Siltstone
Limestone
Dolomite
Diabase in Crystal Spring Fm.
Silty Dolomite
Sed. Breccia/ Conglomerate
Diamictite
Conglomerate
Coarse Sandstone
Sedimentary Breccia
Striated Clasts
Olistolith

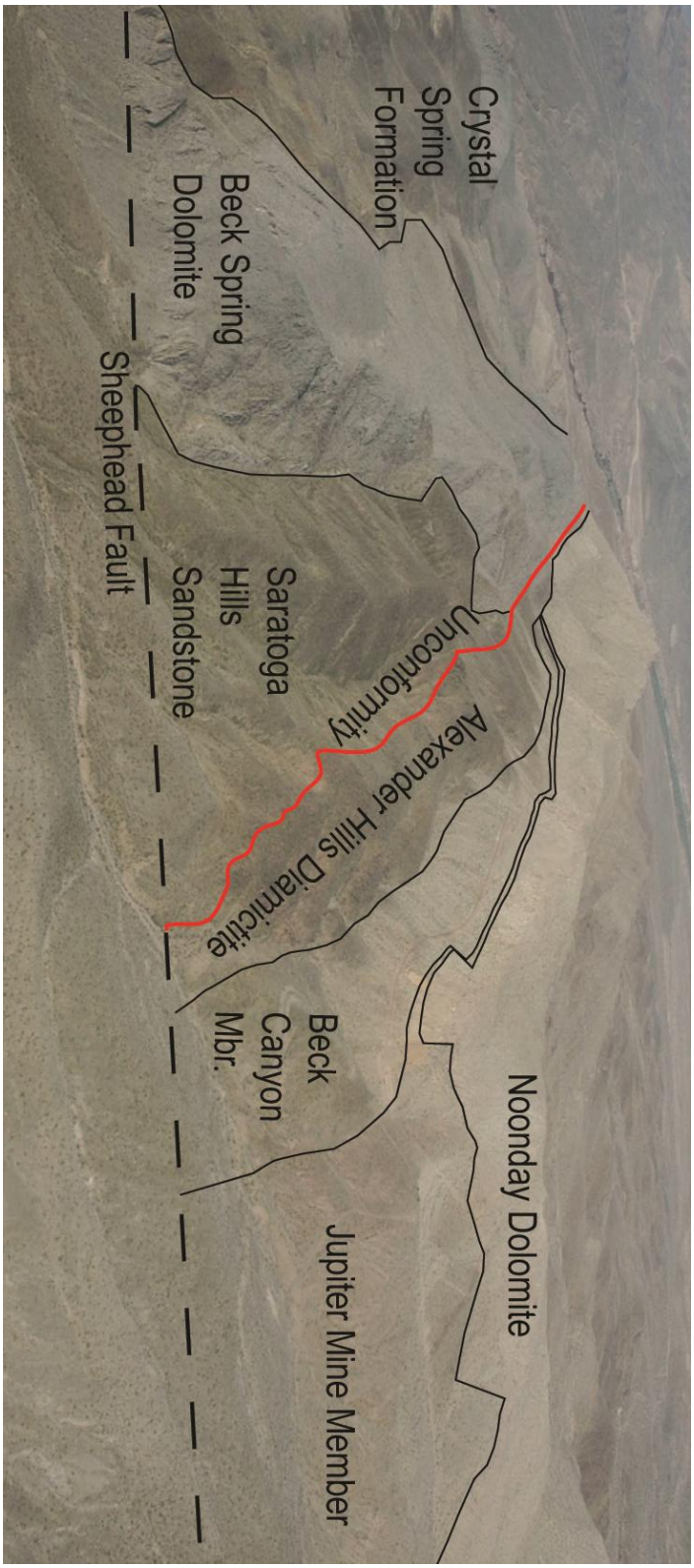

Fig. 4.10. An aerial photograph of the KPF in the Alexander Hills. The distinctive wedge-shaped topography of the Alexander Hills Diamictite-Jupiter Mine Member sandwiched between the Saratoga Hills Sandstone and Noonday Dolomite; Alexander Hills (Photo courtesy of Martin Kennedy)

accommodation space. This relationship is shown in both Figure 4.10, an aerial photograph of the Alexander Mine area with lines indicating the different KPF Members, and in Plate 4, a geologic map of the same area. The KPF can be seen thickening to the south beneath the Noonday Dolomite. Younger units are not truncated to the north, but progressively thin and on lap the regional unconformity at the base of the Alexander Hills Diamictite. A thin (m-scale) interval of

4.7. Wedge-shaped thickening across the Kingston Range

The geologic map of the Kingston Range in Figure 2.10 (see also Plate 2) reveals on a grander scale the same wedge-shaped geometry that has been shown in the Alexander Hills (Plate 4). Km-scale olistoliths (blocks) of the underlying Beck Spring Dolomite are present in the KPF Silver Rule Mine Member (Fig. 2.10: large blue polygons in the green Silver Rule Mine Member) and deposits of the KPF thicken abruptly (see red stars on Plate 2 and in Fig. 2.10) southwest of locations where the Noonday Dolomite is mapped in contact with formations underlying the KPF. The association between these transitions and missing Pahrump Group rocks beneath the footwall sections of the KPF are a function of faulting, differential erosion and deposition. Additionally, this map view of the southward thickening KPF (Fig. 2.10) shows the same relationship as the cross section in Figure 4.9; the thickest part of the preserved KPF deposits thicken from 0-3 km in only 8 km lateral distance. Evidence of synsedimentary normal faulting in the KPF is well documented in the Panamint Range, the southern Nopah Mountains and in the Kingston Range (Burchfiel et al., 1992; Christie-Blick and Levy, 1989; Miller, 1983; Miller, 1985; Partin, 2008; Stewart, 1972, 1976; Wright et al., 1974; Wright et al., 1978) .

Geologic mapping of the Jupiter Mine area (Plate 1) reveals a synsedimentary paleofault separating a footwall section with a thin layer of Gunsight Diamictite from a wedge-shaped section of KPF in the hanging wall. Atop the footwall, the Gunsight Diamictite overlies the middle Crystal Spring Formation and the surface between them is a clear erosion surface. In the hanging wall, the KPF initially overlies the upper Crystal Spring Formation and to the south overlies the Beck Spring Dolomite (dark blue in Plate 1 map), demonstrating that the Crystal Spring Formation and Beck Spring Dolomite have been lifted, tilted and beveled beneath the KPF. At Jupiter Mine, the entire Beck Spring Dolomite and much of the Crystal Spring Formation has been truncated by extensional tectonism during deposition of the KPF.

This sequence of events is made clear by the order of lithologies comprising the Jupiter Mine Member at the Jupiter Mine. The first deposits in the hanging wall, immediately adjacent to the paleofault, are monomictic sedimentary breccia intervals of Beck Spring Dolomite. These deposits extend to the first outcrops of extant Beck Spring Dolomite (south end in Plate 1). Overlying the monomictic sedimentary breccias are fanglomerate deposits comprised of both Beck Spring Dolomite and the Crystal Spring Formation. This pattern clearly supports tectonic unroofing of the Pahrump Group during KPF deposition.

These processes are further demonstrated in a fence diagram of measured sections in the Kingston Range (Fig. 4.11) and in a fence diagram incorporating all measured sections from the eastern and western KPF (Plate 3). The Silver Rule Mine Member records the most active period of tectonic activity. It records the greatest amount of thickening, contains km-scale olistoliths of Beck Spring Dolomite and Crystal Spring Formation, and displays a coarsening-fining-coarsening

Fig. 4.11. Fence diagram of KPF sections in the Kingston Range. BCW=Beck Canyon West, CS=Crystal Spring, BCD=Beck Canyon Divide, HTS=Horsethief Springs, HTM= Horsethief Mine, JM=Jupiter Mine, SM=Snow White Mine (see full fence diagram in Plate 3).

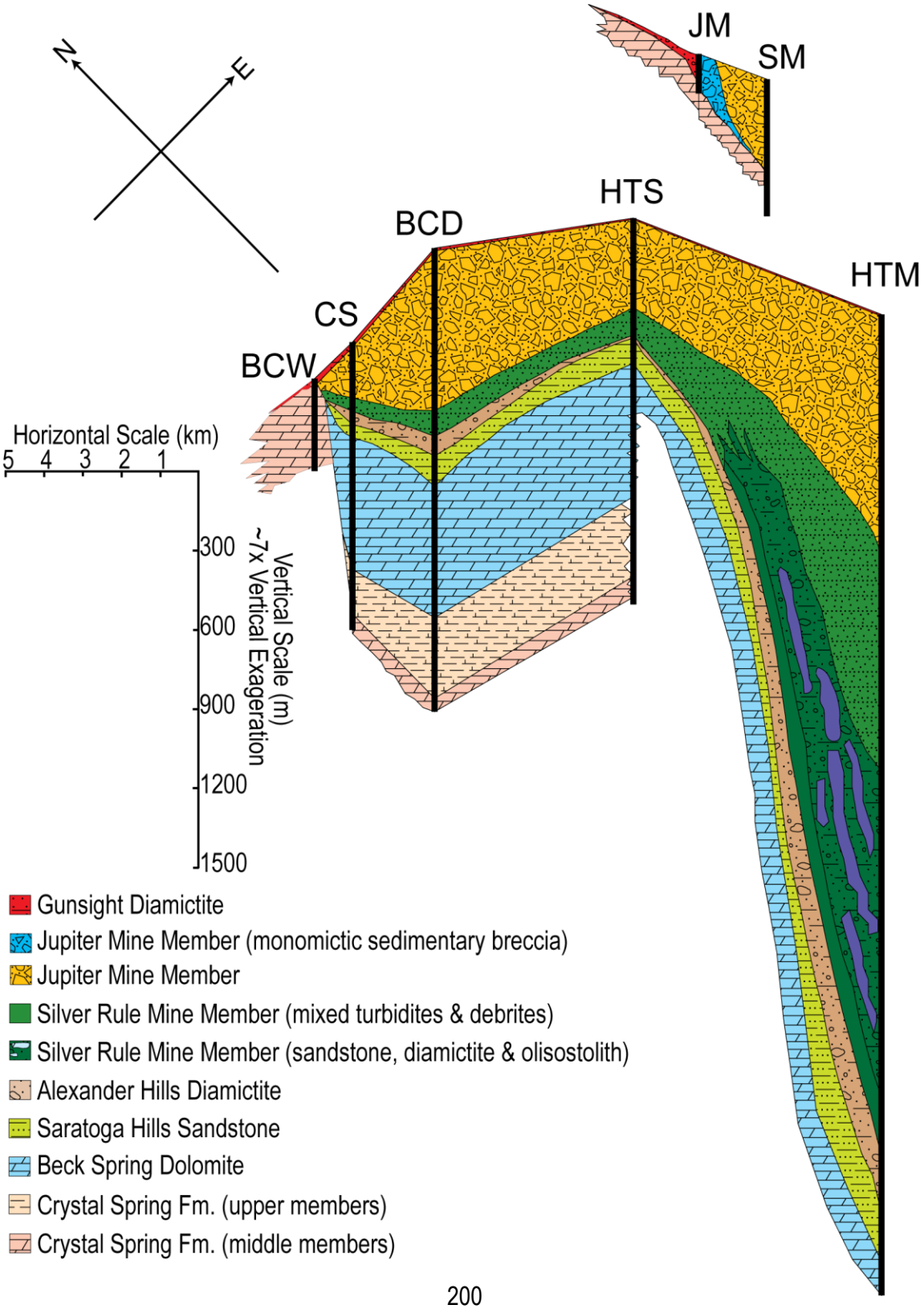
N
E
JM
SM
HTS
BCD
HTM
CS
BCW
Horizontal Scale (km)
5 4 3 2 1
300
600
900
1200
1500
Vertical Scale (m)
~7x Vertical Exageration
Gunsight Diamictite
Jupiter Mine Member (monomictic sedimentary breccia)
Jupiter Mine Member
Silver Rule Mine Member (mixed turbidites & debrites)
Silver Rule Mine Member (sandstone, diamictite & olisostolith)
Alexander Hills Diamictite
Saratoga Hills Sandstone
Beck Spring Dolomite
Crystal Spring Fm. (upper members)
Crystal Spring Fm. (middle members)

upwards trend that is characteristic of a “sediment-balanced” or “sediment-overfilled” extensional basin during maximum subsidence (Ravnas and Steel, 1998).

4.8. Striated Clasts: Evidence for Ice Influence

There is a variety of direct and indirect types of sedimentary evidence that may support ancient glacial sedimentary processes including ice-rafted debris, striated and faceted clasts, striated pavements, diamictite, rapid changes in facies and thickness, deformation structures in diamictite, varves, till pellets and a variety of fabrics (i.e. clast orientation) and grain features (i.e. conchoidal fracturing of matrix grains) (Crowell, 1977; Crowell, 1999; Dott, 1961; Etienne et al., 2007; Harland, 1964). However, most, if not all, of these types of evidence are equivocal by themselves, and a strong argument for ancient glaciations relies upon the existence of multiple lines of evidence and a strong association between a number of sedimentary indicators. The only direct evidence for the influence of ice in the KPF is the presence of striated clasts in the eastern region.

Striated clasts are present in the Alexander Hills Diamictite, within diamictite intervals in the Silver Rule Mine Member and in the Gunsight Diamictite. Clasts are normally siltsone or fine-grained sandstone; rarely, they are quartzite. This reflects the ability of finer-grained lithologies to preserve striations. Siltstone clasts are dark green and often have waxy or polished surfaces. No striated clasts were over 10 cm along their longest axis. In the eastern KPF no striated clasts were found during clast counts. Over a period of 7 years, co-workers and I searched each time we measured or traversed the Alexander Hills Diamictite or Silver Rule Mine Member, and striated

clasts were only found when carefully searched for (n=22 over 7 years). On all these clasts, striations are in 2-3 directions and directions may be up to 90º apart.

There is no systematic relationship between striated clast-bearing diamictite and bounding units. The Alexander Hills Diamictite is overlain sharply by sandstone of the Saratoga Hills Sandstone, in the Silver Rule Mine Member, diamictite is interbedded with sandstone and sedimentary breccias, and the Gunsight Diamictite sharply overlies sedimentary breccia. Their presence in many sections in the eastern KPF indicates that glacial ice was present in some form during deposition of the eastern KPF.

Over the same 7 year period, many searches for striated clasts in the KPF in the Panamint Range were carried out. Both the Surprise and Limekiln Spring Members (Fig. 1.2) were searched thoroughly. No unambiguous striated clasts have been documented in the western KPF and a glacial interpretation for any coarse-grained members there relies entirely on the indirect evidence of abundant diamictite and rapid facies changes or correlation with the east (e.g. Miller, 1983). Coarse-grained deposits in the western KPF provide evidence for tectonism but not for a glacial influence.

4.9. Tidal Bundles

One of the most interesting findings from this study is an interval of rhythmic laminae within the Alexander Hills Diamictite discovered by M.J. Kennedy and interpreted to be tidal bundles (Fig. 2.15). Laminations are arranged in bundles of 7-10 sets of couplets. Couplets are comprised of a light lamina 1-2 sand grains thick and a dark lamina composed of clay. This interval is underlain by

medium-grained sandstone with herringbone cross-stratification. The association between the tidal bundles, striated clasts in the same interval, outsized grains (Fig. 2.15b), and possible till pellets (Fig. 2.15d) indicate that ice occasionally reached sea level. Periods of ice advance may have been driven by ice growth at elevation, and driven by uplift during extension.

5. Discussion

5.1. Glacial vs. Tectonic Influence on the eastern KPF

There is strong evidence in the form of striated clasts for glacial activity during deposition of the KPF. However, there is not strong evidence that glacial processes strongly influenced the architecture or, more importantly, the timing of sedimentation. The KPF is dominated by coarse-grained deposits of the underlying Pahrump Groups and their depositional order in the KPF represents a clear unroofing sequence.

5.2. Basin Evolution of the Eastern KPF

The Saratoga Hills Sandstone is comprised of cm-scale beds of parallel-laminated sandstone, massive sandstone and siltstone. Sandstone beds have rare gentle cross-lamination and siltstone beds sometimes contain mud chips. Near the Crystal Mine, the base of the member is comprised of 5-6 m of pairs of sandstone beds (3-5 cm thick) overlain by cm-thick silt intervals. The overlying laminated Virgin Spring limestone is parallel laminated, composed of ooids and peloids and folded and contorted laminations indicate occasional downslope movement. Cm-thick sandstone intervals are interbedded with the limestone and silt appears between laminae. These

features indicate a transition from a deeper water shelf environment with periodic sand input from storm currents and deposition of silt from suspension to a deeper water condensed carbonate interval with grains, and occasional sand, transported in by storms. This is in agreement with Tucker (1986).

The unconformity that truncates the Virgin Spring limestone is the result of either sea level fall from glaciation, tectonic uplift, or a combination of the two. Erosional truncation in hanging wall sections indicates that while clasts from the underlying Pahrump Group in the Alexander Hills Diamictite provide a clear signal for initiation of tectonism, initial exposure and erosion across the region may have been the result of ice growth and sea level change prior to local tectonism, as indicated by the presence of striated clasts.

The Alexander Hills Diamictite was likely deposited in a glacio-marine setting and underwent gradual downslope reworking (Boulton and Deynoux, 1981) on the same broad shallow shelf on which the Saratoga Hills Sandstone and Virgin Spring limestone were deposited. In the rare instances when bedding contacts can be discerned through the thick weathering rind, there is no evidence of the clinoform geometry expected with very rapid deposition and retransport down oversteepened debris aprons and no evidence of laminations within the diamictite facies hosting outsized clasts expected from rainout of ice rafted debris. The Silver Rule Mine Member records the greatest lateral thickness changes of all the KPF members and represents the most active phase of tectonism in the KPF. Finer-grained sandstones at the base of the member likely record an increase in the rate of accommodation space creation and relative base level rise. Debrites occur sporadically here and increase up section and are interbedded with diamictite, conglomerate,

sedimentary breccia and mega-clasts. Diamictite intervals within the Silver Rule Mine Member with striated clasts are interbedded with coarse-grained deposits and interpreted to be a result of sporadic ice growth and gravity driven debris flows down a rapidly tectonically steepening margin.

The Jupiter Mine Member is dominated by commonly monomictic channelized sedimentary breccia and likely represents terrestrial fanglomerate facies (Hewett, 1956). Tectonism and creation of accommodation space had slowed or stopped and terrestrial facies filled local basins. The transgressive Gunsight Diamictite records either a final pulse of glaciation or retransport of sediments from flooded uplifted land surfaces and subsequent deglacial flooding of Jupiter Mine Member terrestrial deposits. The abrupt and conformable transition to the overlying and regionally continuous platformal Noonday Dolomite and thickness of its microbial mounds (>200 m) suggest flooding was a result of deglacial sea level rise (vs. isostatic loading) and that cessation of tectonism cut off any source of siliciclastic sediments.

5.3. Extensional Architecture of the Eastern KPF

The wedge-shaped architecture of the KPF has been interpreted as the result of tilting and beveling of the underlying Pahrump Group (including the KPF) and subsequent regional deposition of the Noonday Dolomite (Christie-Blick and Levy, 1989; Wright et al., 1974) over a regional angular unconformity. One of the best examples of this architecture, and the best location to use for discussion of different interpretations, is in the Alexander Hills. There, Prave (1999) modified the interpretation of a tilted and beveled Pahrump Group by placing an unconformity below the uppermost diamictite of the KPF, which he suggested was the Gunsight Diamictite filling erosional

channels in the tilted and beveled KPF, thus making the Gunsight Diamictite conformable with the Noonday Dolomite and unconformable with the underlying KPF. He considered the m-scale diamictite interval to be correlative to the Wildrose sub-member diamictite in the western KPF (Fig. 1.2) and correlative to over 2,000 m of KPF deposits in the Silurian Hills (Fig. 4.9). At issue is the lack of an erosional surface below the uppermost diamictite in the Alexander Hills or elsewhere.

This interpretation means that an entire interglacial sequence, which once would have existed above the Jupiter Mine Member, must be missing and the Gunsight Diamictite has fortuitously been deposited on top of coarse-grained facies equivalent to the Surprise Member in the Panamint Range. The only unconformity in the KPF lies near the base of the Formation, not beneath the uppermost diamictite interval. The erosional event responsible for this surface cuts down through the Saratoga Hills Sandstone in the Alexander Hills (Fig. 2.11c), cuts out more than 30 m of sandstone over less than 1 km in Virgin Spring Wash, was responsible for the erosion of almost all of the Virgin Spring Limestone, and is regional in extent.

The wedge-shaped geometry in the Alexander Hills is the result of tilting of down-dropped hanging wall blocks, successive thickening of KPF members into the basin during extension, and thinning of KPF members to the north as the base of the Noonday Dolomite approaches the surface of the unconformity. The wedge-shaped geometry outcrop pattern of the KPF in the Alexander Hills, and elsewhere in the KPF, is not a result of KPF deposition, tilting and beveling. While this series of events would result in a similar outcrop pattern, it is not possible because there is no regional unconformity below the Gunsight Diamictite and I have documented a conformable

interbedded relationship between the Jupiter Mine Member and the Noonday Dolomite (Fig. 2.8 and 2.9a & b).

5.4. Glacial vs. Tectonic Influence on Coarse Grained Rock Deposition

In publications covering the KPF to date, the most convincing evidence for a glacial influence has been the presence of striated clasts in the Alexander Hills Diamictite and the Gunsight Diamictite (Hazzard, 1939; Miller, 1982; Miller, 1983; Miller, 1985), and possible ice rafted debris in the Silver Rule Mine Member (Corsetti and Kaufman, 2003). The abundance of diamictite facies, their thickness and rapidly varying facies has been cited as indirect evidence for a glacial influence (Miller, 1982; Miller, 1985) in the western KPF. Abundant diamictite throughout the KPF and the presence of striated clasts in the eastern KPF are the basis for Miller's (1983; 1985) interpretation that sedimentation in the KPF was strongly influenced by glacial processes.

The presence of diamictite and outsized clasts or lonestones (clasts significantly larger than surrounding grains) has not been shown to be diagnostic of glacial processes in the eastern or western KPF. The abundance of diamictic facies as evidence of glaciations is problematic because these deposits may also result from a variety of mass-flow processes (Crowell, 1957; Dott, 1961; Dott, 1973; Eyles and Januszczak, 2004; Eyles and Januszczak, 2007; Schermerhorn, 1974, 1975). At Sperry Wash, outsized clasts within turbidite facies (Troxel, 1982b) of the Silver Rule Mine Member have been interpreted as dropstones (Abolins et al., 2000; Corsetti et al., 2003) or as lone clasts rolling down tectonically-produced slopes (Troxel, 1982a). As discussed above, outsized clasts at Sperry Wash are grouped along common bedding planes and laterally

associated with diamictites and normally-graded conglomerate beds interpreted to be debris flows (Troxel 1982b). In other sections, similar outsized clast-bearing facies are interbedded with conglomerate and host dam-scale megaclasts and km-scale olistoliths.

The association with tectonically-emplaced olistoliths, the bedding plane parallel orientation of many clasts, and close association of outsize clasts to debrites beds with lonestones suggests that outsized clasts more likely represent the distal edges of debris flows or loose clasts that tumbled down clast-laden slopes (Postma, 1984).

Neoproterozoic Era glacial sediments are commonly and intimately associated with overlying carbonate facies (Hoffman et al., 1998). Globally, these "cap carbonates" may overlie a lower and upper glacial interval in many sections and host a variety of distinctive sedimentary and geochemical features (Hoffman and Schrag, 2002; Kennedy et al., 1998).

The Sourdough Limestone Member in the western KPF is characterized by graphite-rich parallel laminations and depleted $\delta^{13}C$ values (Table 2.1), characteristics shared among lower cap carbonates (Kennedy et al., 1998), and has been interpreted to represent a lower cap carbonate in the western KPF (Prave, 1999). In the eastern KPF, the Virgin Spring and Silurian Hills limestone units also are characterized by graphite-rich parallel laminations but have enriched δ13C values. Bergfeld et al. (1996) argue that the negative carbon isotope values in the Sourdough Limestone are the result of carbon exchange with organic matter in the limestone.

The Noonday Dolomite, overlying the KPF, has been interpreted as an upper cap carbonate based on a number of common characteristics, including its cream color, vertical tubestone facies, abundant marine cements and depleted $\delta^{13}C$ values (Kennedy et al., 1998).

6. Global Models

One of the fundamental questions is what model of climate change is most reasonable given the pattern of widely-spaced coarse-grained Cryogenian intervals. However, the importance of tectonic control on preservation of glacigenic deposits is that local processes may provide the appearance of a globally synchronous event (Fig. 1.1). The record of climate change over the last 600 million years was likely driven by tectonic-scale processes (i.e. chemical weathering, seafloor spreading, uplift and continental position relative to the poles) that gradually transferred carbon between the atmosphere and the lithosphere over 50-100 million year icehouse-to-greenhouse cycles and provided an appropriately located continental platform on which to accumulate ice (Crowell, 1999; Eyles, 2008).

During the Permo-Carboniferous icehouse epoch spanning 350-260 Ma, ice accumulation was driven by a slow withdrawal of carbon from the atmosphere and continental position (Crowell, 1999). The occurrence of Pennsylvanian cyclothems indicates an extensive pattern of sea level change due in part to glacial advance-retreat cycles (Klein and Kupperman, 1992). The present icehouse epoch followed a significantly warmer “greenhouse” period of Earth history, again likely due to gradual tectonic-scale processes such as enhanced carbon dioxide input to the atmosphere due to increased seafloor spreading.

During the present Cenozoic ice age the planet has undergone a slow and gradual 50 Ma change to icehouse conditions where permanent ice has been present on the globe for at least the last 34 Ma (Kent & Muttoni 2008; Lear *et al.* 2008). An extensive sedimentary and geochemical record indicates a climate system with a series of glacial-interglacial cycles, as with the previous icehouse epoch; sudden transitions to warmer conditions after gradual buildup of ice and a see-saw pattern of conditions in one hemisphere opposite to those in the other (Barker & Knorr 2007; Barker *et al.* 2009).

The high-resolution work in younger glacial intervals identifies that with increasing information, glacial events are characterized by increasing spatial and temporal complexity. The Neoproterozoic stratigraphic signal, described in the KPF, seemingly stands in contrast to this and begs the question whether this interval was fundamentally different or if the seeming uniqueness of this record is an artifact of less available stratigraphic information.

7. Conclusion

Tectonic and glacial deposits of the eastern KPF are bounded by the Beck Spring Dolomite and Noonday Dolomite carbonate platforms, overlie a regional unconformity, and record an abrupt change to siliciclastic sedimentation resulting from tectonic uplift. The wedge-shaped packaging of the KPF strata next to tilted and erosionally truncated segments of the underlying Pahrump Group and basement conforms to rotation of the hanging wall and footwall sections in extensional systems (Faerseth et al., 1997; Jackson et al., 2005; Jackson and White, 1989). Coarse-grained facies are primarily the product of local tectonic activity as indicated by: 1)

syndepositional normal faults and erosional beveling of footwall blocks, 2) a systematic and consistent pattern of coarsening upwards from sand and angular cobble debrites to sedimentary breccia and km-scale olistoliths, 3) a transition from marine debris-flow facies to terrestrial fanglomerates, and 4) a systematic pattern of unroofing of the underlying Pahrump group as seen in the sequence of dominant clasts. The occurrence of striated clasts in the Alexander Hills Diamictite and Silver Rule Mine Members indicates a glacigenic influence that is sporadic and limited to specific stratigraphic intervals.

Stratigraphic relationships within the KPF are not consistent with the paradigm of discrete global climate events that determine the properties of the stratigraphic record. In contrast to laterally continuous synchronous glacigenic units capped by distinctive carbonates, the Kingston Peak shows rapid local facies variations adjacent to faults. These faults control the timing of subsidence, local sediment supply through uplift of rift flanks and potentially influence local climate. While evidence of a climate signal is evident in portions of the KPF, it is a second-order signal that coincides with accommodation space controlled by tectonism. Given that local tectonics is largely independent of global climate and that tectonics determines timing of accommodation space deposition of glacial facies in some cases may be a more appropriate proxy for tectonism than global climate.

The coincidental timing of glacial onset and termination with initiation of faults in the Alexander Hills and in the Kingston Range combined with the second-order influence of the climate in these locations suggests that climate influence in the KPF is a product of more local controls (such as uplift). Subtle changes in uplift particularly during a prolonged cold period during the

Cryogenian could account for local onset of glaciation. By contrast, the regionally pervasive signal of flooding and carbonate precipitation of the Noonday Dolomite contrasts with this more localized tectonic signal, and is consistent with deglaciation and sea level rise from a global climate event. That no further evidence for glaciation occurs above the Noonday Dolomite indicates a pervasive change closely timed with the Ediacaran transition.

The Death Valley record is controlled by the timing of tectonic subsidence related to local onset of rifting. It was modified in part by glacial activity and did not experience subsequent glaciation after deposition of the Noonday Dolomite during a major global transgression. This pattern is consistent with a prolonged ice age with rift-induced local glaciation and abrupt global termination preceding the Ediacaran Period. It conforms poorly to the current paradigm of several discrete and pervasive glaciations that control sedimentary processes and supports an alternative model of an enduring Cryogenian glacial epoch leaving a record of regionally diachronous glacial advances, often preserved by tectonically driven accommodation space, and terminated abruptly across the globe at ~635 Ma (Condon et al., 2005).

A possible way to reconcile both diachroneity of Sturtian glacials and the inability to correlate lower carbonates with confidence is that the Cryogenian period is a prolonged cold interval making local climate records more sensitive to uplift by being prone to glaciation. This provides a semblance of multiple ice ages. Glacigenic diamictites developed due to diachronous local tectonism provide no direct evidence of global climate in these local areas and are then diagnostic of local creation of accommodation space. Given that local uplift can subtly influence

glacial patterns in Earth's current glacial state it may be that the climate record within the KPF is the expected discrete glacial-carbonate sequence characteristic of the Neoproterozoic record.

These findings support a model of one long Cryogenian ice age terminated at ~635 Ma The terms "Sturtian" and "Marinoan" glaciations thus become somewhat misleading while the importance of the Sturtian and Marinoan sections in Australia (Kendall et al., 2004) is not diminished as type sections that show lithological and geochemical traits characteristic of Cryogenian glacial intervals capped by transgressive carbonates and the globally synchronous terminal deglaciation and transgression at the end of the Cryogenian Period.

References

Abolins, M., Oskin, R., Prave, T., Summa, C., and Corsetti, F.A., 2000, Neoproterozoic glacial record in the Death Valley region, California and Nevada: GSA Field Guide, v. 2, p. 319-335.

Allen, P.A., and Etienne, J.L., 2008, Sedimentary challenge to snowball Earth: Nature Geoscience, v. 1, p. 817-825.

Barker, S., Diz, P., Vautravers, M.J., Pike, J., Knorr, G., Hall, I.R., and Broecker, W.S., 2009, Interhemispheric Atlantic seesaw response during the last deglaciation: Nature, v. 457, p. 1097-1102.

Barker, S., and Knorr, G., 2007, Antarctic climate signature in the Greenland ice core record: Proceedings of the National Academy of Sciences, v. 104, p. 17278-17282.

Bergfeld, D., Nabelek, P.I., and Labotka, T.C., 1996, Carbon isotope exchange during polymetamorphism in the Panamint Mountains, California, USA: Journal of Metamorphic Geology, v. 14, p. 199-212.

Boulton, G.S., and Deynoux, M., 1981, Sedimentation in glacial environments and the identification of tills and tillites in ancient sedimentary sequences: Precambrian Research, v. 15, p. 397-422.

Burchfiel, B.C., Cowan, D.S., and Davis, G.A., 1992, Tectonic overview of the Cordilleran Orogen in the Western United States, *in* Burchfiel, B.C., Lipman, P.W., and Zoback, M.L., eds., The Cordilleran Orogen; conterminous U.S.: United States (USA), Geol. Soc. Am.

Christie-Blick, N., and Levy, M., 1989, Stratigraphic and tectonic framework of upper Proterozoic and Cambrian rocks in the Western United States, *in* Christie-Blick, N., Levy, M., Mount, J.F., Signor, P.W., and Link, P.K., eds., ???: 28th International Geological Congress field trip guide series 7-21: Washington D.C., American Geophysical Union, p. 7-21.

Cloud, P., Wright, L.A., Williams, E.G., Diehl, P.E., and Walter, M.R., 1974, Giant Stromatolites and Associated Vertical Tubes from the Upper Proterozoic Noonday Dolomite, Death Valley Region, Eastern California: Geological Society of America Bulletin, v. 85, p. 1869-1882.

Condon, D., Zhu, M., Bowring, S., Wang, W., Yang, A., and Jin, Y., 2005, U-Pb Ages from the Neoproterozoic Doushantuo Formation, China: Science, v. 308, p. 95-98.

Condon, D.J., Prave, A.R., and Benn, D.I., 2002, Neoproterozoic glacial-rainout intervals; observations and implications: Geology, v. 30, p. 35-38.

Corsetti, F.A., Awramik, S.M., and Pierce, D., 2003, A complex microbiota from snowball Earth times: Microfossils from the Neoproterozoic Kingston Peak Formation, Death Valley, USA: Proceedings of the National Academy of Sciences of the United States of America, v. 100, p. 4399-4404.

Corsetti, F.A., and Kaufman, A.J., 2003, Stratigraphic investigations of carbon isotope anomalies and Neoproterozoic ice ages in Death Valley, California: GSA Bulletin, v. 115, p. 916-932.

—, 2005, The relationship between the Neoproterozoic Noonday Dolomite and the Ibex Formation: New observations and their bearing on 'snowball Earth': Earth-Science Reviews, v. 73, p. 63-78.

Crowell, J.C., 1957, Origin of pebbly mudstones: Geological Society of America Bulletin, v. 68, p. 993-1009.

—, 1977, The significance of glaciations in Precambrian correlation, *in* Sidorenko, A.V., ed., Correlation of the Precambrian, Volume 1: Moscow, Izd. Nauka, p. 115-131.

—, 1978, Gondwanan glaciation, cyclothems, continental positioning, and climate change: American Journal of Science, v. 278, p. 1345-1372.

—, 1999, Pre-Mesozoic ice ages; their bearing on understanding the climate system, 106 p.

Crowell, J.C., and Frakes, L.A., 1970, Phanerozoic glaciation and the causes of ice ages: American Journal of Science, v. 268, p. 193-224.

Deynoux, M., Miller, J.M.G., Domack, E.W., Eyles, N., Fairchild, I.J., and Young, G.M., 1994, Earth's glacial record: Cambridge, Cambridge University Press, p. 266.

DeYoung, D.P., 2005, The Neoproterozoic Ibex Formation, eastern California: Stratigraphic and Sedimentological Constraints on Ice Age and Carbonate Precipitation Events of Southern Death Valley [MSc thesis]: Riverside, University of California, Riverside.

Dott, R.H., Jr., 1961, Squantum 'tillite,' Massachusetts; evidence of glaciation or subaqueous mass movements?: Geological Society of America Bulletin, v. 72, p. 1289-1305.

—, 1973, Dynamics of subaqueous gravity depositional processes: Reprint Series - American Association of Petroleum Geologists. Tulsa., v. 8, p. 25-49.

Etienne, J.L., Allen, P.A., Rieu, R., and Le Guerroue, E., 2007, Neoproterozoic glaciated basins; a critical review of the snowball Earth hypothesis by comparison with Phanerozoic glaciations: Special Publication of the International Association of Sedimentologists, v. 39, p. 343-399.

Eyles, N., 2008, Glacio-epochs and the supercontinent cycle after ~ 3.0 Ga: Tectonic boundary conditions for glaciation: Palaeogeography, Palaeoclimatology, Palaeoecology, v. 258, p. 89-129.

Eyles, N., and Januszczak, N., 2004, 'Zipper-rift': a tectonic model for Neoproterozoic glaciations during the breakup of Rodinia after 750 Ma: Earth-Science Reviews, v. 65, p. 1-73.

—, 2007, Syntectonic subaqueous mass flows of the Neoproterozoic Otavi Group, Namibia: Where is the evidence for global glaciation?, v. 19, p. 179-198.

Faerseth, R.B., Knudsen, B.E., Liljedahl, T., Midboe, P.S., and Soderstrom, B., 1997, Oblique rifting and sequential faulting in the Jurassic development of the northern North Sea: Journal of Structural Geology, v. 19, p. 1285-1302.

Fairchild, I.J., and Kennedy, M.J., 2007, Neoproterozoic glaciation in the Earth system: Journal of the Geological Society of London, v. 164, p. 895-921.

Harland, B., 1964, Critical evidence for a great infra-Cambrian glaciation: Geologische Rundschau, v. 54, p. 45-61.

Hazzard, J.C., 1939, Possibility of pre-Cambric glaciation in southeastern California: Pan-American Geologist, v. 71, p. 47-48.

Hewett, D.F., 1956, Geology and mineral resources of the Ivanpah Quadrangle, California and Nevada, p. 23-99.

Hoffman, P.F., Kaufman, A.J., Halverson, G.P., and Schrag, D.P., 1998, A Neoproterozoic snowball earth: Science, v. 281, p. 1342-1346.

Hoffman, P.F., and Schrag, D.P., 2002, The snowball earth hypothesis: testing the limits of global change: Terr Nova, v. 14, p. 129-155.

Jackson, C.A.L., Gawthorpe, R.L., Carr, I.D., and Sharp, I.R., 2005, Normal faulting as a control on the stratigraphic development of shallow marine syn-rift sequences; the Nukhul and Lower Rudeis Formations, Hammam Faraun fault block, Suez Rift, Egypt: Sedimentology, v. 52, p. 313-338.

Jackson, J.A., and White, N.J., 1989, Normal faulting in the upper continental crust; observations from regions of active extension: Journal of Structural Geology, v. 11, p. 15-36.

Kendall, B., Creaser, R.A., and Selby, D., 2006, Re-Os geochronology of postglacial black shales in Australia: Constrains on the timing of [ldquo]Sturtian[rdquo] glaciation, v. 34, p. 729-732.

Kendall, B.S., Creaser, R.A., Ross, G.M., and Selby, D., 2004, Constraints on the timing of Marinoan "Snowball Earth" glaciation by 187Re-187Os dating of a Neoproterozoic, post-glacial black shale in Western Canada: Earth and Planetary Science Letters, v. 222, p. 729-740.

Kennedy, M.J., Runnegar, B., Prave, A.R., Hoffman, K.-H., and Arthur, M.A., 1998, Two or four Neoproterozoic glaciations?, v. 26, p. 1059-1063.

Kenny, R., and Knauth, L.P., 2001, Stable isotope variations in the Neoproterozoic Beck Spring Dolomite and Mesoproterozoic Mescal Limestone paleokarst; implications for life on land in the Precambrian: Geological Society of America Bulletin, v. 113, p. 650-658.

Kent, D.V., Muttoni, G., and Anonymous, 2006, Equatorial convergence of India and early Cenozoic climate trends: Earth and Planetary Science Letters, v. 243, p. 847-850.

Kirschvink, J.L., 1992, Late Proterozoic low-latitude global glaciation; the snowball Earth, *in* Schopf, J.W., and Klein, C., eds., The Proterozoic biosphere: A multidisciplinary study: Cambridge, Cambridge Univ. Press, p. 51-52.

Klein, G.D., and Kupperman, J.B., 1992, Pennsylvanian cyclothems: Methods of distinguishing tectonically induced changes in sea level from climatically induced changes

10.1130/0016-7606(1992)104<0166:PCMODT>2.3.CO;2: Geological Society of America Bulletin, v. 104, p. 166-175.

Lear, C.H., Bailey, T.R., Pearson, P.N., Coxall, H.K., and Rosenthal, Y., 2008, Cooling and ice growth across the Eocene-Oligocene transition: Geology, v. 36, p. 251-254.

Levy, M., and Christie-Blick, N., 1989, Pre-Mesozoic palinspastic reconstruction of the eastern Great Basin (Western United States): Science, v. 245, p. 1454-1462.

Liu, Z., Pagani, M., Zinniker, D., DeConto, R., Huber, M., Brinkhuis, H., Shah, S.R., Leckie, R.M., and Pearson, A., 2009, Global Cooling During the Eocene-Oligocene Climate Transition

10.1126/science.1166368: Science, v. 323, p. 1187-1190.

Miller, J.M.G., 1982, Kingston Peak Formation in the southern Panamint Range; a glacial interpretation, *in* Cooper, J.D., Troxel, B.W., and Wright, L.A., eds., Geology of selected areas in the San Bernardino Mountains, western Mojave Desert, and southern Great Basin, California: Geological Society of America Cordilleran Section Field Trip Guidebook and Volume: Shohone, California, Death Valley Publ. Co., p. 155-164.

—, 1983, Stratigraphy and sedimentolgy of the upper Proterozoic Kingston Peak Formation, southern Panamint Range, eastern California [Doctoral thesis]: Santa Barbara, University of California.

—, 1985, Glacial and syntectonic sedimentation: The upper Proterozoic Kingston Peak Formation, southern Panamint Range, eastern California, v. 96, p. 1537-1553.

—, 1987, Paleotectonic and stratigraphic implications of the Kingston Peak-Noonday contact in the Panamint Range, eastern California: Journal of Geology, v. 95, p. 75-85.

Noble, L.F., 1934, Rock formations of Death Valley, California; science, n. s., vol. 80, no. 2069.

Partin, C.A., 2008, Accomodation and climate in the neoproterozoic Kingston peak formation, Southern Panamint range, Death Valley, Ca [MSc. thesis]: Riverside, University of California, Riverside.

Postma, G., 1984, Mass-flow conglomerates in a submarine canyon; Abrioja fan-delta, Pliocene, Southeast Spain: Memoir - Canadian Society of Petroleum Geologists, v. 10, p. 237-258.

Prave, A.R., 1999, Two diamictites, two cap carbonates, two delta (super 13) C excursions, two rifts; the Neoproterozoic Kingston Peak Formation, Death Valley, California: Geology (Boulder), v. 27, p. 339-342.

Ravnas, R., and Steel, R.J., 1998, Architecture of marine rift-basin successions: AAPG Bulletin, v. 82, p. 110-146.

Schermerhorn, L.J.G., 1974, Late Precambrian mixites: Glacial and/or nonglacial?: American Journal of Science, v. 274, p. 673-824.

—, 1975, Tectonic framework of late Precambrian supposed glacials: Geological Journal, Special Issue, p. 241-274.

Schmidt, P.W., Williams, G.E., and McWilliams, M.O., 2009, Palaeomagnetism and magnetic anisotropy of late Neoproterozoic strata, South Australia: Implications for the palaeolatitude of late Cryogenian glaciation, cap carbonate and the Ediacaran System: Precambrian Research, v. 174, p. 35-52.

Sohl, L.E., Christie-Blick, N., and Kent, D.V., 1999, Paleomagnetic polarity reversals in Marinoan (ca. 600 Ma) glacial deposits of Australia; implications for the duration of low-latitude glaciation in Neoproterozoic time: Geological Society of America Bulletin, v. 111, p. 1120-1139.

Stewart, J.H., 1972, Initial deposits in the Cordilleran geosyncline: Evidence of a late Precambrian (<850 m.y.) continental separation: Geological Society of America Bulletin, v. 83, p. 1345-1360.

—, 1976, Late Precambrian evolution of North America: Plate tectonics implication: Geology, v. 4, p. 11-15.

Tripati, A.K., Eagle, R.A., Morton, A., Dowdeswell, J.A., Atkinson, K.L., Bahé, Y., Dawber, C.F., Khadun, E., Shaw, R.M.H., Shorttle, O., and Thanabalasundaram, L., 2008, Evidence for glaciation in the Northern Hemisphere back to 44 Ma from ice-rafted debris in the Greenland Sea: Earth and Planetary Science Letters, v. 265, p. 112-122.

Troxel, B.W., 1967, Sedimentary rocks of late Precambrian and Cambrian age in the southern Salt Spring Hills, southeastern Death Valley, California: Special Report - California Division of Mines and Geology, p. 33-41.

—, 1982a, Basin facies (Ibex Formation) of the Noonday Dolomite, southern Saddle Peak Hills, southern Death Valley, California, *in* Cooper, J.D., Troxel, B.W., and Wright, L.A., eds., Geology of selected areas in the San Bernardino Mountains, western Mojave Desert, and southern Great Basin, California: Geological Society of America Cordilleran Section Field Trip Guidebook and Volume: Shohone, Death Valley Publ. Co., p. 43-48.

—, 1982b, Description of the uppermost part of the Kingston Peak Formation, Amargosa Rim Canyon, Death Valley region, California, *in* Cooper, J.D., Troxel, B.W., and Wright, L.A., eds., Geology of selected areas in the San Bernardino Mountains, western Mojave Desert, and southern Great Basin, California: Geological Society of America Cordilleran Section Field Trip Guidebook and Volume: Shohone, Death Valley Publ. Co., p. 61-70.

Tucker, M.E., 1986, Formerly aragonitic limestones associated with tillites in the Late Proterozoic of Death Valley, California: Journal of Sedimentary Petrology, v. 56/6, p. 818-830, 14 Figs., 3 Tabs.

Wright, L.A., Troxel, B.W., and Prave, A.R., 1992, Field traverse of Proterozoic rock units, Alexander Hills and southern Nopah Range, Death Valley region, CA, Late Phanerozoic Penrose Conference, Geological Society of America, p. 1-11.

Wright, L.A., Troxel, B.W., Williams, E.G., Roberts, M.T., and Diehl, P.E., 1974, Precambrian sedimentary environments of the Death Valley region, eastern California: Shoshone, Death Valley Publ. Co.

—, 1976, Precambrian sedimentary environments of the Death Valley region, eastern California: California Division of Mines and Geology Special Report, v. 106, p. 7-15.

Wright, L.A., Williams, E.G., and Cloud, P., 1978, Algal and cryptalgal structures and platform environments of the lat pre-Phanerozoic Noonday Dolomite, eastern California: Geological Society of America Bulletin, v. 89, p. 321-333.

Zhang, S., Jiang, G., and Han, Y., 2008, The age of the Nantuo Formation and Nantuo glaciation in South China, p. 1-6.

Zhang, S., Jiang, G., Zhang, J., Song, B., Kennedy, M.J., and Christie-Blick, N., 2005, U-Pb sensitive high-resolution ion microprobe ages from the Doushantuo Formation in south China: Constraints on late Neoproterozoic glaciations: Geology, v. 33, p. 473-476.

APPENDIX A: Sample locations, isotopic data and thin section preparation

Key to abbreviations:

Fm (Formation) & Mbr (Member):

bsd=Beck Spring Dolomite

csf=Crystal Spring Formation: biscuit=upper CSF marker bed

kpf=Kingston Peak Formation:

(east) ahd=Alexander Hills Diamictite, gd=Gunsight Diamictite, jmm=Jupiter Mine Member, shs=Saratoga Hills Sandstone, silhl=Silurian Hills Limestone, srmm=Silver Rule Mine Member, vsl=Virgin Spring Limestone

(west) mtngrl=Mountain Girls Member, surpd=Surprise Diamictite, sourl=Sourdough Limestone, wild=Wildrose Diamictite

nd=Noonday Dolomite: bsd-ndd=Noonday Dolomite-Beck Spring Dolomite contact

if=Ibex Formation: saddm=Saddle Peak Member

jf=Johnie Formation

Fm	Mbr	Samp ID	Description	Height	d 13-C	d 18-O	TS
Alexander Hills							
bsd	upper	2	AH BSD below SHS contact		1.2	-3.7	
bsd	upper	3	AH BSD below SHS contact		0.6	-5.0	
bsd	upper	5	AH: BSD noonday looking bed just below SHS		2.3	-6.8	
bsd	upper	6	AH: BSD microbialit just above ND-looking bed				y
bsd	upper	7	AH top of BSD but turning brown		2.1	-2.4	
bsd	upper	8	AH top of BSD microbial		0.5	-5.3	
bsd	upper	9	AH top of BSD microbial		0.3	-6.2	
bsd	upper	10	AH more microbial upper BSD but not in section		-0.7	-6.5	
csf		3	classic stroms great western		1.8	-7.4	y
jf	oolite	3	Alexander Hills J. ooliteite		-4.4	-7.5	
jf	oolite	2(above 2)	Alexander Hills J. ooliteite		-3.7	-6.3	
jf	oolite	2A	Alexander Hills J. ooliteite		-4.1	-7.3	
jf	oolite	3v	Alexander Hills J. ooliteite		-1.4	-7.1	
jf	oolite	4a1	Alexander Hills J. ooliteite		-5.6	-9.2	
jf	oolite	4a2	Alexander Hills J. ooliteite		-5.8	-8.6	
jf	oolite	4b(rpt)	Alexander Hills J. ooliteite		-4.7	-7.8	
jf	oolite	4b1	Alexander Hills J. ooliteite		-4.7	-7.6	
jf	oolite	4b2	Alexander Hills J. ooliteite		1.6	-13.5	
jf	oolite	5a1	Alexander Hills J. ooliteite		-4.9	-7.7	
jf	oolite	5a3	Alexander Hills J. ooliteite		-5.7	-9.2	
jf	oolite	5a4	Alexander Hills J. ooliteite		-5.3	-8.6	
jf	oolite	5b1	Alexander Hills J. ooliteite		-4.5	-7.3	
jf	oolite	5b2	Alexander Hills J. ooliteite		-4.9	-8.5	
jf	oolite	5b2(rpt)	Alexander Hills J. ooliteite		-4.9	-8.3	
jf	oolite	5b3	Alexander Hills J. ooliteite		-5.2	-7.9	
jf	oolite	5b4	Alexander Hills J. ooliteite		-4.8	-7.5	
jf	oolite	E13-1	alex johnnie ooliteite	0.5	-2.7	-8.0	

jf	oolite	E13-2	alex johnnie ooliteite	1	-3.4	-7.6	
jf	oolite	E13-3	alex johnnie ooliteite	1.5	-4.3	-7.1	
jf	oolite	E13-4	alex johnnie ooliteite	2	-4.3	-6.6	
kpf	ahd	1	AH: AHD ooliteite				y
kpf	ahd	1	AH: AHD black clastic limestone		1.3	-15.4	y
kpf	ahd	2	AH: AHD gray carb with odd blk clast		4.1	-8.9	y
kpf	ahd	2	AH: AHD black limestone		1.8	-15.0	y
kpf	ahd	3	AH: matt's blk clast in the AHD		3.9	-15.6	y
kpf	ahd	23	AH AHD massive diamictite				y
kpf	ahd	24	AH AHD massive diamictite				y
kpf	ahd	25	AH AHD massive diamictite				y
kpf	ahd	35	AH Basal AHD w/Virgin clasts		2.1	-11.0	
kpf	ahd	11a	AH CSF clasts in probable AHD		1.8	-1.2	y
kpf	ahd	11a	AH BSD clasts in probable AHD		3.7	0.0	y
kpf	ahd	11b	AH BSD clasts in probable AHD		3.9	0.0	y
kpf	ahd	11c	AH BSD clasts in probable AHD		4.0	0.0	y
kpf	ahd	2	AH: SHS-AHD contact		-2.4	-4.5	
kpf	ahd	22A	AH AHD massive diamictite				y
kpf	ahd	22B	AH AHD massive diamictite				y
kpf	ahd	34m	AH Basal AHD w/Virgin clasts		0.2	-11.7	
kpf	jmm	1	AH: JMM green diamictite for matrix in ts				y
kpf	jmm	1	AH: red ss from JMM ash bed				y
kpf	jmm	2	AH: JMM laminated carb in clast; csf?		2.0	-2.3	
kpf	jmm	3	AH: JMM pinkish granite? Clast				y
kpf	jmm	4	AH JMM sandy beds above possible ash				y
kpf	jmm	4	AH: JMM pinkish ss from "ash beds"				y
kpf	jmm	4	AH: SRMM base at top of roadcut				y
kpf	jmm	5	AH JMM possible ash beds				y
kpf	jmm	5	AH JMM fanglomerate red matrix				y
kpf	jmm	6	AH JMM fanglomerate red matrix				y
kpf	jmm	7	AH JMM fanglomerate red matrix				y
kpf	jmm	8	AH JMM ss				y

kpf	jmm	9	AH JMM ss				y
kpf	jmm	10	AH JMM fanglomerate browner matrix				y
kpf	jmm	11	AH JMM fanglomerate browner matrix				y
kpf	jmm	12	AH JMM coarse ss				y
kpf	jmm	J9???	fang under slide area				y
kpf	shs	1	Alex Hills; SHS base showing trans brwn and grn ss				y
kpf	shs	2	Alex Hills; SHS more gradational grn and brn ss				y
kpf	shs	3	Alex Hills; carbonate from SHS base transitional beds		0.9	-4.7	y
kpf	shs	4	Alex Hills; interbedded carbonate and ss from base SHS transition beds				y
kpf	shs	5	AH fine grained SHS-BSD trans beds		0.5	-3.5	
kpf	shs	6	AH coarse grained SHS-BSD trans beds		0.4	-3.6	
kpf	shs	7	AH: SHS-ish ss in basal AHD				y
kpf	shs	14	AH SHS below Damon's contact				y
kpf	shs	26	AH SHS altered zone				y
kpf	shs	27	AH SHS altered zone				y
kpf	shs	28	AH SHS below altered zone				y
kpf	shs	29	AH SHS top of saddle				y
kpf	shs	30	AH SHS				y
kpf	shs	31	AH SHS				y
kpf	shs	32	AH SHS				y
kpf	shs	2	AH: SHS-AHD contact		-5.4	-13.8	
kpf	shs	4a	AH SHS above trans beds		-2.9	-10.0	
kpf	shs	4b			-0.7	-2.5	
kpf	srmm	1	AH: green lam ss near basal SRMM				y
kpf	srmm	3	AH possible SHS faulted up to parking area				y
kpf	srmm	3	AH: SRMM coarse ss				y
kpf	srmm	4	AH possible SHS faulted up to parking area				y
kpf	srmm	4	AH: lavendar siltstone from SRMM (lower)				y
kpf	srmm	4	AH: green igneous sed rock from mid SRMM under mine				y
kpf	srmm	5	AH: SRMM graded beds down by AHD				y
kpf	srmm	14	AH SRMM Diamictite light grn matrx				y
kpf	srmm	15	AH SRMM Diamictite light grn matrx				y

kpf	srmm	16	AH SRMM Diamictite light grn matrx				y
kpf	srmm	17	AH SRMM Diamictite light grn matrx				y
kpf	srmm	18	AH SRMM fine grained bed				y
kpf	srmm	19	AH SRMM fine grained bed				y
kpf	srmm	20	AH SRMM fine grained bed				y
kpf	srmm	21	AH SRMM basement bearing cg from above SRMM-AHD				y
kpf	srmm	36	AH carbonate bed base of SRMM along road; BSD?		-0.6	-1.8	
kpf	srmm	21A	AH SRMM poss ash bed at base				y
kpf		2	AH: ND-=talus-debris for id qtz grains (JMM or AHD?)				y
nd	bsd-ndd	1b	BSD-NDD sed. contact south of road to Great Western		2.7	-0.1	
nd	bsd-ndd	1c	BSD-NDD sed. contact south of road to Great Western		3.2	-0.5	
nd	bsd-ndd	1d	BSD-NDD sed. contact south of road to Great Western		2.6	-2.4	
nd	bsd-ndd	1e	BSD-NDD sed. contact south of road to Great Western		2.1	-2.6	
nd	bsd-ndd	1f	BSD-NDD sed. contact south of road to Great Western		0.6	-4.2	
nd	bsd-ndd	1g	BSD-NDD sed. contact south of road to Great Western		-0.5	-4.7	
nd	bsd-ndd	1h	BSD-NDD sed. contact south of road to Great Western		-8.4	3.4	
nd	bsd-ndd	1i	BSD-NDD sed. contact south of road to Great Western		-2.2	-7.1	
nd	bsd-ndd	1j	BSD-NDD sed. contact south of road to Great Western		3.0	0.0	
nd	bsd-ndd	1k	BSD-NDD sed. contact south of road to Great Western		0.2	-3.9	
nd	bsd-ndd	2a	ND Breccia above BSD-ND sed contact w/cements		-3.1	-7.6	
nd	bsd-ndd	2b	ND Breccia above BSD-ND sed contact w/cements		-3.0	-6.1	
nd	bsd-ndd	2c	ND Breccia above BSD-ND sed contact w/cements		-3.0	-8.4	
nd	bsd-ndd	2d	ND Breccia above BSD-ND sed contact w/cements		-2.8	-12.7	
nd	clast	2Aa	AH clast and rind		2.1	-1.9	
nd	clast	2c	AH clast and rind		2.3	-2.1	
nd	lower	1	AH NDD w/clasts				y
nd	lower	7	Lower ND below interbedded JMM	2.5	-3.7	-5.9	y
nd	lower	9	Lower ND below interbedded JMM	0	-2.8	-5.9	y
nd	lower	10	Lower ND below interbedded JMM	0.5	-2.8	-5.9	y
nd	lower	11	Lower ND below interbedded JMM	1.5	-2.8	-6.1	y
nd	lower	12	AH silty dolo transition above KP		-3.0	-6.1	y
nd	lower	13	Lower ND below interbedded JMM		-3.1	-5.7	y

nd	lower	13	AH silty dolo transition above KP		-3.2	-6.3	
nd	lower	14	Lower ND below interbedded JMM	3.5	-2.8	-6.1	y
nd	lower	15	Lower ND below interbedded JMM	4	-2.9	-5.8	y
nd	lower	16	Lower ND below interbedded JMM	4.5	-3.0	-5.3	y
nd	lower	17	Lower ND below interbedded JMM	5	-3.1	-5.2	y
nd	lower	18	Lower ND below interbedded JMM	5.5	-2.8	-5.3	y
nd	lower	19	Lower ND below interbedded JMM	1	-3.1	-5.8	y
nd	lower	20	Lower ND below interbedded JMM	2	-2.7	-6.0	y
nd	lower	21	Lower ND below interbedded JMM	3	-2.7	-5.3	y
nd	lower	1 grn	AH: ND disrupted faces near wide tubes (2)		-3.0	-8.5	
nd	lower	1 pnk	AH: ND disrupted faces near wide tubes (2)		-3.1	-8.4	
nd	lower	1 spar	AH: ND disrupted faces near wide tubes (2)		-1.9	-10.6	
nd	lower	1 vein	AH: ND disrupted faces near wide tubes (2)		-4.6	-11.7	
nd	lower	12 bsc	Lower ND below interbedded JMM		1.2	-1.5	y
nd	lower	1a	Lower ND below interbedded JMM		4.7	0.0	y
nd	lower	1b	Lower ND below interbedded JMM		4.0	1.3	y
nd	lower	2Ab	AH clast and rind		-2.8	-5.0	
nd	lower	2Ac	AH clast and rind		-3.7	-5.7	
nd	lower	2Ad	AH clast and rind		-3.0	-5.7	
nd	lower	2Ae	AH clast and rind		-3.4	-5.0	
nd	lower	2Af	AH clast and rind		-4.0	-5.4	
nd	lower	2Ah	AH clast and rind		-3.2	-5.8	
nd	lower	2m	AH clast and rind		-1.8	-6.0	
nd	lower	3a	AH NDD above clast layer		-3.3	-5.5	
nd	lower	3b	AH NDD above clast layer		-3.7	-5.5	
nd	lower	E9	alexander NDF breccia & diamictite for iso				y
nd	bsd-nd	1a	BSD-NDD sed. contact south of road to Great Western		1.3	-2.1	
nd	bsd-nd	2(c)	bsd-nd Contact (see Dave's cement strat notes)		-3.0	-8.4	
nd	bsd-nd	2(1a)	bsd-nd Contact (see Dave's cement strat notes)		-3.5	-7.4	
nd	bsd-nd	2(1A)	bsd-nd Contact (see Dave's cement strat notes)		-2.6	-7.5	
nd	bsd-nd	2(1B)	bsd-nd Contact (see Dave's cement strat notes)		2.4	-10.4	
nd	bsd-nd	2(2A)	bsd-nd Contact (see Dave's cement strat notes)		-11.6	-15.1	

nd	bsd-nd	2(2A)	bsd-nd Contact (see Dave's cement strat notes)		-2.7	-12.7	
nd	bsd-nd	2(2B)	bsd-nd Contact (see Dave's cement strat notes)		-3.6	-14.8	
nd	bsd-nd	2(3A)	bsd-nd Contact (see Dave's cement strat notes)		-3.4	-8.7	
nd	bsd-nd	2(3B)	bsd-nd Contact (see Dave's cement strat notes)		-3.1	-6.8	
nd	bsd-nd	2(3C)	bsd-nd Contact (see Dave's cement strat notes)		-3.5	-9.8	
nd	bsd-nd	2(a)	bsd-nd Contact (see Dave's cement strat notes)		-3.1	-7.6	
nd	bsd-nd	2(b)	bsd-nd Contact (see Dave's cement strat notes)		-3.0	-6.1	
nd	bsd-nd	2(d)	bsd-nd Contact (see Dave's cement strat notes)		-2.8	-12.7	
nd	bsd-nd	2(e)	bsd-nd Contact (see Dave's cement strat notes)		-1.8	-4.5	
nd	upper	3	AH: upper ND purple siltstone with grn minerals				y
nd	upper	5	AH: U. ND thin bedded dolo N. end AH				y
nd	upper	6	AH: U. ND above BSD fault block		-3.5	-6.7	y
unk		2	basement diabase hash near basal SRMM				y
Beck Canyon Weste							
jf	oolite	1	ooliteite at Beck Canyon North		-3.2	-6.3	
jf	oolite	2	ooliteite at Beck Canyon North		-4.1	-7.3	
jf	oolite	3	ooliteite at Beck Canyon North	1.2	-5.1	-7.5	
jf	oolite	4	ooliteite at Beck Canyon North	2	-5.4	-8.2	
jf	oolite	5	ooliteite at Beck Canyon North	2.25	-5.1	-7.9	
jf	oolite	6	ooliteite at Beck Canyon North		-6.7	-6.5	
Beck Cayon Divide							
kpf	ahd	1	clast from basal AHD		-3.8	-15.4	
kpf	ahd	2	laminated carb silt below basal AHD		-3.5	-15.4	
kpf	ahd	4	AHD matrix				y
kpf	ahd	5	AHD?: finer mtx				y
kpf	ahd	6	AHD?: crs mtx				y
kpf	ahd	10	upper AHD: mtx				y
kpf	ahd	11	AHD: mtx				y
kpf	ahd	2(rpt)	laminated carb silt below basal AHD		-2.9	-13.2	
kpf	shs	3	basal SHS (???) oriented for ts				y
kpf	srmm	7	SRMM marker: oncoids		-2.8	-3.2	y
kpf	srmm	8	below marker: grn ss interval				y

kpf	srmm	9	below marker: pbl bed in grn ss				y
kpf	srmm	13	marker bed: 2 pcs below oncoidal zone				y
kpf	srmm	14	interbedded diamictites green mtx is 14-1,3,5 brn mtx is 14-2,4,4		1.1	-8.0	
kpf	srmm	15	white dolo clast (nd?) where from?		-2.3	-3.2	
kpf	srmm	17	SRMM marker bed in drainage under flyiong saucer		0.9	-11.6	y
kpf	srmm	6-1	SRMM marker bed: 6-1 thru 6-8 is section and 6-6a is chert piece		-2.1	-7.8	
kpf	srmm	6-1(rpt)	SRMM marker bed: 6-1 thru 6-8 is section and 6-6a is chert piece		-1.1	-10.9	
kpf	srmm	6-2	SRMM marker bed: 6-1 thru 6-8 is section and 6-6a is chert piece	0.5	1.1	-11.5	y
kpf	srmm	6-2(rpt)	SRMM marker bed: 6-1 thru 6-8 is section and 6-6a is chert piece	0.5	1.1	-10.1	y
kpf	srmm	6-3	SRMM marker bed: 6-1 thru 6-8 is section and 6-6a is chert piece	1	1.2	-11.6	
kpf	srmm	6-3(rpt)	SRMM marker bed: 6-1 thru 6-8 is section and 6-6a is chert piece	1	1.2	-10.2	
kpf	srmm	6-4	SRMM marker bed: 6-1 thru 6-8 is section and 6-6a is chert piece	1	1.9	-9.7	
kpf	srmm	6-4(rpt)	SRMM marker bed: 6-1 thru 6-8 is section and 6-6a is chert piece	1.5	1.9	-8.3	
kpf	srmm	6-5	SRMM marker bed: 6-1 thru 6-8 is section and 6-6a is chert piece	1	2.2	-8.7	
kpf	srmm	6-5(rpt)	SRMM marker bed: 6-1 thru 6-8 is section and 6-6a is chert piece	2	2.2	-7.3	
kpf	srmm	6-6	SRMM marker bed: 6-1 thru 6-8 is section and 6-6a is chert piece	2.5	2.1	-12.6	
kpf	srmm	6-6(rpt)	SRMM marker bed: 6-1 thru 6-8 is section and 6-6a is chert piece	2.5	2.1	-11.2	
kpf	srmm	6-6A	SRMM marker bed: 6-1 thru 6-8 is section and 6-6a is chert piece		-2.1	-9.2	
kpf	srmm	6-7	SRMM marker bed: 6-1 thru 6-8 is section and 6-6a is chert piece	1	2.9	-5.0	
kpf	srmm	6-7(rpt)	SRMM marker bed: 6-1 thru 6-8 is section and 6-6a is chert piece	3	2.9	-3.6	
kpf	srmm	6-8	SRMM marker bed: 6-1 thru 6-8 is section and 6-6a is chert piece		3.7	-5.6	
kpf	srmm	6-8(rpt)	SRMM marker bed: 6-1 thru 6-8 is section and 6-6a is chert piece		0.1	-12.2	
kpf	srmm	14(1)	interbedded diamictites green mtx is 14-1,3,5 brn mtx is 14-2,4,5		-3.6	-10.4	y
kpf	srmm	14(1)(rpt)	interbedded diamictites green mtx is 14-1,3,5 brn mtx is 14-2,4,6		-2.3	-11.7	y
kpf	srmm	14(2)	interbedded diamictites green mtx is 14-1,3,5 brn mtx is 14-2,4,7		-0.9	-11.5	y
kpf	srmm	14(2)(rpt)	interbedded diamictites green mtx is 14-1,3,5 brn mtx is 14-2,4,8		-0.9	-11.7	y
kpf	srmm	14(3)	interbedded diamictites green mtx is 14-1,3,5 brn mtx is 14-2,4,9		-4.2	-11.2	y
kpf	srmm	14(3)(rpt)	interbedded diamictites green mtx is 14-1,3,5 brn mtx is 14-2,4,10		-1.3	-10.5	
kpf	srmm	14(4)	interbedded diamictites green mtx is 14-1,3,5 brn mtx is 14-2,4,11		-0.2	-12.6	y
kpf	srmm	14(4)(rpt)	interbedded diamictites green mtx is 14-1,3,5 brn mtx is 14-2,4,12		0.1	-12.3	y
kpf	srmm	14(5)	interbedded diamictites green mtx is 14-1,3,5 brn mtx is 14-2,4,13		-1.8	-9.5	y
kpf	srmm	14(5)(rpt)	interbedded diamictites green mtx is 14-1,3,5 brn mtx is 14-2,4,14		-1.6	-8.9	y

kpf	srmm	14(6)	interbedded diamictites green mtx is 14-1,3,5 brn mtx is 14-2,4,15		0.2	-11.1	y
kpf	srmm	14(6)(rpt)	interbedded diamictites green mtx is 14-1,3,5 brn mtx is 14-2,4,6		0.6	-10.9	y
Blacksmith Hills							
csf		13	quartzite under ND				y
nd	lower	1	pink quartzite from NDF				y
nd	lower	2	quartzite-ndf contact for grain contact				y
nd	lower	3	ndf tubes		-3.4	-10.0	
nd	lower	4	3-4 m buff carbonate bed above tubes; ndf? Bottom	0	-3.9	-13.5	
nd	lower	5	3-4 m buff carbonate bed above tubes; ndf? Middle	1.5	-3.5	-12.5	
nd	lower	6	3-4 m buff carbonate bed above tubes; ndf? Top	3	-3.4	-12.0	
Blacksmith Mine							
jf	oolite	F1	bl mine j ooliteite bottom shale	-0.5	-4.2	-12.5	
jf	oolite	F2	bl mine j ooliteite bottom shale	-0.3	-5.3	-11.4	
jf	oolite	F3	bl mine j ooliteite bottom shale	-0.1	-4.4	-8.5	
jf	oolite	F4	bl mine base ooliteite	0.1	-2.7	-7.6	
jf	oolite	F4a	bl mine very base ooliteite…dark surface	0	-2.3	-7.7	
jf	oolite	F5	bl mine ooliteite up 30 cm	0.4	-4.0	-7.3	
jf	oolite	F6	bl mine j ooliteite up 80 cm	0.9	-3.4	-5.4	
jf	oolite	F7	bl mine j ooliteite up 120 cm	1.3	-4.2	-7.1	
jf	oolite	F8	bl mine j ooliteite up 150 cm	1.6	-4.9	-7.4	
jf	oolite	F9	bl mine j ooliteite up ~2 m	2	-5.3	-7.1	
jf		F12	bl mine carb cemented s.s. right above NDF		-3.3	-7.4	
Cooper Mine							
kpf	sour l	8		2.6	-2.8	-15.2	
kpf	sour l	9		2	-3.0	-12.4	
kpf	sour l	11		1.6	-3.1	-15.2	
kpf	sour l	12		1.3	-3.5	-12.6	
kpf	sour l	13		1	-3.3	-12.3	
kpf	sour l	14		0.6	-4.0	-12.5	
kpf	sour l	15		0.3	-3.5	-14.5	
kpf	sour l	16		0	-4.1	-14.6	
kpf	sour l	19	top sdl nice slab	2.6	-3.7	-14.6	

kpf	unl	1	1m ls bed 100m laterally from sdl-wildrose contact	32m+1	-3.7	-15.8	
kpf	unl	2	1m ls bed 100m laterally from sdl-wildrose contact	32m+.8	-4.3	-13.3	
kpf	unl	3	1m ls bed 100m laterally from sdl-wildrose contact	32m+.6	-3.6	-14.0	
kpf	unl	4	1m ls bed 100m laterally from sdl-wildrose contact	32m+.2	-3.3	-15.8	
kpf	unl	5	1m ls bed 100m laterally from sdl-wildrose contact	32m+0	-3.7	-15.2	
kpf	wild d	6	ls clast in wildrose	2.7	-2.8	-15.0	
kpf	wild d	7	wildrose mtx	2.7	-3.3	-12.3	
kpf	wild d	1A-a	odd clast from wildrose		-2.1	-14.8	
kpf	wild d	1A-b	odd clast from wildrose		5.0	-15.4	
kpf		18a			-2.6	-15.4	
kpf		18b			-6.8	-17.5	
nd	sent pk	1	basal sentinal peak		-2.0	-9.3	
Corral Section							
kpf	srmm	ahd1	Kingston Range-CorralHTS (Corsetti)-SRMM Marker	0	-1.9	-8.1	
kpf	srmm	ahd2	Kingston Range-CorralHTS (Corsetti)-SRMM Marker	0.5	-1.4	-8.3	
kpf	srmm	ahd3	Kingston Range-CorralHTS (Corsetti)-SRMM Marker	1	-0.5	-4.5	
kpf	srmm	ahd4	Kingston Range-CorralHTS (Corsetti)-SRMM Marker	1.5	1.0	-3.8	
kpf	srmm	KPONC	Kingston Range-HTS (Corsetti)-SRMM Marker	4	1.1	-2.2	
Coyote Canyon							
kpf	wildd	2	basal wildrose w/white carb clasts for iso		5.3	-15.1	
Cresent Mine							
bsd		2a	pisoid marker bed…bsd?		-1.3	-11.6	
bsd		3Ba	possible mottled BSD		-1.8	-15.6	
bsd		3Bb	possible mottled BSD		-1.1	-12.6	
Crystal Spring							
csf		3	silicified CSF or diamictite				y
kpf	ahd	1	AHD clast: vsl		2.0	-14.5	
kpf	ahd	2	AHD: grn mtx				y
kpf	ahd	3	AHD: vsl lam clast		-1.1	-16.7	
kpf	ahd	4	AHD: blk mtx		1.0	-13.2	y
kpf	ahd	5	AHD: mtx w/cycles (?)		0.5	-13.9	y
kpf	ahd	7	AHD: basal AHD layer mtx				y

kpf	ahd	8	AHD: basal AHD layer clast		-6.4	-15.0	y
kpf	shs	11	carb layer at top of SHS		2.1	-23.7	
kpf	shs	12	SHS: basal hang wall concretionary SHS for ts				y
kpf	srmm	5	lam possibly tidal SRMM over AHD contact				y
kpf	srmm	7	SRMM: first SRMMish for mtx				y
kpf	srmm	10	green bed				y
Excelsior Mine							
csf	biscuit	30	Excelsior Mine; CSF marker bed	0	-0.8	-5.0	
csf	biscuit	31	Excelsior Mine; CSF marker bed	1.5	-0.9	-4.6	
csf	biscuit	32	Excelsior Mine; CSF marker bed	3	-0.7	-4.3	
csf	biscuit	33	Excelsior Mine; CSF marker bed	4.5	-2.5	-3.8	
csf	biscuit	34	Excelsior Mine; gray "BSD" like clast from CSF marker bed	2.25	-4.0	-4.2	
Far North							
kpf	jmm	1-3	kp mtx of diamictite under ND				y
Galena Canyon							
jf	oolite	BMO-1	Blk Mtn J ooliteite		-0.7	-11.5	
jf	oolite	BMO-2	Blk Mtn J ooliteite		-1.4	-10.4	
jf	oolite	BMO-3	Blk Mtn J ooliteite		-3.8	-8.8	
jf	oolite	BMO-4	Blk Mtn J ooliteite		-3.2	-9.8	
jf	oolite	BMO-5	Blk Mtn J ooliteite		-6.8	-8.5	
Goler Wash							
csf		7	south side road carb block: white carb at base		-4.1	-18.7	
csf		8	south side road carb block: gray carb in middle		-3.1	-18.1	
csf		9	south side road carb block: gray sdl like top		-1.8	-17.3	
csf		10	possible white CSF w/diabase shot w/grn veins and algal buildups		-3.8	-12.7	
csf		11	possible upper CSF above fault lam and deformed		-3.7	-16.7	
csf		12	downstream section of white par lam dolo (across NDD fault)		-2.5	-9.5	
csf		13	upstream section wht lam dolo		-4.3	-10.1	
kpf	sour l	2			-1.6	-16.1	
kpf	sour l	2	sdl section along road		-3.9	-17.8	
kpf	sour l	3			-1.8	-15.5	
kpf	sour l	3			-2.2	-16.0	

kpf	sour l	4			-2.5	-16.2	
kpf	sour l	4			-1.9	-15.3	
kpf	sour l	5			-2.7	-16.7	
kpf	sour l	5			-1.4	-14.6	
kpf	sour l	6			-2.1	-15.8	
kpf	sour l	6			-1.1	-13.0	
kpf	sour l	10			-1.8	-15.1	
kpf	sour l	11			-1.4	-15.0	
kpf	sour l	13			-1.4	-16.5	
kpf	sour l	14			-1.2	-14.8	
kpf	sour l	15			-1.1	-15.7	
kpf	sour l	16			-2.2	-14.7	
kpf	sour l	17			-1.5	-15.6	
kpf	sour l	18			-2.8	-16.8	
kpf	sour l	19			-2.3	-16.4	
kpf	sour l	20			-3.4	-16.3	
kpf	sour l	21			-2.6	-16.3	
kpf	sour l	22			-2.6	-15.7	
kpf	sour l	23			-2.2	-15.2	
kpf	sour l	24			-0.9	-10.8	
kpf	sour l	25			-2.2	-15.7	
kpf	sour l	1a	sdl: very dark basal		-3.2	-17.0	
kpf	sour l	1a(rpt)			-2.7	-17.1	
kpf	sour l	1b			-2.8	-17.1	
kpf	sour l	1c			-2.8	-17.0	
kpf	sour l	1d			-2.7	-17.1	
kpf	sour l	1e			-3.0	-17.4	
kpf	surp d	2	surprise: white carb clast for iso		-0.6	-18.3	
kpf	surp d	3	surprise: striped carb clast for iso		-2.0	-17.6	
kpf	surpd	1	possible SDL clast in base Surprise		-5.2	-17.1	
kpf	wildd	8	just above #7 is a laminate wht carb		-2.7	-10.8	
kpf	wildd	10	white megaclast		-5.4	-17.1	

nd	lower	1	bedded white dolo over NDD (?) that may be olisostrome material		-3.8	-7.5	
nd	lower	14	white NDD (above fault)		-3.7	-7.8	
nd	lower	3A	possible NDD in SDL debris wash		-3.7	-11.0	
nd	lower	3C	possible NDD in SDL debris wash		-4.6	-18.0	
nd	lower	3D	possible NDD in SDL debris wash		-2.2	-11.0	
Goler Wash							
kpf		2	odd dist. Pyritic clasts in diamictite				y
nd	upper	2	shale above ndf				y
nd	upper	3	im fill above shale				y
nd	upper	4	lower nd2				y
nd	upper	5	upper nd2				y
nd	upper	6	karst in nd2				y
Horsethief Mine							
kpf	ahd	2	black AHD mtx		-7.6	-12.5	y
kpf	ahd	3	gritty AHD mtx, diff from above?				y
kpf	ahd	2(rpt)	black AHD mtx		0.6	-10.0	
kpf	jmm	6	brn ss below ND				y
kpf	jmm	7	diamictite below brown ss				y
kpf	srmm	6	diabase rich volc breccia (SRMM) (missing)				y
kpf	srmm	7	fine silty lams (tidal?) from SRMMbelow first fang facies				y
kpf	srmm	8	sandy bed hosting ash				y
kpf	wildd	5	wildrose diamictite				y
nd	lower	3	contact between ND mnd and lam: lam		-2.9	-6.6	
nd	lower	4	contact between ND mnd and lam: mound		-3.3	-6.2	
Horsethief Spring							
kpf	ahd	8	lower AHD mtx				y
kpf	jmm	2	Kingston Range; black shale from JMM mbr near Horsethief Springs roadcut				y
kpf	jmm	3	JMM fanglomerate, mesquite mtns, with BSD clasts		5.3	-0.1	
kpf	shs	7	SHS under AHD contact				y
kpf	srmm	1	SRMM marker bed from Franks paper		0.4	-2.5	
kpf	srmm	1	Kingston Range-Bennie p/u for MJK-SRMM Onco Bed		4.3		

kpf	srmm	2	mid upper SRMM marker		-1.7	-5.8	
kpf	srmm	2	Kingston Range-Bennie p/u for MJK-SRMM Onco Bed		3.6		
kpf	srmm	3	Kingston Range-Bennie p/u for MJK-SRMM Onco Bed		1.0		
kpf	srmm	4	Kingston Range-Bennie p/u for MJK-SRMM Onco Bed		2.0		
kpf	srmm	5	Kingston Range-Bennie p/u for MJK-SRMM Onco Bed		0.4		
kpf	srmm	9	SRMM grn mtx diamictite odd clast				y
kpf	srmm	10	SRMM grn mtx diamictite for mtx				y
kpf	srmm	11	green bed? Big pyrite				y
kpf	srmm	1 dark	oncolite from Kingston Range; KPF1(?) Oncolite bed		-2.9	-22.7	y
kpf	srmm	1 light	oncolite from Kingston Range; KPF1(?) Oncolite bed		-1.3	-6.6	
kpf	srmm	1(onco?)	oncolite from Kingston Range; KPF1(?) Oncolite bed		0.3	-9.7	
kpf	srmm	1D1	oncolite from Kingston Range; KPF1(?) Oncolite bed		-4.1	-26.2	
kpf	srmm	1L1	oncolite from Kingston Range; KPF1(?) Oncolite bed		-3.7	-23.6	
kpf	srmm	shs1	Kingston Range-HTS (Corsetti)-SRMM Marker	3.5	-2.5	-8.8	
kpf	srmm	shs2	Kingston Range-HTS (Corsetti)-SRMM Marker	3	-2.5	-11.2	
kpf	srmm	shs3	Kingston Range-HTS (Corsetti)-SRMM Marker	2.5	-2.8	-5.2	
kpf	srmm	shs4	Kingston Range-HTS (Corsetti)-SRMM Marker	2	-0.3	-5.7	
kpf	srmm	shs5.5	Kingston Range-HTS (Corsetti)-SRMM Marker	1	-2.1	-5.8	
kpf	srmm	shs5.5	Kingston Range-HTS (Corsetti)-SRMM Marker	1.5	-2.0	-6.1	
kpf	srmm	shs6	Kingston Range-HTS (Corsetti)-SRMM Marker	0.5	-2.5	-8.0	
kpf	srmm	shs7	Kingston Range-HTS (Corsetti)-SRMM Marker	0	-4.0	-2.1	
Ibex Hills							
bsd	upper	11a	LS (?) under crs ss…bsd?		3.0	-2.4	
bsd	upper	11A-a	Pinkish top BSD?		1.8	-7.0	
bsd	upper	11A-b	Pinkish top BSD?		1.8	-5.2	
bsd	upper	11b	LS (?) under crs ss…bsd?		2.2	-3.8	
bsd	upper	11c	LS (?) under crs ss…bsd?		3.4	-1.2	
bsd	upper	12a	BSD across VSL/BSD s.side		2.3	-10.5	
bsd	upper	12b	BSD across VSL/BSD s.side		2.7	-5.1	
bsd		1A	BSD s. end VSL block		3.4	-1.8	
if		1	damon's quartz bed				y
if		1.2.1	Damons Section	1	-2.5	-8.1	

if	1.2.10	Damons Section	5.5	-2.6	-7.6	
if	1.2.11	Damons Section	6	-2.7	-8.4	
if	1.2.12	Damons Section	6.5	-2.5	-8.2	
if	1.2.13	Damons Section	7	-2.5	-8.9	
if	1.2.14	Damons Section	7.5	-2.6	-8.0	
if	1.2.15	Damons Section	8	-2.6	-7.3	
if	1.2.16	Damons Section	8.5	-2.8	-8.8	
if	1.2.17	Damons Section	9	-2.7	-7.7	
if	1.2.18	Damons Section	9.5	-2.6	-7.6	
if	1.2.19	Damons Section	10	-3.0	-7.5	
if	1.2.2	Damons Section	1.5	-2.5	-7.2	
if	1.2.20	Damons Section	2	-2.8	-9.1	
if	1.2.21	Damons Section	2.5	-2.9	-8.8	
if	1.2.22	Damons Section	3	-2.8	-7.9	
if	1.2.23	Damons Section	3.5	-2.7	-8.3	
if	1.2.24	Damons Section	4	-2.8	-8.3	
if	1.2.3	Damons Section	2	-2.6	-7.2	
if	1.2.4	Damons Section	2.5	-2.7	-8.2	
if	1.2.5	Damons Section	3	-2.5	-8.4	
if	1.2.6	Damons Section	3.5	-2.6	-10.0	
if	1.2.7	Damons Section	4	-2.4	-7.9	
if	1.2.8	Damons Section	4.5	-2.5	-7.4	
if	1.2.9	Damons Section	5	-2.2	-10.8	
if	IBX 40-1	Damons Section	13	-2.2	-7.8	
if	IBX 40-10	Damons Section	13.5	-1.8	-8.9	
if	IBX 40-11	Damons Section	14	-2.3	-7.5	
if	IBX 40-12	Damons Section	14.5	-2.6	-7.7	
if	IBX 40-13	Damons Section	15	-2.1	-6.0	
if	IBX 40-14	Damons Section	15.5	-3.3	-21.4	
if	IBX 40-2	Damons Section	16	-2.3	-7.4	
if	IBX 40-3	Damons Section	16.5	-2.1	-7.5	
if	IBX 40-4	Damons Section	17	-1.8	-8.1	

if		IBX 40-5	Damons Section	17.5	-2.4	-7.6	
if		IBX 40-6	Damons Section	18	-2.6	-7.8	
if		IBX 40-7	Damons Section	18.5	-2.6	-7.2	
if		IBX 40-8	Damons Section	19	-2.6	-8.2	
if		IBX 40-9	Damons Section	19.5	-2.8	-7.4	
kpf	ahd	3	AHD w/vsl				y
kpf	jmm	13	JMM massive gray clast BSD?		-2.6	-8.6	
kpf	vsl	2	ooid chert from vsl				y
kpf	vsl	2	laminated from base above cover		1.6	-18.7	
kpf	vsl	4	laminated		2.4	-14.8	
kpf	vsl	5	laminated		2.4	-10.2	
kpf	vsl	7	laminated		1.2	-12.6	
kpf	vsl	8	laminated		2.7	-9.8	
kpf	vsl	8	big slab of top		2.7	-14.1	
kpf	vsl	9	laminated		2.5	-11.7	
kpf	vsl	10	laminated		2.6	-13.0	
kpf	vsl	11	laminated		2.2	-9.4	
kpf	vsl	12	laminated		3.3	-9.5	
kpf	vsl	13	laminated		2.9	-14.6	
kpf	vsl	14	laminated		3.3	-13.8	
kpf	vsl	15	laminated		2.5	-11.9	
kpf	vsl	16	laminated		2.2	-15.6	
kpf	vsl	17	laminated		2.4	-14.7	
kpf	vsl	18	very basal vsl from found contact		3.1	-17.4	
kpf	vsl	10a	color trans		0.3	-14.8	
kpf	vsl	10b	color trans		2.3	-18.9	
kpf	vsl	10c	color trans		2.0	-15.3	
kpf	vsl	10d	color trans		1.8	-16.7	
kpf	vsl	10e	color trans		2.2	-10.6	
kpf	vsl	10f	color trans		1.0	-13.2	
kpf	vsl	10g	color trans		2.5	-8.8	
kpf	vsl	13a	VSL across VSL/BSD contact s.side		1.6	-16.9	

kpf	vsl	13b	VSL across VSL/BSD contact s.side		1.9	-16.6	
kpf	vsl	1a	lam base of VSL above crs ss		1.5	-16.9	
kpf	vsl	1B	VSL across fault abutting BSD		2.5	-19.2	
kpf	vsl	1b	lam base of VSL above crs ss		1.7	-17.0	
kpf	vsl	2a	lam with onlap and cherty bits?		2.7	-14.9	
kpf	vsl	2b	lam with onlap and cherty bits?		2.8	-15.5	
kpf	vsl	3a	lt gray allochems above cherty		1.9	-15.7	
kpf	vsl	3b	lt gray allochems above cherty		1.7	-15.2	
kpf	vsl	4A	laminated		2.4	-14.8	
kpf	vsl	4a	lt gray flakey from base		2.8	-10.4	
kpf	vsl	4b	lt gray flakey from base		3.1	-12.2	
kpf	vsl	4c	lt gray flakey from base		2.0	-9.9	
kpf	vsl	5a	med gray…attached to #6		1.5	-13.2	
kpf	vsl	5b	med gray…attached to #6		0.4	-8.9	
kpf	vsl	5c	med gray…attached to #6		1.1	-11.5	
kpf	vsl	6a	v. lt gray flakey		1.9	-11.8	
kpf	vsl	6b	v. lt gray flakey		2.9	-11.1	
kpf	vsl	6c	v. lt gray flakey		3.3	-10.3	
kpf	vsl	6d	v. lt gray flakey		3.2	-10.5	
kpf	vsl	7a	dark gray lam ls		1.7	-14.5	
kpf	vsl	7b	dark gray lam ls		0.7	-11.9	
kpf	vsl	9a	thin bed w/discolor zone		1.8	-15.9	
kpf	vsl	9b	thin bed w/discolor zone		2.6	-11.9	
kpf	vsl	9c	thin bed w/discolor zone		0.6	-13.1	
kpf		1	top of vsl with ss layer		1.7	-16.7	
kpf		11	white carb of Valjean in debris				y
Jubilee Mine							
bsd		4	Virgin Wash BSD karst: BSD assoc w/sandy NDD infills		2.6	-3.5	
bsd		5	Virgin Wash BSD karst: BSD below diamictite		3.5	-0.2	
bsd		6	Virgin Wash BSD karst: lam bsd under diamictite		2.5	-3.1	
bsd		7	Virgin Wash BSD karst: more BSD under NDD fill		2.9	-3.7	
bsd		9	Virgin Wash BSD karst: BSD above fill		2.9	-2.4	

bsd		10	Virgin Wash BSD karst: BSD at BSD-NDD		3.0	-2.3	
jf		13	Virgin Wash JF: sharp ss-carb contact				y
jf		13	around ooliteiter		2.3	-4.9	
jf		14	around ooliteiter		-2.8	-6.0	
kpf	gd	1	diamict matrix wrom within basal Noonday; Martin and Karl walked to it				y
kpf	gd	3	Virgin Wash: kp matrix from diamict channels in BSD				y
nd	lower	3a	see Karl's cement strat notes		-2.1	-4.9	
nd	lower	3b	see Karl's cement strat notes		-1.2	-6.8	
nd	lower	3c	see Karl's cement strat notes		-0.3	-4.9	
nd	lower	3d	see Karl's cement strat notes		-1.7	-8.0	
nd	lower	3e	see Karl's cement strat notes		-2.9	-8.1	
nd	lower	3f	see Karl's cement strat notes		-2.1	-7.6	
nd	lower	3g	see Karl's cement strat notes		-1.5	-14.7	
nd	lower	3h	see Karl's cement strat notes		-2.3	-7.3	
nd	lower	3i	see Karl's cement strat notes		-2.2	-8.4	
nd		8	Virgin Wash BSD karst: NDD fill in karst		-2.3	-6.5	
nd		11	Virgin Wash BSD karst: NDD above BSD-NDD		-2.4	-6.2	
Jupiter Mine							
cs	biscuit?	1	section of carbonate in KPF from above saddle	0	-0.8	-3.8	
cs	biscuit?	2	section of carbonate in KPF from above saddle	0.66	1.1	-3.5	
cs	biscuit?	3	section of carbonate in KPF from above saddle	1.3	0.3	-6.2	
cs	biscuit?	4	section of carbonate in KPF from above saddle	2	1.1	-2.9	
cs	biscuit?	5	section of carbonate in KPF from above saddle	2.6	0.7	-2.7	
cs	biscuit?	6	section of carbonate in KPF from above saddle	3	0.9	-2.7	
cs	biscuit?	7	section of carbonate in KPF from above saddle	3.3	1.8	-5.4	
cs	biscuit?	8	section of carbonate in KPF from above saddle	3.6	2.7	-3.6	
cs	biscuit?	9	section of carbonate in KPF from above saddle	4.3	0.5	-4.0	
cs	upper	I6	back 40; CSF marker bed algal rollup		-0.7	-3.3	
csf		3A	JP CSF/KPF for slabbing				y
csf		A10	dark fine-grained from L.Saddle				y
csf		A7	transitional talc layer from CSF above talc-tremolite				y
csf		A8	laminated CSF from L.Saddle area				y

csf		B5	brescciated from CSF near L.Saddle				y
csf		C13	paleocurrent sample				y
csf		C8	pink confusing rock from between carb and diabase N. of L.Saddle				y
csf		D14	lower diamictite matrix				y
csf		D20	out of coarser grained layer				y
csf		D2b	dark gray clast, I guess from above L.Saddle				y
csf		G13	Pioneer Ridge; rhyolite from dike above excelsior				y
csf		G14	CSF Marker Bed; top buff carb		-0.1	-3.3	
csf		G19	very coarse diabase from by snow white				y
if		28	"ibex?" from backside				y
if		28A	"ibex?" from backside		-4.4	-9.1	
jf		J4	laminated johnnie(not upside down) N.End				y
kpf	gd	D13	transition clays under KPF				y
kpf	gd	D15	upper fine grain diamictite matrix				y
kpf	gd	D22	matrix of red diamictite				y
kpf	gd	D5	diamictite w/poss diabase matrix				y
kpf	gd	F19	J.Ridge; poss volcanic in diamictite				y
kpf	gd	I4	J.Ridge; red matrix ss above CSF/KPF				y
kpf	jmm	2	"scary" bsd in breccia				y
kpf	jmm	29	BSD talus		3.8	-0.2	
kpf	jmm	H7	from fine-grained section fanglomerate under big slide in NDF				y
kpf	jmm	H9	channel material in BSD Talus layer				y
kpf	wedge	1	small m-bed gray dolo base wedge s.end	n	0.8	-4.5	
kpf	wedge	2	small m-bed gray dolo base wedge s.end	n	2.3	-2.5	
kpf	wedge	3	small m-bed gray dolo base wedge s.end	n	1.8	-4.0	y
kpf	wedge	19	gray carb base wedge caps NDD #2	0	0.4	-10.5	
kpf	wedge	20	gray carb base wedge caps NDD #2	2.5	1.4	-4.5	
kpf	wedge	21	gray carb base wedge caps NDD #2	5	1.5	-3.7	
kpf	wedge	22	poss clast from wedge mid dolo layer		-2.0	-3.9	
kpf	wedge	E6	gray carb NDF#3; above pink quartzite		0.1	-7.7	
kpf	wedge	E7	gray carb NDF#3; middle		1.1	-1.8	
kpf	wedge	E8	gray carb NDF#3; top		1.1	-3.8	y

kpf	wedge	F20	tan carb by lower diamictite under NDD#2				y
kpf	wedge	F21	J.Ridge; white/pink altered ss from top plateau				y
kpf	wedge	F23	J.Ridge; brown shale that is main slope former from top plateau along w/poss clasts				y
kpf	wedge	H13-1	wedge; section of NDF-like carbonate	1	-0.1	-3.7	
kpf	wedge	H13-2	wedge; section of NDF-like carbonate	2	0.4	-3.7	
kpf	wedge	H13-3	wedge; section of NDF-like carbonate	3	-0.7	-3.9	
kpf	wedge	H13-4	wedge; section of NDF-like carbonate	4	-1.7	-4.4	y
kpf	wedge	H13-5	wedge; section of NDF-like carbonate	5	-2.4	-3.7	
kpf	wedge	H13-6	wedge; section of NDF-like carbonate	6	-3.7	-2.8	
kpf	wedge	H13-7	wedge; section of NDF-like carbonate	7	-3.8	-3.1	
kpf	wedge	H14	dark rock from top of NDF#2				y
kpf	wedge	H15	wedge; cap of grains on top gray carb				y
kpf	wedge	H16	wedge; beginning qtzite beds over qtzite caps or lenses in carb				y
kpf	wedge	H17	wedge; quartzit to do ts fro rvs grading				y
kpf	wedge	H18	NDF#1; brown cap rock				y
kpf	wedge	I12	wedge; carb next to "CSF"like carb for iso		-1.6	-5.8	
kpf	wedge	I7	some sample from north 40 around faulted marker bed				y
kpf	wedge	I9	wedge; under NDD 3; looks like fault breccia				y
kpf	wedge	J2	igneous looking rock from under diamictite at north end of J.Ridge				y
nd	lower 1	1	NDD #1; ts for diff between lam and other grains	0	-3.3	-6.2	
nd	lower 1	2	NDD #1, ts of lams that Karl thinks are mech.	1	-2.6	-7.4	
nd	lower 1	4	NDD #1	5	-2.7	-7.0	
nd	lower 1	5	NDD #1	10	-2.8	-7.2	
nd	lower 1	6	NDD #1	20	-3.0	-7.5	
nd	lower 1	7	NDD #1	30	-2.5	-7.2	
nd	lower 1	8	NDD #1	40	-3.2	-11.4	
nd	lower 2	10	NDD #2 (middle); clast from base		-0.6	-5.3	
nd	lower 2	12	NDD #2	0	-2.7	-6.6	
nd	lower 2	15	NDD #2	8	-2.7	-7.2	
nd	lower 2	16	NDD #2	12	-3.1	-6.5	
nd	lower 2	17	NDD #2	16	-3.2	-5.8	

nd	lower 2	18	NDD #2	20	-2.8	-7.9	
nd	lower 2	11c	NDD #2 (middle); clast from base		-0.5	-6.1	
nd	lower 2	11m	NDD #2 (middle); clast from base		-1.0	-7.6	
nd	lower 2	13c	NDD #2 (middle); clast from base	2	2.3	-1.6	
nd	lower 2	13m	NDD #2 (middle); clast from base	2	-2.9	-7.2	
nd	lower 2	14mud	NDD #2 (middle)	4	-2.6	-7.1	
nd	lower 2	14spar	NDD #2 (middle)	4	-2.7	-6.5	
nd	lower 2	9c	NDD #2 (middle); clast from base		2.8	-1.9	
nd	lower 2	9m	NDD #2 (middle); clast from base		-2.8	-6.3	
nd	lower 3	23	NDD #3 (top)	0	-2.9	-7.0	
nd	lower 3	24	NDD #3 (top)	3	-3.2	-6.9	
nd	lower 3	25	NDD #3 (top)	6	-3.0	-7.6	
nd	lower 3	26	NDD #3 (top)	9	0.9	-6.8	
nd	lower 3	27	NDD #3 (top)	12	-3.0	-7.3	
nd	lower 3	E4	NDD #3: samples of matrix around clasts		-1.2	-5.8	
nd	lower 3	E5	NDD #3: base of NDF		-1.6	-3.8	
nd	lwr1cmnt	H1	cements from debris layer at base of NDF across from snow white		-2.4	-6.6	
nd	lwr1cmnt	H3	cements from debris layer at base of NDF across from snow white		-2.5	-10.0	
nd	lwr1cmnt	H4	cements from debris layer at base of NDF across from snow white				4
nd	lwr1cmnt	H6	cements from debris layer at base of NDF across from snow white		-2.1	-4.7	
nd		H8	under slide area; NDF/JF trans rock w/cross lams				y
Saddle Peak Hills							
bsd		1	fetid blk dolo base measured section		0.4	-7.1	
bsd		2	lam bsd from upper bsd		2.0	-2.5	
bsd		2	blk dolo from BSD as above		1.8	-10.0	
bsd		3	blk fetid dolo as above		1.5	-9.2	
if	sd pk m	12A	interformational conglomerate above Saddle Peak S.B.	8.7	-5.3	-13.8	
if	sd pk m	12B	interformational conglomerate above Saddle Peak S.B.	11.5	-5.6	-13.5	
kpf	ahd	3	AHD mtx facies a				y
kpf	ahd	4	AHD mtx facies b				y
kpf	srmm	1	silty carb section below ND	24	-3.9	-5.4	

kpf	srmm	2	silty carb section below ND	0	-2.0	-7.3	
kpf	srmm	3	silty carb section below ND	16	-3.4	-6.5	
kpf	srmm	4	silty carb section below ND	10	-1.5	-8.7	
kpf	srmm	5	silty carb section below ND	124	-3.6	-5.1	
kpf	srmm	6A	silty carb section below ND	215	-3.3	-4.6	
kpf	srmm	6B	silty carb section below ND	215	-3.0	-4.6	
kpf	srmm	7A	silty carb section below ND	215	-3.0	-4.5	
kpf	srmm	7B	silty carb section below ND	240	-3.1	-5.3	
kpf	srmm	8A	silty carb section below ND	240	-3.2	-5.3	
kpf	srmm	8B	silty carb section below ND	340	-2.0	-4.5	
nd	lower	9	NDF tubes	340	-3.1	-5.4	
nd	lower	10a	NDF Tubes	4	-2.7	-5.9	
nd	lower	10b	NDF Tubes	4	-2.6	-5.8	
nd	lower	10B	NDF Tubes	2.5	-2.6	-5.8	
nd	lower	10c	NDF Tubes	4	-2.9	-5.9	
nd	lower	10C	NDF Tubes	9.7	-2.9	-5.9	
Saratoga Hills							
kpf	ahd	1	AHD mtx 15m above vsl				y
kpf	ahd	4	AHD: undolo vslk clast from grn diamictite		2.6	-12.3	
kpf	ahd	5	AHD: grn diamictite mtx		-8.8	-14.7	y
kpf	ahd	6	bsd: this is crs ss at top of bsd that makes up clasts in AHD				y
kpf	ahd	8	AHD: mtx from upper AHD clast count				y
kpf	ahd	9	AHD: grn diamictite above rhythmites				y
kpf	shs	6	SHS lam				y
kpf	srmm	5	SRMM ss w/pyrite				y
kpf	srmm	7	shale w/Py				y
kpf	vsl	30	mjk collected		-0.2	-14.8	
kpf	vsl	32	mjk collected		-0.3	-15.1	
kpf	vsl	33	mjk collected		0.3	-17.0	
kpf	vsl	34	mjk collected		0.8	-14.9	
kpf	vsl	39	mjk collected		-14.1	-23.3	
kpf	vsl	40	mjk collected		-0.2	-18.7	

kpf	vsl	41	mjk collected		2.5	-14.6	
kpf	vsl	42	mjk collected		2.1	-14.8	
kpf	vsl	43	mjk collected		1.3	-13.3	
kpf	vsl	44	mjk collected		1.5	-15.0	
kpf	vsl	31a	mjk collected		-0.8	-15.4	
kpf	vsl	31b	mjk collected		-1.2	-14.6	
kpf	vsl	37a	mjk collected		0.1	-19.9	
kpf	vsl	37b	mjk collected		0.1	-19.7	
kpf	vsl	39B	mjk collected		0.2	-15.2	
kpf	vsl	40B	mjk collected		0.6	-13.7	
kpf	vsl	45a	mjk collected		1.9	-14.0	
kpf	vsl	45b	mjk collected		-0.4	-17.1	
kpf	vsl	45c	mjk collected		1.1	-14.3	
kpf	vsl	46a	mjk collected		1.1	-14.3	
kpf	vsl	46b	mjk collected		-0.5	-15.7	
nd	lower	6	SaH: barite crust from mound		-3.3	-5.5	
nd	lower	7	SaH: very top surface of mounds		-3.6	-5.7	
nd	lower	1a	Karl's cements…see Dave's cement strat notes		-3.3	-10.3	
nd	lower	1b	Karl's cements…see Dave's cement strat notes		-3.1	-8.9	
nd	lower	1c	Karl's cements…see Dave's cement strat notes		-2.8	-9.3	
nd	lower	1d	Karl's cements…see Dave's cement strat notes		-3.3	-8.5	
nd	lower	2a	Karl's cements…see Dave's cement strat notes		-3.3	-9.7	
nd	lower	2b	Karl's cements…see Dave's cement strat notes		-3.0	-8.1	
nd	lower	3a	Karl's cements…see Dave's cement strat notes		-0.8	3.6	
nd	lower	3b	Karl's cements…see Dave's cement strat notes		-2.3	-12.3	
nd	lower	4a	Karl's cements…see Dave's cement strat notes		-3.8	-8.5	
nd	lower	4b	Karl's cements…see Dave's cement strat notes		-2.7	-7.3	
nd	lower	5a	Karl's cements…see Dave's cement strat notes		-6.5	-9.5	
nd	lower	5b	Karl's cements…see Dave's cement strat notes		-6.3	-10.9	
Silurian Hills							
jf	oolite	3	possible JF ooliteite		-4.5	-9.9	
kpf	silh l	1	SHL collected by karl,martin,paul	2	-0.1	-15.1	

kpf	silh l	4	SHL collected by karl,martin,paul	9	-0.1	-16.6	
kpf	silh l	5	SHL collected by karl,martin,paul	10	0.5	-16.2	
kpf	silh l	6	SHL collected by karl,martin,paul	11	0.9	-13.9	
kpf	silh l	10	SHL collected by karl,martin,paul	19	1.3	-12.4	
kpf	silh l	11	SHL collected by karl,martin,paul	20	4.4	-12.6	
kpf	silh l	12	SHL collected by karl,martin,paul	21	5.5	-8.5	
kpf	silh l	13	SHL collected by karl,martin,paul	22	2.9	-11.3	
kpf	silh l	13	nodule ?	2	0.9	-16.0	
kpf	silh l	14	SHL collected by karl,martin,paul	23	3.4	-10.7	
kpf	silh l	14	nodule ?	3	0.5	-14.6	y
kpf	silh l	15	ls	4	0.6	-15.6	y
kpf	silh l	16	SHL collected by karl,martin,paul	27	4.7	-10.3	
kpf	silh l	16		5	0.6	-12.7	y
kpf	silh l	17	SHL collected by karl,martin,paul	28	3.8	-10.6	
kpf	silh l	17		6	0.5	-16.0	y
kpf	silh l	18		7	-1.2	-13.3	y
kpf	silh l	19	ash or carb?				y
kpf	silh l	20	ls	8	0.0	-13.6	y
kpf	silh l	21		9	1.3	-14.3	y
kpf	silh l	22		10	3.2	-16.9	
kpf	silh l	23		11	3.3	-13.3	
kpf	silh l	24		12	5.6	-8.5	
kpf	silh l	25		13	3.4	-7.3	
kpf	silh l	26		14	2.8	-11.0	
kpf	silh l	27		15	2.9	-11.2	
kpf	silh l	29		17	4.9	-10.5	
kpf	silh l	30		18	5.8	-10.0	
kpf	silh l	31		19	5.9	-10.9	
kpf	silh l	32		20	4.3	-9.3	
kpf	silh l	33		21	6.7	-13.5	
kpf	silh l	34		22	4.2	-15.3	
kpf	silh l	36	ls karst	24	3.6	-15.9	

kpf	silh l	38	karst fill	26	-0.5	-15.2	
kpf	silh l	12a	interbedded ss and ash base limestone	1	-1.5	-16.1	
kpf	silh l	12b		1	-4.4	-16.1	
kpf	silh l	15a	SHL collected by karl,martin,paul	24	4.7	-10.7	
kpf	silh l	15b	SHL collected by karl,martin,paul	25	4.9	-11.1	
kpf	silh l	18a	SHL collected by karl,martin,paul	29	3.2	-13.7	
kpf	silh l	18b	SHL collected by karl,martin,paul	30	1.9	-13.9	
kpf	silh l	18ya	SHL collected by karl,martin,paul	31	3.4	-11.1	
kpf	silh l	18yb	SHL collected by karl,martin,paul	32	1.4	-18.2	
kpf	silh l	19A	SHL collected by karl,martin,paul	35	3.2	-14.9	
kpf	silh l	19a	SHL collected by karl,martin,paul	33	4.0	-15.1	
kpf	silh l	19b	SHL collected by karl,martin,paul	34	3.1	-15.4	
kpf	silh l	1A	SHL collected by karl,martin,paul	3	4.3	-12.7	
kpf	silh l	20A	SHL collected by karl,martin,paul	37	2.9	-14.4	
kpf	silh l	20Ba	SHL collected by karl,martin,paul	38	5.0	-17.2	
kpf	silh l	20Bb	SHL collected by karl,martin,paul	39	3.2	-16.2	
kpf	silh l	27vein		15	2.1	-21.2	
kpf	silh l	28a		16	3.1	-14.5	
kpf	silh l	28b		16	2.4	-14.0	
kpf	silh l	28vein		16	3.1	-22.2	
kpf	silh l	2a	SHL collected by karl,martin,paul	4	0.6	-14.2	
kpf	silh l	2b	SHL collected by karl,martin,paul	5	0.2	-14.4	
kpf	silh l	35a		23	3.3	-16.7	
kpf	silh l	35b		23	2.4	-14.6	
kpf	silh l	36Aa		24	0.3	-16.9	
kpf	silh l	36Ab		24	1.3	-14.1	
kpf	silh l	36Ac		24	1.9	-15.0	
kpf	silh l	36Ad		24	1.8	-14.9	
kpf	silh l	36Ae		24	1.7	-14.7	
kpf	silh l	36Af		24	1.7	-14.4	
kpf	silh l	37a	sandy as over ls	25	4.3	-20.1	
kpf	silh l	3a	SHL collected by karl,martin,paul	7	-0.5	-14.2	

kpf	silh l	3b	SHL collected by karl,martin,paul	8	-0.5	-15.5	
kpf	silh l	7a	SHL collected by karl,martin,paul	12	3.0	-16.2	
kpf	silh l	7b	SHL collected by karl,martin,paul	13	2.5	-24.3	
kpf	silh l	8a	SHL collected by karl,martin,paul	14	2.8	-15.1	
kpf	silh l	8b	SHL collected by karl,martin,paul	15	2.3	-18.2	
kpf	silh l	9a	SHL collected by karl,martin,paul	17	3.0	-13.7	
kpf	silh l	9b	SHL collected by karl,martin,paul	18	2.8	-17.4	
kpf		1	Rhythmite ash at top of overturned dark limestone				y
kpf		2	pink dolo w/ribs can see lams clearly & orange dolo		0.1	-19.0	
kpf		5	diabase "sill": big crystals at base of sill				y
kpf		6	diamictite mtx above blk ls				y
kpf		1a	pink dolo bed w/orange dolo front		-0.7	-17.8	
kpf		1b	pink dolo bed w/orange dolo front		-0.9	-13.4	
kpf		5a	upper blk ls color change		3.9	-13.9	
kpf		5b	upper blk ls color change		3.7	-13.5	
nd		1	section abobe KPF; NDF limestone?		-4.2	-17.6	
nd		2	section abobe KPF; NDF limestone?		-4.4	-14.1	
nd		3	section abobe KPF; NDF limestone?		-3.9	-9.3	
nd		4	section abobe KPF; NDF limestone?		-4.1	-11.2	
nd		5	section abobe KPF; NDF limestone?		-4.4	-14.5	
nd		6	section abobe KPF; NDF limestone?		-3.9	-13.3	
nd		7	section abobe KPF; NDF limestone?		-4.2	-14.3	
nd		8	section abobe KPF; NDF limestone?		-4.4	-15.5	
nd		9	section abobe KPF; NDF limestone?		-3.5	-9.9	
nd		1A	section abobe KPF; NDF limestone?		-4.6	-13.0	
Silver Rule Mine							
kpf	ahd	2	AHD dark mtx		0.5	-13.2	y
kpf	ahd	2	AHD: mtx from clast count				y
kpf	ahd	3	AHD vsl clast		4.9	-2.1	
kpf	ahd	4	AHD sandy mtx				y
kpf	ahd	4	tabular clast from basal AHD zone		-7.4	-15.5	
kpf	ahd	5	AHD mtx from clast count				y

kpf	ahd	4(rpt)	tabular clast from basal AHD zone		-7.3	-14.6	
kpf	shs	1	SHS base no carb				y
kpf	shs	2	SHS lam ss @ 19-20 stfs				y
kpf	shs	3	SHS lam ss for slab				y
kpf	srmm	5	fine grain (glacial flower?) above debris flow in SRMM				y
kpf	srmm	6	poss tidalite from basal SRMM				y
Sourdough Canyon							
kpf	sour l	1	mjk collected along roadcut		-2.4	-13.7	
kpf	sour l	2	mjk collected along roadcut		-2.9	-13.3	
kpf	sour l	3	mjk collected along roadcut		-1.8	-13.0	
kpf	sour l	3	sourdough ls section (see notes)	1.2	-3.8	-12.6	
kpf	sour l	4	mjk collected along roadcut		-2.5	-12.8	
kpf	sour l	4	sourdough ls section (see notes)	1.8	-3.5	-13.5	
kpf	sour l	5	sourdough ls section (see notes)	1.9	-3.2	-13.6	
kpf	sour l	6	sourdough ls section (see notes)	2.5	-2.6	-13.3	
kpf	sour l	7	sourdough ls section (see notes)	3.1	-3.3	-11.9	
kpf	sour l	8	sourdough ls section (see notes)	3.7	-2.7	-13.0	
kpf	sour l	10	mjk collected along roadcut		-1.5	-15.2	
kpf	sour l	10	sourdough ls section (see notes)	5.3	-1.9	-11.7	
kpf	sour l	11	mjk collected along roadcut		-3.3	-12.5	
kpf	sour l	11	sourdough ls section (see notes)	6	-3.6	-11.3	
kpf	sour l	12	sourdough ls section (see notes)	7	-1.9	-12.6	
kpf	sour l	13	sourdough ls section (see notes)	8	-1.6	-13.2	
kpf	sour l	14	sourdough ls section (see notes)	9	-2.4	-13.1	
kpf	sour l	15	sourdough ls section (see notes)	10	-2.7	-13.8	
kpf	sour l	17	sourdough ls section (see notes)	12	-1.8	-12.0	
kpf	sour l	18	sourdough ls section (see notes)	13	-1.5	-12.6	
kpf	sour l	19	sourdough ls section (see notes)	14	-2.2	-11.5	
kpf	sour l	20	sourdough ls section (see notes)	15	-1.5	-13.0	
kpf	sour l	21	sourdough ls section (see notes)	16	-2.1	-12.5	
kpf	sour l	22	sourdough ls section (see notes)	17	-2.2	-13.8	
kpf	sour l	24	sourdough ls section (see notes)	19	-2.4	-13.7	

kpf	sour l	25	sourdough ls section (see notes)	20	-2.9	-12.4	
kpf	sour l	26	sourdough ls section (see notes)	21	-2.5	-14.0	
kpf	sour l	12a	mjk collected along roadcut		-3.5	-14.4	
kpf	sour l	12b	mjk collected along roadcut		-2.3	-13.6	
kpf	sour l	1B	sourdough ls section (see notes)	0	-3.1	-13.7	
kpf	sour l	25A	sourdough ls section (see notes)	20.3	-2.7	-14.4	
kpf	sour l	2a	sourdough ls section (see notes)	0.6	-3.1	-13.1	
kpf	sour l	2b	sourdough ls section (see notes)	0.6	-2.6	-16.3	
kpf	sour l	5A-a	sourdough ls section (see notes)	1.9	-2.9	-13.0	
kpf	sour l	5A-b	sourdough ls section (see notes)	1.9	-3.3	-11.0	
kpf	sour l	5A-c	sourdough ls section (see notes)	1.9	-3.6	-12.4	
kpf	sour l	5A-d	sourdough ls section (see notes)	1.9	-2.7	-13.0	
kpf	sour l	6a	mjk collected along roadcut		-1.7	-12.7	
kpf	sour l	6b	mjk collected along roadcut		-2.1	-12.5	
kpf	sour l	7a	mjk collected along roadcut		-2.1	-12.2	
kpf	sour l	7a	sourdough ls section (see notes)	3.1	-3.8	-11.6	
kpf	sour l	7b	mjk collected along roadcut		-1.8	-13.2	
kpf	sour l	7b	sourdough ls section (see notes)	3.1	-3.3	-12.6	
kpf	sour l	7c	sourdough ls section (see notes)	3.1	-3.3	-12.5	
kpf	sour l	7d	sourdough ls section (see notes)	3.1	-3.4	-12.5	
kpf	sour l	7e	sourdough ls section (see notes)	3.1	-2.5	-12.9	
kpf	sour l	7f	sourdough ls section (see notes)	3.1	-2.8	-13.8	
kpf	sour l	8A	sourdough ls section (see notes)	4	-3.2	-13.3	
kpf	sour l	9a	mjk collected along roadcut		-2.0	-13.0	
kpf	sour l	9b	mjk collected along roadcut		-2.1	-13.1	
kpf	unl	1	unnamed limestone (see notes)	1	4.3	-14.8	
kpf	unl	4	unnamed limestone (see notes)	4	5.1	-14.9	
kpf	unl	5	unnamed limestone (see notes)	5	5.6	-14.9	
kpf	unl	6	unnamed limestone (see notes)	6	3.8	-15.3	
kpf	unl	7	unnamed limestone (see notes)	7	1.2	-11.6	
kpf	unl	8	unnamed limestone (see notes)	8	5.1	-14.9	
kpf	unl	9	unnamed limestone (see notes)	9	2.5	-11.5	

kpf	unl	10	unnamed limestone (see notes)	10	4.9	-14.6	
kpf	unl	2a	unnamed limestone (see notes)	2	2.7	-15.3	
kpf	unl	2b	unnamed limestone (see notes)	2	2.8	-15.2	
kpf	unl	3a	unnamed limestone (see notes)	3	0.6	-13.0	
kpf	unl	3b	unnamed limestone (see notes)	3	4.0	-15.3	
kpf	unl	7Aa	unnamed limestone (see notes)	7	0.7	-11.3	
kpf	unl	7Ab	unnamed limestone (see notes)	7	0.9	-11.9	
kpf	unl	7Ac	unnamed limestone (see notes)	7	0.5	-11.8	
kpf	unlim+	11	alabaster white carb cycle above Wildrose		-2.3	-9.7	
kpf	unlim+	12	alabaster white carb cycle above Wildrose		-2.0	-8.8	
kpf	unlim+	13	alabaster white carb cycle above Wildrose		-2.9	-10.3	
kpf	unlim+	14	alabaster white carb cycle above Wildrose		-2.4	-9.1	
kpf	unlim+	15	alabaster white carb cycle above Wildrose		-2.4	-9.7	
kpf	unlim+	16	carb 15-20 m above alb white cycle		-5.0	-14.3	
kpf		17	siltstone above SDL for meta grade				y
Southern Saddle Peak Hills							
if	sd pk m	2	SS: thickly lam blk siltstone + limestone (4 pcs + slab)		-6.4	-11.5	y
if	sd pk m	3					y
if	sd pk m	5	SSgrn qtzite below SP Mbr				y
if	sd pk m	2(rpt)	SS: thickly lam blk siltstone + limestone (4 pcs + slab)		-4.7	-10.6	y
kpf		7	SS: grn qtzite from JMM s. facies just below Bennies knob of Limestone				y
kpf		8	SS: graded beds from creek, above diamictite				y
kpf		9	SS: black siltstn from drainage above diamict (boumas)				y
Valjean Hills							
if		3	white carb clast from chocolate		4.7	-1.7	
if		22	ND clast in noonday rich breccia		-2.3	-10.8	
if		23	Lam ND in noonday rich breccia		-2.3	-10.4	
if		24	megaclast piece ND		-2.1	-9.6	
kpf		1	lower dark green shale				y
kpf		4	white carb clast from kp		2.4	-2.2	
kpf		5	lower kpf: gravel cgl				y
kpf		11	odd featues in siltstone				y

kpf		36			4.9	-2.8	
Virgin Spring							
kpf	ahd	1	lam dolo in AHD		1.9	-14.4	y
kpf	vsl	4	mjk collected; perhaps not vsl		3.3	-15.4	
kpf	vsl	7	mjk collected; perhaps not vsl		3.5	-15.5	
kpf	vsl	7	mjk collected; perhaps not vsl		4.3	-18.2	
kpf	vsl	8	mjk collected; perhaps not vsl		5.9	-15.0	
kpf	vsl	9	mjk collected; perhaps not vsl		2.9	-15.3	
kpf	vsl	9	mjk collected; perhaps not vsl		5.8	-16.1	
kpf	vsl	11	mjk collected; perhaps not vsl		5.5	-16.9	
kpf	vsl	12	mjk collected; perhaps not vsl		5.3	-22.0	
kpf	vsl	13	mjk collected; perhaps not vsl		2.7	-15.4	
kpf	vsl	13	mjk collected; perhaps not vsl		4.9	-18.3	
kpf	vsl	14	mjk collected; perhaps not vsl		1.4	-24.8	
kpf	vsl	15	mjk collected; perhaps not vsl		3.6	-15.1	
kpf	vsl	15	mjk collected; perhaps not vsl		-1.2	-12.2	
kpf	vsl	16	mjk collected; perhaps not vsl		2.1	-15.3	
kpf	vsl	27	mjk collected; perhaps not vsl		1.9	-15.1	
kpf	vsl	28	mjk collected; perhaps not vsl		1.8	-15.2	
kpf	vsl	29	mjk collected; perhaps not vsl		2.1	-14.7	
kpf	vsl	30	mjk collected; perhaps not vsl		3.4	-13.3	
kpf	vsl	10a	mjk collected; perhaps not vsl		5.3	-18.2	
kpf	vsl	10b	mjk collected; perhaps not vsl		4.0	-14.5	
kpf	vsl	11a	mjk collected; perhaps not vsl		2.8	-15.7	
kpf	vsl	11b	mjk collected; perhaps not vsl		2.8	-15.1	
kpf	vsl	13A	mjk collected; perhaps not vsl		1.8	-13.7	
kpf	vsl	13Ba	mjk collected; perhaps not vsl		1.2	-14.7	
kpf	vsl	13Bb	mjk collected; perhaps not vsl		0.9	-13.2	
kpf	vsl	14a	mjk collected; perhaps not vsl		2.8	-15.5	
kpf	vsl	14b	mjk collected; perhaps not vsl		1.8	-14.4	
kpf	vsl	6a	mjk collected; perhaps not vsl		3.3	-19.5	
kpf	vsl	6b	mjk collected; perhaps not vsl		1.9	-22.5	

Wareagle Mine							
nd	lower	1	WAR-BLOCK LAM CEMENTS&DISRUPTION (see Toms strat notes)		-1.5	-10.5	
nd	lower	1-mtx	WAR-BLOCK LAM CEMENTS&DISRUPTION (see Toms strat notes)		-1.4	-5.5	
nd	lower	1-vein	WAR-BLOCK LAM CEMENTS&DISRUPTION (see Toms strat notes)		-1.4	-8.0	
nd	lower	2 in	inside tube		-2.7	-6.1	
nd	lower	2 out	outside tube		-2.7	-6.0	
nd	lower	B1	War slab from creek...see Tom's cement strat notes		-3.5	-9.3	
nd	lower	B10	War slab from creek...see Tom's cement strat notes		-3.8	-8.9	
nd	lower	B2	War slab from creek...see Tom's cement strat notes		-3.9	-9.7	
nd	lower	B3	War slab from creek...see Tom's cement strat notes		-3.1	-8.3	
nd	lower	B4	War slab from creek...see Tom's cement strat notes		-7.3	-22.1	
nd	lower	B5	War slab from creek...see Tom's cement strat notes		-2.4	-7.6	
nd	lower	B6	War slab from creek...see Tom's cement strat notes		-1.9	-7.3	
nd	lower	B7	War slab from creek...see Tom's cement strat notes		-3.1	-8.0	
nd	lower	B8	War slab from creek...see Tom's cement strat notes		-3.6	-9.1	
nd	lower	B9	War slab from creek...see Tom's cement strat notes		-3.3	-14.1	
nd	lower	C in	WAR-BIG BLOCK LAM CEMENTS AND DISRUPTION ZONE		-2.7	-7.5	
nd	lower	C out	WAR-BIG BLOCK LAM CEMENTS AND DISRUPTION ZONE		-2.5	-6.3	
nd	lower	mwi	War Eagle Tubes		-3.6	-7.8	
nd	lower	mwo	War Eagle Tubes		-2.7	-6.8	
nd	lower	wbi	War Eagle Tubes		-3.7	-7.8	
nd	lower	wbo	War Eagle Tubes		-3.1	-6.9	
nd	upper	20	IM Fill Section	1	-3.2	-8.0	
nd	upper	21	IM Fill Section	2	-3.2	-8.6	
nd	upper	22	IM Fill Section	3	-2.8	-9.0	
nd	upper	23	IM Fill Section	4	-2.5	-8.3	
nd	upper	24	IM Fill Section	5	1.3	-15.0	
nd	upper	26	IM Fill Section	6	-4.0	-9.7	
nd	upper	27	IM Fill Section	7	-4.2	-9.9	
nd	upper	28	IM Fill Section	8	-2.7	-8.5	
nd	upper	29	IM Fill Section	9	-3.4	-9.3	
nd	upper	30	IM Fill Section	10	-3.3	-8.1	

nd	upper	31	IM Fill Section	11	-4.4	-9.7	
nd	upper	32	IM Fill Section	12	-3.7	-9.6	
nd	upper	33	IM Fill Section	13	-4.6	-10.3	
nd	upper	34	IM Fill Section	14	-1.8	-7.0	
nd	upper	35	IM Fill Section	15	-0.3	-5.9	
nd	upper	36	IM Fill Section	16	-0.4	-5.7	
nd	upper	39	IM Fill Section	18	-4.1	-9.5	
nd	upper	40	IM Fill Section	19	-4.6	-9.6	
nd	upper	41	IM Fill Section	20	-4.3	-8.9	
nd	upper	42	IM Fill Section	21	-4.6	-7.7	
nd	upper	43	IM Fill Section	22	-1.4	0.7	
nd	upper	44	IM Fill Section	23	-2.8	-4.3	
nd	upper	24A	IM Fill Section	5	-0.4	-5.1	
nd	upper	24B	IM Fill Section	5	-0.2	-4.9	
Wildrose Canyon							
kpf	mtn girl	4	gray ls clast in mtn girl		-6.0	-13.5	
kpf	sour l	1	Sourdough Section along road	1	0.7	-13.9	
kpf	sour l	4	Sourdough Section along road	4	0.9	-13.9	
kpf	sour l	5	Sourdough Section along road	5	1.6	-13.5	
kpf	sour l	8	Sourdough Section along road	7	1.9	-14.1	
kpf	sour l	10	Sourdough Section along road	9	3.1	-13.1	
kpf	sour l	11	Sourdough Section along road	10	4.3	-11.3	
kpf	sour l	22	upper sdl cycle in dolo & ls	8	-2.4	-12.9	
kpf	sour l	23	upper sdl cycle in dolo & ls	7	-3.3	-14.7	
kpf	sour l	24	upper sdl cycle in dolo & ls	6	-3.4	-14.3	
kpf	sour l	25	upper sdl cycle in dolo & ls	5	-6.3	-17.3	
kpf	sour l	26	lower sdl cycle ib dolo & ls	4	-3.2	-16.5	
kpf	sour l	27	lower sdl cycle ib dolo & ls	3	1.0	-14.1	
kpf	sour l	28	lower sdl cycle ib dolo & ls	2	2.5	-10.8	
kpf	sour l	30	lower sdl cycle ib dolo & ls	1	-1.3	-13.4	
kpf	sour l	12a	Sourdough Section along road	11	4.4	-14.0	
kpf	sour l	12b	Sourdough Section along road	11	4.5	-14.3	

kpf	sour l	13b	sourdough handsamp from n.side road		-4.4	-11.3	
kpf	sour l	13v	sourdough handsamp from n.side road		-5.2	-11.2	
kpf	sour l	1a	dolo contact in sdl under top dolo (these are all north side road)		-6.4	-16.7	
kpf	sour l	1b	dolo contact in sdl under top dolo (these are all north side road)		-0.9	-15.5	
kpf	sour l	2a	Sourdough Section along road	2	4.7	-13.2	
kpf	sour l	2a	almost upper dolo contact in sdl		-4.6	-16.6	
kpf	sour l	2b	Sourdough Section along road	2	4.8	-13.1	
kpf	sour l	2b	almost upper dolo contact in sdl		-4.9	-17.1	
kpf	sour l	3a	Sourdough Section along road	3	1.5	-13.7	
kpf	sour l	3a	top sdl dolo		-5.4	-17.2	
kpf	sour l	3b	Sourdough Section along road	3	1.4	-13.7	
kpf	sour l	3b	top sdl dolo		3.7	-15.6	
kpf	sour l	7a	Sourdough Section along road	6	-4.6	-7.2	
kpf	sour l	7b	Sourdough Section along road	6	1.8	-14.1	
kpf	sour l	7v	Sourdough Section along road	6	1.4	-12.8	
kpf	sour l	9a	Sourdough Section along road	8	2.7	-12.5	
kpf	sour l	9b	Sourdough Section along road	8	2.9	-12.3	
kpf	unl	5	first dolo bed in un-named		-2.0	-12.4	
kpf	unl	6	first limestone bed in un-named		0.9	-14.0	
kpf	unl	7	gray ls clast around un-named		-0.8	-13.7	
kpf	unl	8	gray ls clast around un-named		1.5	-13.2	
kpf	unl	9	dolo clast around un-named		4.7	-13.0	
kpf	unl	11	un-named ib dolo & ls	10	2.4	-11.4	
kpf	unl	12	un-named ib dolo & ls	9	4.2	-12.5	
kpf	unl	13	un-named ib dolo & ls	8	4.7	-13.5	
kpf	unl	14	un-named ib dolo & ls	7	3.4	-12.1	
kpf	unl	15	un-named ib dolo & ls	6	0.8	-14.2	
kpf	unl	16	un-named ib dolo & ls	5	-1.9	-12.0	
kpf	unl	17	un-named ib dolo & ls	4	-2.5	-12.6	
kpf	unl	18	un-named ib dolo & ls	3	-2.3	-12.7	
kpf	unl	20	un-named ib dolo & ls	2	-1.7	-12.2	
Winters Pass NE Hills							

kpf	gd	1	kp mtx?				y
kpf	gd	2	bsm below kp (?)…is there kp?				y
kpf	gd	5	coarse ss pbl layer				y
Winters Pass Hills							
kpf	gd	1	WP: clast from orange brown diamictite				y
kpf	gd	2	WP: choc brown matrix of choc diamictite				y
nd	lower	1A(c)	sample for cement strat project		-2.9	-12.9	
nd	lower	1A(a)	sample for cement strat project		-3.6	-6.0	
nd	lower	1A(b)	sample for cement strat project		-3.7	-6.1	
nd	lower	1A(d)	sample for cement strat project		-3.0	-11.1	
nd	lower	3 botroid	WP: travertine vein (2)		-8.2	-11.4	y
nd	lower	3 lam	WP: travertine vein (2)		-7.8	-11.0	
nd	lower	3A	big slab tube		-2.2	-6.4	y
nd	lower	3B	big slab tube		-3.0	-6.2	
nd	lower	3C	big slab tube		-3.3	-9.6	
nd	lower	3D	big slab tube		-2.8	-7.5	
nd	lower	crust	sample for cement strat project		-3.4	-4.9	
nd	lower	WP1cmnt	North Winters Pass tubes		-3.0	-9.5	
nd	lower	WP1I	North Winters Pass tubes		-2.7	-6.9	
nd	lower	WP1O	North Winters Pass tubes		-3.2	-6.4	
nd	lower	WP-A inside	North Winters Pass tubes		-2.1	-6.8	
nd	lower	WP-A outside	North Winters Pass tubes		-3.0	-6.2	
kpf	gd	8	mtx of wildrose				y
Wood Canyon							
kpf	sour l	6		6	-3.4	-15.3	
kpf	sour l	7.5	light zone right above 7E	7.5	-2.6	-13.7	
kpf	sour l	15.6	spar inside lens	15.6	-4.3	-16.4	
kpf	sour l	15.7	upper contact	15.7	-3.5	-16.7	
kpf	sour l	19		19	-1.8	-14.6	
kpf	sour l	20		20	-2.3	-15.8	

kpf	sour l	21		21	-2.4	-16.5	
kpf	sour l	22		22	-3.0	-17.3	
kpf	sour l	30		31	-2.2	-16.1	
kpf	sour l	41		41	-5.8	-17.2	
kpf	sour l	44	lam,fold grey LS (10m over 43)	60	-4.7	-18.2	
kpf	sour l	10a		10	-2.4	-13.1	
kpf	sour l	10b		10	-2.5	-13.9	
kpf	sour l	10v		10	-3.0	-14.6	
kpf	sour l	11a		11	-2.3	-15.1	
kpf	sour l	11b		11	-2.3	-14.9	
kpf	sour l	12a		12	-2.2	-15.9	
kpf	sour l	12b		12	-2.2	-15.9	
kpf	sour l	13.8a	x-cut vein	13.8	-2.2	-15.6	
kpf	sour l	13.8b	x-cut vein	13.8	-2.1	-16.1	
kpf	sour l	13a		13	-2.0	-16.4	
kpf	sour l	13b		13	-2.1	-16.3	
kpf	sour l	14a		14	-2.4	-16.1	
kpf	sour l	14b		14	-2.5	-16.2	
kpf	sour l	15.5a	gray lower contact spar lens	15.5	-3.0	-15.4	
kpf	sour l	15.5a1a	gray lower contact spar lens	15.5	-3.0	-16.5	
kpf	sour l	15.5b	gray lower contact spar lens	15.5	-1.8	-12.8	
kpf	sour l	15.5x	gray lower contact spar lens	15.5	-3.4	-12.8	
kpf	sour l	15.9a1	tigmatic spar vein in lm facies	15.9	-2.9	-16.2	
kpf	sour l	15.9a2	tigmatic spar vein in lm facies	15.9	-3.0	-16.2	
kpf	sour l	15.9b1	tigmatic spar vein in lm facies	15.9	-2.9	-16.3	
kpf	sour l	15.9b2	tigmatic spar vein in lm facies	15.9	-2.9	-16.5	
kpf	sour l	15b		15	-3.4	-16.3	
kpf	sour l	16a	grading into coarser brown recrystal facies	16	-2.8	-16.5	
kpf	sour l	16a2	grading into coarser brown recrystal facies	16	-2.9	-16.9	
kpf	sour l	16b		16	-2.7	-16.6	
kpf	sour l	16v		16	-3.0	-16.4	
kpf	sour l	17a		17	-2.5	-16.8	

kpf	sour l	17b		17	-2.4	-16.7	
kpf	sour l	18b		18	-2.0	-15.2	
kpf	sour l	1a		0	-3.3	-15.7	
kpf	sour l	1b		0	-3.6	-15.9	
kpf	sour l	1c		0	-3.7	-16.0	
kpf	sour l	22.3b	under overturned vein	22.3	-3.4	-17.1	
kpf	sour l	22.3v	under overturned vein	22.3	-2.9	-13.4	
kpf	sour l	22.8b	top contact overturned vein	22.8	-4.1	-17.2	
kpf	sour l	23a		23	-2.9	-17.1	
kpf	sour l	23b		23	-2.8	-17.2	
kpf	sour l	24a1		24	-2.5	-15.5	
kpf	sour l	24a2		24	-2.3	-15.7	
kpf	sour l	24b1		24	-2.4	-15.7	
kpf	sour l	24b2		24	-2.3	-15.7	
kpf	sour l	25a1		25	-2.3	-15.0	
kpf	sour l	25a1(rpt)		25	-2.3	-15.0	
kpf	sour l	25a2		25	-2.4	-15.0	
kpf	sour l	25a2(rpt)		25	-2.3	-14.9	
kpf	sour l	25b		25	-2.4	-15.0	
kpf	sour l	25b(rpt)		25	-2.3	-14.9	
kpf	sour l	26a1		26	-2.6	-15.1	
kpf	sour l	26a1(rpt)		26	-2.6	-15.1	
kpf	sour l	26a2		26	-2.6	-15.3	
kpf	sour l	26a2(rpt)		26	-2.7	-15.1	
kpf	sour l	26b		26	-2.4	-15.2	
kpf	sour l	26b(rpt)		26	-2.3	-15.2	
kpf	sour l	27b		27	-2.9	-16.1	
kpf	sour l	28a		28	-2.7	-15.7	
kpf	sour l	28b		28	-2.7	-15.1	
kpf	sour l	29a		29	-2.3	-16.8	
kpf	sour l	29b		29	-2.3	-16.9	
kpf	sour l	2a		1.5	-2.4	-13.1	

kpf	sour l	2b		1.5	-2.5	-13.2	
kpf	sour l	30a		30	-2.0	-16.4	
kpf	sour l	30b		30	-2.2	-16.7	
kpf	sour l	31a		31	-2.4	-16.4	
kpf	sour l	32a		32	-2.1	-16.3	
kpf	sour l	32a2		32	-2.3	-16.3	
kpf	sour l	32b		32	-2.3	-16.5	
kpf	sour l	33b		33	-2.1	-16.1	
kpf	sour l	34a		34	-2.1	-16.0	
kpf	sour l	34b		34	-2.2	-16.3	
kpf	sour l	35a		35	-2.3	-16.3	
kpf	sour l	36a		36	-2.9	-17.6	
kpf	sour l	36b		36	-2.9	-17.9	
kpf	sour l	37a	top of all carb SDL	37	-2.6	-17.6	
kpf	sour l	37b	top of all carb SDL	37	-2.9	-17.7	
kpf	sour l	3a		3	-2.2	-12.4	
kpf	sour l	3b		3	-2.3	-12.4	
kpf	sour l	40a		40	-2.6	-17.8	
kpf	sour l	40b		40	-2.5	-17.8	
kpf	sour l	42a		42	-4.8	-20.2	
kpf	sour l	42b		42	-4.6	-20.0	
kpf	sour l	43a	carbonate in SS; 5-10 m above top of IB SDL/SS	50	-3.9	-17.2	
kpf	sour l	43b		50	-4.1	-17.6	
kpf	sour l	45a	last major LS cycle (44+10m) trans to med ss (spotty)	70	-2.9	-17.2	
kpf	sour l	4a		4	-2.6	-13.8	
kpf	sour l	4b		4	-2.6	-13.8	
kpf	sour l	5a		5	-2.4	-13.1	
kpf	sour l	5b		5	-2.7	-13.5	
kpf	sour l	6.3a	upper dark carb contact of ss lens	6.3	-3.4	-15.6	
kpf	sour l	6.3b	upper dark carb contact of ss lens	6.3	-2.9	-14.9	
kpf	sour l	6.5a1		6.5	-3.0	-14.9	
kpf	sour l	6.5a2		6.5	-3.1	-15.3	

kpf	sour l	6.5a3		6.5	-3.1	-15.2	
kpf	sour l	6.5b1		6.5	-3.1	-15.1	
kpf	sour l	6.5b2		6.5	-3.1	-15.4	
kpf	sour l	6.5b3		6.5	-3.3	-15.8	
kpf	sour l	6.6a	slab from discolored zone below "vein"	6.6	-2.1	-12.5	
kpf	sour l	6.6b	slab from discolored zone below "vein"	6.6	-1.6	-12.1	
kpf	sour l	6.6v	slab from discolored zone below "vein"	6.6	-1.9	-12.6	
kpf	sour l	6A	s.s. channel or boudin	6	-4.1	-15.0	
kpf	sour l	7a1	slab just below vein…top is 7m	7	-2.7	-13.7	
kpf	sour l	7a3	slab just below vein…top is 7m	7	-3.0	-14.1	
kpf	sour l	7B	cement below sand	6.9	-3.2	-16.0	
kpf	sour l	7b1	slab just below vein…top is 7m	7	-2.7	-13.8	
kpf	sour l	7B-1		6.9	-3.2	-15.5	
kpf	sour l	7b2	slab just below vein…top is 7m	7	-3.0	-13.8	
kpf	sour l	7b3	slab just below vein…top is 7m	7	-3.0	-14.3	
kpf	sour l	7b4	slab just below vein…top is 7m	7	-3.7	-14.9	
kpf	sour l	7Bv	cement below sand	6.9	-3.4	-15.4	
kpf	sour l	7D	cement over vein calcite (7C)	7.3	-3.7	-15.2	
kpf	sour l	7D-1	cement over vein calcite (7C)	7.3	-3.8	-15.7	
kpf	sour l	7Dv	cement over vein calcite (7C)	7.3	-3.1	-14.9	
kpf	sour l	7E	light colored SDL over upper cement (in slabw/7D)	7.4	-3.1	-14.7	
kpf	sour l	7v1	slab just below vein…top is 7m	7	-3.3	-14.6	
kpf	sour l	7v2	slab just below vein…top is 7m	7	-3.1	-14.8	
kpf	sour l	8a1		8	-2.7	-12.2	
kpf	sour l	8a2		8	-2.5	-11.2	
kpf	sour l	8b		8	-2.7	-12.1	
kpf	sour l	9a		9	-2.5	-11.9	
kpf	sour l	9b		9	-2.3	-11.7	
nd		46		110	-0.3	-9.4	
nd		47		115	-0.9	-11.2	
nd		48		120	-1.6	-10.1	
nd		49		125	-2.0	-11.3	

nd	50		130	-1.8	-12.2	
nd	51	alt sandy red zone between cycles	140	-2.6	-8.8	
nd	52		145	-2.3	-9.2	
nd	53		150	-2.7	-10.5	
nd	54		155	-2.9	-10.3	
nd	55		160	-2.5	-9.4	
nd	56	has brown contact	170	-2.5	-8.9	
nd	57		175	-2.3	-8.7	
nd	58	Limy/sandy trans to next unit	178	-4.0	-10.8	
nd	59		180	-5.1	-11.8	
nd	61		190	-5.2	-13.2	
nd	62		200	-5.1	-13.0	
nd	63		210	-4.7	-14.6	
nd	65	buff bed	213	-3.7	-13.8	
nd	66	grn bed	214	-4.8	-16.3	
nd	67	buff bed	215	-4.2	-12.6	
nd	68		220	-4.6	-12.7	
nd	69		225	-4.6	-11.9	
nd	70		230	-2.2	-12.9	
nd	72		235	-2.1	-6.7	
nd	73		240	-0.9	-6.1	
nd	74		245	-1.8	-5.6	
nd	75		250	0.1	-7.0	
nd	49c		125	-1.8	-11.5	
nd	60a		185	-5.1	-12.4	
nd	60b		185	-5.2	-12.6	
nd	64a		212	-4.7	-12.0	
nd	64b	grn bed	212	-5.7	-12.9	
nd	71a		230	-1.5	-7.0	
nd	71b		230	-1.6	-6.9	

Appendix B: Clast Counts

Key: AHD=Alexander Hills Diamictite, Q=quartzite, Bi=basement-igneous, Bm=basement-metamorphic, CSFc=Crystal Spring Formation-carbonate, CSFs=Crystal Spring Formastion-sandstone, CSFd=Crystal Spring Formation-diabase, BSD=Beck Spring Dolomite, SHS=Saratoga Hills Sandstone, SHSc=Saratoga Hills Sandstone-coarse, VSL=Virgin Spring Limestone

	Q	Bi	Bm	CSFc	CSFs	CSFd	BSD	SHS	SHSc	VSL
AHD										
11/20/2005-Beck Canyon Divide-basal Alexander Hills Diamictite-.6x.6m										
Matrix: bimodal, black calcite cemented medium-grained sand with 15-20% pebble fragments of black limestone, BSD and Q										
Count	5	1								21
Max Size	3	5								5
Average Size										
11/20/2005-Beck Canyon Divide-basal Alexander Hills Diamictite-1x.5m										
Matrix: bimodal, black calcite cemented medium-grained sand with 15-20% pebble fragments of black limestone, BSD & Q										
Count	12		6							52
Max Size	7		9							9
Average Size										
12/3/2005-Crystal Spring-basal Alexander Hills Diamictite-1x1m										
Matrix: bimodal, silt and medium-grained sub-angular quartz sand (also pebble size siltstone ripups of kp1)										
Count	5	2								21
Max Size	4	3								7
Average Size										

12/3/2005-Crystal Spring-basal Alexander Hills Diamictite-.5x1m Matrix: bimodal, silt and medium-grained sub-angular quartz sand (also pebble size siltstone ripups of kp1)								
Count	7	2			1			15
Max Size	8	3			3			6
Average Size								

12/3/2005-Crystal Spring-basal Alexander Hills Diamictite-1x2m Matrix: bimodal, silt and medium-grained sub-angular quartz sand (also pebble size siltstone ripups of kp1)								
Count	3	1	1			1		48
Max Size	3	5	8			4		12
Average Size								

3/19/2006-Ibex Hills-basal Alexander Hills Diamictite-3x3m Mtrix: bimodal, calcite-rich black silty and sub-angular quartz grains								
Count	2							42
Max Size	10							24
Average Size								

12/16/2006 - Silverule Mine - basal Alexander Hills Diamictite - .5x2m Matrix: black calcitic with rounded to sub-rounded qtz sand								
Count	6	3	1	1	10	3	8	22
Max Size	3	7	4	2	5	5	3	4.5
Average Size	2	4	4	2	1.75	4	2.125	1.636

2/28/2005-Alexander Hills-30m above basal Alexander Hills Diamictite-.5x.5m Matrix: coarse sub-rounded to angular sand with ca. 5% sub-cm pebbles of quartzite, tan carbonate and siltstone								
Count	10	2	3	2		3		
Max Size	8	5	5	6		2		
Average Size	3.7	3	3.333	4.5		2		

2/28/2005-Alexander Hills-30m above basal Alexander Hills Diamictite-.5x.5m Matrix: coarse sub-rounded to angular sand and siltstone						
Count	4	1	4		1	1
Max Size	5	2	20		3	4
Average Size	3.5	2	7.5		3	4

2/28/2005-Alexander Hills-30m above basal Alexander Hills Diamictite-.5x.5m Matrix: coarse sub-rounded to angular sand with ca. 2% sub-cm pebbles of quartzite, tan carbonate and siltstone						
Count	4	4	1	2		1
Max Size	7	3	4	30		5
Average Size	5.5	1.75	4	16.5		5

2/28/2005-Alexander Hills-30m above basal Alexander Hills Diamictite-.5x.5m Matrix: coarse sub-rounded to angular sand and siltstone						
Count	14	5	1		2	2
Max Size	20	6	5		5	5
Average Size	4.5	4.6	5		3.5	4.5

11/20/2005-Beck Canyon Divide-middle Alexander Hills Diamictite-1x1m Matrix: greenish with well-rounded quartz and silt						
Count	28	1				2
Max Size	12	6				9
Average Size						

3/19/2006-Ibex Hills-upper Alexander Hills Diamictite-1x1m Matrix: bimodal, orage silt and sub-rounded med-grained quarts sand						
Count	35					
Max Size						
Average Size						

12/18/2006 - Saratoga Hills - upper Alexander Hills Diamictite -1x1m Matrix: coarse green and white poorly sorted								
Count	20	5				25		
Max Size	8	5				8		
Average Size	3.65	3.2				3.24		

12/16/2006 - Silverule Mine - upper Alexander Hills Diamictite - .7x2.2m Matrix: green with fine- to med-grain sand and silt or brown with med- to coarse-grain sand								
Count	12	4				12	6	5
Max Size	9	10				5	8	5
Average Size	4.208	6				2.458	4.167	4.1

12/16/2006 - Silverule Mine - upper Alexander Hills Diamictite -1x3.5m Matrix: green with fine- to med-grain sand, some calcite and sub-rounded to sub-angular quartz grains								
Count	14	10		1		17	1	15
Max Size	9	10		6		7	12	7
Average Size	4.143	4.1		6		3.353	12	3.1

2/27/2005-Alexander Hills-Alexander Hills Diamictite-1x1m Matrix: brown fine sand and silt with coarse sub-rounded sand grains								
Count	8	9	1	13	6	5		1
Max Size	7	6	3	12	16	4		2
Average Size	3.875	3.778	3	4.538	6.333	2.8		2

11/21/2005-Blackwater Mine-Alexander Hills Diamictite Matrix: greenish-yellow, fine-grained quartz sand								
Count	2	11	3			2		50
Max Size	5	10	4			4		6
Average Size								

12/10/2005-Crystal Spring-Alexander Hills Diamictite-1x1m Matrix: bimodal, carbonate-rich silt and rounded quartz sand						
Count	9	2	6	1	4	28
Max Size	25	18	7	5	3	10
Average Size						

12/10/2005-Crystal Spring-Alexander Hills Diamictite-1x1m Matrix: bimodal, carbonate-rich silt and rounded quartz sand						
Count	10		4		16	17
Max Size	32		5		7	11
Average Size						

12/10/2005-Crystal Spring-Alexander Hills Diamictite-1x1m Matrix: bimodal, carbonate-rich silt and rounded quartz sand						
Count	7	5	7	8	13	7
Max Size	40	20	10	8	20	8
Average Size						

1/13/2006-Horsethief Mine-Alexander Hills Diamictite-2x2m Matrix: bimodal, silt and sub-rounded to sub-angular sand with abundant angular pebbles						
Count	15	1		21		
Max Size	5	8		10		
Average Size						

12/18/2006 - Saratoga Hills - Alexander Hills Diamictite -1x2m Matrix: green silty-fine sand & calcitic and brown with med- to coarse-sand					
Count	30	22	1	20	1
Max Size	17	12	8	8	2
Average Size	5.133	4.864	8	2.95	2

2/8/2006-Virgin Spring Wash-Alexander Hills Diamictite-1x1m Matrix: bimodal, orange silt and coarse quartz sand (abundant quartz and Virgin Spring Limestone pebbles)										
Count	5						1			15
Max Size	6						4			7
Average Size										
TTL Count Basal Portion	**40**	**9**	**7**	**1**	**1**	**0**	**11**	**4**	**8**	**221**
TTL Count Middle Portion	**60**	**13**	**0**	**9**	**4**	**0**	**0**	**6**	**0**	**6**
TTL Count Upper Portion	**81**	**19**	**0**	**1**	**0**	**0**	**0**	**54**	**7**	**20**
TTL Count Entire Section	**267**	**91**	**12**	**41**	**11**	**21**	**23**	**89**	**48**	**366**

Silver Rule Mine Member

11/20/2005-Beck Canyon Divide-Silver Rule Mine Member diamictite facies-2x2m Matrix: calcite-rich grey-green medium quartz sand										
Count	4						25			4
Max Size	4						20			3
Average Size										

12/3/2005-Crystal Spring-Silver Rule Mine Member diamictite facies-1x1m Matrix: bimodal, carbonate-rich silt and rounded quartz sand										
Count	7			3			8			18
Max Size	3			6			4			3
Average Size										

12/3/2005-Crystal Spring-Silver Rule Mine Member diamictite facies-1x2m Matrix: Bimodal, silt and coarse quartz sand										
Count	18	13	1	5						12
Max Size	10	10	5	3						60
Average Size										

1/31/2006-Horsethief Mine-Silver Rule Mine Member diamictite facies-1x1m Matrix: non-calcitic orange silt and angular to rounded coarse-grained quartz sand										
Count				9			20			
Max Size				2			3			
Average Size										
12/17/2006 - Silverule Mine - Silver Rule Mine Member diamictite facies, near Silver Rule Mine Member oncoid marker bed - 1.25x1m Matrix: black calcitic with rounded qtz grains										
Count	19	15					9	26	2	26
Max Size	12	6					6	10	4	7
Average Size	3.7	3.1					3.6	2.3	3.0	3.0
12/2/2005-Snow White-Silver Rule Mine Member diamictite facies-1x1m Matrix: brownish, silt and medium-grained quartz sand										
Count					18	12	9	4		
Max Size										
Average Size										
TTL Count	**48**	**28**	**1**	**17**	**0**	**0**	**62**	**26**	**2**	**60**
Jupiter Mine Member										
12/3/2005-Crystal Spring-Jupiter Mine Member fanglomerate-.5x.5m Matrix: bimodal, fine grained sand and coarse-grained sub-angular quartz sand										
Count	14			9			62			
Max Size	10			3			25			
Average Size										
1/31/2006-Horsethief Mine-Jupiter Mine Member conglomerate/fanglomerate-1x2m Matrix: bimodal, orange silt and medium-grained quartz sand										
Count	9			8			144			
Max Size	7			4			20			
Average Size										

12/23/2005-Silurian Hills-Jupiter Mine Member diamictite-1x1m Matrix: bimodal, silt and sub-rounded to sub-angular medium-grained quartz							
Count		17	3	2			
Max Size							
Average Size							

12/2/2005-Snow White-Jupiter Mine Member fanglomerate-1x1m Matrix: bimodal quartz silt and sub-angular coarse-grained quartz sand						
Count	43		17	10	20	10
Max Size	30		5	5	50	3
Average Size						

12/2/2005-Snow White-Jupiter Mine Member debris flow-1x1m Matrix: silt with minor sub-rounded medium grained quartz sand						
Count	12				25	
Max Size	20				40	
Average Size						

Gunsight Mine Diamictite

12/8/2005-Wareagle Mine-Gunsight Mine Diamictite-2x2m										
Matrix: medium-grained quartz sand and sub-rounded coarse-grained quartz sand										
Count	12			25						
Max Size	15			12						
Average Size										
2/8/2006-Wareagle Mine-Gunsight Diamictite-1x2m										
Matrix: bimodal, coarse sub-rounded to angular sand and siltstone										
Count			22	18				15		
Max Size			14	15				8		
Average Size										
TTL Count	**12**	**0**	**22**	**43**	**0**	**0**	**0**	**15**	**0**	**0**